

# **Evaluation of Gait Transitional Stability for Adults with Ankle-foot Impairments**

**Imran Mahmood**

**Submitted in accordance with the requirements for the degree of  
Doctor of Philosophy**

**The University of Leeds  
School of Mechanical Engineering**

**April, 2019**

The candidate confirms that the work submitted is his own, except where work which has formed part of jointly-authored publications has been included. The contribution of the candidate and the other authors to this work has been explicitly indicated below. The candidate confirms that appropriate credit has been given within the thesis where reference has been made to the work of others.

This copy has been supplied on the understanding that it is copyright material and that no quotation from the thesis may be published without proper acknowledgement.

The candidate performed the major tasks of the work presented in these published papers, such as the development of algorithm, experimental procedures, data analysis and the results. The co-authors reviewed and guided the candidate and provided valuable feedback.

The right of Imran Mahmood to be identified as Author of this work has been asserted by him in accordance with the Copyright, Designs and Patents Act 1988.

## ABSTRACT

Walking stability is essential for performing daily living activities with independence, dignity and confidence. Statistics reveal that patients with lower limb impairments are continually increasing with an increase in accidents or sports-related injuries, neurological deficiencies, and elderly population. The recovery from such impairments usually took a significantly long time and affect patient's health, psychology, social issues, and increased healthcare costs.

A survey of the literature reveals that the pre-assessment of such patients can potentially reduce stability risks, however, the existing assessment techniques are lacked to quantify stabilities with distinct criteria, during gait transitional phases, and varying degrees of lower limb impairments. On the other hand, various wearable orthoses are prescribed clinically or available commercially to assist gait deficiencies, however, their impacts on walking stabilities have remained unclear.

This research introduces new applications of control engineering theory to assess gait dynamic stabilities using mathematical models, distinct analysis criteria, and over varying walking terrains. The ankle-foot deficiencies such as foot drop, Charcot-Marie-Tooth, eversion, and inversion are imitated with a uniform degree of impairments using healthy subjects and adjustable orthoses. The gait dynamic stabilities are assessed using frequency models of neuromechanical signals such as centre-of-pressure and centre-of-mass acceleration as a resultant output and input (O/I) responses generated by the neuromotor. The Nyquist and Bode methods are employed to quantify stability margins from gain and phase plots of the modelled signals. The results illustrated the significant impact of imitated impairments on walking stabilities compared to an unrestricted healthy walk. The stability margins during weight loading gait phases showed stable magnitudes quantified from CoP waveforms and unstable responses from CoM-acceleration using  $99\pm 0.5\%$  best fit models. During weight unloading gait phases, both the outputs and inputs showed unstable margins. The results are also compared by applying prior stability assessment approaches.

Evaluation of gait contractile dynamics such as damping ratio, peak gain, and natural frequency using vertical CoM-oscillations provide important information about lower limbs contractile dynamics with/without the effect of the wearable orthosis. This pilot study provided proof of concept for neuromechanical balance control assessment applying control engineering theory and with ankle-foot impairments, nevertheless, these methods could be equally applicable for stability assessments in patients with knee or hip joint impairments and/or by wearing other lower limb prosthetics or exoskeleton devices.

*To my father, my beloved mother (late) and my family for their endless support. To my wife, Anam, who has been patient and supportive during the completion of this thesis and to my little son, Muhammad Asher Mahmood, who was the source of happiness.*

## ACKNOWLEDGEMENTS

All praise and acclamations belong to Almighty Allah (SWT) who has, out of his endless bounties, provided me with the opportunity and enabled me to achieve my goals successfully. I would like to take this opportunity to thank everyone who helped and supported me throughout my PhD study.

I offer my sincerest gratitude to my supervisor *Professor Abbas Dehghani* for his tireless support, encouragement and guidance throughout the entire PhD study. None of my work would have been possible without his kind supervision.

I am grateful to *Dr Uriel Martinez-Hernandez* for their continuous support and guidance throughout the entire research. Thanks to my entire fellow graduate students at the Institute of Design, Robotics and Optimization (iDRO) at the University of Leeds as well as my friends from other Schools of the University.

I must thank my parents who have been a constant source of inspiration for me. They have provided me with values that rank high in morals and character. I give my deepest love to my parents and the rest of the family members for their love, encouragement and support throughout my PhD study and my entire life. I would like to express my special thanks to my beloved wife, *Anam* and my lovely son *Muhammad Asher Mahmood* for their patience, encouragement and moral support.

I also would like to thank all the volunteers who participated in this study. Finally, I would like to thank my sponsor, University of Engineering and Technology Lahore, Pakistan for providing financial support to pursue my PhD study.

## LIST OF CONTENTS

<b>Abstract .....</b>	<b>iii</b>
<b>Acknowledgement .....</b>	<b>v</b>
<b>List of Contents .....</b>	<b>vi</b>
<b>List of Figures .....</b>	<b>xi</b>
<b>List of Tables .....</b>	<b>xv</b>
<b>List of Abbreviations .....</b>	<b>xxi</b>
<b>List of Publication Related to This Thesis .....</b>	<b>xxiv</b>
<b>CHAPTER 1 INTRODUCTION .....</b>	<b>1</b>
1.1 Background .....	1
1.2 Motivation .....	3
1.3 Aims and Objectives .....	5
1.3.1 Aims .....	5
1.3.2 Objectives .....	5
1.4 Scope of this Research .....	6
1.5 Contributions of this research .....	6
1.6 Organization of the Thesis .....	7
<b>CHAPTER 2 LITERATURE REVIEW .....</b>	<b>10</b>
2.1 Introduction .....	10
2.2 Lower limbs Biomechanics .....	10
2.2.1 Basic Anatomy .....	10
2.2.2 Planes and axes of movements .....	11
2.2.3 Gait cycle .....	12
2.2.4 Lower limb joints kinematics and kinetics .....	13
2.2.5 Neural Control of Gait .....	16
2.3 Walking Stabilities and Lower Limb Impairments .....	18
2.3.1 Ankle-foot joint as an end effector .....	18
2.3.2 Ankle-foot Impairments and Wearable Orthosis .....	22
2.3.3 Static and Dynamic Balance Control .....	26
2.4 Gait Dynamic Stability Assessment Methods .....	28
2.4.1 Gait Parameters Variability .....	28
2.4.2 Correlation Coefficient Methods .....	29
2.4.3 Lyapunov Exponent Method .....	30
2.4.4 Floquet Multiplier (FM) Method .....	32

2.4.5	Whole Body Angular Momentum approach .....	32
2.4.6	Extrapolated-CoM and BoS Difference .....	33
2.4.7	Nyquist and Bode (N&B) stability Methods .....	35
2.4.8	Clinical/experimental limitations of stability assessments .....	37
2.5	Stability Evaluation for varying terrains .....	37
2.6	Lower limb contractile dynamics .....	38
2.7	Gaps of knowledge .....	41
2.7.1	Methodological .....	42
2.7.2	Performance .....	42
2.7.3	Applications .....	42
2.8	Summary .....	43
<b>CHAPTER 3 EXPERIMENTAL PROTOCOL AND ANALYTICAL PROCESSES .....</b>		<b>44</b>
3.1	Introduction .....	44
3.2	Requirements and Specifications .....	44
3.3	Wearable Ankle-foot orthoses Designs .....	46
3.3.1	Adjustable ankle-foot orthosis design .....	46
3.3.2	Wedge foot insoles design .....	48
3.4	Experimental Protocol and Procedures .....	49
3.4.1	Imitated Ankle-foot Impairments .....	49
3.4.2	Motion Capture System and Trials .....	50
3.4.3	Visual3D Motion Analysis System .....	52
3.4.4	Spaciotemporal, Kinematic and Kinetic variations in Gait .....	53
3.4.5	Validation of Imitated Ankle-foot Impairments .....	61
3.5	Gait Dynamic Stability Measurement Signals .....	64
3.6	Modelling and Stability Analysis Algorithms .....	65
3.6.1	Linearity and time invariance of measured Signals .....	65
3.6.2	Modelling in Time and Frequency Domains .....	67
3.6.3	Nyquist and Bode (N&B) stability methods .....	69
3.6.4	Stable and Unstable Gait .....	76
3.7	Comparison between past and proposed stability measures .....	76
3.8	Effect of extreme walking speeds on transitional stability .....	78
3.9	Statistical Analyses .....	78
3.10	Summary .....	79

<b>CHAPTER 4 GAIT TRANSITIONAL STABILITY ASSESSMENT USING COP IMPULSIVE RESPONSES FOR LEVEL WALK .....</b>	<b>81</b>
4.1 Introduction .....	81
4.2 Hypotheses .....	81
4.3 Methods.....	82
4.3.1 Subjects and Trials.....	82
4.3.2 CoP-velocity waveforms and Pre-processing.....	84
4.3.3 Linearity in Measured Waveforms .....	86
4.3.4 Time and Frequency Domain Models .....	87
4.3.5 Nyquist and Bode Stability Methods .....	88
4.3.6 Extrapolated CoM and Gait parametric variability Methods .....	89
4.3.7 Body mass index (BMI) impact on transitional stability.....	89
4.3.8 Statistical Analysis.....	89
4.4 Results.....	90
4.4.1 Stability Margins from Nyquist and Bode Methods.....	90
4.4.2 Margins of stability using Extrapolated-CoM (XCoM) Method.....	97
4.4.3 Variability in Gait kinematic and kinetic parameters .....	99
4.4.4 BMI effect on stability.....	100
4.4.5 Controller design for unstable gait transitions.....	100
4.4.6 Effect of walking speed on transitional stability .....	101
4.5 Discussion .....	102
4.6 Summary .....	109
<b>CHAPTER 5 SOMATOSENSORY FORWARD COM-OSCILLATIONS IMPACTS ON GAIT TRANSITIONAL STABILITIES.....</b>	<b>110</b>
5.1 Introduction .....	110
5.2 Hypotheses .....	110
5.3 Methods.....	111
5.3.1 Experimental Protocol .....	111
5.3.2 Data Processing .....	112
5.3.3 Time and Frequency domain Modelling.....	113
5.3.4 Correlation Coefficients.....	119
5.3.5 Statistical Analysis.....	119
5.4 Results.....	119
5.4.1 Modelling Results .....	119
5.4.2 Loading Phases Stability Margins .....	120
5.4.3 Unloading Phases Stability Margins.....	122



5.4.4	Variability in Principal Components .....	125
5.4.5	Spearman Correlations .....	125
5.4.6	Comparison between CoP and CoM stability outcomes .....	126
5.4.7	Spatiotemporal, kinematic and kinetic parameters.....	126
5.4.8	Body mass index (BMI) impact on transitional stability.....	127
5.4.9	Controller design for unstable gait transitions.....	128
5.4.10	Effect of walking speed on transitional stability .....	129
5.5	Discussion .....	130
5.5.1	Methodological Considerations.....	131
5.5.2	Stability Margins .....	133
5.6	Summary .....	138
<b>CHAPTER 6 VERTICAL COM-OSCILLATIONS IMPACTS ON GAIT STABILITIES AND CONTRACTILE DYNAMICS .....</b>		<b>139</b>
6.1	Introduction.....	139
6.2	Hypotheses.....	139
6.3	Methods.....	140
6.3.1	Experimental Protocol.....	140
6.3.2	Data Processing .....	141
6.3.3	Modelling of whole body vertical vibrations .....	142
6.3.4	Nyquist and Bode Stability Analysis.....	146
6.3.5	Statistical Analysis .....	147
6.4	Results.....	147
6.4.1	Stability margins and Contractile properties .....	147
6.4.2	Body mass index (BMI) effect on transitional stability .....	151
6.4.3	Controller design for unstable gait transitions.....	152
6.4.4	Effect of walking speed on transitional stability .....	153
6.5	Discussion .....	154
6.5.1	Loading phases vibrations impact on contractile properties ....	155
6.5.2	Whole body vertical-vibrations impacts on Dynamic Stabilities .....	157
6.6	Summary .....	160
<b>CHAPTER 7 EVALUATION OF GAIT TRANSITIONAL STABILITY FOR RAMP ASCEND AND DESCEND WALKS.....</b>		<b>161</b>
7.1	Introduction.....	161
7.2	Hypothesis.....	161
7.3	Methods.....	162

7.3.1	Experimental Protocol .....	162
7.3.2	Data Collection .....	162
7.3.3	Data Processing .....	163
7.3.4	Time and Frequency domain Models .....	165
7.3.5	Nyquist and Bode stability methods .....	167
7.3.6	Lower limb joints angles and moments .....	168
7.3.7	Statistical Analysis.....	168
7.4	Results .....	168
7.4.1	Ramp Ascend activity.....	169
7.4.2	Ramp Descend activity .....	173
7.4.3	Variability in joints angles and moments .....	178
7.5	Discussion .....	181
7.5.1	Stability margins quantified using Neuromotor Outputs (CoP).....	181
7.5.2	Stability margins quantified using Neuromotor Inputs ( $a_{CoM-AP}$ ).....	182
7.5.3	Stability margins quantified using Neuromotor Inputs ( $a_{CoM-vertical}$ ) .....	186
7.6	Summary .....	194
<b>CHAPTER 8 SUMMARY, CONCLUSIONS AND FUTURE WORK .....</b>		<b>195</b>
8.1	Summary and Assessment of the Research Objectives.....	195
8.2	Relevance of Research .....	197
8.3	Conclusions .....	198
8.4	Limitations .....	203
8.5	Future Works.....	204
<b>REFERENCES .....</b>		<b>207</b>
<b>Appendix A: Literature Review Summary .....</b>		<b>220</b>
<b>Appendix B: Ethical Approval.....</b>		<b>229</b>
<b>Appendix C: Angles and Moments Ramp walk .....</b>		<b>230</b>
<b>Appendix D: Demographic data .....</b>		<b>236</b>
<b>Appendix E: Stability Margins .....</b>		<b>237</b>
<b>Appendix F: Efficiency of predictively .....</b>		<b>239</b>
<b>Appendix G: List of all Publications .....</b>		<b>240</b>
G.1 Publications from Thesis (I. Mahmood, main author) .....		240
G.2 Other Publications (I. Mahmood, co-author) .....		241

## LIST OF TABLES

Table 2.1: Gait cycle breakdown in phases and sub-phases and lower limb joints range of motions. summarised from [58].....	21
Table 2.2: Common Ankle-foot related abnormalities [59-61]. .....	22
Table 2.3: Studies evaluated gait dynamic stability on inclined surface. ....	38
Table 2.4: Studies evaluated lower limb contractile dynamics using Bode plot and system identification methods.....	40
Table 2.5: Comparison between gait dynamic stability assessment techniques. .	41
Table 3.1: Imitated ankle-foot impairments using healthy subjects. ....	45
Table 3.2: Common ankle-foot forward and rotational impairments. ....	46
Table 3.3: Specifications of adjustable dynamic response (ADR) AFO joint. ....	47
Table 3.4: Orthoses restrictions applied to imitate ankle-foot impairments. ....	49
Table 3.5: Level walk lower limb joints angles and moments mean (standard deviation) data for forward and rotational impairments and walking speed group. ....	58
Table 3.6: Spatiotemporal parameters mean (standard deviation) data for forward and rotational ankle-foot impairments for a level walk. ....	60
Table 3.7: Evaluation of lower limb angles and moments from studies included Charcot-marie tooth patients.....	62
Table 3.8: PCA applications relevant to current study for waveform reduction and/or linearity analysis. ....	66
Table 3.9: Examples of Transfer functions minimum phase (MP) versus non-minimum phase (NMP).....	71
Table 3.10: Nyquist and/or Bode methods in lower limb biomechanics modelling and stability analysis. ....	75
Table 3.11: Trials for walking speed effect on gait transitional stability.....	78
Table 3.12: Statistically comparative walking conditions. ....	79
Table 4.1: Quantified and compared stability margins for loading phases of AFO restricted conditions. ....	92
Table 4.2: Quantified and comparison of stability margins for unloading phases of AFO restricted conditions.....	92
Table 4.3: Spearman correlation coefficients illustrate intralimb interaction between loading and unloading phases of AFO restrictions.....	93
Table 4.4: Quantified and compared Stability margins for loading phases of rotational foot impairments.....	93
Table 4.5: Spearman correlation illustrate intralimb interaction between loading and unloading phases of rotational impairments and walking speed groups.....	94
Table 4.6: Quantified and compared stability margins for unloading phases of rotational foot impairments.....	94

Table 4.7: Quantified and compared stability margins for loading phases of level walk at self-selected walking speeds.....	95
Table 4.8: Quantified and compared stability margins for unloading phases of level walk at self-selected walking speeds.....	95
Table 4.9: Comparison of margin of stability for forward ankle-foot impairments applying extrapolated-CoM method. ....	98
Table 4.10: Comparison of margins of stability for self-selected walking speeds applying extrapolated-CoM method. ....	98
Table 4.11: Comparison of margins of stability for rotational impairments applying extrapolated-CoM method. ....	99
Table 4.12: Controller design outcomes.....	101
Table 4.13: Summary of discussion regarding first hypothesis. ....	107
Table 4.14: Summary of discussion regarding second hypothesis.....	107
Table 5.1: Stability margins (mean± Std.), variances, and coefficient of determinant quantified for loading phases of AFO restricted conditions. ....	120
Table 5.2: Stability margins (mean± Std.), variances, and models coefficient of determinant quantified for loading phases of rotational foot restrictions. ....	121
Table 5.3: Stability margins (mean± Std.), variances, and models coefficient of determination quantified for loading phases of self-selected walking speeds. ....	122
Table 5.4: Stability margins (mean± Std.), variances, and models coefficient of determination quantified for unloading phases of AFO restricted conditions. ....	123
Table 5.5: Stability margins (mean± Std.), variances, and models coefficient of determination quantified for unloading phases of rotational foot restrictions. ....	124
Table 5.6: Stability margins (mean± Std.), variances, and models coefficient of determination quantified for unloading phases of self-selected walking speeds. ....	124
Table 5.7: Spearman’s correlation between normal walk and AFO restricted conditions, rotational restrictions and walking speed groups. ....	125
Table 5.8: Controller design for unstable CoM-oscillations models.....	129
Table 5.9: Summary of discussion and hypothesis outcomes.....	136
Table 6.1: The AFO restrictions and their operating ranges. ....	140
Table 6.2: Contractile properties of walking conditions during loading phases. ....	148
Table 6.3: Stability margins for loading phases of AFO restricted walking conditions. ....	149
Table 6.4: Stability margins for unloading phases of AFO restricted walking condition.....	150
Table 6.5: Stability margins for loading phases of walking speed group. ....	151
Table 6.6: Stability margins for unloading phases of walking speed group. ....	151

Table 6.7: Comparison of contractile properties using SMD models and empirical CoM-vibrations models for different walking speeds.....	156
Table 6.8: Summary of discussion regarding second hypothesis. ....	159
Table 7.1: Loading phases stability margins quantified using anterior-posterior CoP-velocity. ....	169
Table 7.2: Unloading phases stability margins quantified using anterior-posterior CoP-velocity. ....	170
Table 7.3: Loading phases stability margins quantified using anterior-posterior CoM-vibrations. ....	171
Table 7.4: Unloading phases stability margins quantified using anterior-posterior CoM-vibrations. ....	171
Table 7.5: Loading phases stability margins quantified in vertical direction. ...	172
Table 7.6: Unloading phases stability margins quantified in vertical direction. ....	172
Table 7.7: Contractile properties quantified using vertical CoM-vibrations. ....	173
Table 7.8: Loading phases stability margins quantified using CoP-velocity.....	174
Table 7.9: Unloading phases stability margins quantified using CoP-velocity. ....	174
Table 7.10: Loading phases stability margins quantified using anterior-posterior CoM-vibrations. ....	175
Table 7.11: Unloading phases stability margins quantified using anterior-posterior CoM-vibrations. ....	176
Table 7.12: Loading phases stability margins quantified using vertical CoM-vibrations.....	177
Table 7.13: Unloading phases stability margins quantified using vertical CoM-vibrations.....	177
Table 7.14: Contractile properties quantified using vertical CoM-vibrations. ...	178
Table 7.15: Lower limb joints angles (ROMs) and peak moments (mean $\pm$ Std.) for Ramp Ascend activity. ....	179
Table 7.16: Lower limb joints angles (ROMs) and peak moments (mean $\pm$ Std.) for Ramp Descend activity.....	180
Table 7.17: First hypothesis concluded based on output stability margins evaluated for ramp ascend activity.....	183
Table 7.18: First hypothesis concluded based on output stability margins quantified for ramp descend activity.....	184
Table 7.19: First hypothesis concluded based on input (AP) stability margins quantified for ramp ascend activity.....	187
Table 7.20: First hypothesis concluded based on input (AP) stability margins quantified for ramp descend activity.....	188
Table 7.21: First hypothesis concluded based on input (vertical) stability margins quantified for ramp ascend activity.....	191

Table 7.22: First hypothesis concluded based on input (vertical) stability margins quantified for ramp descend activity.....	192
Table 7.23: Second hypothesis concluded based on contractile properties evaluated for ramp ascend and descend activities.....	193
Table 8.1: Overall Stability Margins and Hypothesis evaluation for a Level ground Walk.....	199
Table 8.2: Overall Stability Margins and Hypothesis evaluation for Ramp Ascend (A) and Descend (D) Walks.....	200
Table 8.3: Efficiency of stability evaluation for level walking conditions.....	203

## LIST OF FIGURES

Figure 1.1: Neuromotor balance control illustrating biomechanical signals. ....	5
Figure 1.2: Pilot study with respect to gait phases, application, and terrain conditions. ....	6
Figure 1.3: Thesis organization Flowchart. ....	7
Figure 2.1: Anatomy of lower limb illustrating segments and joints. adapted from [45] .....	11
Figure 2.2: Anatomical planes and axes of motion. Adapted and modified from [46] .....	12
Figure 2.3: Gait cycle breakdown. (a) Gait phases and sub-phases. adapted and modified from [47], (b) Spatial parameters of a Gait. adapted from [48]...	13
Figure 2.4: Lower limb joints angles and moments in Sagittal plane. (a) ankle joint angle, (b) ankle joint moment, (c) knee joint angle, (d) knee joint moment, (e) hip joint angle, (f) hip joint moment. ....	14
Figure 2.5: Ground reaction forces and center of pressure waveforms for stance phase. gait phases in (a) adapted [31], CoP foot path adapted [52].....	15
Figure 2.6: Neuromotor control loop. (a) Flow of sensory feedback between various modules – adapted from [54], (b) Closed loop integration of various modules – adapted from [55] .....	16
Figure 2.7: Lower limb muscles activation patterns illustrated for a level walk in forward direction. adapted from [33].....	17
Figure 2.8: Resemblance between muscle spindle instantaneous firing rate (IRF) musculotendon length and force in stretching. modified and adapted from [56] .....	18
Figure 2.9: Intralimb interaction illustrated in gait transitional phases. animation part of figure adapted from [58].....	19
Figure 2.10: Energy transformation in transitional phases. adapted and modified from [32] .....	20
Figure 2.11: Examples of static and dynamic base of support (BoS). adapted from [62] .....	23
Figure 2.12: Commercially available AFO. (a) AFO by BRACEABILITY for foot drop, (b) AFO by Ottobock for foot drop, (c) AFO by HEALIOS for foot drop , (d) AFO by ORTHOBMI for heel pressure off, (e) AFO brace walker, (f) PRAFO Kodel ankle support. adapted from [63-68] .....	24
Figure 2.13: Adjustable dynamic response lower limb orthoses. (a, b) AFO by Ultraflex systems, (c, d) AFO by Beckerorthopedic, (e, f) KAFO by Ultraflex systems, (g, h) KAFO by Beckerorthopedic. adapted from [19, 69] .....	25
Figure 2.14: Active orthoses illustrated for different actuation types. (a) Series elastic actuator (SEA) AFO, (b) Magneto-rheological fluid brakes AFO, (c) Pneumatic rotary actuator AFO, (d) Artificial pneumatic muscles AFO, (e) Shape memory alloy actuator based AFO. adapted from [70-74] .....	26

Figure 2.15: Equilibrium conditions in quiet stance. (a) disturbance effects in COM [75], (b) human body pendulum like rotational stability [77].....	27
Figure 2.16: Intraclass correlation coefficient evaluation. (a) time series data, (b) Expanded view line fitted for windows of 4 strides, (c) ICC evaluated from log-log curve. adapted from [10] .....	30
Figure 2.17: Lyapunov exponent stability evaluation method. (a) EMG time series, (b) State space constructed using four EMGs data, (c) expanded view of orthogonal section to the mean state space data, (d) Lyapunov exponent evaluated from averaged rate of divergence. adapted from [85].	31
Figure 2.18: Floquet exponent method illustrate Poincare section of the state space shown in Figure 2.14(b). adapted from [85] .....	32
Figure 2.19: Inverted pendulum model of lower limb. ....	33
Figure 2.20: Margin of stability (MoS) in AP direction with maximum BoS measure from toe of leading foot. adapted and modified [91].....	35
Figure 2.21: Postural control model and stability margins illustrated. (a) Balance control model of static posture with force perturbation and ankle angle [37], (b) Gain and phase margins computed from Bode plots [34]. ....	36
Figure 2.22: Natural frequency and damping ratio ( $\theta$ ) defined w.r.t pole location in Laplace plane. adapted from [101] .....	39
Figure 3.1: Assembling of an adjustable ankle-foot orthosis. (a) Simulation of medial and lateral components, (b) Physical assembly of AFO. ....	47
Figure 3.2: Wedged foot insoles design for rotational impairments. (a) wedged insoles, (b) foot rotational impairments adapted from [122]. ....	48
Figure 3.3: Reflective markers attached to the lower limbs.....	50
Figure 3.4: Motion capture system shown for level and inclined walks. ....	51
Figure 3.5: Model building in Visual3D software. (a) markers positions, (b) kinetic model, (c) kinematic model with virtual foot design. ....	53
Figure 3.6: Ankle, knee and hip joints angles (N=11 subjects) for forward AFO restricted impairments during a level walk. ....	54
Figure 3.7: Ankle, knee and hip joints angles (N=11 subjects) for rotational impairments and walking speed group during a level walk.....	55
Figure 3.8: Ankle, knee and hip joints moments (N=11 subjects) for forward AFO restricted impairments during a level walk. ....	56
Figure 3.9: Ankle, knee and hip joints moments (N=11 subjects) for rotational impairments and walking speed group during a level walk.....	57
Figure 3.10: Ankle foot angle (N=11 subjects) in rotational (ML) direction. ....	58
Figure 3.11: Peak joints angles and moments comparison between AFO imitations and CMT patients data. ....	63
Figure 3.12: Rate of change in CoP and GRFs illustrate impulsive responses (N=11 subjects). ....	64
Figure 3.13: Hierarchical approach of empirical modelling, applied to the CoM-vibrations data from imitated walking conditions.....	68



Figure 3.14: Lower limb modelled using plant outputs responses and unit impulse inputs.....	69
Figure 3.15: Stable and unstable equilibrium conditions.....	74
Figure 3.16: Mathematical interpretation of critical point of instability (-1, 0j)..	74
Figure 3.17 Stance phase of a gait cycle divided into sub-phases. adopted from [58].....	76
Figure 3.18 Gait dynamic stability assessment methods categorised based on discrete and continuous time series input waveforms.....	77
Figure 3.19: Hierarchical layout of biomechanical data collection. ....	80
Figure 4.1: Neuromuscular control loop shown with restricted ankle-foot motions. The neuromotor responds to the imbalances in body's CoM with resultant effect measured from CoP trajectory. Wearable orthoses used to restrict ankle-foot motion in the forward and lateral directions. The CoP trajectories showing greater variations during loading (L) and unloading (U) phases. ....	82
Figure 4.2: Ankle-foot impairments imitated using wearable orthoses. (a) AFO and wedged insoles are illustrated, (b) Experimental trials recorded in motion capture lab.....	83
Figure 4.3: The CoP-velocity (actual and averaged) impulsive responses for loading and unloading phases, each present ~20% of stance. ....	83
Figure 4.4: The residual analysis performed for optimum cut-off frequency selection. (a) normal/preferred speed walk, (b) with dorsiflexion ROM restriction 'DRR'. ....	85
Figure 4.5: The averaged CoP-velocity impulsive responses filtered (1 <sup>st</sup> order, 30Hz) and unfiltered waveforms. (a) Loading phase data, (b) unloading phase data from normal speed trials.....	85
Figure 4.6: The CoP-velocity impulses as linear combination of PCA models after removing artefacts and reducing the dimension. (a) Loading phase data, (b) Unloading phase data from normal walk trials.....	86
Figure 4.7: The pole-zero map of frequency models (11 subjects) in the s-plane. (a) Loading phase with poles on the left half show stable and minimal phase system, (b) Unloading phase with poles on the right half of s-plane show unstable and non-minimum phase system. ....	88
Figure 4.8: Nyquist plots loading phases of normal walk trials (11 subjects). ....	88
Figure 4.9: Bode plots for loading phases of normal walk trials (11 subjects)....	89
Figure 4.10: Nyquist plots loading phase AFO conditions, stability margins calculated w.r.t unity circle passing through point (-1, 0). Loading phases transfer functions cut unit circle (1 <sup>st</sup> zoom) at points (2 <sup>nd</sup> zoom) and differences of these points from (-1,0) give stability margin.....	90
Figure 4.11: Nyquist plots for AFO restricted conditions, stability margins calculated w.r.t unity circle passing through point (-1, 0). Unloading phases transfer function plots and stability margins computed from (-1,0). ....	91

Figure 4.12: Comparison of stability margins for forward direction ankle-foot impairments (mean 95% of CI), ‘★’ presents significant difference with normal walk, ‘■’ present significant difference with AFO free-mode walk. (a) Phase margins during loading phases, (b) Gain margins during unloading phases, (c) Phase margins during unloading phases. .... 96

Figure 4.13: Comparison of stability margins for rotational restrictions and walking speed groups (mean 95% of CI). ‘★’ present significant difference with normal walk. (a) Phase margins during loading phases, (b) Gain margins during unloading phases, (c) Phase margins during unloading phases. .... 97

Figure 4.14 Effect of body mass index (BMI) on gait transitional stability. BMI categorised into subgroups i.e. low (21.1±1.9), Medium (25.22±0.6), High (27.85±0.35), stability margins shown for (a) loading phase, (b) unloading phase..... 100

Figure 4.15 Controller design to stabilize the unstable gait phases. .... 101

Figure 4.16 Stability trends with effect of walking speeds. .... 102

Figure 5.1: Neural postural control loop showing the sensory feedback provided to the brain by proprioception, hear, and sight senses and an error signal generated in brain used to reweight muscles activation to provide stabilizing toques to the lower limb joints. The resultant imbalances measured from body CoM-vibrations in the direction of motion. .... 111

Figure 5.2: (a) The impact forces illustrate maximum magnitudes and oscillatory response during heel impact and relatively low magnitude oscillations during unloading phases. (b) The RMS value showing the power density spectrum of CoM-vibrations. .... 112

Figure 5.3: Residual analysis to estimate the cut-off frequency of filtering, performed using CoM-vibrations data from unrestricted normal walk. ... 113

Figure 5.4: Principal component analysis illustrate the resultant waveforms for AFO restricted conditions, waveforms plotted with 90±1% variance explained by PC1. For conditions with low values the PC2 was also plotted..... 114

Figure 5.5: Principal component analysis illustrate the resultant waveforms for rotational restrictions and walking speed groups, and waveforms plotted with 90±1% variance explained by PC1. For conditions with lower values the PC2 also plotted. .... 115

Figure 5.6: Various empirical linear models simulated for loading phases CoM-vibrations, the best fit model selected based on coefficient of determinant ( $R^2$ ) and root mean square error (RMSE). .... 116

Figure 5.7: Equivalent transfer functions illustrated for the polynomial and sinusoidal models. .... 117

Figure 5.8: Pole-zeros map showed for both loading and unloading transfer functions (TFs) using unrestricted normal walk trials. .... 117

Figure 5.9: Bode plots examples illustrated for the loading and unloading phases transfer functions using normal walk mean trials (S: subjects). The critical stability margins quantified for: (a) minimum phase margins at 0dB gain crossover frequencies, (b) minimum gain margins at $\pm 180^\circ \pm 2k\pi$ phase crossover frequencies. ....	118
Figure 5.10: Flow diagram illustrating the comparison between stability outcomes quantified by applying different methods. ....	119
Figure 5.11: Stability margins comparison for loading phases of AFO restricted conditions using Bar plot (mean $\pm$ 95 CI), ‘★’ illustrate significant difference with a normal walk, ‘■’ illustrate significant difference with a AFO free-mode walk. ....	121
Figure 5.12: Stability margins comparison for loading phases of rotational impairments and walking speed groups using Bar plots (mean $\pm$ 95 CI), ‘★’ illustrate significant difference w.r.t a normal walk. ....	122
Figure 5.13: Stability margins comparison for unloading phases of AFO restricted conditions using Bar plot (mean $\pm$ 95 CI), ‘★’ illustrate significant difference with a normal walk, ‘■’ illustrate significant difference with a AFO free-mode walk. ....	123
Figure 5.14: Stability margins comparison for unloading phases of rotational impairments and walking speed groups using Bar plots (mean $\pm$ 95 CI), ‘★’ illustrate significant difference w.r.t a normal walk. ....	124
Figure 5.15: Stability margins quantified from input CoM-vibrations TFs compared with outcomes from respective output CoP-velocity TFs. (a) Loading phases phase margins, (b) Unloading phases gain margins, (c) Unloading phases phase margins. ....	127
Figure 5.16 Effect of body mass index (BMI) on gait transitional stability. BMI categorised into subgroups i.e. low ( $21.1 \pm 1.9$ ), Medium ( $25.22 \pm 0.6$ ), High ( $27.85 \pm 0.35$ ), stability margins shown for (a) loading phase, (b) unloading phase. ....	128
Figure 5.17 Walking speed effect on transitional stability. (a, b) Loading Phases, (c, d) Unloading Phases. ....	130
Figure 6.1: (a) Experimental trials recorded in motion lab wearing Ankle-foot orthosis. Restrictions applied for dorsiflexion and/or plantarflexion ankle motions, (b) interlimb joints coordination and resultant reponses measured using CoP (output) and GRF (CoM input). ....	140
Figure 6.2: The rate of change in CoM-acceleration showing the oscillatory response. (a) actual CoM-oscillations, (b) RMS CoM-oscillations. ....	141
Figure 6.3: Residual analysis method applied to select cut-off frequency. ....	142
Figure 6.4: CoM-oscillations illustrated for walking conditions with ankle-foot orthosis. AFO free-mode walk: (a) loading phase, (b) unloading phase; (c) dorsi-plantarflexion ROM restrictions: (c) loading phase, (d) unloading phase; dorsi-plantarflexion resistive torques: (e) loading phase, (f) unloading phase; dorsiflexion ROM restriction: (g) loading phase, (h) unloading phase; dorsiflexion resistive torque: (i) loading phase, (j) unloading phase. ....	143

Figure 6.5: CoM-oscillations (vibrations) illustrated for walking speed group. Slow speed walk: (a) loading phase, (b) unloading phase; Normal speed walk: (c) loading phase, (d) unloading phase; Fast speed walk: (e) loading phase, (f) unloading phase..... 144

Figure 6.6: Linear regression model fitted to CoM-vibrations (oscillations) data for normal walking trials. (a) Loading phase, (b) Unloading phase. .... 145

Figure 6.7: Pole-zero map illustrated for Loading phases transfer functions, the poles lie on imaginary axis showing the unstable, undamped system and zeros on right half showing the non-minimal phase system. .... 146

Figure 6.8: Bode plots of loading phases showing the gain margins, phase margins, and respective cut-off frequencies for normal speed walking trials..... 146

Figure 6.9: Bode plots of unloading phases showing the gain margins, phase margins, and respective cut-off frequencies for normal speed walking trials..... 147

Figure 6.10 Effect of body mass index (BMI) on gait transitional stability. BMI categorised into subgroups i.e. low ( $21.1\pm 1.9$ ), Medium ( $25.22\pm 0.6$ ), High ( $27.85\pm 0.35$ ), stability margins shown for (a) loading phase, (b) unloading phase..... 152

Figure 6.11 Stable output response for unstable loading phase plant model. .... 153

Figure 6.12 Stable output response for unstable unloading phase plant model. 153

Figure 6.13 Walking speed effect on transitional stability. (a, b) Loading Phases, (c, d) Unloading Phases..... 154

Figure 7.1: Input, output neuromechanical responses and interlimb joints coordination illustrated for a balance control..... 162

Figure 7.2: Experimental data collection for imitated ankle-foot impairments in motion capture lab..... 163

Figure 7.3: Walking activities, gait transient phases, ankle-foot impairments and measurement signals hierarchy. .... 163

Figure 7.4: Mean CoP-velocity and RMS CoM-vibrations raw data illustrate the impulsive responses during stance phase transitions. .... 164

Figure 7.5: Residual analysis method applied to select cut-off frequencies for three measurements signals..... 165

Figure 7.6: PCA reconstructed waveforms illustrated using normal walk trials for a ramp ascend activity. .... 166

Figure 7.7: Pole-zero map illustrating the stability of modelled I/O's TFs for normal walk data. .... 167

Figure 7.8: Comparison of anterior-posterior stability margins quantified from CoM-vibrations (input) and CoP-velocity (output) for a ramp ascend and descend walks..... 189

Figure 8.1: Mean Stability margins quantified from neuromotor outputs (CoP). .... 201

Figure 8.2: Mean Instability margins quantified from <i>forward</i> CoM-acceleration (somatosensory Input).....	201
Figure 8.3: Mean Instability margins quantified from <i>vertical</i> CoM-acceleration (somatosensory Input).....	202
Figure 8.4: Applications of current study for Neuromotor balance control evaluation during gait transitional phases. images adapted from [189-194] .....	206

## ABBREVIATIONS

<b>3D</b>	three dimensions
<b>%</b>	percentage
<b>A</b>	ascend
<b>ACL</b>	anterior cruciate ligament
<b>ADF</b>	activities of daily living
<b>ADR</b>	adjustable response devices
<b>AFO</b>	ankle-foot orthosis
<b>AFJ</b>	ankle-foot joint
<b>AP</b>	anterior-posterior
<b>BoS</b>	base of support
<b>Bn</b>	billion
<b>CI</b>	confidence interval
<b>CMT</b>	Charcot-Marie-Tooth
<b>CoM</b>	centre of mass
<b>CoP</b>	centre of pressure
<b>D</b>	descend
<b>dB</b>	decibel (unit for gain)
<b>deg</b>	degree
<b>DOF</b>	degree of freedom
<b>DPRT</b>	dorsi-plantarflexion resistive torques
<b>DRT</b>	dorsiflexion resistive torque
<b>DPRR</b>	dorsi-plantarflexion range-of-motion restriction
<b>DRR</b>	dorsiflexion range-of-motion restriction
<b>E</b>	elderly
<b>EMG</b>	electromyography
<b>FD</b>	foot drop
<b>FDP</b>	foot drop and plantarflexion
<b>FM</b>	Floquet Multiplier

<b>GM(s)</b>	gain margin(s)
<b>GRF</b>	ground reaction force
<b>H</b>	healthy
<b>HC</b>	heel contact
<b>I</b>	impaired
<b>ICC</b>	intraclass correlation coefficient
<b>IMU</b>	inertial measurement unit
<b>IP</b>	inverted pendulum
<b>I/O</b>	input or output
<b>IRF</b>	instantaneous firing rate
<b>KE</b>	kinetic energy
<b>L</b>	loading
<b>LDS</b>	local dynamic stability
<b>LTI</b>	linear time-invariant
<b>ML</b>	medial-lateral
<b>MOCAP</b>	motion capture
<b>MoS</b>	Margin of stability
<b>MP</b>	Minimum phase
<b>MR</b>	magnetorheological
<b>N&amp;B</b>	Nyquist and Bode
<b>NMP</b>	non-minimum phase
<b>PCA</b>	principal component analysis
<b>PC</b>	principal component
<b>PC1</b>	first principal component
<b>PM(s)</b>	phase margin(s)
<b>PE</b>	potential energy
<b>RMS</b>	root mean square
<b>RMSE</b>	root mean square error
<b>ROM(s)</b>	range of motion(s)

<b>R<sup>2</sup></b>	coefficient of determinant
<b>SEA</b>	series elastic actuator
<b>SIT</b>	system identification toolbox
<b>SMD</b>	spring mass damper
<b>Std.</b>	standard deviation
<b>TF</b>	transfer function
<b>TO</b>	toe-off
<b>U</b>	unloading
<b>UK</b>	United Kingdom
<b>USA</b>	United States of America
<b>w.r.t</b>	with respect to
<b>XCoM</b>	extrapolated centre of mass
<b>Y</b>	young



## LIST OF PUBLICATIONS RELATED TO THIS RESEARCH

Following peer review conference papers are published. These methods and analysis are related to Chapters 3-6 of the current thesis.

1. I. Mahmood, U. Martinez-Hernandez, and A. A. Dehghani-Sanij, "Rate-Dependant Gait Dynamic Stability Analysis for Motor Control Estimation," in *Advances in Cooperative Robotics*, ed: WORLD SCIENTIFIC, 2016, pp. 454-463. DOI: <https://doi.org/10.1142/10261>
2. I. Mahmood, U. Martinez-Hernandez, and A. A. Dehghani-Sanij, "Gait dynamic stability analysis and motor control prediction for varying terrain conditions," in *IEEE Mechatronics (MECHATRONICS)/17th International Conference on Research and Education in Mechatronics (REM)*, 2016 11th France-Japan & 9th Europe-Asia Congress on, 2016, pp. 290-295. DOI: 10.1109/MECATRONICS.2016.7547157
3. Mahmood I., Martinez-Hernandez U., Dehghani-Sanij A.A. (2017) Towards Behavioral Based Sensorimotor Controller Design for Wearable Soft Exoskeletal Applications. In: Ibáñez J., González-Vargas J., Azorín J., Akay M., Pons J. (eds) *Converging Clinical and Engineering Research on Neurorehabilitation II. Biosystems & Biorobotics*, vol 15. Springer, Cham. DOI: [https://doi.org/10.1007/978-3-319-46669-9\\_209](https://doi.org/10.1007/978-3-319-46669-9_209)
4. I. Mahmood, U. Martinez Hernandez, and A. A. Dehghani-Sanij, "Gait Dynamic Stability Analysis for simulated Ankle-foot impairments and Bipedal robotics applications," presented at the 6th Mechatronics Forum International Conference, 2018.

Following Journal papers are submitted (1 and 2) or planned to be submitted (3) including level ground walk stability evaluations in Chapters 3-6 of current thesis:

1. Mahmood, U. Martinez Hernandez, and A. A. Dehghani-Sanij, "Evaluation of Neuromotor Balance Control during Gait Transitional Phases," *ASME Journal of Biomechanical Engineering*. (Under review, 2019)
2. Mahmood, U. Martinez Hernandez, and A. A. Dehghani-Sanij, "Evaluation of Neuromotor Balance Control during Gait Transitional Phases with Rotational ankle-foot Impairments," *Human Movement Science*. Elsevier. (Under review, 2019)
3. Mahmood, U. Martinez Hernandez, and A. A. Dehghani-Sanij, "Wearable orthosis impacts on vertical dynamics of lower limbs during weight loading and unloading gait transitions," *Journal of Biomechanics*. Elsevier. (submitted, 2019)

The outcomes from Chapter 7 (Ramp Ascend Descend walk) are planned to be published accordingly.

# CHAPTER 1

## INTRODUCTION

### 1.1 Background

Mobility plays an important role in one's life considering the independence of life and freedom of performing activities of daily living (ADL). Considering human locomotion, walking over varying terrains such as level ground, ramp or stairs ascend/descend are everyday experiences of people either inside the home or outside to access a building, footpath, parks, public transport etc. That is the resultant of a complex but well-synchronised coordination between various lower limb joints, bones, muscles, and sensory systems. The complexity of bipedal motion becomes significant when there is a deficiency in gait leading to poor balance control and high metabolic cost. A walking disability may be resulted from one or more joints failure (ankle, knee, and hip) and caused by various factors like spinal cord injury, central nervous system dysfunction, stroke, heart attack, sports injuries, and accidents. The problem domain becomes severe considering the age factor, degree of impairment, and cause of injury.

Locomotory disabilities are continuously increasing worldwide with a growing population and enhancing the health care cost as well. Considering national (UK) statistics, 6.5 million people suffer through mobility deficiency, 6 million people have a lift and carrying problem, and 2.4 million have a lack of coordination [1]. The NHS bears the falling cost of £2Bn, skin pressure cure of £2.1Bn, and in total, the cost for stroke and social services until the patient's health ranged to £9.8Bn [1]. In literature, motor disorder and ageing are reported as major causes of poor balance control and accountable for risk of fall particularly in elderly [2]. Considering USA statistics, every year, 2.8 million elderly people are treated with fall injuries and one out of five falls causes a serious injury such as broken bones or head injury. The medical costs for fall injuries were reported over \$50Bn in the USA in 2015 [3]. In Australia, fall is reported as a major health issue in 30% of the elderly population (3 million in 2010) and 40% of fall injuries are reported as fatal. With that incident rate, the cost related to fall injuries is expected to increase to \$1.4Bn by 2051 [4]. A study [5] shows about 75% of people with incomplete spine cord injury are deficient in dynamic balance and falls every year. Fall is reported to be a leading cause of dominant injuries or accidental deaths in the older age [6].

These statistics and costs of treatment brought researchers attention to evaluate gait stabilities periodically with growing age to diagnose balancing issues and suggest

preventive measures clinically and technologically. Clinical stability assessments are analytical and relied on physical observations, questioner, and scaling methods [7-9] without any sophisticated instruments involved. In research methods [10, 11], walking stabilities are assessed using high tech equipment (motion capture system, Tekscan force measurement soles, IMU sensors etc.), resultant measurement signals are extracted from body limbs, and numerical algorithms are applied to provide precise stability quantification. Despite a great deal of research being conducted on human balance control, the research-based methods are lacked to be applied in clinical environments. This is because of varying outcomes reported, lack of distinct criteria and hence qualitative data.

In biomechanics, a walking activity is studied in periods named gait cycle (e.g. heel to heel foot contact). A gait cycle is further divided into events and phases. The research methods quantified human stability either in static condition with/without external perturbations or while performing dynamic activities. In a dynamic gait, studies used lower limb signals either for the whole gait cycle [6] or evaluated at discrete events [10]. The methods applied to the whole gait cycle require a bunch of time series data to be precise and predict outcomes in a unit-less factor. The normal range of this factor is quantified from healthy subjects and used to define a stable/unstable walk. In discrete events based stability evaluation [12], the limits of lower limb movements (angular or linear) are quantified from healthy individuals and with respect to these limits any testing subjects are compared. Most of the earlier studies evaluated elderly and/or healthy subjects by applying these methods for a level ground walk. More recently, two studies from the same author also reported stabilities on inclined surfaces, among these, a first study [13] evaluated healthy subjects, and second [14] evaluated both healthy and elderly. In the published literature, there is no study found that has evaluated stability for a deficient or impaired gait on inclined surfaces.

Clinically, a range of wearable orthoses or exoskeletons is recommended for assistance or rehabilitation [15]. There are intensive researches ongoing to make these devices adaptable, lightweight, and stronger. Most of the commercially available orthoses/exoskeletons [16-19] are made of metallic structures attached to the body rigidly for efficient power transmission. Earlier studies reported that the impact forces generated due to inertial changes at lower extremity transmitted from ankle to head [20], affected whole body center of mass (CoM) and hence somatosensory feedback [21, 22], and considered as one of the major reasons for worsening the lower limb joints diseases and neuromuscular injuries [23]. On the other end, an optimum range of impact forces is also essential as somatosensory feedback to the neuromotor for appropriate muscles activation and balance control [24-26]. To the author's

knowledge, these impact forces effects on gait dynamic stabilities are not investigated before in viewpoint of the wearable orthosis.

## 1.2 Motivation

Considering increasing patients with stability issues, cost of treatment, and a gap between advanced research methods and clinical stability assessments, there is a need of more robust techniques, with clearly defined stability criteria that can provide a qualitative database to be compared with abnormalities. Including the lower limbs motion, more specifically, the end effector is ankle-foot joint (AFJ). It transfers the two-thirds of body weight lying at two-thirds of body height while maintaining body stability like an inverted pendulum [27]. The AFJ motion is complex by the fact that it requires maximum power, involves more phases, and greater variation in the range of motion necessary for forwarding and upward body propulsion. Successful negotiation between body weight transfer and the ground contact is performed by the ankle-foot joint, hence, it is vital in a bipedal walk. The stability issues resulted from ankle-foot joint impairments are the main theme of the current study.

Research methods applied so far reported varying stability outcomes. Among the most dependable dynamic stability assessments, studies applied local dynamic stability method and reported the age-related difference between young and elderly with diversified outcomes [6]. In another widely used method, margins of stability (MoS) are quantified as body's extrapolated-CoM (XCoM) difference from its base of support (BoS). In this method, stability criteria are reported in either way i.e. increased XCoM movement w.r.t BoS implies more stability as well in some cases declared as an indication of poor balance control [28]. Both of these two popular research methods have standardising issues, that included a lack of distinct reference to define and quantify stability or instability, instead, these methods reported various ranges in different studies [6, 28, 29]. Further, almost all prior research-based methods quantify gait dynamic stability either using whole gait cycle waveforms or at discrete gait events and lacked to quantify inner gait phases. In particular, transitional phases (double limb support) are critical considering dynamic gait stability during which body weight is transferred from one limb (accelerate) to other (decelerate) [30, 31], energies are transformed from max kinetic to max potential [32], neuromotor program is modulated [2], and leg muscles are maximally activated [33]. More specifically, these gait phases have been remained unquantified mainly due to methodological limitations. In short, the confusion in stability evaluation criteria and inadequacy of transitional phases make the differential diagnostic challenging with these methods.

In comparison, however, recent studies [34-36] introduced control engineering methods to assess gait dynamic stability. In these studies, Nyquist and Bode methods

are applied successfully to distinguish patients with knee deficiencies and healthy subjects. These studies quantified knee joint stability using knee angular trajectories for whole/initial stance. These methods involved a mathematical model of a system to be evaluated and reported with distinct cut-off thresholds to quantify stability/instability. Another prior study [37] also applied these methods for robustness assessment in static postural control in the presence of external perturbations. In that study, the shank angle is modelled with impulsive force input perturbations and reported a decrease in postural robustness in elderly compared with young subjects. Also, previously, these methods are widely applied for plant control e.g. electric motor control in medical/industrial robots, however, their application in gait stability assessments is relatively new with the benefit of distinct criteria.

Another encounter in gait stability assessment is the use of appropriate signals. For example, in local dynamic stability methods, large datasets are applied using either combination of kinematic variables (mostly five reported) collected from various body segments (foot, ankle, shank, knee, thigh, hip, trunk, pelvis, EMGs) [6, 10, 11]. The margin of stability method evaluates body's XCoM and BoS difference, whereas BoS boundaries are quantified from either foot centre of pressure (CoP) [29, 38] or heel [28] or toe [39, 40] positions. In neuromotor balance control (Figure 1.1), the sensory information is reported to be estimated from body's CoM rather local joint variables, and more recent studies reported that CoM-acceleration is used to scale magnitude and timing of initial burst in the muscle [41, 42]. Further, the path of the foot CoP provides resultant information where all the reaction forces are concentrated [43]. The CoM-acceleration [2, 9] or rate of change in CoP [31, 43, 44] has been widely applied earlier to quantify gait stabilities, however, the supportive analysis techniques limited their scope for assessment of transitional phases stabilities. In conclusion, an assessment technique that uses resultant biomechanical stability measures (CoP, CoM, or their derivatives), apply distinct criteria, evaluate gait transitional phases, and applicable for varying terrains with/without impairments can accomplish above-highlighted limitations in existing approaches and potentially suitable for clinical applications. For example, the applications included transitional stability evaluation during weight loading and unloading phases before and after a therapeutic procedure, to distinguish normal versus impaired gait, and the impact of wearable assistive devices.

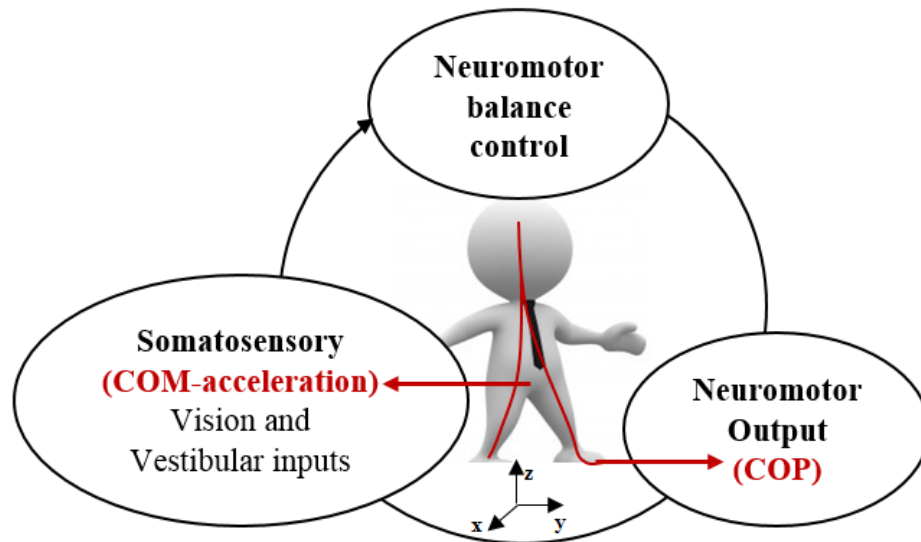


Figure 1.1: Neuromotor balance control illustrating biomechanical signals.

## 1.3 Aims and Objectives

### 1.3.1 Aims

The aims of the current study are:

- To introduce gait dynamic stability assessment *methods* with distinct criteria and using net neuromotor balance control signals;
- To evaluate *gait transitional stabilities* with ankle-foot joint impairments and/or with the effect of the wearable orthosis.

### 1.3.2 Objectives

The following objectives are defined in this research to achieve the above aims:

- To extract appropriate biomechanical signals that can be used to evaluate transitional phases gait stabilities.
- To establish supporting analytical techniques to these signals with clear fixed thresholds to determine stable or unstable gait.
- To evaluate gait transitional stabilities for varying terrains i.e. level, ramp ascends and descend ADLs.
- To evaluate somatosensory neuromotor feedbacks (impact forces) effects on gait stability in healthy and impaired gait, and varying terrains.
- To evaluate lower limb contractile properties with/without the effect of ankle-foot orthosis and adjustments made to clinically prescribed ranges.
- To provide a qualitative database for clinical applications with the effect of healthy and uniform ankle-foot impairments.

## 1.4 Scope of this Research

This research introduces control engineering theory in gait dynamic stability evaluation during weight loading and unloading phases in both healthy and imitated ankle-foot impairments. The distinct criteria, redundancy in measurements using resultant biomechanical signals, easy computation, and uniform database make these methods potentially applicable in the clinical environment. The prospective applications of current research are:

- To evaluate lower limb joints (ankle, knee, hip) or segments (shank, thigh, pelvis, trunk, tendon, muscles) impairments effect on walking stabilities.
- To evaluate wearable devices, orthoses, foot pads, prostheses, exoskeletons, and walking surfaces impact on gait dynamic stabilities.

## 1.5 Contributions of this research

This research contributes to the biomedical engineering field with an evaluation of patients having stability issues, estimation of the effect of assistive devices, and rehabilitation effectiveness for short or long recoveries. The implementation of Nyquist and Bode (N&B) methods for stability evaluation during gait transitional phases, with ankle-foot joint deficiencies, and for a level/ramp walk presents this study as a preliminary work as illustrated in Figure 1.2.

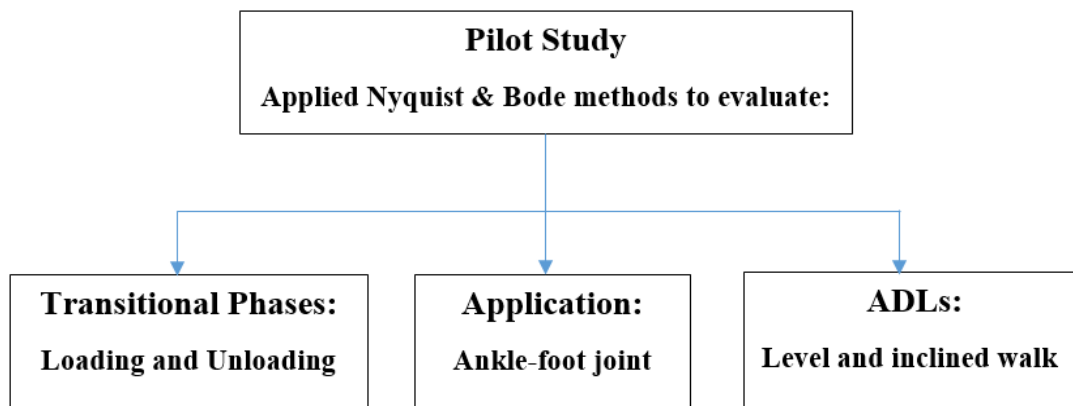


**Figure 1.2: Pilot study with respect to gait phases, application, and terrain conditions.**

Parts of this thesis are published in peer-reviewed conferences and submitted as journal papers as listed in Appendix G. Contributions of the current research study are summarised here:

1. An adjustable ankle-foot orthosis (AFO) and wedged foot insoles are designed to imitate uniform degree of ankle-foot impairments, the resultant lower limb joints range of motion are validated with earlier forward and rotational ankle-



foot patients data. Furthermore, preferred walking speed trials are also conducted to be compared with deficient ankle-foot motions.

2. Balance control resultant signals (i.e. CoP, CoM-accelerations) modelled in time and frequency domains using system identification approach.
3. Introduced and defined Nyquist and Bode methods to analyse neuromotor control signals and quantified stability margins.
4. Evaluated vertical and forward CoM-oscillations (shocks) impact on gait dynamic stability and limb contractile (attenuation) properties.
5. Intralimb correlations are defined between opposite limb loading and unloading phases using neuromotor time domain responses quantified by CoP-velocity.
6. Along with the level walk, transitional phases stability margins are evaluated on an inclined pathway ( $\pm 5^\circ$ , up/down) with healthy subjects and imitated impairments.

## 1.6 Organization of the Thesis

The thesis is organised into eight chapters. The block diagram in Figure 1.3 illustrates workflow in the chapters, and thereafter, the outline of each chapter is summarised.

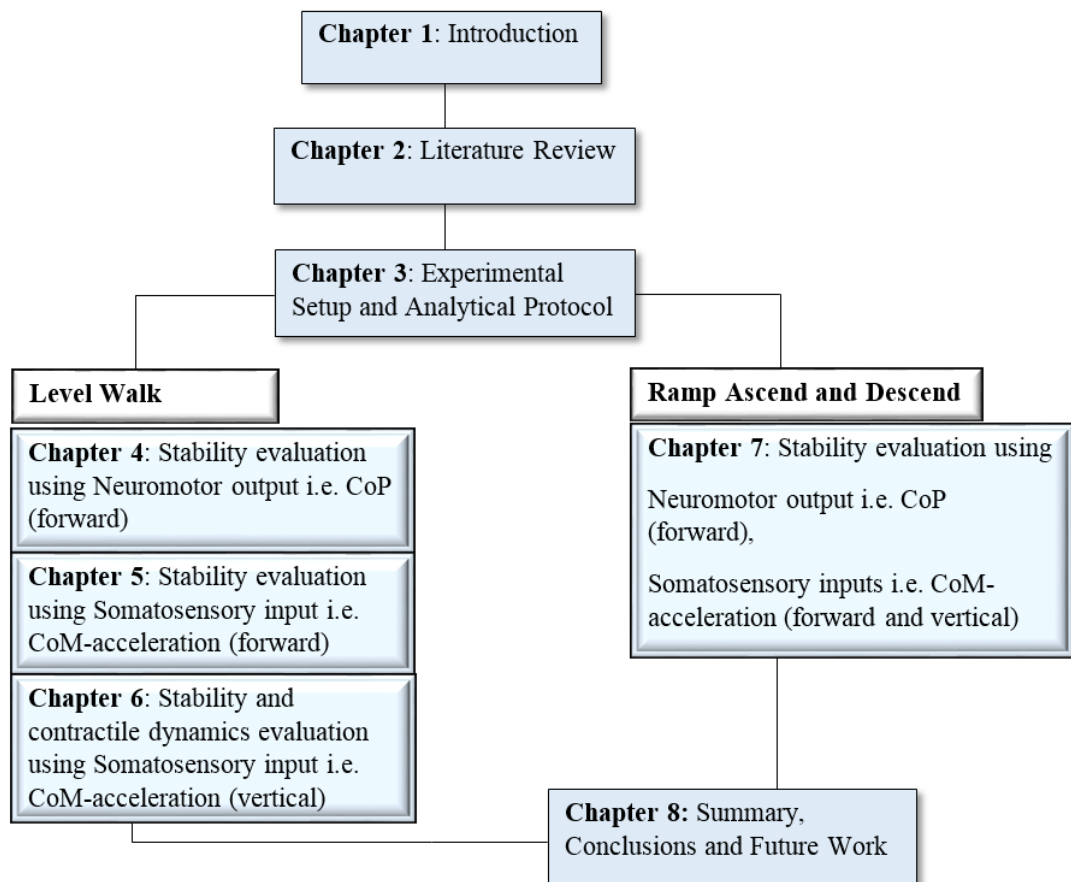


Figure 1.3: Thesis organization Flowchart.

**Chapter 1** introduces the background, motivation, aims and objects to evaluate gait dynamic stabilities during transitional phases with/without ankle-foot impairments in adults. Furthermore, the scope and contributions of current research are described in this chapter.

**Chapter 2** presents a literature review in support of the biomechanics of walking stability. Initially, lower limb joints, range of motions, gait cycle, and neural control are described. Then, the role of the ankle-foot joint in maintaining walking stability is discussed along with associated ankle-foot abnormalities. After that basic theory of postural control is described and static and dynamic balance are differentiated. All prior, gait dynamic stability assessment methods are discussed with merits and demerits. Lastly, gaps of knowledge are described with methodological, performance, and applications perspectives.

**Chapter 3** consists of two parts, the first part highlights the differential diagnosis issue with varying degree of ankle-foot impairments in group-based studies and elucidated by an imitation approach. Wearable orthoses are designed to restrict ankle-foot motions in forwarding and rotational directions, and trials were conducted using a motion capture system, force platforms, and eleven healthy subjects. Lower limbs joints angles and moments are evaluated in Visual3D motion analysis software and validated with tracteries from actual patients data. In the second part, balance control related biomechanical signals are sorted and analysis tools are established including linearity testing, time and frequency models, and N&B stability methods.

**Chapter 4** presents gait transitional stabilities applying N&B methods and using rate of change in CoP for ten walking conditions grouped into forward (5 conditions), rotational impairments (2) and walking speeds (3). The stability margins (N&B) were compared statistically within each group, with extrapolated-CoM method, and with discrete points variability in joints angles and moments. The stabilities were evaluated in both anterior-posterior (forward) and medial-lateral directions. Further, the intralimb interaction was quantified between opposite limbs loading and unloading phases from time series CoP-velocity waveforms.

**Chapter 5** presents gait transitional stabilities applying N&B methods and using the rate of change in CoM-acceleration in forwarding direction for ten (healthy and impaired) walking conditions. Different linear models were applied using a system identification approach. The results were compared statistically within each group and with PCA variability in CoM-acceleration waveforms, discrete parametric variability, and correlation methods. Also, a comparison was made between stability margins quantified from somatosensory inputs modelled in this chapter and neuromotor outputs in Chapter 4 for respective walking conditions.

**Chapter 6** presents contractile properties of lower limbs and gait transitional stabilities using rate of change in CoM-acceleration (impact forces) in the vertical direction. The N&B methods were implemented for forwarding impairments and preferred walking speed groups. Stability margins were explained by variability in joints angles and moments. The contractile dynamics were quantified for the body's impact loading and also compared with earlier spring-mass-damper model based outcomes.

**Chapter 7** presents gait transitional stabilities and contractile properties for a slope ascend/descend walk applying N&B methods and using the rate of change in CoP and CoM-acceleration signals. The results were compared statistically within each group and with parametric variability method. Further, the stability margins quantified from CoP and CoM-acceleration were compared in forwarding direction as neuromotor O/Is.

**Chapter 8** describes the summary of work done in current research, the contributions and conclusions drawn, limitations, and implications of this pilot study as a part of future work.

## **CHAPTER 2**

### **LITERATURE REVIEW**

#### **2.1 Introduction**

This chapter mainly consists of three sections covering lower limb biomechanics, ankle-foot joint impairments and supportive devices, and gait dynamic stability assessment techniques. In the first section, lower limbs anatomy, planes of movements, joints kinematic and kinetic waveforms and nomenclature are discussed. A detailed breakdown of the gait cycle and the neuromotor control loop is described for gait sub-phases. In the second section, ankle-foot deficiencies and stability issues are defined along with existing research approaches proposed to overcome them. In relation to that, different assistive ankle-foot orthoses are discussed with their performance and limitations. In the third section, the gait dynamic stability assessments are mainly the focus with respect to ankle-foot impairments and/or impacts of wearable devices. Different previously published stability assessment methods are discussed with merits and demerits. Lower limb contractual properties and dynamic stability assessments for varying terrains are reviewed in the ending sections. Finally, the gaps of knowledge are discussed with the requirements of new stability measures.

#### **2.2 Lower limbs Biomechanics**

##### **2.2.1 Basic Anatomy**

In biomechanics, a lower limb skeleton is mainly described by segments and joints. The segments include the pelvis, thigh, shank, and foot parts as shown in Figure 2.1. The relative movements between two consecutive segments are defined by joints e.g. ankle joint (between foot and shank), knee joint (between shank and thigh) and hip joint (between thigh and pelvis). A movement in the limb skeleton is actuated by a parallel neuromuscular system consisting of muscles, tendons, ligaments and nerves. The nerves provide inner/outer sensory information e.g. walking environment, joints relative positions, muscles activity. Resultant moments are generated by each muscle group belonging to each joint to execute dynamic motions. Both the skeleton and muscular system work together to perform an efficient walk.

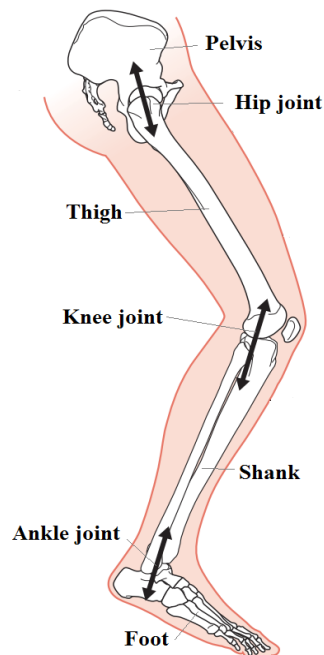


**Figure 2.1: Anatomy of lower limb illustrating segments and joints. adapted from [45]**

### 2.2.2 Planes and axes of movements

Lower limb joints exhibit rotational and transitional motions. Using a state space, these motions are presented in three dimensions (3D i.e. x, y, z) and each pair of these axes define a plane. Considering human biomechanics, a segment or joint movements are divided into three planes named sagittal, frontal, and transverse planes as illustrated in Figure 2.2. In an upright stand still posture, a plane dividing front and back sides are called coronal/frontal plane, and perpendicular to that, a plane dividing right and left is called sagittal/median plane, and perpendicular to both of the defined planes, a plane dividing the body into top and bottom halves is called transverse plane. Similarly, each plane divides the body movements in opposite axes ( $\pm$ ). Sagittal plane describes body motions in anterior (front) and posterior (back) axes, a frontal plane describes in medial (inward) and lateral (outward) axes and transverse plane divides body movements in superior (top) and inferior (bottom) axes. Likewise, the joints rotations are defined w.r.t to planes and axes. For example, the ankle joint rotation in the sagittal plane is called dorsiflexion/plantarflexion (flexion/extension) and in a frontal plane named as eversion/inversion (abduction/adduction). Similarly, the flexion/extension and abduction/adduction movements are defined for knee and hip joints.

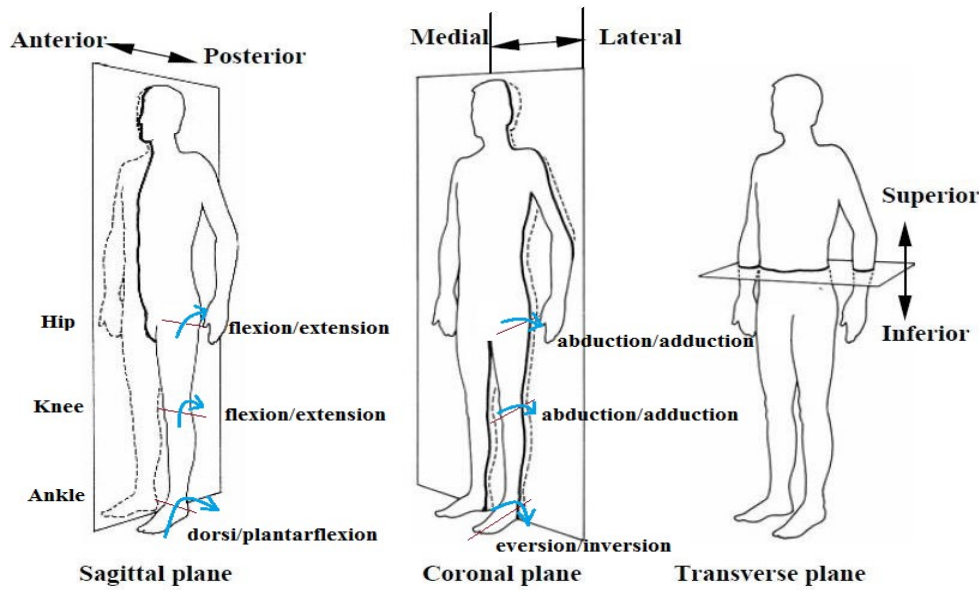


**Figure 2.2: Anatomical planes and axes of motion. Adapted and modified from [46]**

### 2.2.3 Gait cycle

During a level walk, lower limb joints and segments illustrate periodically repeated motions and a unit cycle of that repetitive motion is called gait cycle or stride. A gait cycle presents the interval between one heel contact (HC) to next HC of the same limb or from one toe-off (TO) to the next TO as shown in Figure 2.3(a). A gait cycle consists of two main phases i.e. stance phase for which foot remains in contact with the ground and swing phases during which foot remains in the air. Conventionally, a stance phase is measured as first ~60% of a gait cycle starting from HC, and the swing phase is presented as next ~40% of a gait cycle ending at next HC. A stance phase is further divided into sub-phases such as loading phase, mid-stance, terminal stance, push-off phase. Similarly, a swing phase is divided into initial swing, mid swing, and terminal swing phases. Further, in a gait cycle, discrete events are also defined and each presents a single instant of time in a gait cycle such as heel contact, toe off, foot flat, heel-off etc. These events are particularly important to distinguish the start and end of a gait cycle. All lower limb kinematic and kinetic waveforms are described for one gait cycle and all wearable supportive devices are designed and controlled based on detecting gait sub-phases and events.

In addition to that, a gait cycle is also divided w.r.t single and double limb support phases, and both phases are repeated twice in a gait cycle alternatively. Starting from HC of a stance phase, during first double limb support, one limb executes weight loading and opposite limb undergoes weight unloading in parallel and vice versa during second double limb support phase that ends at TO. The loading and unloading phases define gait transitional phases during which stance to swing and swing to

stance transitions take place in opposite limbs. Historically, time and distance parameters are evaluated between events and phases also called spatiotemporal parameters. In biomechanics, these parameters are evaluated (Figure 2.3b) w.r.t right and/or left foot and nomenclated as step length/time, stride length/time, walking velocity, stance time, swing time, single limb support time, and double limb support time.

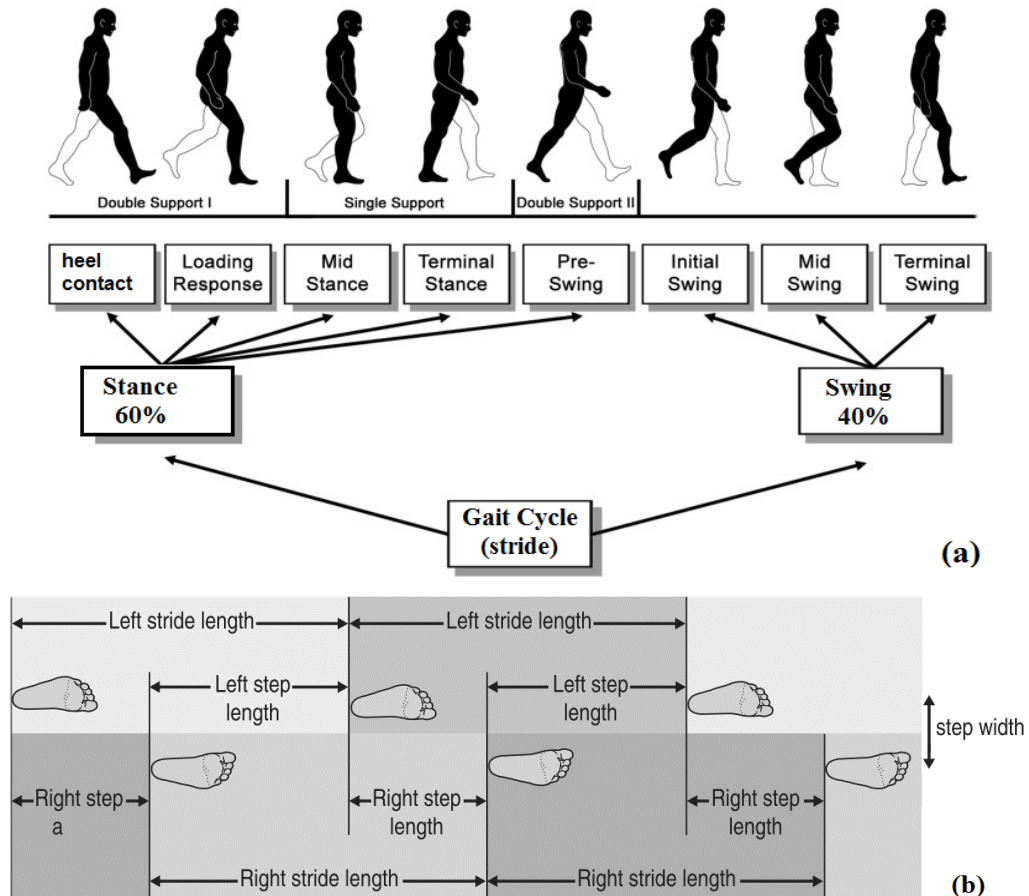


**Figure 2.3: Gait cycle breakdown. (a) Gait phases and sub-phases. adapted and modified from [47], (b) Spatial parameters of a Gait. adapted from [48]**

### 2.2.4 Lower limb joints kinematics and kinetics

In biomechanics research, gait performance is evaluated using joints kinematic and kinetic trajectories. These include 3D waveforms of angles, moments, ground reaction forces, and muscles activities. Lower limb joints have their maximum movements in a sagittal plane and conventionally this plane is used for evaluating differential outcomes such as between healthy and impaired subjects. Almost all wearable orthoses are designed to support sagittal plane motions. In the frontal plane, the joints rotations (abduction/adduction) are significantly small and rarely analysed. Similarly, ground reaction forces (GRF) have maximum magnitudes in vertical (gravitational) direction and relatively small magnitudes in anterior-posterior (AP) and medial-lateral (ML) directions. The AP and ML GRFs are resultant of shear stresses generated

between foot and ground surface. With ankle as the centre point, the product of vertical GRF and ‘CoP in AP’ or ‘CoP in ML’ axes define ankle joint moments in AP and ML directions respectively. The lower limb joints angles and moments are plotted in Figure 2.4 (level ground walk).

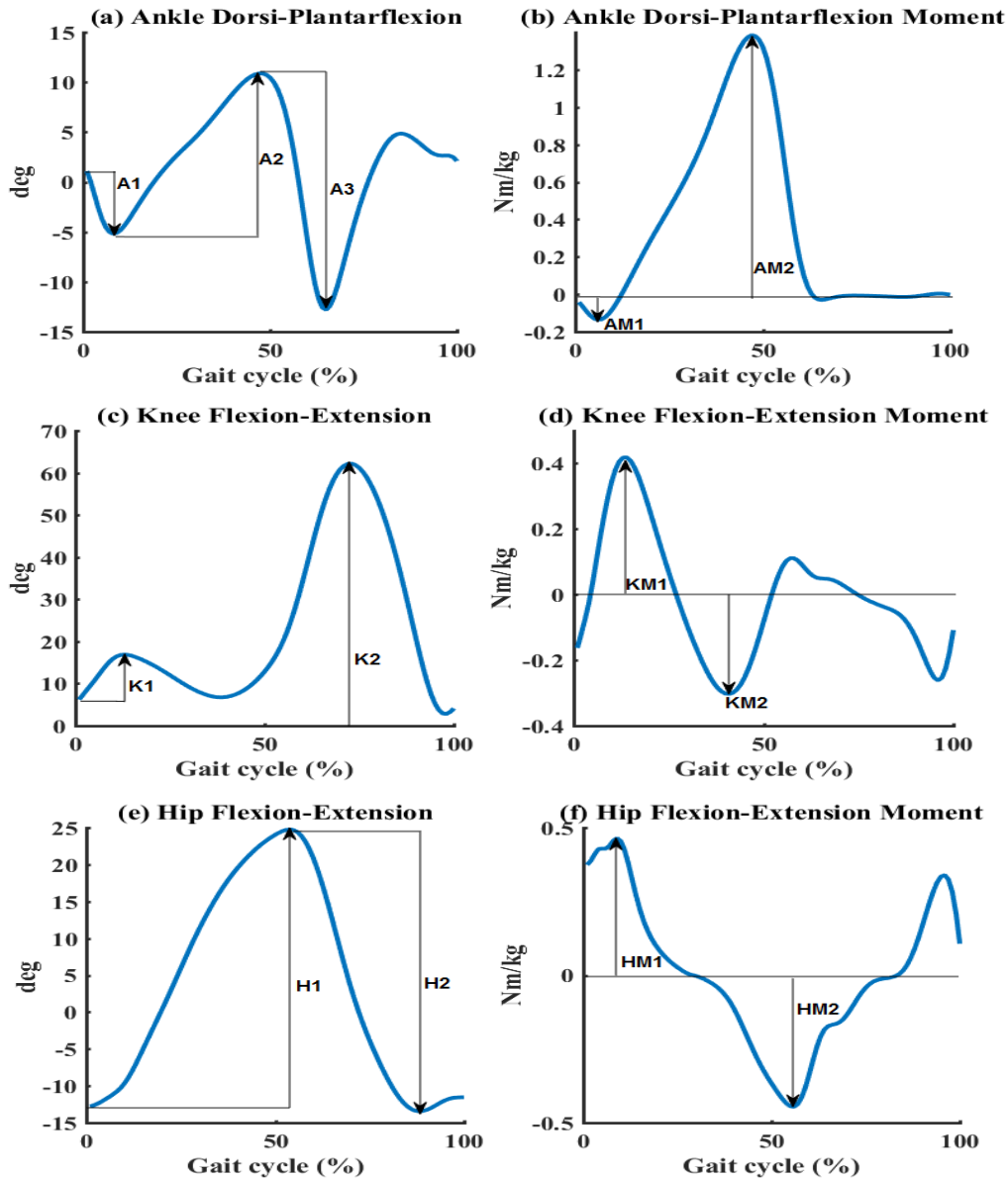


**Figure 2.4: Lower limb joints angles and moments in the Sagittal plane. (a) ankle joint angle, (b) ankle joint moment, (c) knee joint angle, (d) knee joint moment, (e) hip joint angle, (f) hip joint moment.**

Abbreviations in Figure 2.4: Peak definitions adapted from [49, 50]. A1: initial plantarflexion angle, A2: peak dorsiflexion angle, A3: peak plantarflexion angle, AM1: peak plantarflexion moment, AM2: peak dorsiflexion moment, K1: peak knee flexion stance, K2: peak knee flexion swing, KM1: peak knee flexion moment, KM2: peak knee extension moment, H1: peak hip extension angle stance, H2: peak hip flexion angle swing, HM1: peak hip flexion moment, HM2: peak hip extension moment.



During the level walk, joints angles and moments continuously change w.r.t gait phases in order to adapt to walking surfaces. The resultant body movements are presented by the centre of mass (CoM) and centre of pressure (CoP) trajectories. Body's CoM is a 3D point and presents a weighted average of all body segments. The CoP presents a 2D point under the foot plantar where all resultant forces get balance. The CoP is the neuromuscular response to the imbalances taking place in CoM, however, CoP trajectory is independent of the CoM [51]. Both CoP and CoM linked together in the form of GRF vector such that the vector head presents CoM-acceleration (force/mass) and vector tail presents CoP displacement. While performing dynamic gait activities, body gained balance control by a complex interaction between inter/intra limbs joints. The individual limb contribution is quantifiable from CoP and CoM waveforms, that is why the rate of change in these signals is widely used to quantify gait dynamic stabilities. The GRF and CoP waveforms are illustrated in Figure 2.5.

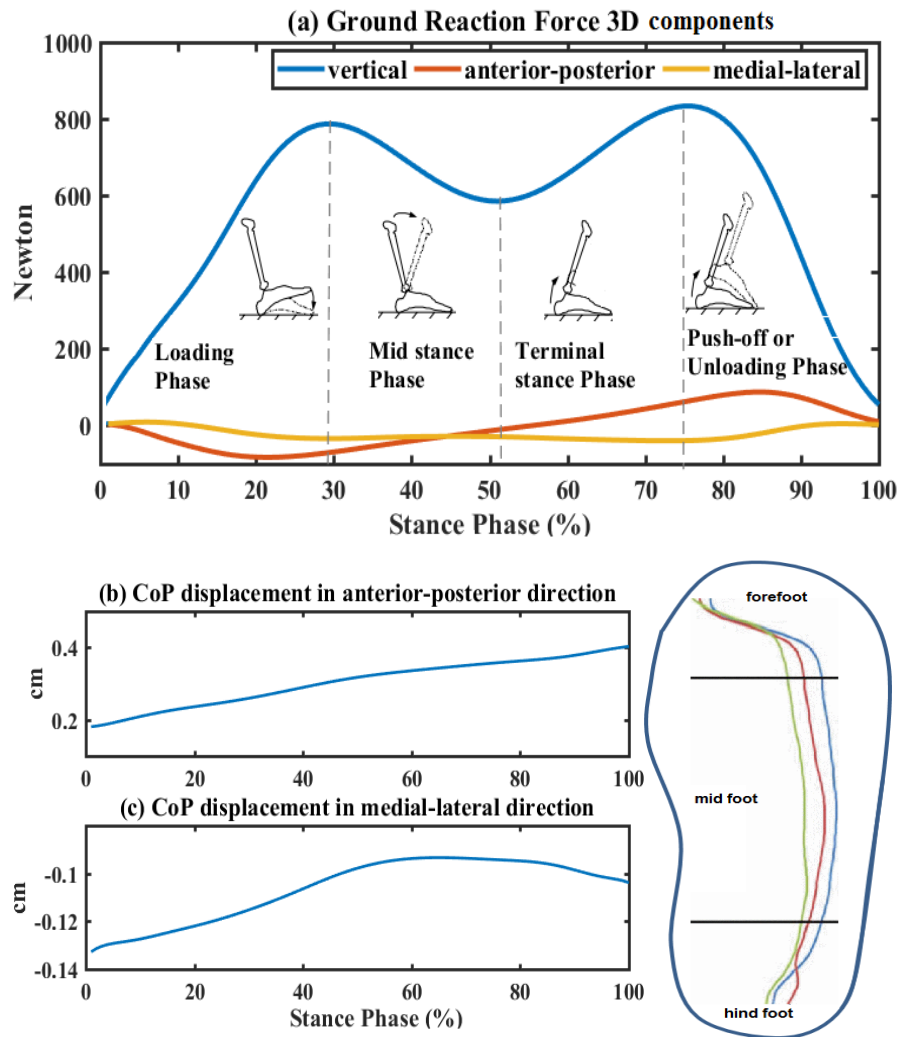
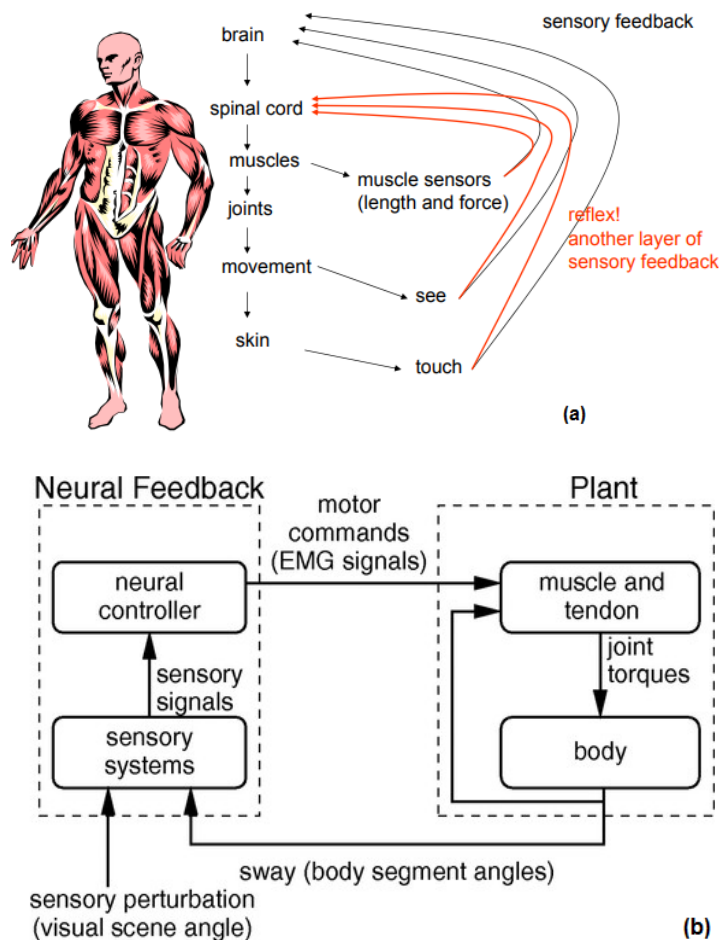


Figure 2.5: Ground reaction forces and centre of pressure waveforms for the stance phase. gait phases in (a) adapted [31], CoP foot path adapted [52]

### 2.2.5 Neural Control of Gait

In bipedal locomotion, neuromotor control provides forward progression and maintains stability. Lower limb neuromuscular system consists of a network of neuromotor, spine, muscles, tendons, ligaments and bones. These modules are integrated into a closed loop (Figure 2.6a) in which sensory organs, neuromotor, and muscles-bone act as a sensor, controller, and plant respectively (Figure 2.6b). The sensory information is received in neuromotor through proprioception (70%), vestibular (20%) and visual (10%) senses [53]. Each joint resultant moment presents net activity by a group of associated muscles. The muscles activity is measured by fibre length, area, and mass during its expansion and contraction. A neuromuscular chain in lower limbs is also used to damp impact forces by its contractual properties. Muscles work in groups for performing different functional tasks such as balance control, and each group is referred to as muscles synergies or modules. Each joint movement is supported by a module (a group of muscles).



**Figure 2.6: Neuromotor control loop. (a) Flow of sensory feedback between various modules – adapted from [54], (b) Closed loop integration of various modules – adapted from [55]**

While performing a dynamic gait activity, the mass and inertia of each body segment change continuously and the net effect is expressed by either CoM position, velocity, acceleration, and/or jerk data. The neural control responds to feedback from CoM and spine motor control pool of muscles with bursts of activity illustrated around heel contact and toe-off for a level walk [33]. These impulsive activation patterns of lower limb muscles are illustrated in Figure 2.7. Due to a complex interaction between inter/intralimb muscles, the net response of limb dynamics is frequently studied using resultant forces and moments [30].

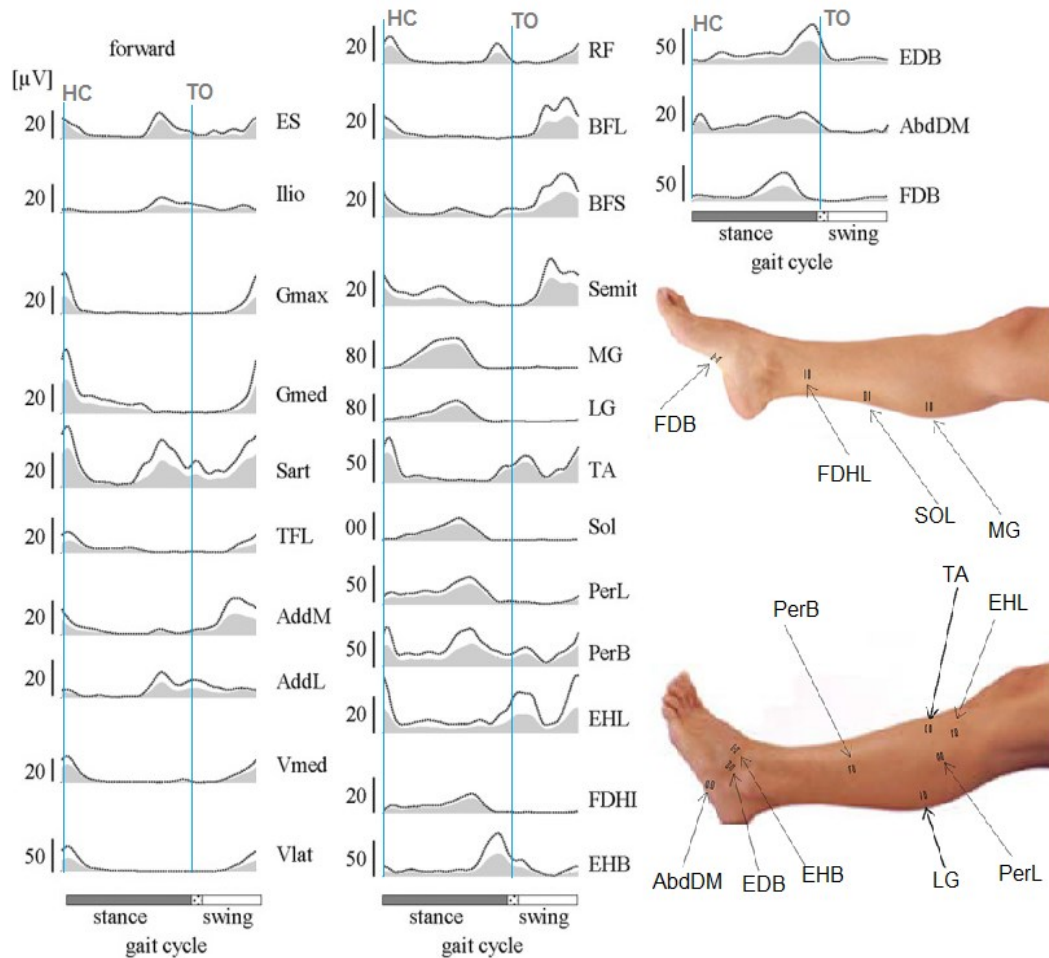


**Figure 2.7: Lower limb muscles activation patterns illustrated for a level walk in forwarding direction. adapted from [33]**

Recent studies [56] reported that the instantaneous firing rate of muscles stretch (lengthening) is closely associated with acceleration and rate of change in force produced in the muscles fibre in the presence of perturbations. The muscles lengthening is proportional to the force rate as illustrated in Figure 2.8 and these transient responses act as proprioceptive feedback in standing balance control. Another study [41] investigated muscles contributions in whole body CoM acceleration in during forwarding balance loss while stepping. The results illustrated that the lost balance is achieved through a complex interaction of lower limb muscles

in the forward direction such that Gastrocnemius and Hamstrings accelerate body's CoM throughout, and Soleus and Vasti muscles of stepping leg decelerate the CoM after heel contact. The Gastrocnemius and Soleus muscles are responsible for vertical CoM support.

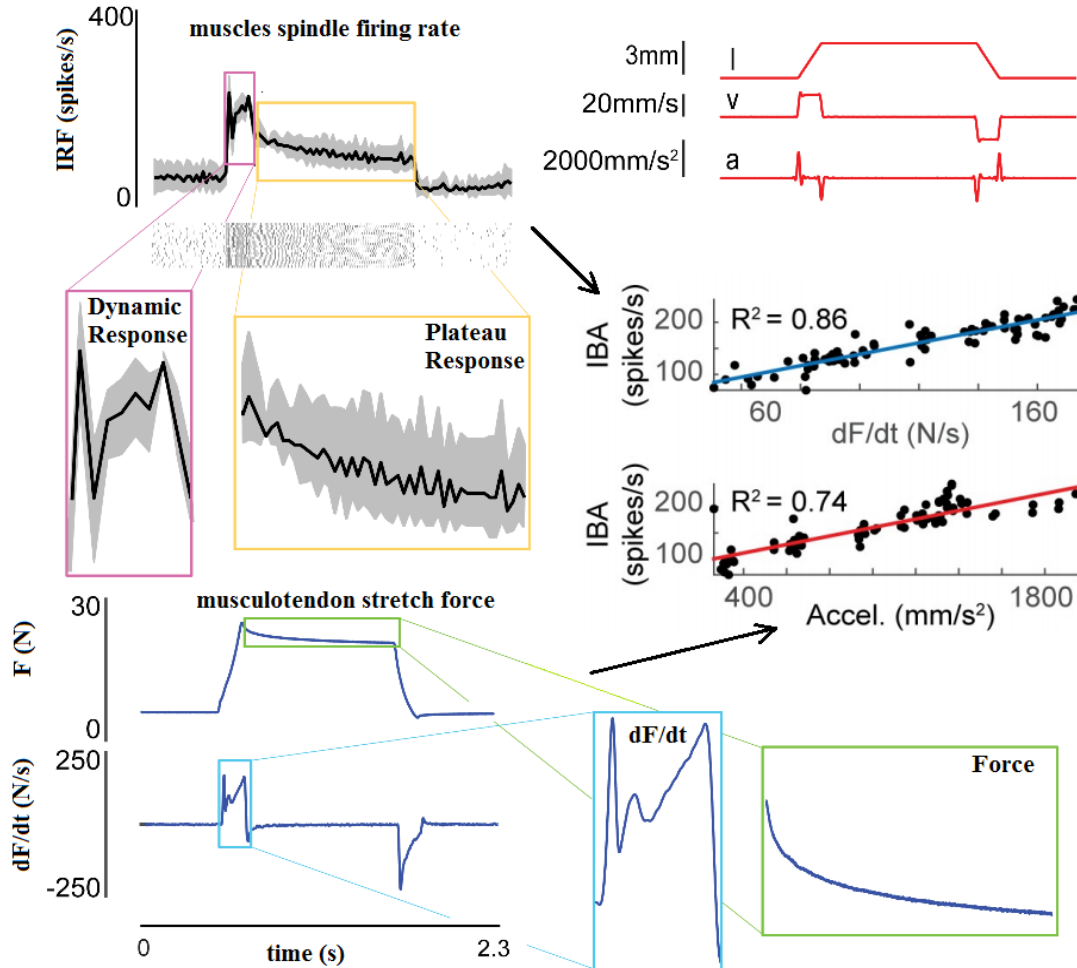


**Figure 2.8: Resemblance between muscle spindle instantaneous firing rate (IRF) musculotendon length and force in stretching. modified and adapted from [56]**

## 2.3 Walking Stabilities and Lower Limb Impairments

### 2.3.1 Ankle-foot joint as an end effector

In dynamic gait, the ankle joint is critical to maintain balance and generate forward propulsion simultaneously. Body's CoM moves like an inverted pendulum at almost two-thirds of body height and varied continuously by hip, knee, and ankle joints in a kinematic chain. The end-effector in this chain is ankle-foot which also defines the base of support in terms of area of foot contact with the ground. Among lower limb joints, ankle-foot generates maximum torque 172.5Nm and power 300watt, thresholds reported with a body weight of 75kg [57]. The ankle-foot joint works in two modes i.e. open kinematic chain when the foot is off the ground and close kinematic chain

where the foot is in contact with the ground. Close chain motion is complicated by the fact that GRF blocks the foot motion and shank moves relative to the fixed foot. However, to maintain the stability, other joints coordinate and compensate the motions especially in the case of the impaired ankle-foot joint.

All wearable devices are designed and controlled based on gait events and phases detections. These events or phases are mostly detected using kinematic or kinetic trajectories from shank/ankle/foot. Among these, the heel contact and toe-off events are of particular importance to distinct gait transitions from swing to stance and vice versa. The gait is divided into two main phases based on ankle joint functionality i.e. double limb and single limb support time. There are two double limb support periods in a gait cycle, in each, body weight is transferred from one limb to opposite named gait transitional phases. These included weight loading (~25-30% of stance from HC) and weight unloading phases (~25% of stance towards TO) [31] as illustrated in Figure 2.9 from vertical GRF signal. During these phases, body's CoM sways maximum from its base of support (BoS) and CoP works to keep CoM within BoS, these limits of movements are used to define gait stabilities [51].

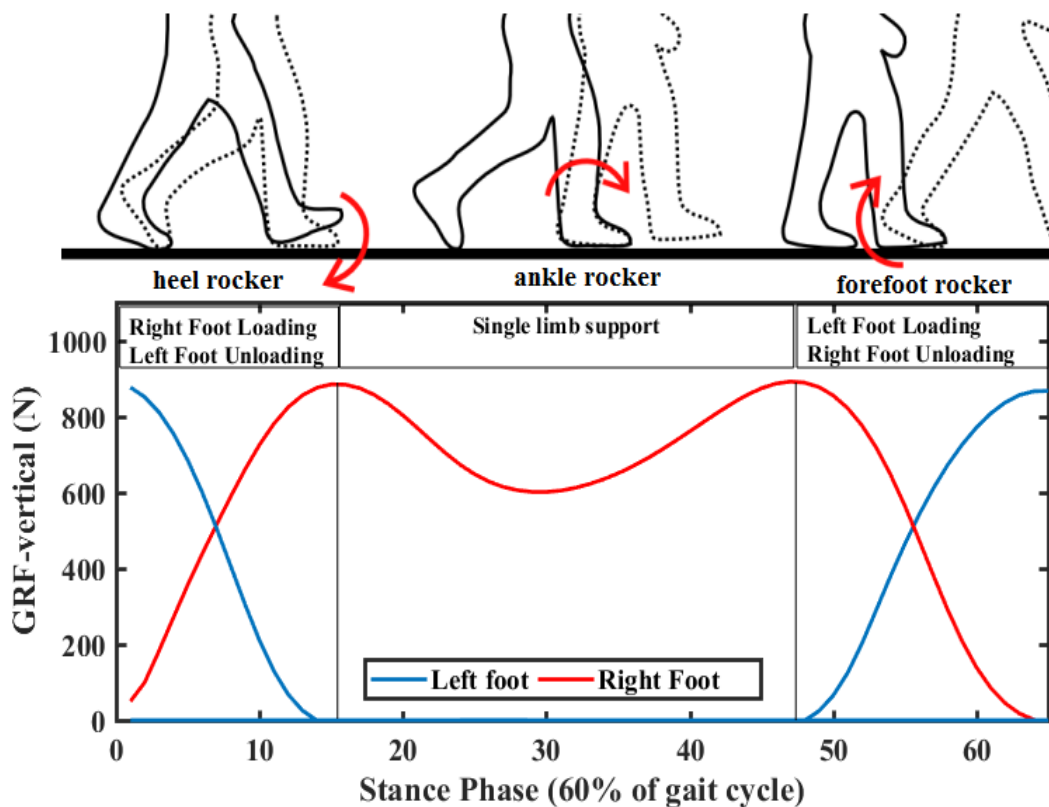


**Figure 2.9: Intralimb interaction illustrated in gait transitional phases. the animation part of figure adapted from [58]**

During the loading phase, heel acts as a rocker between heel contact to foot flat and breaking moment is generated by ankle plantarflexion muscles to deceleration the foot towards the ground. The shank-ankle-foot assembly acts as a linear spring and absorbs

impact energies generated maximally during the loading phase. During unloading phases, forefoot acts as a rocker between maximum dorsiflexion to toe-off and push-off moment generated by the ankle plantarflexion muscles. Maximum positive work is performed by the ankle joint in this phase and energies absorbed previously released along with propulsion to accelerate the limb forward. Considering energy spectrums, during single limb support potential energy (PE) is maximum and in double limb support kinetic energy (KE) is maximum. Gait KE is a function of the body's CoM-velocity. During loading and unloading phases, sharp transitions of KE to PE take place at different rates as illustrated in Figure 2.10. The KE raised up every time CoM raised from either of the limbs.

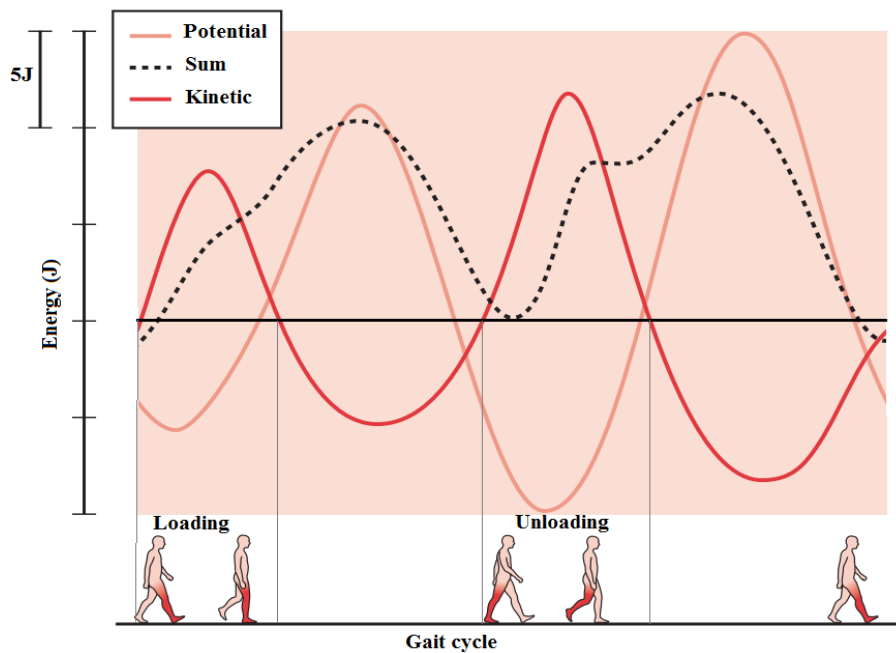


**Figure 2.10: Energy transformation in transitional phases. adapted and modified from [32]**

Summarising, the loading and unloading phases are critical toward dynamic balance control as illustrated by GRF, kinetic energy, and CoP waveforms, and muscles activation patterns during stance to swing and swing to stance phases transitions. The rate of change in kinetic parameters remains relatively steady during the single limb support phase. The kinematic ROMs for lower limb joints during loading and unloading phases are summarised in Table 2.1.

**Table 2.1: Gait cycle breakdown in phases and sub-phases and lower limb joints range of motions. summarised from [58]**

<b>Phases</b>	<b>Double limb support</b>				<b>Single limb support</b>			
<b>sub-phases</b>	<b>Weight Loading</b>		<b>Weight Unloading</b>		<b>Stance phase</b>		<b>Swing Phase</b>	
<b>Joint</b>	<b>Heel Contact</b>	<b>Foot flat</b>	<b>Terminal Stance</b>	<b>Toe-off</b>	<b>Initial Mid-stance</b>	<b>Late Mid-stance</b>	<b>Initial Swing</b>	<b>Terminal Swing</b>
Ankle	neutral	plantar flexes up to 10°	heel rise	max plantarflexion (20°)	slight plantarflexion	max dorsiflexion (10°)	max plantarflexion	neutral
Knee	knee extended	knee flexes 15°	full extension	flexes up to 40°	slight flexion	extended	maximum flexion (60°)	max extension (0°)
Hip	flexed up to 25°	stable 25° flexion	max extension (20°)	flexes to ~0° (neutral)	flexed, relative adduction	extended, relative adduction	flexion towards 25°, relative abduction	flexion, relative abduction
Pelvis	level	laterally drop to swing leg	anterior rotation and posterior depression	less anterior rotation, begin anterior elevation	towards stance leg	laterally drop to swing leg, medially rotated away from stance leg	laterally drop to swing leg, medially rotated to aligned with swing leg	

### 2.3.2 Ankle-foot Impairments and Wearable Orthosis

Ankle-foot joint (AFJ) as an end effector provides a supportive moment, dynamic stability, and absorbs impact loads. Since the ankle-foot joint is the prime focus of current research, it can be observed there are greater variations in kinetic data (moment, power) and less symmetrical kinematic (angles) waveforms comparative to other joints. That's why a small deficiency in the ankle-foot impact the overall gait performance significantly. The major reasons for AFJ disabilities include stroke, poor motor control, accidental or sports injuries, falling, nerve damage or weakness in the elderly. The AFJ impairments are summarised in Table 2.2.

**Table 2.2: Common Ankle-foot related abnormalities [59-61].**

<b>AFJ Diseases</b>	<b>Simple Meaning</b>	<b>Cause</b>	<b>Postural Effects</b>	<b>Statistics</b>
Charcot Marie Tooth	muscle weakness in the feet, ankles, legs	damage the peripheral nerves	weaken gait	25000 patients in the UK
Foot drop or steppage	foot lifting in swing and toe drag	muscular weakness	foot slap with ground	-
everted or inverted foot	fallen or high arches	abnormal bones/ joint pathology	pain in legs, ankle or foot	-
Cerebral palsy	muscle stiffness	neurological disorder	lack of coordination & movements	1 in 400 people in the UK
Multiple sclerosis	poor muscle movements	motor neuron degenerates,	difficult to balance and coordinate	100,000 patients in the UK
Polio	temporal or permanent paralysis	viral infection	shrinking of muscles	-
Hemiparesis	weakness of entire left/right side	brain injury/stroke	-	-
Parkinson Disease	involuntary shaking, physiotherapy reg.	brain disorder, nerve damage	poor stability, fear of fall	127,000 patients in the UK
Tendon injuries		temporary rupture	-	-



Fall is the most drastic outcome with lower limb impairments, especially in elderly people. Clinically, various supportive devices are prescribed to assist patients suffering from gait deficiencies. The simplest forms are crutches and walking frames with/without wheels. These non-wearable devices increase the base of support (BoS) (stability) and body's CoM remains within BoS most of the time in a gait cycle as illustrated in Figure 2.11. On the other end, wearable devices (orthoses) provide assistance directly to the affected joint and prescribed for long term usage. Most commercial lower limb orthoses are passive (without any electronic control) and the ongoing researches in this area are designing active/semi-active (electronics involved) devices. The active devices are more robust and adaptive with sensor, controller, and motor feedback control loop. However, the device interaction along with the user's own intent of motion makes the active orthoses design quite challenging. The devices weight and power supply also made active orthoses difficult to carry for a longer time span. Adjustable orthoses are designed and provided to the patients based on prescriptions from orthopaedic specialists.

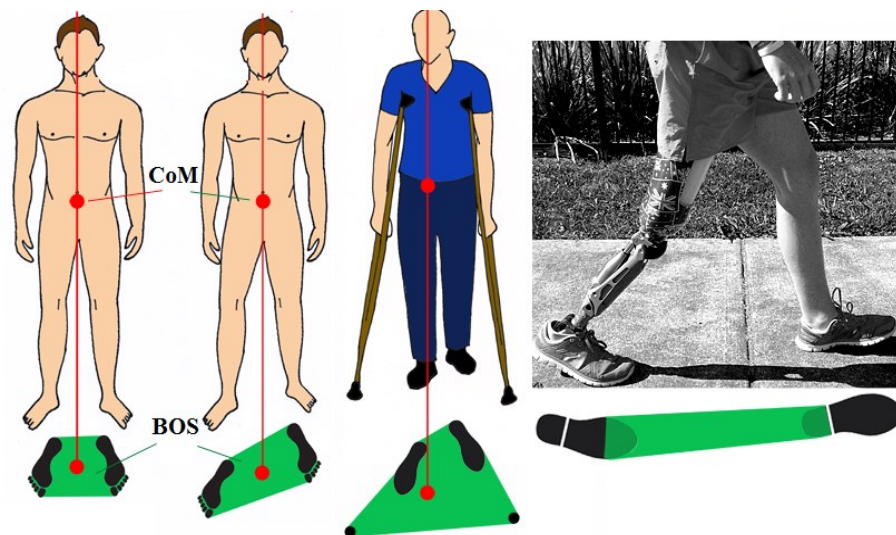


**Figure 2.11: Examples of the static and dynamic base of support (BoS). adapted from [62]**

Portable active/semiactive orthoses are not yet commercially available, however, active orthoses are widely used for rehabilitation purposes (e.g. physiotherapy) under the observation of experts. Both active and passive types of orthoses are designed to provide joint moments (accelerating or decelerating) and/or restrict the angular range of motion within limits as per the requirement of each gait phase. In research studies, the performance of these devices is mostly examined using the moment and angular trajectories from lower limb joints and rarely investigated with dynamic stability point of view. Examples of commercially available ankle-foot orthoses (AFO) are illustrated in Figure 2.12. The AFOs (a-c) are designed to support foot drop as a consequence of weak dorsiflexion muscles during both swing and loading phases.

Foot drop may be caused by fatigue, balance issues, dementia, Parkinson, stroke, traumatic brain injury, multiple sclerosis and peroneal palsy. The AFO (d) is designed to support contractures and plantarflexion problems such as to relieve the pressure at the heel. Similarly, AFO (e, f) is used to maintain joint alignments in case of fractures taking place in the ankle-foot joint. These AFOs are not tuneable and patients can purchase them without any prescription.



**Figure 2.12: Commercially available AFO. (a) AFO by BRACEABILITY for foot drop, (b) AFO by Ottobock for foot drop, (c) AFO by HEALIOS for foot drop, (d) AFO by ORTHOBMI for heel pressure off, (e) AFO brace walker, (f) PRAFO Kodel ankle support. adapted from [63-68]**

Adjustable AFOs are prescribed to the patients by the doctors and orthoses are tuned by an expert to meet individual patient's requirements. The examples of adjustable response devices (ADR) are illustrated in Figure 2.13. An AFO in (a) is prescribed for soleus spasticity (hemiplegia) management, loss of dorsiflexion ROM, frequent falling with the clinical goal to maintain and increase the length of soleus muscles. An AFO in (b) is prescribed to post-stroke, post-polio, foot drop, foot slap and ankle instability problem. Clinical target is to tune AFO stiffness and ROMs to acquire normal gait like symmetry and walking speed. In Figure 2.13(c), the AFO has a motion limiter made of stainless steel urethane and provides variable plantarflexion stops along with load dampening. The AFO showed in Figure 2.13(d) is designed to adjust plantar/dorsiflexion motion by restriction their ROMs. There are four dorsiflexion stop positions and infinitely adjustable plantarflexion motion. Similarly, combined knee ankle joints adjustable orthoses (KAFO) are illustrated (e-h) to make up knee joint deficiencies along with/without ankle joint impairments. The structure of these orthoses is made of rigid metallic materials for effective assistance to the joints.



**Figure 2.13: Adjustable dynamic response lower limb orthoses. (a, b) AFO by Ultraflex systems, (c, d) AFO by Beckerorthopedic, (e, f) KAFO by Ultraflex systems, (g, h) KAFO by Beckerorthopedic. adapted from [19, 69]**

The active orthoses are reported in research studies and not commercially accessible at this stage. The examples of active AFOs are illustrated in Figure 2.14. There are various design techniques summarised here briefly. The SEA in (Fig. 2.14a) is also called robotic tendon consists of series helical spring with a small DC motor and that makes AFO wearable by reducing motor and battery sizes [70]. The robotic tendon works as helical spring stores kinetic energy in stance phase between FF to HO by extension and then releases energy at toe-off to provide push-off. The magnetorheological (MR) is a smart fluid with iron particles mixed into the oil as carriers. When MR fluid is subjected to an electromagnetic field (current based), its viscosity increases significantly as shown in Figure 2.14(b) [71]. The MR damper generates resistive torque and damps the motions. An AFO using pneumatic rotary actuator operated by compressed gas ( $\text{CO}_2$ ) via the pressure regulators is shown in Figure 2.14(c) [72]. Two separate regulators are used to adjust gas pressures corresponding to plantarflexion and dorsiflexion torques. The assistive torque direction is switched via two solenoid valves depending on gait events information from force sensors. Another generation *semiactive* pneumatic AFO's works based on artificial pneumatic muscles (Fig. 2.14d) [73]. Artificial pneumatic muscles are attached parallel to carbon fibre shank and provide plantarflexion assistive torques. Lastly, shape memory wires are actuated by current (heat) as shown in Figure 2.14(e) [74]. In heating mode wires length is increased and in cooling mode, (of current) wires

gain the original shape. This extension and contraction of SMA wires work like an artificial muscle to provide motions.

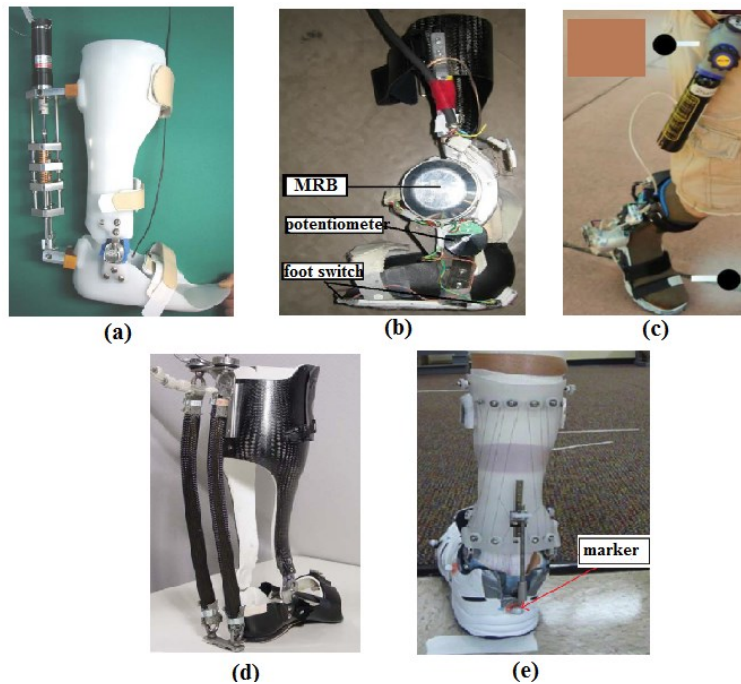


**Figure 2.14: Active orthoses illustrated for different actuation types. (a) Series elastic actuator (SEA) AFO, (b) Magneto-rheological fluid brakes AFO, (c) Pneumatic rotary actuator AFO, (d) Artificial pneumatic muscles AFO, (e) Shape memory alloy actuator based AFO. adapted from [70-74]**

Both research-based and clinically prescribed AFOs showed increased structural loads and improvement in performance from passive to active designs. These loads are further increased with other wearable devices such as lower limb prosthetic and exoskeleton. In literature, lower limbs angles and moments trajectories are compared to evaluate the effectiveness of these devices, however, there is no study found regarding gait dynamic stability evaluation (CoP, CoM signals) by wearing devices except clinically applied non-instrumented tests. Along with that, rigid metallic structures (frames) of these devices are expected to produce more impact loads during heel strike and change the shear forces under the foot plantar. The impact loads and net stabilities are related to the body's CoP or CoM displacements or higher order signals. Thus, the ability to acquire or maintain balance with ankle-foot impairments and by wearing orthoses is required to be investigated.

### 2.3.3 Static and Dynamic Balance Control

Bipedal balance control is mainly categorised w.r.t static and dynamic gait activities. The static activities include standstill posture, sit-to-stand, stand-to-sit, bending forward/backwards, whereas, dynamic activities include a level walk, walk on the inclined path (ascend/descend), stairs (up/down) etc. In a static posture, body's CoM lies approximately directly over the CoP and all linear and rotary forces are in

equilibrium about CoM [75]. In reality, there are small oscillations in the human head even in standstill posture and hence body's overall CoM moves to and fro like an inverted pendulum. Body's CoM shifts from its equilibrium point are called postural sway. In response, CoP also moves in an effort to bring CoM back to equilibrium. An excessive postural sway in elderly or pathological gait is reported as a prediction of fall [75] and poor balance control in CMT patients [76]. Considering CoM equilibrium, the body's stability can be categorised into three forms i.e. stable, unstable and neutral as illustrated in Figure 2.15.

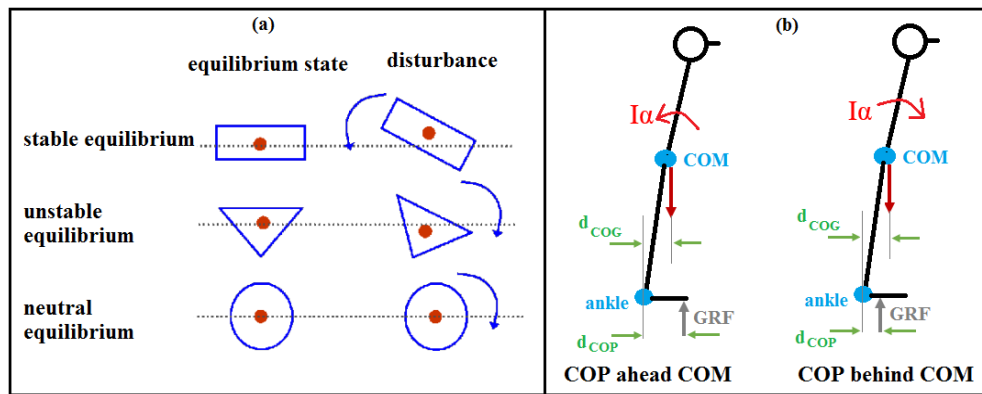


**Figure 2.15: Equilibrium conditions in quiet stance. (a) disturbance effects in COM [75], (b) human body pendulum-like rotational stability [77].**

A stable equilibrium is a condition in which an object comes back to equilibrium after a slight disturbance applied as shown above in Figure 2.15(a). Oppositely in an unstable equilibrium, an object never comes back after a disturbance is applied. A condition in which an object's CoM does not move up/down upon applying disturbance is called neutral equilibrium. Considering human body inverted pendulum model in Figure 2.15, when CoP moves ahead to the CoM, a counter-clockwise moment ( $I\alpha$ ) is provided to the trunk by the ankle joint to regain the stable equilibrium (Eq. 2.1). Oppositely, when CoP is behind the CoM, a clockwise moment is generated in the trunk by the ankle joint and balance is either lost or body fell forward. A decrease in CoM height increases the stability because it gives more degree of freedom to the CoM to move within the base of support [75].

$$(GRF \times d_{COP}) - (W \times d_{COM}) = I\alpha \quad (2.1)$$

where ' $I$ ' presents the body's moment of inertia about ankle in the sagittal plane, ' $\alpha$ ' presents forward angular acceleration of CoM.

Clinically, static and dynamic stabilities are evaluated using Berg balance scale, Romberg test, and Timed up and go test in which series of tasks are performed by the subjects, questionnaires asked, and an expert matched and/or scaled the observations with some known reference [78, 79]. These methods do not involve sophisticated

instruments and are least accurate compared to research-based methods discussed in the next section. Further, static stabilities are also evaluated by improvising perturbations in standstill posture [80]. A static posture provides good theoretical understanding about human balance control, however, the focus of current literature review is on dynamic gait stability evaluations.

## **2.4 Gait Dynamic Stability Assessment Methods**

The methods published to quantify gait dynamic stability are described in this section. The applications related to each method are summarised in Table A.1 (Appendix A) at the end.

### **2.4.1 Gait Parameters Variability**

Parametric variabilities are the oldest and simplest technique reported in the literature to assess gait dynamic stability and still widely employed in support to advance stability techniques (discussed in subsequent sections). The parameters include spatiotemporal (time and distance), peak magnitudes of lower limbs kinematics (joints angles, CoP, CoM), and kinetics (joints moments, GRF). These parameters are computed using either body mounted sensors (IMU sensors) or motion capture system with force plates and built-in analysis tools i.e. OpenSim, Matlab toolbox, Visual-3D, Anybody software. In gait-related studies, variability is quantified either using discrete parameters and getting mean and standard deviation (Std.) or using whole time-series waveform and applying principal component analysis (PCA) [81]. PCA is a data analysis technique that reduces a large correlated data in a small number of uncorrelated variables called principal components (details in Chapter 3 section 3.6.1). PCs explain variance in the data in decreasing percentages and initial few PCs explain maximum variances which are further used for comparing different gait conditions.

An increase in parametric variability is an indication of decreased stability [81]. In literature, studies that applied parametric variability for stability evaluations are summarised in Appendix A (Table A.1). The main limitations included less stability related information from a single parameter which implies a combination of discrete parameters (e.g. ankle, knee, hip peak angles and moments) required to be conclusive. That also induces complexity while developing neuromotor balance control patterns. These parameters are reported to be better in explaining the inter/intralimb coordination and difficult to explain whole body/limb dynamic stability [82]. Secondly, the criteria of increased variability as poor stability also indicates adaptability in a positive sense. Therefore distinction in good and bad variability is ambiguous. Thirdly, there are no distinct criteria to declare a system stable/unstable

except comparing with control subjects. Further, the rate of change in neighbouring discrete points is unpredictable which is important for evaluating gait transitional changes. In conclusion, variability method is less conclusive to predict dynamic stabilities alone and ongoing researches used this as a supportive tool.

#### **2.4.2 Correlation Coefficient Methods**

These are statistical methods of comparing gait parameters evaluated from both control and impaired subjects. These coefficients give the strength and direction of the relationship between two variables. Depending on normal or non-normal distribution in the data, the Pearson coefficient or Spearman coefficient is used respectively. A correlation is measured between 0 to 1 either in a positive or negative direction. The correlation coefficient is considered strong (0.6 – 0.79), very strong (0.8 – 1), moderate (0.4 – 0.59) and weak (<0.4). In gait stability evaluations, the correlation coefficient is computed either using discrete parameters extracted from waveforms (spatiotemporal, peak angles, peak moments) or using derived parameters (e.g. in negative exponent models – stability time, static sway, transitional sway [9, 83]).

Another form is the intraclass correlation coefficient (ICC) which evaluates a long-range correlation using long-range time series data and predict reliability (agreement) between two variables. Comparative to Pearson/Spearman coefficient, ICC predicts both correlation and agreement between two variables [84] and long-time series makes ICC method resistant to internal and environmental perturbations (error tolerances). In ICC method, the time series is integrated first and then windowed into equal lengths (i.e. 'n' spans). For each of the window lengths, a line is fitted and residual variance  $f(n)$  is calculated w.r.t this line. Generally, a linear relationship exists in the log-log curve between  $F(n)$  and 'n' as illustrated in Figure 2.16. The slope of the linearly fitted line gives a measure of ICC. An ICC is quantified between 0 to 1 with sub-ranges poor (<0.5), moderate (0.5 – 0.75), good (0.75 – 0.9), and excellent (>0.9). In gait stability, ICC values >0.5 is considered stable (positive long-range correlation), <0.5 means more fluctuations [10]. Longtime series are mostly constructed using tri-axial accelerometer data collected from trunk [11]. Gait stability related studies which have evaluated correlation coefficients are summarised in Appendix A (Table A.1). A correlation did not provide critical cut-off between stable or unstable conditions. An ICC computed from long range strides did not predict transitional stabilities or stability changeovers during gait sub-phases.

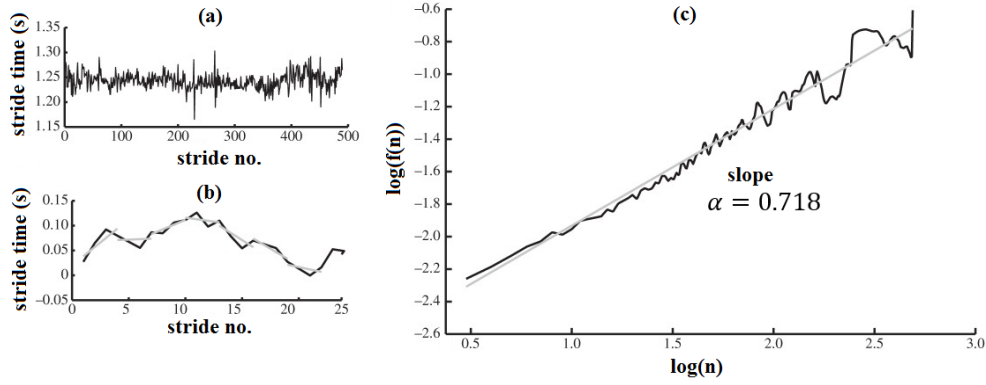


**Figure 2.16: Intraclass correlation coefficient evaluation. (a) time series data, (b) Expanded view line fitted for windows of 4 strides, (c) ICC evaluated from the log-log curve. adapted from [10]**

### 2.4.3 Lyapunov Exponent Method

Lyapunov exponent also called local dynamic stability (LDS) method is a non-linear time series analysis technique in which data is plotted in state space with a sufficient number of independent variables. After the parametric variability method, Lyapunov is the oldest technique used to quantify gait dynamic stability and here this method is described briefly following earlier studies [85, 86]. In gait-related LDS applications, a time series is constructed (Figure 2.17a) using either combination of 3D kinematic variables (position, velocity, acceleration, jerk, EMG outputs and/or their derivatives [10]), and required too larger time series data in each variable. The strides are equally sampled and all subjects have the same number of strides. After constructing a state space (Figure 2.17b), Euclidian distances are computed (Figure 2.17c) between nearest neighbouring points starting from initial state i.e.  $d_j(0)$  (where the distance between two trajectories approaches to zero) to the entire stride length  $d_j(i)$ . A Lyapunov exponent is thus evaluated (Eq.'s 2.2 to 2.4) using the rate of divergence of distances between neighbouring points and gives a measure of sensitivity to local perturbations.

$$d(t) = De^{\lambda_1 t} \quad (2.2)$$

where  $d(t)$  is mean displacement at any time  $t$ ,  $D$  is an initial separation in neighbouring points and  $\lambda_1$  is Lyapunov exponent. Taking the log of both sides of Eq. 2.2:

$$\ln[d_j(i)] = \lambda_1(i\Delta t) + \ln[D_j] \quad (2.3)$$

where  $d_j$  is Euclidian distance between  $j^{th}$  pair of neighbouring points and  $i$  is discrete time steps. Euclidian distances between neighbouring points are averaged over stride time such that  $\lambda^*$  gives the slope of a linear fit to the exponential curve (Figure 2.17d).

$$y(i) = \frac{1}{\Delta t} \langle \ln[d_j(i)] \rangle \quad (2.4)$$



where  $\langle \cdot \rangle$  denotes the average of values of  $j$  pairs of neighbouring points.

Stability is defined as a dynamic system's sensitivity towards perturbations and if these perturbations are infinitely small then this is called local stability, and if perturbations are finite then this is called global stability [87]. The natural fluctuations in human gait are described as local perturbations. A negative value of Lyapunov exponent ( $\lambda^*$ ) indicates local stability and positive exponent predicts local instability. A larger exponent (slopes of linear fit) indicates greater sensitivity towards local perturbations. A divergence of slopes of linear fits between 0 and 1 stride gives short-term exponent ( $\lambda_S^*$ ) and between 4 to 10 strides gives long-term exponent ( $\lambda_L^*$ ). The  $\lambda_S^*$  is more sensitive to local perturbations than  $\lambda_L^*$  and  $\lambda_S^*$  is also used to predict fall probability. The implementation of local dynamic stability algorithm is illustrated in Figure 2.17 for four EMG sensors data used to create state space [85].

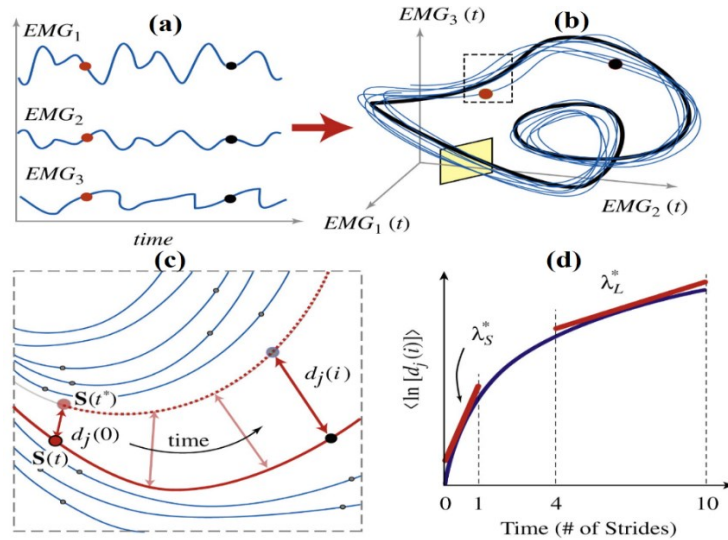


**Figure 2.17: Lyapunov exponent stability evaluation method. (a) EMG time series, (b) State space constructed using four EMGs data, (c) expanded view of the orthogonal section to the mean state space data, (d) Lyapunov exponent evaluated from averaged rate of divergence. adapted from [85]**

The applications of the LDS method for gait dynamic stability assessment are summarised in Appendix A (Table A.1). LDS methods have few limitations such as large data sets (strides per subject) required to construct state space for a precise exponent estimation. Secondly, there are no distinct cut-off thresholds to distinguish stable and unstable gait [34]. The Lyapunov method has the same attraction towards local perturbations and unwanted noise in the data (no exponent growth due to noise). This sensitivity towards noise also raises the question which kinematic parameters should be used and what is the efficiency of prediction e.g. a large value of  $\lambda_S^*$  is used to predict fall probability. Lastly, there are different algorithms (e.g. Rosensein-Kantz, Wolf) and measurement signals reported to quantify Lyapunov exponents that induces standardising issues and varying outcomes from different studies [6].

### 2.4.4 Floquet Multiplier (FM) Method

Floquet multiplier method belongs to the same generic type to which the Lyapunov exponent method belongs. Both methods require a state space construction using kinematic variables and evaluate exponent convergence/divergence [10, 11, 85]. In the Floquet method, gait waveforms are repeated over time and presented as Poincaré sections for each discrete stride point as illustrated in Figure 2.18. The mean of all trajectories is calculated in each Poincaré section which acts as a fixed point ( $S^*$ ) and across which state variables are perturbed. Periodicity in variables is the key assumption in this method such that a cycle ( $S_{k+1}$ ) is a function ( $f$ ) of the current cycle ( $S_k$ ).

$$S_{k+1} = f(S_k) \quad (2.5)$$

$$[S_{k+1} - S^*] = j(S^*)[S_k - S^*] \quad (2.6)$$

where  $j(S^*)$  present the Eigenvalues or rate at which small perturbations grow or decay also called Floquet multiplier (FM). If  $FM < 1$  then perturbations in  $S_k$  shrinks in  $S_{k+1}$  and the system remains stable. A maximum value of Floquet multiplier is used to predict exponential stability and any random discrete point could be used for stability evaluation. Floquet multiplier method rarely applied in gait stability analysis due to its additional limitations along with Lyapunov exponent method. Floquet method is mostly reported along with Lyapunov exponent stability methods. The mean of all waveforms used in the Poincaré section (fixed point) underestimates the exact evaluation of maximum FM [10]. Further, a random selection of Poincaré section may be good stability predictor in a theoretical system (bipedal robots) and less practical for a human walk because it is not strictly repetitive.

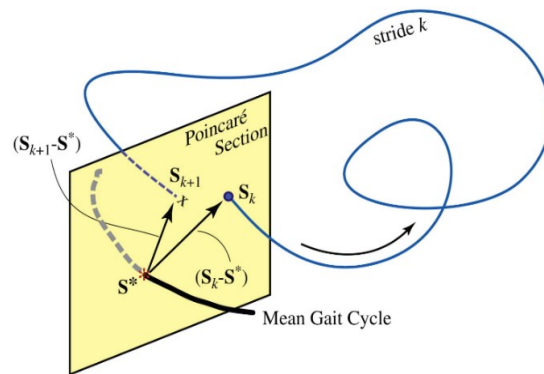


**Figure 2.18: Floquet exponent method illustrates the Poincaré section of the state space shown in Figure 2.14(b). adapted from [85]**

### 2.4.5 Whole Body Angular Momentum approach

Another method reported whole-body angular momentum to quantify gait dynamic stability [88], however, its application was found rare in the literature. In this method,

the time rate of change in angular momentum is evaluated using Eq. 2.7. A higher rate of change in  $\vec{H}$  is measured from peak-to-peak (max-min) waveforms and indicates balance is challenging to control.

$$\frac{d\vec{H}}{dt} = \vec{M}_{ext}, \quad \vec{M}_{ext} = \vec{r} \times \overline{GRF} \quad (2.7)$$

where  $\vec{r}$  presents position vector quantified from foot CoP and  $\overline{GRF}$  presents ground reaction force vector. Like previous methods, this method also did not provide information about inner gait phases (transitional phases) and had not any distinct criteria of evaluating stabilities.

#### 2.4.6 Extrapolated-CoM and BoS Difference

A widely reported dynamic stability assessment method quantifies limits of body's CoM sways w.r.t BoS in anterior-posterior and medial-lateral directions. The motivation behind is an inverted pendulum (IP) model. As illustrated earlier in Figure 2.15(b) for a static posture, the difference in CoP and CoM in AP direction generate destabilising moment and in response, a balancing moment is generated in the ankle joint to displace CoP back to equilibrium. It is well known in bipedal stability that vertical projection of CoM within/outside BoS define the stability of walk, however, Pai and his group [89] extended this concept by introducing CoM velocity concept in addition. According to him, even if CoM lies within BoS but CoM velocity directed outward then the balance may be impossible and oppositely if CoM velocity directed towards BoS with CoM outside then the balance may be achievable. Hof et al. [12, 90] illustrated this concept by a relatively simple mathematical derivation using IP model in Figure 2.19 and summarised here (Eq.'s 2.8 to 2.12). Starting with Euler's equation:

$$\sum M = I\alpha \quad (2.8)$$

where  $M$  presents resultant moments,  $I = ml^2$ ,  $I$  moment of inertia,  $m$  presents mass of pendulum and  $l$  present effective length.

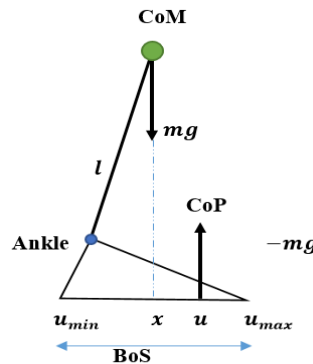


**Figure 2.19: Inverted pendulum model of the lower limb.**

$$GRF \times u - W \times x = I\alpha$$

For  $GRF = W = mg$

$$mg(u - x) = -ml^2\left(\frac{\ddot{x}}{l}\right)$$

$$u - x = -\frac{\ddot{x}}{g/l} = -\frac{\ddot{x}}{\omega_o^2}$$

where  $\omega_o = \sqrt{g/l}$  present natural frequency of CoM-oscillations.

$$\ddot{x} = \omega_o(x - u) \quad (2.9)$$

This differential equation (Eq. 2.9) is solved with initial CoM position and velocity  $x_o$  and  $v_o$  (details in [90]),  $x(t)$  is the solution with the condition CoM will not pass the CoP i.e.  $x(t) \leq u$ .

$$x_o + \frac{v_o}{\omega_o} \leq u \quad (2.10)$$

The Eq. 2.10 interprets that as long as  $x_o + \frac{v_o}{\omega_o}$  remains within BoS defined by  $u_{min} \leq u \leq u_{max}$ , the body remains stable and as this quantity exceeds BoS, the body becomes unstable. The equivalent representation of this quantity using CoM and BoS notions is presented as:

$$XCoM = CoM + v_{CoM}/\omega_o \quad (2.11)$$

where XCoM presents extrapolated-CoM and further margin of stability (MoS) can be computed w.r.t BoS as:

$$MoS = XCoM - BoS \quad (2.12)$$

A margin of stability (meter/centimetre) predicts the impulse disturbance required to make a subject unstable and computed in anterior-posterior and medial-lateral directions. Similarly, XCoM and BoS (boundaries of the foot) are also computed in the respective directions. In literature, different foot positions are used to define BoS. For example, the CoP (max, min) positions are used in above derivation to define BoS. In other studies, heel or toe markers are also used in AP direction, and medial and lateral ankle joint markers are used to define BoS in perpendicular (ML) direction [28, 91].

Stability criteria – for a dynamic gait cycle, the MoS(s) are quantified as the shortest distance between BoS and XCoM [28]. For example in Figure 2.20, toe marker is used to define BoS (foot boundary) and the shortest distance between XCoM and leading foot toe marker is quantified at heel contact and toe-off events to define margins of stabilities. When XCoM remains within BoS (e.g. at HC), MoS quantifies stable margins (positive), and when XCoM lies outside the BoS (e.g. at TO) then MoS quantifies unstable margins (negative). A decrease in MoS implies a decrease in stability, and oppositely, an increase in MoS implies better stability. However, an

increased MoS (CoM sway w.r.t BoS) has also been used as an indication of poor balance control.

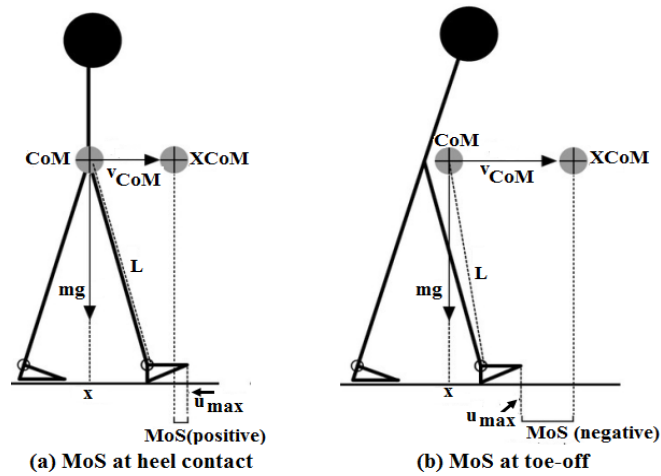


**Figure 2.20: Margin of stability (MoS) in AP direction with maximum BoS measure from the toe of the leading foot. adapted and modified [91]**

In literature, the applications of MoS(s) for gait dynamic stability assessments are summarised in Appendix A (Table A.1). This method also has a few limitations. For example, the BoS is assumed constant without counting foot rollover (means double limb support time zero) whereas practically CoP (or BoS) trajectories change significantly and CoM accelerate and decelerate maximum during this double support transition [12]. This also implies that gait transitional phases are not quantifiable by this method. The stability criteria are loose such that in some studies, a decrease in MoS implies poor stability, and in others, an increase in MoS also indicates poor balance control [28]. Lastly, the MoS(s) are quantified at the discrete event (HC, TO) which may not necessarily present critical stability margins considering inner gait phases.

#### 2.4.7 Nyquist and Bode (N&B) stability Methods

Nyquist and Bode are stability analysis techniques from control engineering theory and widely used in plant modelling and controller design applications in biomedical robotics. Considering gait biomechanics, Bode plots are used to evaluate lower limb contractile dynamics and vibration impacts using spring-mass-damper (SMD) models [37, 80, 92, 93]. More recent studies [34-36, 94] applied N&B methods for gait stability analysis using lower limb joints kinematic/kinetic data in the sagittal plane. An earlier study quantified robustness, gain, and phase margins for an open loop postural control both experimentally and using inverted pendulum models [37]. Earlier studies also applied these methods for gait transitional stability evaluation using CoM and CoP higher order waveforms which showed impulsive behaviours [95-97]. These methods are briefly described here with further details being discussed in Chapter 3 (section 3.6.3). In these methods, a continuous variable is selected that

presents lower limb kinematic/kinetic and modelled in time and frequency domains (transfer function – TF) using system identification methods. The roots of a TF are plotted in the complex plane (s-plane) and the existence of denominator roots on the left half of s-plane shows stable system otherwise it is unstable. A range of frequencies are put into TF (models) and Nyquist or Bode plots are constructed as shown in Figure 2.21 (Bode plots). These methods have strict mathematical notions (cut-off reference) across which stability margins are quantified. The stability outcomes are in the form of gain margin (GM) and phase margin (PM). A GM presents amplitude difference from cut-off reference i.e. 0 decibel gain in gain plot and a PM presents time difference from cut-off i.e.  $\pm 180^\circ \pm 2k\pi$  in respective phase plot. The major advantage in these methods is distinct cut-off thresholds (0 dB,  $\pm 180^\circ \pm 2k\pi$ ) which is used to quantify stability/instability margins independent to comparing with control subjects.

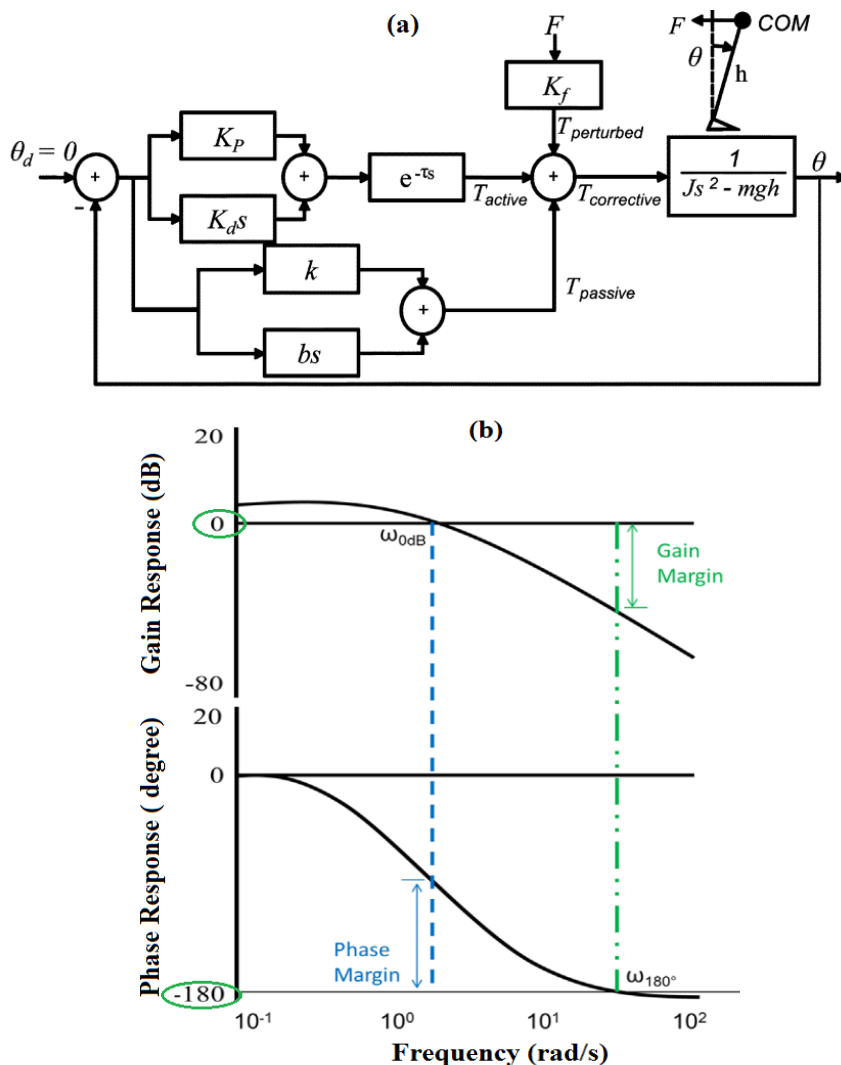


**Figure 2.21: Postural control model and stability margins illustrated. (a) Balance control model of static posture with force perturbation and ankle angle [37], (b) Gain and phase margins computed from Bode plots [34].**

The applications of N&B methods for gait stability analysis are quite recent and related studies reported in Appendix A (Table A.1). These methods are still required to be established considering which gait signals are appropriate, how to evaluate steady-state gait phases, identify the models, and settle the stability margins norms.

#### **2.4.8 Clinical/experimental limitations of stability assessments**

The stability assessment techniques discussed here (section 2.4) are implemented previously in the laboratory environment and mostly for healthy subjects. A literature survey conducted in Appendix A (Table A.1) illustrated that only eight studies (out of 45) involved impaired subjects. The main reasons included variance in the degree of impairments, ethical constraints regarding more unstable patients and research regarding gait dynamic stability evaluation is in developmental phases considering methods and experimental equipment. For example, the variance in a cluster of patients suffering through Charcot-Marie-tooth or foot drop impairments makes a differential diagnostic difficult while comparing with a healthy subjects group. Further, more severe patients require harness support which also affect the stability assessments for independent walking.

Considering measuring instruments, most of the prior studies collect data from human subjects using motion capture system and force platforms which were fixed in the laboratory environment. For more practical scenarios, a portable real-time system is more realistic. The ongoing research regarding gait dynamic stability assessments involved optimisation of existing methods with objectives to reduce the measurement signals and complexing of analysing algorithms (also focused on this thesis). These measures would potentially enhance the application of current methods towards real-time stability assessment and control the patient's instability using preventive hardware. However, such assessment and application are suitable for an individual patient by eliminating the variance issue showed in previous group-based studies. Further, the Footscan pressure insoles and IMU sensors can provide real-time measurements from human subjects.

### **2.5 Stability Evaluation for varying terrains**

In literature, gait dynamic balance control is mostly assessed for a level ground walk. Only three recent publications [13, 14, 98] found in which dynamic stability evaluated on inclined (up/down) surfaces, however, biomechanics of ascending and descending walks are widely reported earlier. In these studies, parametric variability (standard deviation), local dynamic stability, and extrapolated-CoM methods are applied using control subjects and outcomes are summarised in Table 2.3. In one study [14], young and older adults evaluated with no age-related stability difference found. The

evaluation of dynamic stability during transitional phases is yet missing to interpret on an inclined pathway for both healthy and impaired subjects.

**Table 2.3: Studies evaluated gait dynamic stability on an inclined surface.**

Study	Equipment/Method Used	Measurement Signals	Outcomes
Vieira et. al. [13]	treadmill, motion cameras, MoS, LDS, parametric variability	CoM, toe marker, trunk 3D velocities and accelerations	downward walk – high variability, low MoS ML, no effect on LDS, upward walk – low stability LDS
Vieira et. al. [14]	treadmill, motion cameras, MoS, LDS, parametric variability	CoM, toe marker, trunk 3D velocities, accelerations	both LDS and MoS showed no age-related difference
Pickle et. al. [98]	motion capture system, extrapolated CoM method (MoS)	CoM, foot placement estimator and capture point from IPM	CoM effects stability metrics, however, no clear relationship found between these

## 2.6 Lower limb contractile dynamics

Lower limb’s anatomical structure mainly consists of rigid bones and soft muscles. Bones provide strength and muscles to generate force and damping characteristics. During a gait cycle, impact forces are generated and act as input signals to retune limb muscles such that the effect of impact forces reduced at the joints and tendons [99]. Therefore, a limb structure not only absorbs shocks but also reweights the sensory feedback in a balance control loop [80]. Thus, the vibration sensations act as somatosensory feedback in postural stability [76]. The damping characteristics of the lower limb are defined by contractile dynamics, included natural frequency, damping factor and peak gains. In literature, these properties are quantified using direct gait measurements (CoM-acceleration), or inverted pendulum (IP) or spring-mass-damper (SMD) walking models. A literature survey is conducted in Table 2.4 including studies those quantified contractile dynamics. The contractile properties evaluated mostly for healthy/impaired gait, foot inserts, however, no study found that quantified wearable ankle-foot orthosis impacts with/without clinical range adjustments. The contractile properties are defined below with support of Figure 2.22.

1) Damping Ratio ( $\zeta$ ) - The damping ratio is a dimensionless quantity that quantifies the system’s ability to attenuate oscillations/vibrations in response to a disturbance. Practically, an underdamped system has  $0 < \zeta < 1$  and an undamped system has  $\zeta = 0$  [100]. A decrease in damping ratio implies more oscillations resulted from heel contact. The formula for computing damping ratio is presented in Matlab as Equation 2.13.

$$\zeta = -\cos(\theta) \quad (2.13)$$



where ' $\theta$ ' is the angle from origin to pole location.

2) Natural Frequency ( $\omega_n$ ) – presents the frequency of CoM oscillations, which is used to analyse the response of a system. The formula for computing natural frequency is presented in Matlab as Equation 2.14.

$$\omega_n = |s| \quad (2.14)$$

where ' $s$ ' is pole location. Since the natural frequency of oscillations depends on poles location, hence, the pole which presents maximum natural frequency is used for analysis.

3) Peak Gain ( $M_r$ ) - it presents the maximum magnitude in the gain plot. For a normal gait performance, peak gains are required to maintain the range of healthy subjects data in order to provide optimum somatosensory inputs to the neuromotor for balance control.

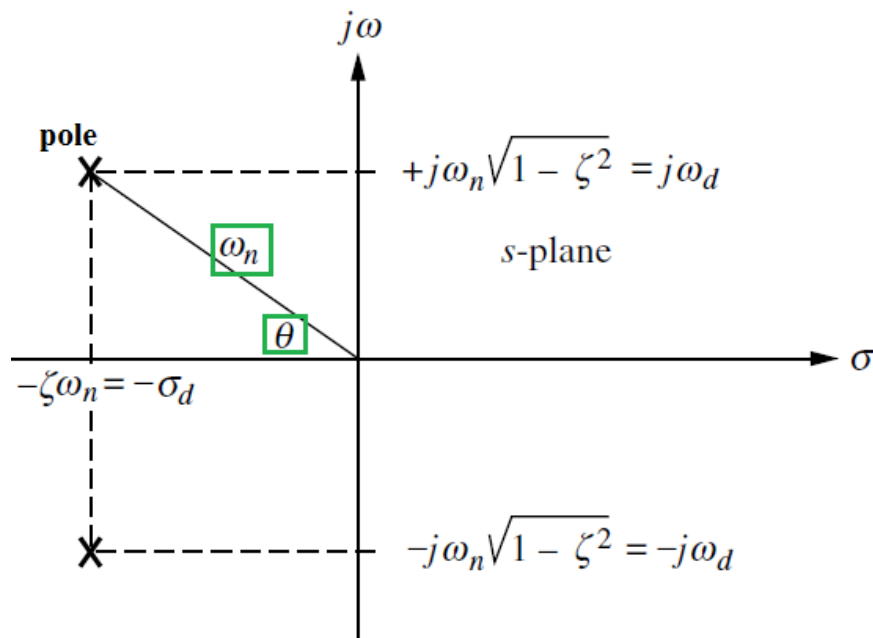


**Figure 2.22: Natural frequency and damping ratio ( $\theta$ ) defined w.r.t pole location in the Laplace plane. adapted from [101]**

**Table 2.4: Studies evaluated lower limb contractile dynamics using Bode plot and system identification methods.**

<b>Study</b>	<b>Purpose</b>	<b>Equipment/Method Used</b>	<b>Measurement Signals</b>	<b>Outcomes</b>
Hong et. al. [102]	spring like gait dynamics in young and elderly	Force plates, motion capture, SMD model	vertical GRF, CoP, step length, damping ratio, stiffness	experimental GRF is achieved from SMD model and model (spring, mass, damper) constants define contractile dynamics
Kim et. al. [103]	compliant leg stiffness evaluation at varying speeds	Force plates, motion capture, SMD model	vertical GRF, CoM, damping ratio, stiffness, natural frequency	leg stiffness increases with walking speed
Enders et. al. [104]	evaluate the damping of super-imposed gait waveforms during running and sprinting	accelerometer, wavelet analysis method, hard and soft walking surfaces	damping coefficient, amplitude, frequency	hard surface walk produced lower damping coefficient compared to soft surface
Khassetarash et. al. [105]	damping in soft tissue vibration and energy dissipation in running	accelerometer	damping ratio	both parameters increased at low frequency vibration of soft tissues
Zadpoor et. al. [106]	effect of fatigue on GRF and vibrations of lower soft tissues	SMD model simulation	GRF, damping ratio, stiffness	vibrations amplitude increased with no effect on GRF
Wakeling et. al. [22]	heel strike generated vibrations relation with muscles activity	accelerometer, force plates	GRF, vibr. frequency, soft tissue acceleration,	muscles activity increased and damp the vibrations
Chi et. al. [21]	effect of impact loads in walking and running	SMD model simulation, force plate	GRF, stiffness, damping ratio, energy	knee angle and foot mass effect impact transients in gait
Smeathers J. E. [93]	heel strike generated vibrations evaluation	accelerometer, Fourier transform	natural frequency, damping ratio, gain	transient vibrations mainly damped by the leg
Hidler et al. [92]	Contractile properties evaluated for a spastic gait stimulated at tibial nerve and Bode plots constructed from ankle moments signals, (H=10, I=10)	Biodex Medical system, tibial nerve stimulator, EMGs (1000Hz), system identification	Ankle joint moment, EMG signals	Patients with higher spasticity preserved contractile dynamics and with less spasticity showed fast response in contractile properties

## 2.7 Gaps of knowledge

Based on the literature reviewed, gait dynamic stability assessment techniques are compared here and various discriminating factors are evaluated in Table 2.5. These factors establish methodological, performance, and application related gaps of knowledge. Stability methods are grouped into time and frequency domains. The time domain methods are further categorised based on continuous time series (Lyapunov, Floquet, and correlation methods) and discrete point evaluations (parametric variability, extrapolated-CoM).

**Table 2.5: Comparison between gait dynamic stability assessment techniques.**

Gait stability methods  Factors	Time domain Methods				Frequency domain
	Continuous		Discrete		N&B <sup>5</sup> methods
	LDS <sup>1</sup> ( $\lambda$ )	ICC <sup>2</sup>	MoS <sup>3</sup>	parametric variability <sup>4</sup>	
distinct stability criteria <sup>a</sup>	no	no	no	no	yes
time-series data	large	large	medium	medium	medium
gait transitional stabilities	no	no	no	no	yes
the efficiency of algorithm <sup>b</sup>	no	yes	no	no	yes
required signals	multiple	multiple	two	multiple	single
critical stability margins <sup>c</sup>	no	no	no	no	yes
time and/or magnitude outputs	scale (ratio)	scale (ratio)	mag.	both	both
varying terrains	no	no	no	yes	yes
orthoses impacts	no	no	no	no	yes
fall prediction	yes*	no	no	no	no

<sup>1</sup>LDS: local dynamic stability (Lyapunov exponent and Floquet multiplier methods), <sup>2</sup>ICC: intraclass, Spearman/Pearson correlation coefficients, <sup>3</sup>MoS: margins of stability (extrapolated-CoM and BoS difference), <sup>4</sup>Parametric variability: discrete spatiotemporal, peak angles/moments, <sup>5</sup>N&B: Nyquist and Bode stability methods, <sup>a</sup> compare the outcomes from control subjects to define stable or unstable margins, <sup>b</sup> the best fit model (system identification) predict the accuracy of quantifying stability, <sup>c</sup> minimum stability point in a gait phase or cycle, \* conditionally (noise in data also increase Lyapunov exponent).

### 2.7.1 Methodological

A common and major limitation in these methods is lack of *distinct cut-off thresholds* to define stable or unstable system and with respect to which stability margins they are quantifiable. Earlier methods strictly depend on comparison with control subjects to quantify stability/instability.

Secondly, these methods need *multiple signals* from lower limbs (e.g. at least 5 variables and/or their derivatives in continuous time series) or evaluate stability at *discrete points/parameters* (HC and TO events, peaks of waveforms) to quantify stability. Whereas in stability biomechanics, two signals CoP or CoM are widely reported as resultant measures of body's balance control such that the CoP responds to imbalances in CoM to gain the equilibrium. Furthermore, these discrete points are not guaranteed to present critical stability (minimum stable).

Thirdly, both long-range time series or discrete event evaluations did not provide stability information specifically about *transitional phases* of a gait cycle. That included the time span when one limb is in weight loading phases and opposite limbs in weight unloading phases and during which most of the limb muscles, GRFs, and energies showed highly transient responses.

Lastly, the *heel contact generated vibrations* reported to have greater impacts on neuromotor balance control (limb's contractile dynamics, somatosensory feedback) and degeneration of impairments. However, there is no study found that evaluated wearable orthoses (rigid structures) generated vibrations impacts on gait stabilities.

### 2.7.2 Performance

All stability methods evaluate internal/external perturbations in body's equilibrium. The *sensitivity* of a particular method *to quantify instability* gets affected by varying degree of impairments in patients involved (no prior study found with ankle-foot patients involved). Therefore, a uniformly restricted imitated impairments can illustrate the sensitivity of a method to determine critical stabilities prior to applying a method for a group of patients.

The *efficiency* of quantifying a stability margin is not predictable in time domain methods. Along with no hardbound criteria, long time series or discrete evaluation, and multiple variables involved reduce the reliability. Further, a dynamic system is described by two distinct time and amplitude outputs whereas time domain methods either scaled the stability or gives distance limits.

### 2.7.3 Applications

In literature, the stability assessment methods are applied for a level ground walk using healthy and impaired gait. Recently a couple of studies (Table 2.4) applied to

time domain methods to assess stability on inclined surfaces (ramp ascend/descend). Considering the above methodological limitations, there is a need for stability assessment tools to evaluate gait transitional stabilities for *ramp ascend/descend* activities.

Despite a great deal of research in *wearable orthoses/exoskeletons*, their impact on gait dynamic stability is not reported very much in literature. A few studies (Table 2.3) evaluated gait stability with AFO using Berg balance test, Time up and go test, and parametric variability. There is a gap of evaluating orthoses impacts on gait transitional stabilities with clinical ranged adjustments.

In conclusion, all stability assessment techniques have their own merits and demerits. However, the time domain methods are lacked to evaluate gait transitional stabilities, along with distinct criteria, and using resultant biomechanical signals considering balance control. In comparison, recently applied frequency domain methods are found to be more promising. These methods, however, require to establish further considering methodological, performance, and applications norms for both healthy and impaired gait. Therefore, the current study fills these gaps of knowledge and proceed with Nyquist and Bode stability assessments for dynamic gait activities.

## **2.8 Summary**

This chapter presented a comprehensive literature review regarding stability aspects of weight loading and unloading gait transitions. Firstly, the body's anatomical planes and axes of movements were described for lower limbs. A gait cycle is a fundamental repetitive period, essential to describe lower limbs biomechanics, and discussed with a breakdown into events, phases, and sub-phases. The parameters used to define lower limbs biomechanics such as spatiotemporal, joints angles and moments were defined along with neuromotor balance control aspects. The ankle-foot joint as an end-effector plays an important role to maintain stability, the common impairments related to ankle joint and wearable orthoses used to support were discussed. In literature, human balance control is measured w.r.t static and dynamic activities and fundamentals of balancing are defined using a static posture (i.e. inverted pendulum model). Hence, static stability measurements were discussed briefly and dynamic stability methods were covered in details along with reported studies related to each method. Furthermore, the body's vertical contractile dynamics and stability at varying terrains are reviewed. Lastly, a critical comparison was made between published gait dynamic stability methods and limitations were sorted into methodological, performance, and application domains. These gaps of knowledge define motivation of current study i.e. to develop and establish a dynamic stability assessment technique for gait transitional phases with distinct criteria.

## **CHAPTER 3**

# **EXPERIMENTAL PROTOCOL AND ANALYTICAL PROCESSES**

### **3.1 Introduction**

This chapter presents the experimental setup and analytical procedures used in this study. In the first part, ankle-foot orthoses are designed to imitate forward and rotational ankle-foot impairments. The experiments performed in motion capture laboratory, with details such as restricted motion ankle-foot impairments, procedures, and ethical review are described. The recorded motion capture data is analysed using Visual-3D motion analysis software. The lower limb joints angles and moments are computed and compared with previously reported patients data to validate the imitated impairments. In the second part, the analytical procedures are established for the collected data. The principal component analysis is used to remove artefacts and linearize the waveforms. The time and frequency domain linear modelling of waveforms is described in details. Lastly, the Nyquist and Bode methods are introduced to quantify gait dynamic stabilities.

### **3.2 Requirements and Specifications**

In lower limbs, the ankle-foot joint as an end effector illustrates greater degrees of freedom (DOF) and plays important role in balance control by transferring body weight to the ground and providing proprioceptive feedback to the neural system. Considering ankle joint DOFs, the types and degrees of impairments were reported earlier in wide ranges in patients having ankle-foot problems [107]. These greater variances made difficult to differentiate control versus impaired subjects in order to prove some hypothesis or to establish a new gait assessment method. Also, the ethical constraints demand to care for selection and experimentation with such patients. On the other hand, a few prior types of research adopted a restricted motions approach to imitate impairments using healthy subjects which introduces uniformity among the testing subjects. Following that, various ankle-foot impairments were imitated in this study with the main objective to establish new stability assessment techniques. The studies reported with restricted motions or imitated impairments are summarised in Table 3.1.

Practically, an ankle-foot impairment was exhibited in biomechanical data by its reduced motions such as dorsiflexion, plantarflexion, inversion, and eversion. A Charcot-Marie-Tooth (CMT) is a heterogeneous ankle-foot disease with multiple subgroups including failures of one or more of mentioned muscles groups [50, 108].

**Table 3.1: Imitated ankle-foot impairments using healthy subjects.**

Study	Purpose	Lower limb restrictions
Lugade et. al. [43, 109]	CoP comparison for four-foot position	plantigrade, equinus, inverted and everted foot walks imitated
Rabiei. M., et al. [110]	Foot pronation (everted foot)	6° laterally wedged insole used for imitation
Houx. L., et al. [15]	Thresholds of equinus in children	+10° ankle dorsiflexion, -10°, -20° ankle plantarflexion restriction using AFO
Huang. P. T., et al. [111]	biomechanics of reduced ankle plantarflexion (push-off) ability	plantarflexion reduced 0-20° using an ankle-foot orthosis
Choi. H., et al. [112]	ankle-foot orthosis stiffness impact on Achilles tendon and gastrocnemius muscles	ankle dorsiflexion stiffness provided at four levels (0.25, 1, 2, and 3.7 Nm/°) using AFO
Soares. at al., [113]	influence of wedges on lower limb kinematics and kinetics	five-foot insoles with different height, shape, and placements
Addison. et al. [114]	foot pads used to understand heel impacts	hard and soft foot pads compared with control subjects
Creaby. et al. [23]	insoles effects on impact loading in level walk	flat and heel-cup insoles used
Romkes. J. et al. [115]	unilaterally restricted ankle motion effect on kinematics	ankle plantarflexion motion restricted
Perry. S. D., et.al. [116]	inverted/everted foot effect on impact loading	10° varus/everted wedge and 10° valgus/inverted wedge shoes used
Kondo. H. [117]	effect of ankle dorsiflexion restrictions on kinematic, kinetics and muscles activity	dorsiflexion restrictions imitated using AFO divided into two groups <7°, and ≥7°
Pauser. J., et al. [118]	partial body weight bearing with an ankle-foot orthosis	orthosis support off-loading for hindfoot and forefoot

For example, foot drop or foot slap is resultant of weak dorsiflexion leg muscles. In forward ankle motion, either dorsiflexion and/or plantarflexion muscles get weaker. In the rotational direction, mostly inverted foot muscles and rarely everted muscles get weaker [108]. The inverted or everted foot impairments take place in hindfoot or forefoot, independent to forward impairments. Three main types of ankle-foot impairments are focused in this study and summarised in Table 3.2.

**Table 3.2: Common ankle-foot forward and rotational impairments.**

Ankle-foot impairments		muscles failure
Charcot-marie tooth (CMT)	Foot drop / Foot Slap (1)	dorsiflexion muscles failure
	Spastic / Equinus gait (2)	plantarflexion muscles failure
	Eversion (3)	everted foot muscles
	Inversion (4)	inverted foot muscles
	(1) and (2)	dorsi-plantarflexion muscles failure
	(1), (2) and (3)/(4)	dorsi-plantarflexion and inversion/eversion muscles failure

### 3.3 Wearable Ankle-foot orthoses Designs

An adjustable ankle-foot orthosis was designed to restrict dorsiflexion or dorsi-plantarflexion restrictions in forward (anterior-posterior) direction. The pairs of wedged insoles were designed to restrict inverted or everted ankle-foot motions in rotational (medial-lateral) direction.

#### 3.3.1 Adjustable ankle-foot orthosis design

A passive ankle-foot orthosis was designed to be worn by healthy adult subjects (foot lengths  $26 \pm 1$ cm; leg lengths  $40 \pm 5$ cm). The rigid orthosis consists of three parts i.e. shank assembly, foot part, and an adjustable joint. The shank part was designed with aluminium thin sheet and consists of two vertical bars slightly angled to acquire medial and lateral shapes of the legs (Figure 3.1a) and a circular collar welded at the top ends (at leg's COM). The bottom end of this frame was screwed to an adjustable ankle-foot orthosis on the lateral side and a free hinge joint was screwed on the medial side. The joint was made by Ultraflex systems [119] and has adjustable dynamic response characteristics (ADR). The joint is tuneable in dorsiflexion and/or plantarflexion directions w.r.t resistive torques and/or rigid ROMs. The detailed specifications are mentioned in Table 3.3. The foot part was cast using a carbon fibre kit from easy-composites and a standard male shoe size mould (UK number 9). The



top portion of shoe was cut to remove the mould and make it wearable with varying foot lengths. Further, the front of the shoe was made slightly wedge ( $10^\circ$ ) with the ground to allow forefoot plantarflexion motions just like leaf spring action in commercial shoes. A leather insole placed inside the shoe for foot safety. The carbon fibre shoe was assembled to the orthosis frame with adjustable and hinge joints on lateral and medial sides respectively. The AFO was designed to apply restrictions at the ankle joints and the forefoot portion was free to flex. The leather straps are riveted to collar part of shank and forefoot part of the shoe. These straps are adjustable with hard Velcro inside and make the device wearable with appropriate tightening. The designed orthosis has a total weight of 0.5kg and the complete assembly is illustrated in Figure 3.1b.

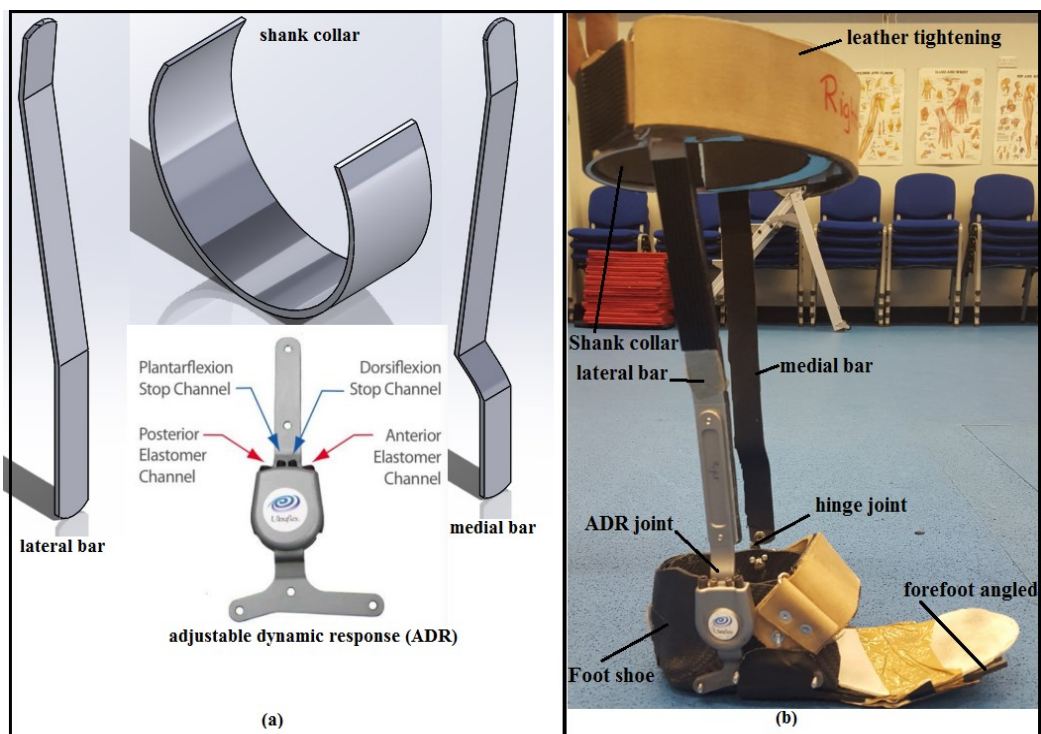


**Figure 3.1: Assembling of an adjustable ankle-foot orthosis. (a) Simulation of medial and lateral components, (b) Physical assembly of AFO.**

**Table 3.3: Specifications of adjustable dynamic response (ADR) AFO joint.**

Parameter	Range
dorsiflexion resistive torque	67.5Nm
plantarflexion resistive torque	67.5Nm
dorsiflexion range of motion	0-40°
plantarflexion range of motion	0-40°
subjects' supporting weight	50-114kg

### 3.3.2 Wedged foot insoles design

Pairs of wedged insoles were designed for inverted foot and everted foot simulations. In previous studies, during the walk, the peak sole compressive stress was reported as  $420\pm 150$  kPa [120] and peak shear stresses reported as  $21.2\pm 5$  kPa at the heel and  $37\pm 7.6$  kPa at forefoot [121]. Considering these specifications, the Styrofoam was selected as potential material to design foot insoles for rotational impairments. The Styrofoam material has good compressive strength (high load 100, thickness 1inch, compressive strength 690kPa, shear strength 35kPa). A Styrofoam sheet was cut in the shape of foot soles (UK numbers 8 and 9) using a hot wire cutter. The insoles were wedged to moderate range following previously reported [50, 108] with  $-10^\circ$  from medial to lateral sides for inverted foot and  $+10^\circ$  from lateral to medial side for the everted foot. The insoles were cut into two pieces i.e. forefoot and hind foot. That allows forefoot plantarflexion excursion which was restricted otherwise due to restricted forefoot motion with stiff insoles. Further, the rotational impairments influence either hind foot or forefoot, therefore, a split insoles design support the evaluations of either case. Both parts were joined together using gaffer tape. The insoles are portable to perform dynamic activities and worn by the subjects using Velcro straps as shown in Figure 3.2.

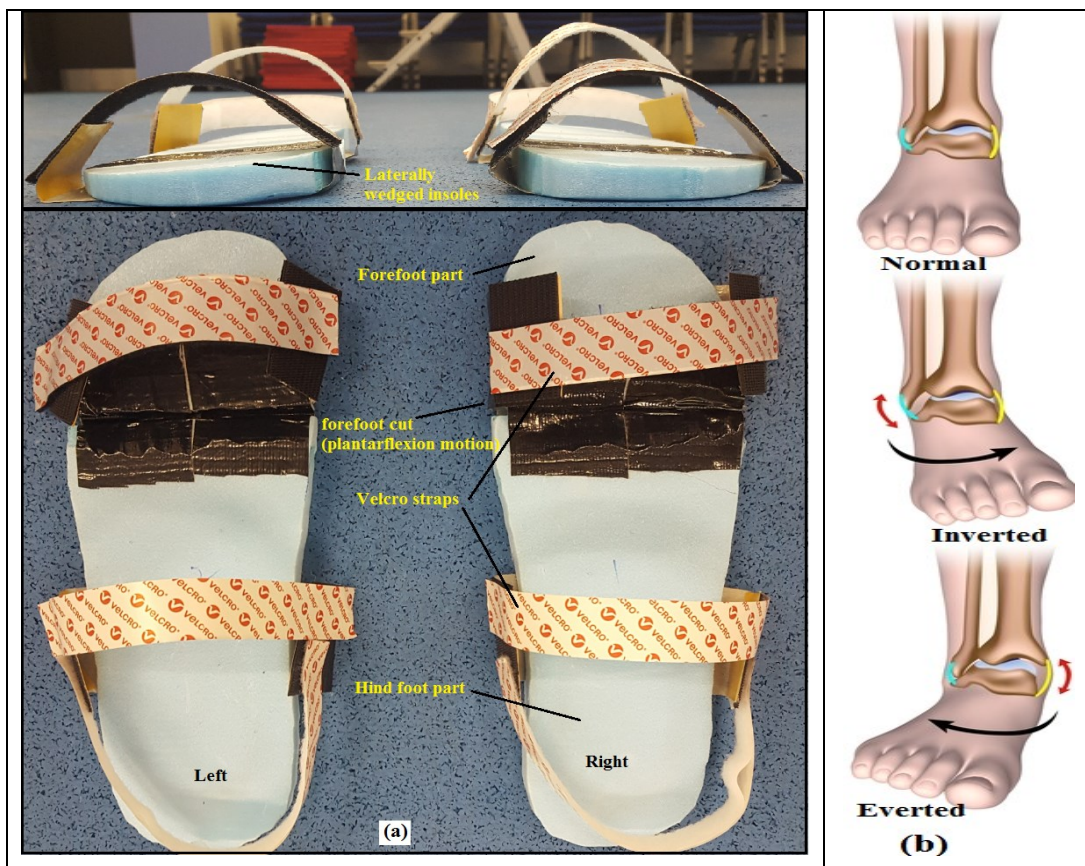


**Figure 3.2: Wedged foot insoles design for rotational impairments. (a) wedged insoles, (b) foot rotational impairments adapted from [122].**

### 3.4 Experimental Protocol and Procedures

#### 3.4.1 Imitated Ankle-foot Impairments

Ankle-foot orthoses (AFO) are clinically prescribed to assist ankle joint deficiencies. In this study, an AFO was used to imitate ankle-foot impairments applying moderate to severe range restrictions in the forward direction. The restricted ankle-foot motions not only imitated ankle-foot impairments but also used to evaluate wearable orthoses performance in dynamic balance control. In a moderate range, an AFO was tuned w.r.t stiffness by improvising resistive torques to the ankle-foot motions. In a severe range, the AFO was tuned to restrict ankle joint full range of motions. An AFO free mode condition was simulated as a reference to compare with restricted motions. In this study, forward AFO restricted impairments were imitated unilaterally (using dominant foot) whereas rotational impairments are imitated bilaterally based on the inherent nature of these impairments. The rotational impairments are simulated in moderate ranges i.e.  $-10^\circ$  for inversion and  $+10^\circ$  for eversion. A summary of imitating impairments, abbreviations, AFO tuning parameters, and corresponding representation of a specific disease is presented in Table 3.4.

**Table 3.4: Orthoses restrictions applied to imitate ankle-foot impairments.**

<b>Forward Impairments (unilateral)</b>	<b>Abbreviation</b>	<b>AFO Adjustment</b>	<b>Disease</b>
<b>Moderate Range</b>			
dorsiflexion resistive torque	DRT	$33 \pm 1 \text{Nm}$	Foot slap/drop
dorsiflexion and plantarflexion resistive torques	DPRT	$\pm 33 \pm 1 \text{Nm}$	CMT
<b>Severe Range</b>			
dorsiflexion range-of-motion restriction	DRR	$40 \pm 5^\circ$	Foot slap / drop
dorsiflexion and plantarflexion range-of-motion restriction	DPRR	$\pm 40 \pm 5^\circ$	CMT
<b>Rotational Impairments (bilateral)</b>	<b>Abbreviation</b>	<b>AFO Adjustment</b>	<b>Disease</b>
<b>Moderate Range</b>			
Medially wedged insoles	Eversion	$+10^\circ$	Eversion
Laterally wedged insoles	Inversion	$-10^\circ$	Inversion

### 3.4.2 Motion Capture System and Trials

Prior to starting experimentation, ethical approval was obtained from the local ethical review board at the University of Leeds. The letter of authority is attached in Appendix B. In an ethical review, a detailed procedure was described and followed in the following steps. Firstly, the subjects were briefed about experimental details and their volunteer participation was ensured. The schedule was prepared for two-week experiments in motion capture lab and a rota was informed to all participants. Each subject participated in three experiments i.e. level walk, ramp, and steps. Each experiment took two hours on an average and was conducted on different days for each participant. At the day of the experiment, the subjects have informed the details of a consent form and each participant signed it. Each subject's anthropological data (age, height, weight, foot length etc.) was recorded first and then the reflective markers were attached to the naked body. The anatomical positions of markers are illustrated in Figure 3.3. Each subject's dominant foot was observed with a simple activity i.e. a football was rolled towards subjects and the limb he/she used to respond was noted. Later, subjects were asked verbally and confirmed this finding.

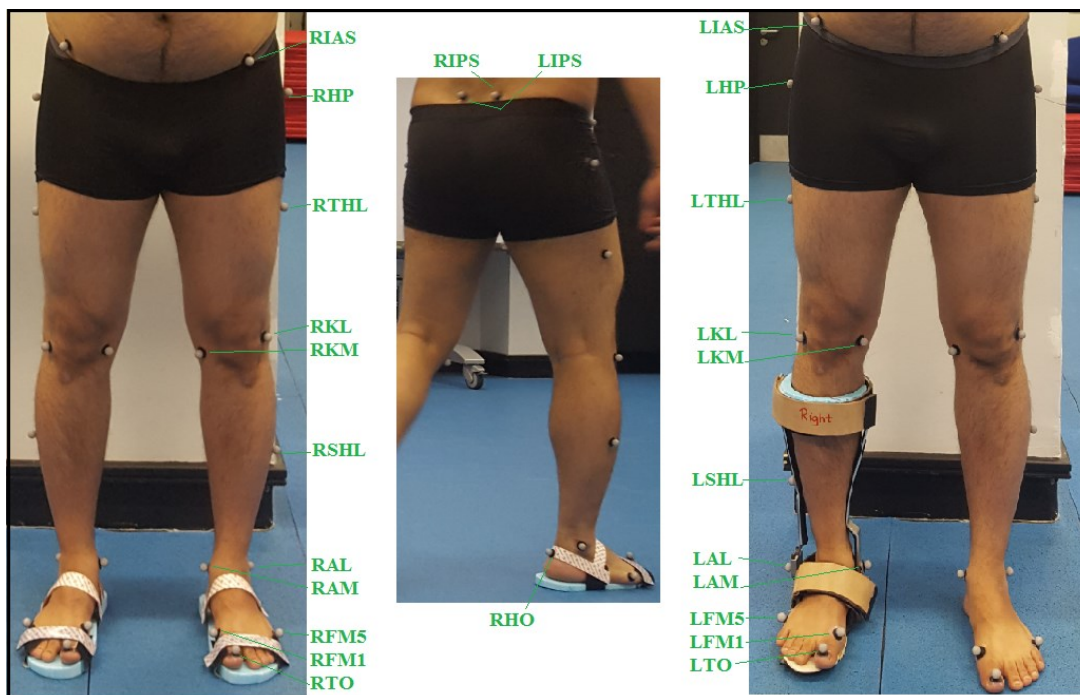


**Figure 3.3: Reflective markers attached to the lower limbs.**

The local motion capture facility consists of 12 motion capture cameras (Oqus cameras) and two force platforms (AMTI Gen 5 BP400600-2000). The supportive operating system is Qualysis track manager. The arrangement of the experimental setup is illustrated in Figure 3.4. The calibration of force plates and cameras was already set in that facility for a level walk. However, the motion capturing volume (work envelop of markers) was calibrated using a wand with a recommended standard

deviation <1mm that was achieved. The data recordings were performed at 1000Hz for the force plates and 400Hz for motion cameras. After setting the equipment, the instructions were given to each subject about walking pathway (8 meters) and start and end points such that first foot placed on one force plate and opposite on second force plate. For each of the walking conditions, the subjects were first asked to get familiar with/without a restricted motion and then the trials were recorded. Initially, static trials were recorded with subjects arms open and stand still upright posture. Static trials help in developing the skeleton model for each subject in the subsequent section. In the first phase, trials were recorded for the subject's self-selected slow, normal, and fast speeds. In the second phase, the trials were recorded by wearing wedged insoles i.e. for the everted and inverted foot. Both in walking speeds and rotational impairments, the markers were attached directly to the body (i.e. shank, ankle, and foot). Lastly, the trials were recorded from each subject by wearing an AFO and tuning the restrictions as described earlier in Table 3.4. By wearing AFO, it is impossible to attach markers directly to the body, hence, the markers were placed at the shank segment, shoe heel and ankle joint as illustrated earlier in Figure 3.4. A total of five trials were recorded per subject per walking condition.

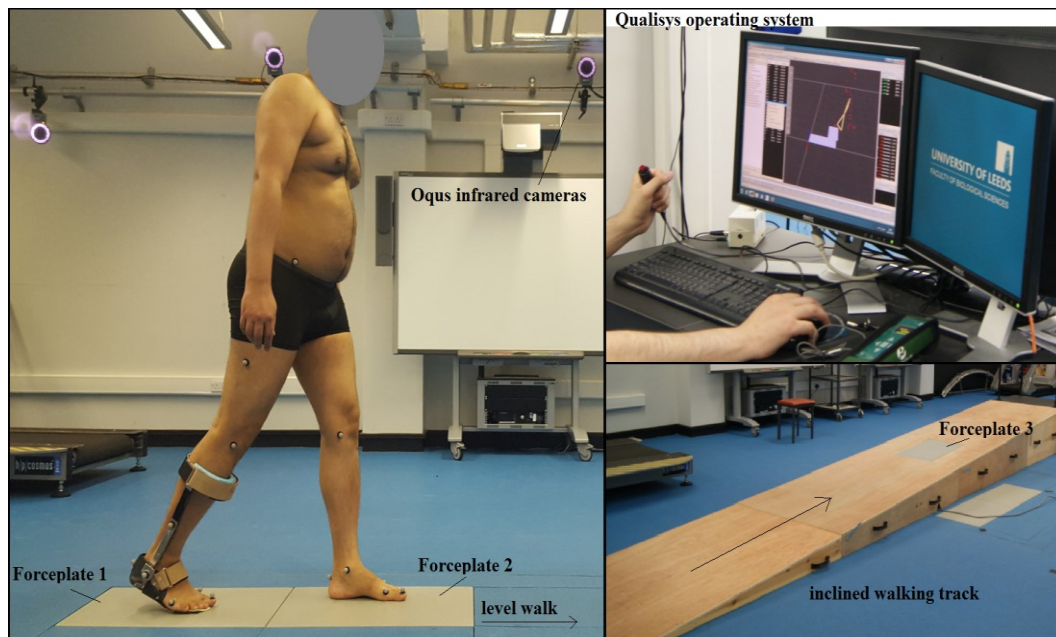


**Figure 3.4: Motion capture system is shown for level and inclined walks.**

For ramp ascend and descend activities, a wooden ramp of slope  $\pm 5^\circ$  and length 8 meters was placed in motion capture arena. A portable force plate was adjusted in the middle of the wooden pathway which consisted of four adjoining pieces. The force plate coordinates (x, y, z) were calibrated by measuring its four corners using CalTester apparatus with the detailed procedure described by c-motion [123]. The coordinates are estimated first without and then with interfacing force plate power cable in the system. In switching on the condition, the CalTester again positioned at

four corners of force plate and loads applied manually through CalTester. The Qualysis recordings were exported to Visual3D software as C3D files and positions of the centre of pressure (CoP) were noted. These CoP values were updated in the Qualysis software force plate settings. Finally, the working volume of reflective markers attached to the body was calibrated using a wand as described earlier for a level walk. For ramp ascend and descend activities, the trials were recorded for forward and rotational impairments following the procedures adopted earlier for a level walk.

### **3.4.3 Visual3D Motion Analysis System**

Visual3D is an advanced biomechanics analysis software designed by C-motion for 3D motion capture data [123]. The data captured using Qualysis software was in the form of QTM files. From Qualysis the markers and force plate data exported in the form of C3D files for each trial. The extracted C3D files were imported into Visual3D software. The reflective markers were labelled w.r.t anatomical positions as shown in Figure 3.5. The markers trajectories were interpolated and filtered to fill missing trajectories. Using markers coordinates of static trials, lower limb exoskeleton models were developed for each subject. Models were constructed using anthropological data (mass, height etc.), landmarks (virtual markers generated by interpolation) and built-in bone segments were adjusted at related markers positions e.g. pelvis, thighs, shank, and foot. The hip, knee and ankle joints presented in-between two segments (Fig. 3.5b). The stepwise model construction followed by C-motion supporting documents [124]. Further, the virtual foot was constructed in each subjects model using landmarks. A virtual foot helps to establish a neutral ankle angle by removing offsets and recommended for kinematic data collection.

After constructing models, the dynamic trials (C3D files) recorded from each subject were applied to respective models. A built-in event detection algorithm was applied to detect heel contact (HC) and toe-off (TO) gait events. The model-based data computed in anterior-posterior and medial-lateral directions for each of the walking conditions included lower limb joints angles, moments, and spatiotemporal parameters. In the anterior-posterior or forward direction, low limbs have their maximum ROMs, hence, mainly focused in subsequent sections. The temporal parameters require events detection from both limbs which were not possible for a ramp walk because a single portable force plate being used. The force plates raw data was extracted between HC and TO events and exported to Matlab software for stability analysis (discussed in section 3.5). The angles and moments data were filtered at 6Hz cut-off frequency using 4<sup>th</sup> order Butterworth filter [125, 126]. Each trial consists of 101 samples presenting a gait cycle (stance plus swing). The heel contact and toe-off events were used to detect stance and swing phases.

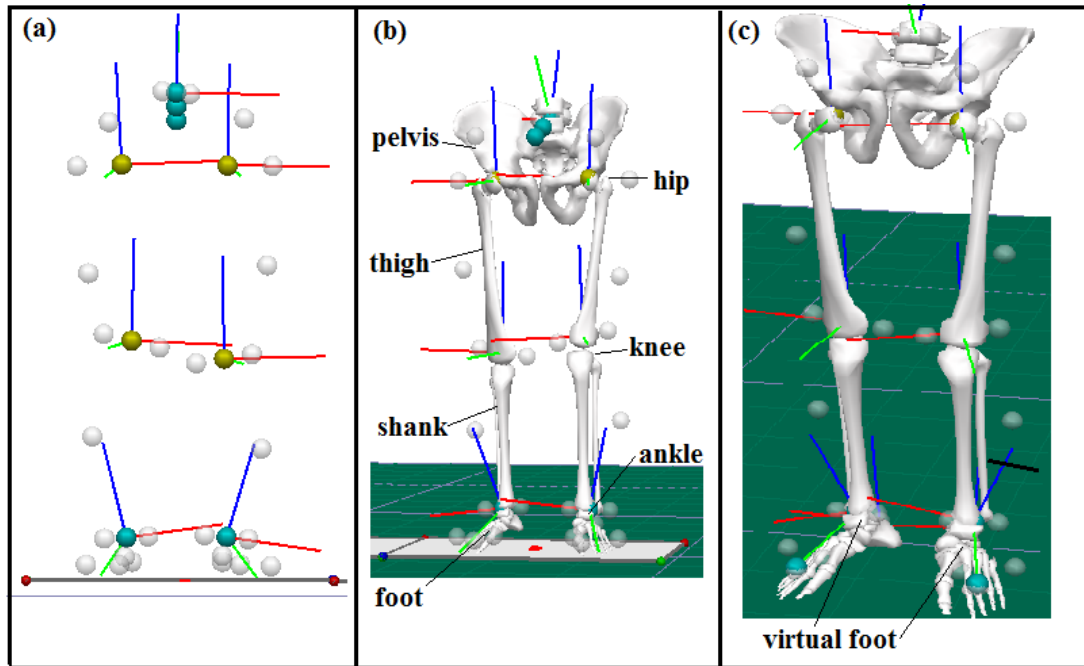


**Figure 3.5: Model building in Visual3D software. (a) markers positions, (b) kinetic model, (c) kinematic model with virtual foot design.**

#### **3.4.4 Spatiotemporal, Kinematic and Kinetic variations in Gait**

The angles and moments waveforms of lower limb joints (i.e. ankle, knee, and hip) are illustrated in Figures 3.6-3.10 for a level walk. The data (mean  $\pm$  Std.) presented in three groups i.e. walking speed, forward, and rotational impairments. The moment's data also exhibited net muscular force excursion in response to ankle-foot imitated impairments [51]. From angle waveforms, the range of motions (ROM) is computed for each of the three joints. The definition of ROMs and peak moments are followed from earlier studies [49, 50] and presented in Chapter 2 (section 2.2.3). For ramp ascend and descend activities, the corresponding plots are illustrated in Appendix C and discrete parameters are presented in Chapter 7 (Tables 7.9 and 7.10).

For statistical analysis, the mean value computed for each subjects parametric data. The normality in each parameter (sample size 11) was tested applying the Shapiro Wilk test ( $p > 0.05$ ). Observing normal distributions, a T-test was applied pairwise using SPSS-V23. In AFO restricted forward impairments, an AFO free mode walk was the reference to compare other restricted conditions. In walking speed and rotational impairments, a normal walk trials used as a reference. A parameter is considered statistically significant if  $p < 0.05$ . These discrete parameters were summarised in Tables 3.5 and 3.6 for a level walk and in Chapter 7 for a ramp walk where the bold numeric illustrating statistically significant differences in respective walking groups.

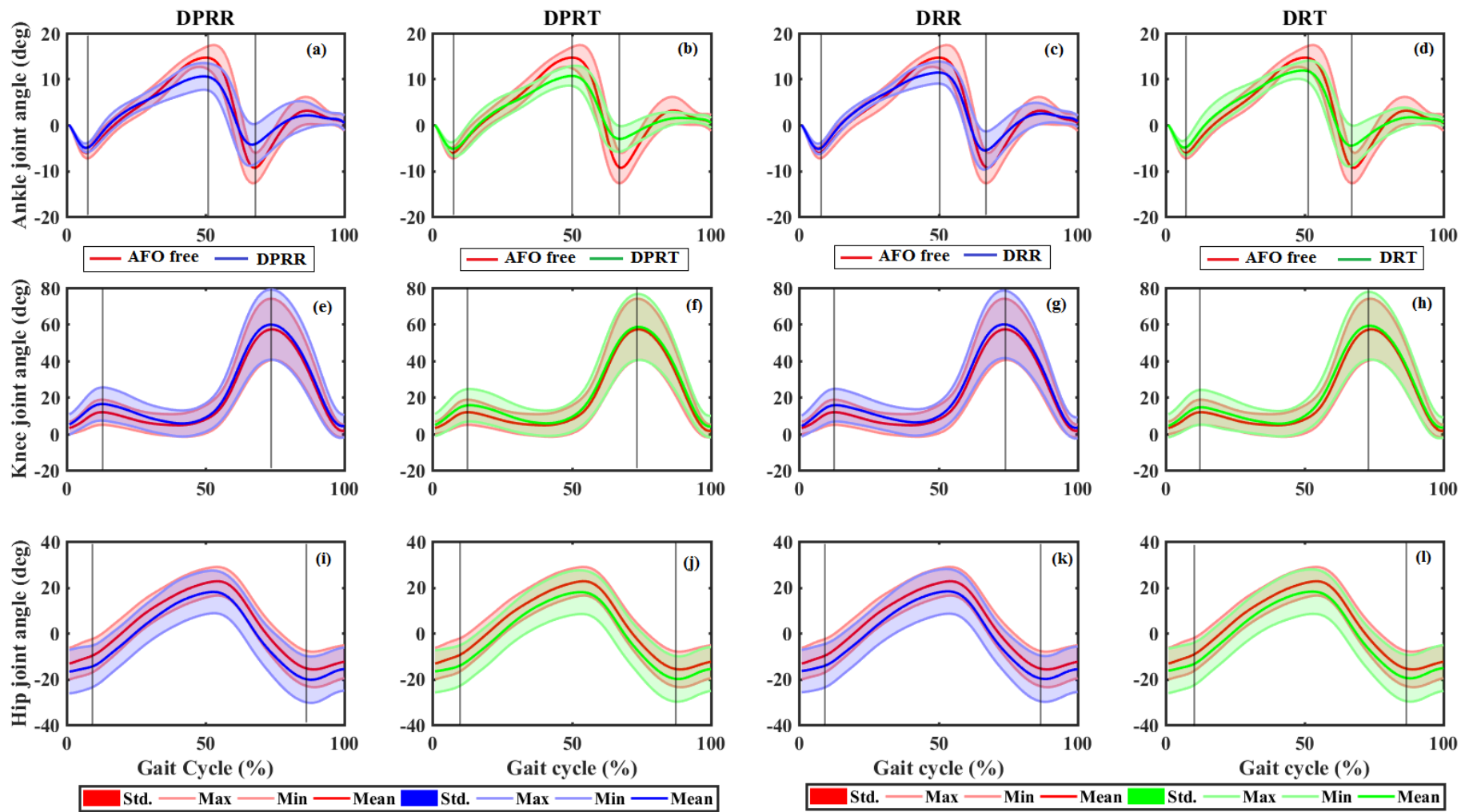


Figure 3.6: Ankle, knee and hip joints angles (N=11 subjects) for forward AFO restricted impairments during a level walk.



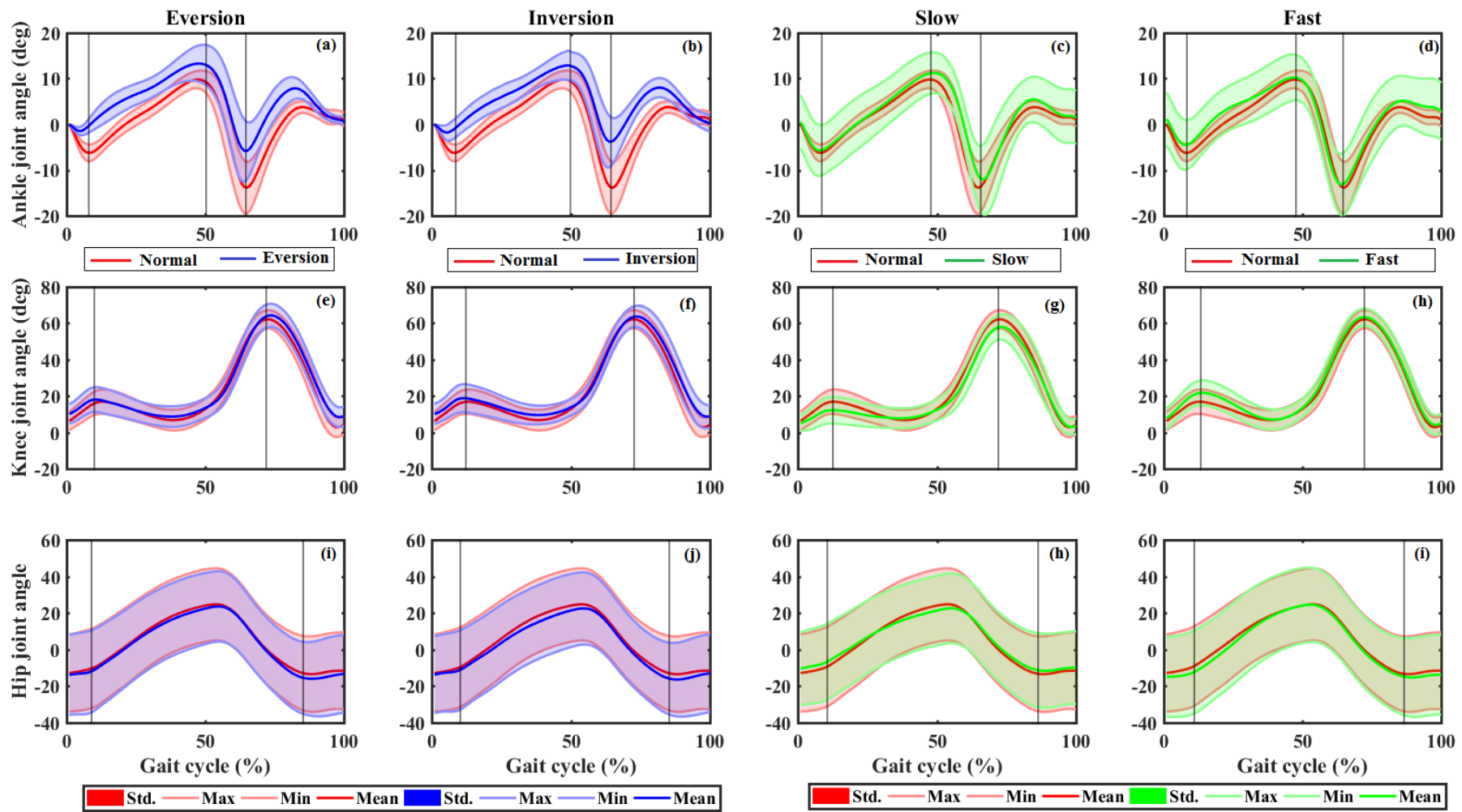


Figure 3.7: Ankle, knee and hip joints angles (N=11 subjects) for rotational impairments and walking speed group during a level walk.

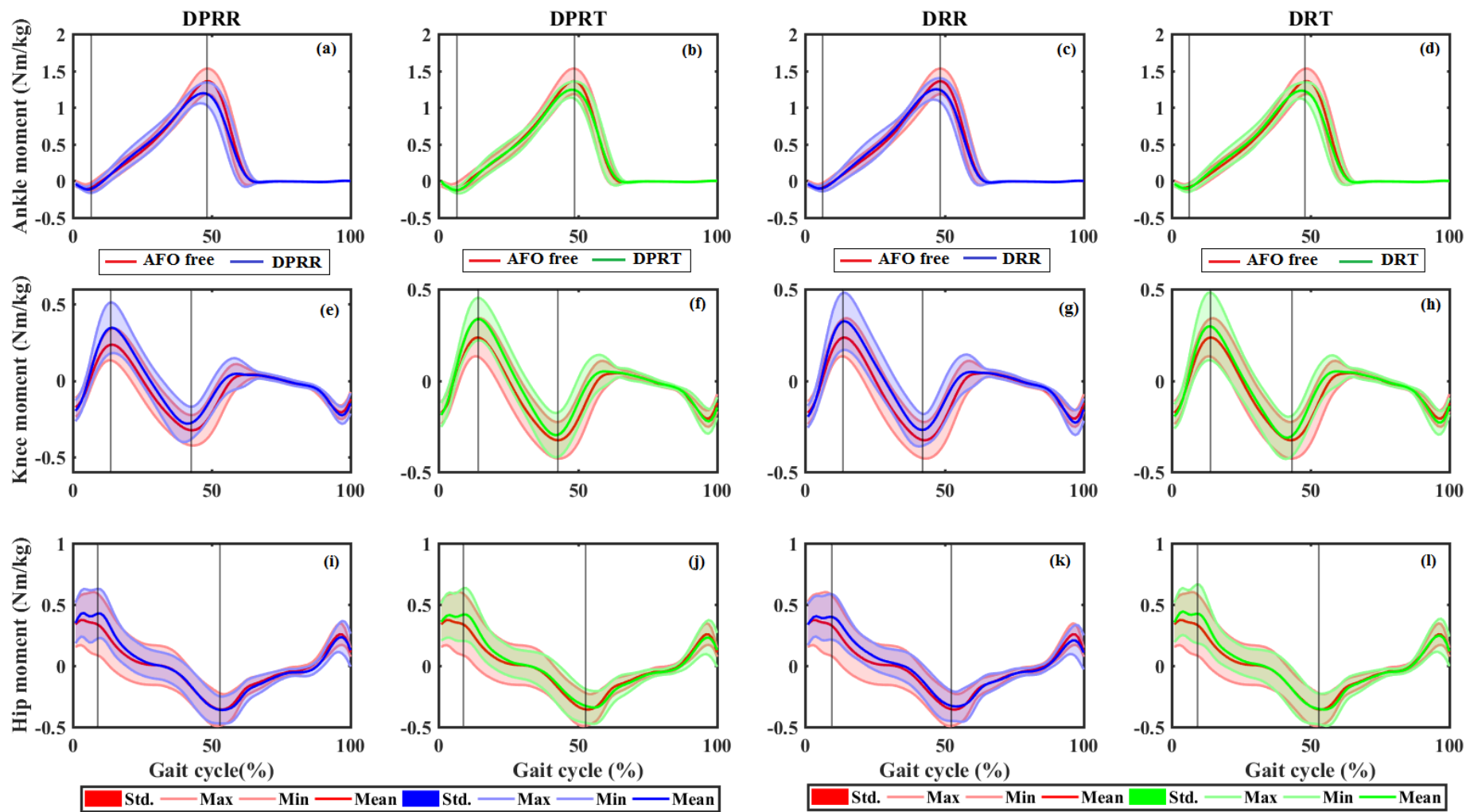


Figure 3.8: Ankle, knee and hip joints moments (N=11 subjects) for forward AFO restricted impairments during a level walk.

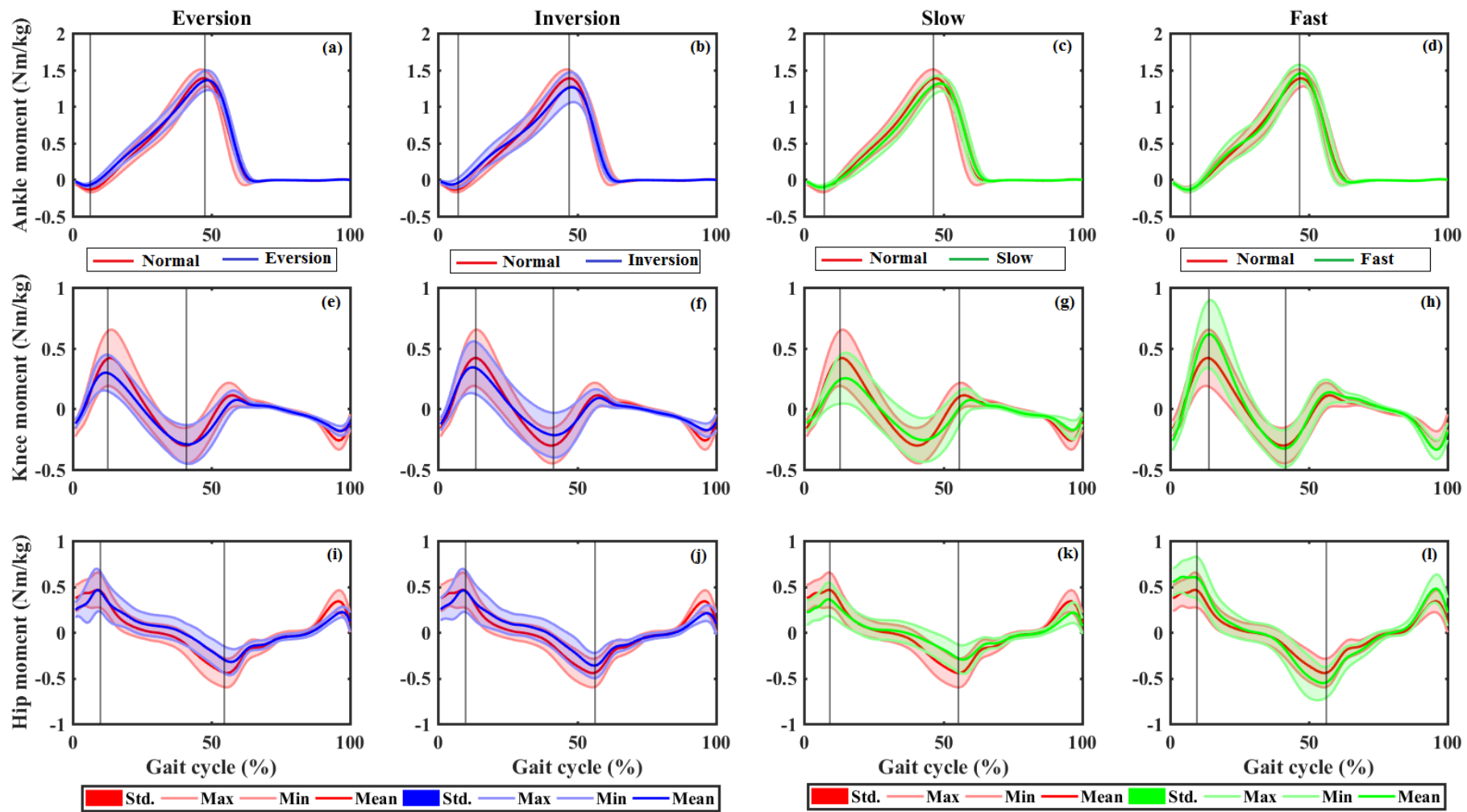


Figure 3.9: Ankle, knee and hip joints moments (N=11 subjects) for rotational impairments and walking speed group during a level walk.

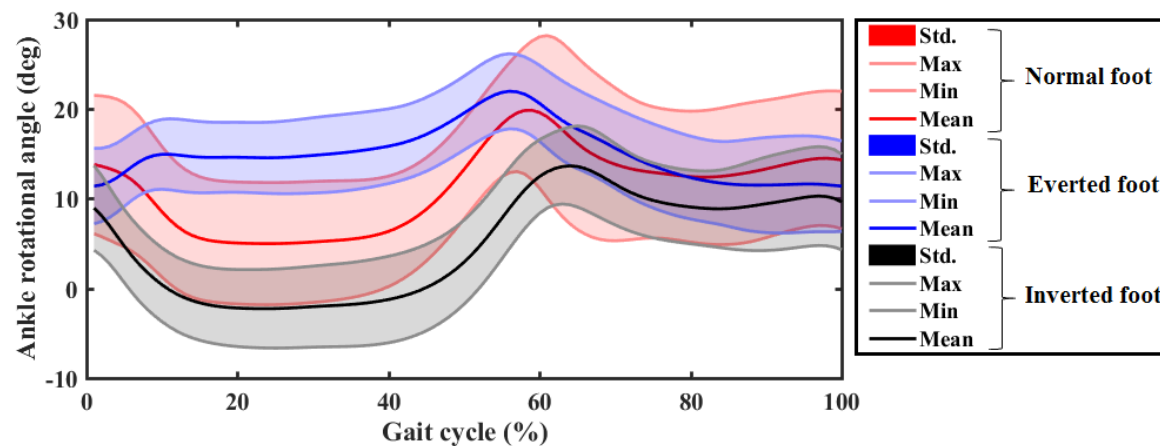


Figure 3.10: Ankle foot angle (N=11 subjects) in the rotational (ML) direction.

Table 3.5: Level walk lower limb joints angles and moments mean (standard deviation) data for forward and rotational impairments and walking speed group.

Parameters	AFO (free)	DPRR	DPRT	DRR	DRT	Normal	Eversion	Inversion	Slow	Fast
Initial peak plantarflexion angle (deg)	5.91 (1.44)	5.12 (1.01)	5.47 (1.44)	5.26 (1.16)	5.17 (1.59)	6.28 (1.82)	<b>1.56</b> (1.00)	<b>2.03</b> (1.74)	6.63 (2.09)	<b>5.54</b> (1.85)
Peak dorsiflexion angle stance (deg)	22.01 (2.49)	<b>16.07</b> (3.13)	<b>16.58</b> (1.72)	<b>17.13</b> (2.0)	<b>17.21</b> (2.06)	16.45 (2.08)	15.25 (3.8)	<b>15.07</b> (3.15)	17.3 (2.77)	15.29 (2.95)
Peak plantarflexion angle stance (deg)	15.9 (6.80)	<b>11.40</b> (5.28)	<b>10.48</b> (5.28)	12.62 (3.57)	<b>12.01</b> (4.31)	21.73 (4.36)	<b>18.53</b> (4.33)	<b>15.31</b> (5.12)	21.46 (4.14)	22.31 (3.93)
Knee flexion angle stance (deg) Cont....	8.96 (4.86)	<b>11.53</b> (4.96)	<b>11.27</b> (4.17)	<b>11.72</b> (4.36)	<b>10.52</b> (4.35)	11.19 (3.75)	<b>8.07</b> (2.44)	8.90 (3.70)	<b>7.23</b> (4.30)	<b>14.36</b> (3.6)

<b>Table 3.5(a) Continue</b>	<b>AFO (free)</b>	<b>DPRR</b>	<b>DPRT</b>	<b>DRR</b>	<b>DRT</b>	<b>Normal</b>	<b>Eversion</b>	<b>Inversion</b>	<b>Slow</b>	<b>Fast</b>
Knee flexion angle swing (deg)	58.04 (14.93)	60.88 (17.62)	59.28 (16.43)	60.69 (16.8)	60.06 (16.8)	62.33 (4.98)	64.42 (6.38)	63.89 (5.69)	<b>58.38</b> (6.75)	63.51 (4.79)
Hip extension angle in stance (deg)	37.63 (7.78)	37.07 (9.86)	36.68 (9.11)	37.25 (9.55)	36.81 (9.98)	37.24 (3.72)	37.52 (8.0)	36.40 (5.04)	<b>33.41</b> (3.49)	<b>39.53</b> (4.46)
Hip flexion angle in swing (deg)	40.28 (7.69)	40.74 (10.45)	40.06 (9.74)	40.27 (10.31)	40.11 (9.72)	38.90 (4.51)	40.68 (7.71)	39.97 (6.0)	<b>34.75</b> (3.02)	<b>40.90</b> (4.81)
Peak dorsiflexion moment (Nm/kg)	1.392 (0.175)	<b>1.233</b> (0.154)	<b>1.275</b> (0.127)	1.288 (0.15)	<b>1.273</b> (0.13)	1.402 (0.117)	1.365 (0.131)	<b>1.268</b> (0.198)	<b>1.33</b> (0.106)	<b>1.478</b> (0.139)
Peak plantarflexion moment (Nm/kg)	0.1006 (0.05)	0.126 (0.044)	<b>0.136</b> (0.043)	0.112 (0.035)	<b>0.141</b> (0.04)	0.139 (0.035)	<b>0.083</b> (0.024)	<b>0.079</b> (0.033)	<b>0.107</b> (0.026)	0.142 (0.027)
Peak knee flexion moment (Nm/kg)	0.317 (0.101)	0.307 (0.1)	0.267 (0.2)	0.295 (0.09)	0.298 (0.11)	0.314 (0.14)	0.305 (0.16)	<b>0.221</b> (0.18)	<b>0.272</b> (0.18)	<b>0.351</b> (0.13)
Peak knee extension moment (Nm/kg)	0.249 (0.1)	0.356 (0.16)	0.349 (0.11)	0.339 (0.147)	0.306 (0.18)	0.43 (0.23)	<b>0.305</b> (0.14)	<b>0.352</b> (0.2)	<b>0.265</b> (0.2)	<b>0.628</b> (0.27)
Peak hip flexion moment (Nm/kg)	0.345 (0.225)	<b>0.414</b> (0.1783)	<b>0.412</b> (0.179)	0.390 (0.166)	<b>0.419</b> (0.199)	0.420 (0.148)	0.382 (0.193)	0.395 (0.189)	<b>0.309</b> (0.151)	<b>0.564</b> (0.175)
Peak hip extension moment (Nm/kg)	0.341 (.097)	0.370 (.096)	0.362 (.127)	0.3432 (.118)	0.38 (.115)	0.401 (0.118)	<b>0.296</b> (0.091)	<b>0.322</b> (0.106)	<b>0.276</b> (0.134)	<b>0.508</b> (0.164)

Bold letters illustrate a statistically significant difference ( $p < 0.05$ ) applying T-test pairwise.

**Table 3.6: Spatiotemporal parameters mean (standard deviation) data for forward and rotational ankle-foot impairments for a level walk.**

Parameters	AFO (free)	DPRR	DPRT	DRR	DRT	Normal	Eversion	Inversion	Slow	Fast
Stride duration (s)	1.248 (0.097)	1.237 (0.106)	1.222 (0.078)	1.207 (0.078)	1.22 (0.117)	1.127 (.106)	<b>1.341</b> (0.140)	<b>1.301</b> (.170)	<b>1.34</b> (0.176)	<b>1.025</b> (0.077)
Initial double limb support (s)	0.157 (0.025)	0.151 (0.023)	0.150 (0.024)	0.143 (0.018)	0.144 (0.022)	.126 (.019)	<b>0.152</b> (0.032)	<b>0.147</b> (0.039)	<b>0.175</b> (0.039)	<b>0.103</b> (0.014)
step length (m)	0.581 (0.038)	<b>0.630</b> (0.606)	<b>0.633</b> (0.056)	<b>0.634</b> (0.044)	<b>0.642</b> (0.054)	.636 (.077)	<b>0.596</b> (0.051)	0.591 (0.045)	<b>0.57</b> (.066)	<b>0.706</b> (0.056)
Walking velocity (m/s)	0.962 (0.109)	0.982 (0.124)	1.00 (0.138)	1.014 (0.103)	1.015 (0.143)	1.132 (.151)	<b>0.915</b> (0.103)	<b>0.938</b> (0.115)	<b>0.86</b> (0.138)	<b>1.356</b> (0.141)

Bold letters illustrate a statistically significant difference ( $p < 0.05$ ) applying T-test pairwise.

### 3.4.5 Validation of Imitated Ankle-foot Impairments

The imitated ankle-foot impairments were validated using kinetic and kinematic data from prior studies. As mentioned earlier, CMT is the most diversified ankle-foot disease that might include forward and/or rotational impairments of varying degrees in different planes. In the forward direction, the outcomes from AFO restricted ankle-foot deficiencies are validated using CMT patients data from five published studies. A total of twelve parameters were evaluated from CMT patients ankle, knee, and hip joints trajectories for a level ground walk as summarised in Table 3.7. For comparison, the definitions of these discrete parameters were kept consistent with this study by evaluating each parameter directly from joints reported waveforms. This is because some studies reported parameters using an absolute reference (from zero axes) and others followed peak-to-peak differences (ROMs). Also, the markers placements, calibrations, different motion capture systems used, and analysis tools introduce offsets. Therefore staying consistent with the current study, the measurements were estimated directly from waveforms to minimise the offsets.

A comparison of this study with CMT studies is illustrated in Figure 3.11. For each parameter, a difference in normal subjects data (mean) and impaired subjects data (mean) was plotted. The data collected from five published CMT studies for healthy and impaired subjects such as foot drop (FD), and foot drop plus plantarflexion failures (FDP). Similarly, in the current study, the corresponding data was compared with a walk with AFO free mode (healthy), dorsiflexion restricted conditions (DRR, DRT impairments), and dorsi-plantarflexion restrictions (DPRR, DPRT impairments) respectively. The results showed significant variations in CMT patients data from one study to another compared to AFO restricted motions imitations. Overall, the parameters in this study (AFO imitations) are determined in range to that of CMT studies (marked with an asterisk) as shown in Figure 3.11. However, in imitated approach, the ankle joint showed more closeness with CMT studies w.r.t angles and moments compared to knee and hip joints which perform the compensatory mechanisms for a deficient gait. This might be because healthy subjects have better compensatory control compared to real patients. Considering rotational impairments, the peak difference in ankle eversion-inversion angle were found  $6.66^{\circ}(\pm 5.63)$  in the everted foot and  $6.77^{\circ}(\pm 2.49)$  in inverted foot compared to a normal condition. The foot insoles used for simulation had wedges  $\pm 10^{\circ}$  which implies that the subjects were flexible to accommodate rotational impairments to a certain degree. These ranges imitate moderate impairments and are consistent with a previous study [110]. The trajectories with rotational impairments were mostly reported for CMT patients who also had forward impairments in combination. Hence, direct validation of discrete parameters for rotational impairments alone is not possible.

**Table 3.7: Evaluation of lower limb angles and moments from studies included Charcot-Marie tooth patients.**

Parameters	Study 1 [127]			Study 2 [107]			Study 3 [15]			Study 4 [50]			Study 5 [128]	
	N	FD	FDP	N	FD	FDP	N	FD	FDP	N	FD	FDP	N	FDP
Peak dorsiflexion angle stance (deg)	18.5	16	22.5	18	17	13	15	12.13	10	10	12	16	20	20
Peak plantarflexion angle stance (deg)	16	16	1	20	6	14	10	10	6	10	5	5	20	10
Knee flexion angle stance (deg)	21.1	23.7	25.2	20	20	15	13	16	20	15	10	15.5	20	16
Knee flexion angle swing (deg)	65.6	65.5	62.3	62	57	55	60	60	62	55	65	45	65	55
Hip extension angle in stance (deg)	-	-	-	-	-	-	37	0	44	35	37	29	40	40
Hip flexion angle in swing (deg)	45	48.1	42	-	-	-	41.5	0	49	37	45	26	42	40
Peak dorsiflexion moment (Nm/kg)	1.1	1.2	0.9	1.2	1.0	1.0	1.4	1.22	0.8	1.25	1.6	0.5	1.2	0.9
Peak plantarflexion moment (Nm/kg)	0.15	0.01	0	0.1	-	-	0.1	0.06	0.08	0.25	0	0	0.2	0.015
Peak knee flexion moment (Nm/kg)	0.46	0.51	0.46	0.5	0.25	0.1	0.38	0.39	0.1	0.9	1.4	0.7	0.6	0.4
Peak knee extension moment (Nm/kg)	0.13	0.2	0.04	0.2	0.15	0.35	0.22	0.15	0.1	0.1	0	0	0.25	0.15
Peak hip flexion moment (Nm/kg)	-	-	-	-	-	-	0.39	0.34	0.42	0.25	0	0.5	0.5	0.5
Peak hip extension moment (Nm/kg)	0.5	0.36	0.43	-	-	-	0.55	0.58	0.5	1.4	1.6	1.4	0.4	0.45

N: normal/control subjects, FD: foot drop or dorsiflexion failure, FDP: foot drop and plantarflexion failure.



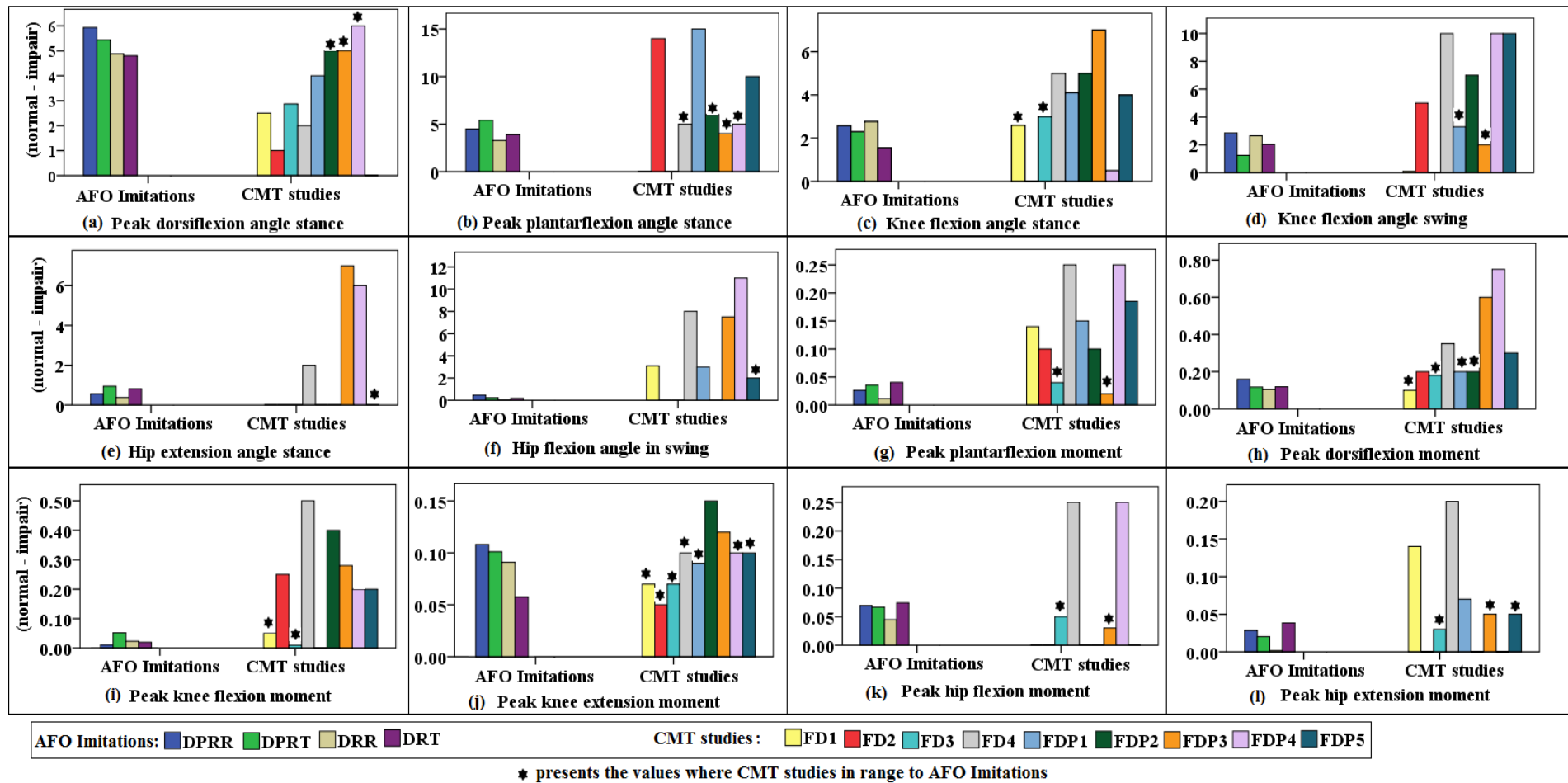
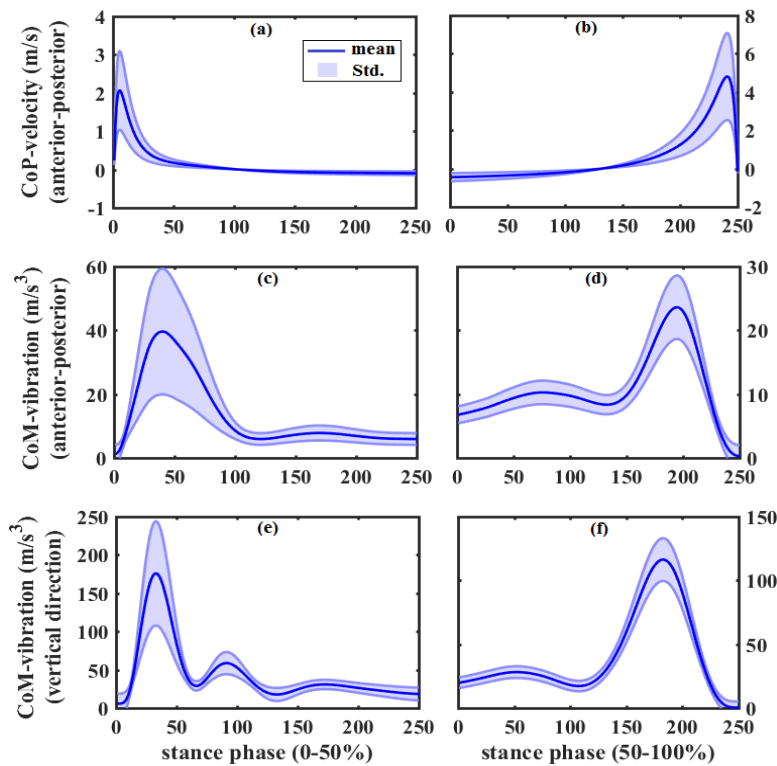


Figure 3.11: Peak joints angles and moments comparison between AFO imitations and CMT patients data.

### 3.5 Gait Dynamic Stability Measurement Signals

In this study, the force plates data were collected as the centre of pressure (CoP) and ground reaction forces (GRF) as 2D and 3D signals respectively. Bipedal dynamic activities take place by continuous transformations of kinetic and potential energies from one limb to another while interacting with the ground/environment. These gait transitions are also named as weight loading and weight unloading phases. The lower limbs joints (ankle, knee, and hip) generate moments and angular motions through muscles illustrated by bursts of activities during these transient phases (i.e. around HC and TO). Recent studies reported that the amplitude and timing of these bursts scaled according to CoM-acceleration signals [42]. Thus the CoM-acceleration information is essential to accurately generate muscles activities in response to perturbations provided here by restricting ankle-foot motions. Summarising, the rate of change in CoM-acceleration provides sensory inputs and the rate of change in CoP provides resultant output responses. Both signals illustrate impulsive responses as shown in Figure 3.12 for loading and unloading phases and variations in their amplitudes and time delays are modelled to quantify stabilities. The CoM-accelerations have maximum magnitudes in vertical and anterior-posterior directions and CoP has a maximum displacement in the anterior-posterior direction. Following prior studies [2, 31, 129], these signal were analysed in the directions of their maximum variations.



**Figure 3.12: Rate of change in CoP and GRFs illustrate impulsive responses (N=11 subjects).**

### **3.6 Modelling and Stability Analysis Algorithms**

The proposed stability methods require mathematical models of the plant (system) either in a linear or non-linear form. A non-linear approach is normally avoided due to the complexity of analysis and predictive accuracies. For linear models, the plant outputs are required to satisfy the linearity assumption. In this section, the requirements and procedures applied to analyse the plant outputs are discussed theoretically, however, the implications for individual signals are discussed in subsequent chapters.

#### **3.6.1 Linearity and time invariance of Measured Signals**

Before modelling, the linearity in the measured waveforms is required to be evaluated. The time domain waveforms illustrated transient responses of the system with varying amplitudes decay/rise over time. The baseline of unstimulated plant returns to the starting point in output impulsive signals. That illustrated the system (plant) returns towards the starting point with zero inputs [130]. In this modelling scenario, principal component analysis can be applied to determine whether a system can be modelled as a linear system or not. A small number of principal components (PCs) those explain larger variances over time give the indication of a linear and time-invariant system. Oppositely, if PCs changes significantly over time then that indicates a non-linear and time-varying system [130]. Therefore, PCA is implemented in the current study to verify linear time-invariant (LTI) system responses. The PCA implementation for the individual signal is presented in subsequent chapters.

PCA is a dimension reduction technique in which a data set is transformed to orthogonal coordinates each called principal component (PC). These components are mutually uncorrelated, independent, and capture maximum information from the original data set. The components which explain maximum variances are retained while those with lesser variances are discarded. PCA has multiple applications including data processing, dimension reduction, clustering, and wavelet analysis. Depending on the application, the variables are included in the input dataset. In this study, the objective is to linearize the system by removing the artefacts in the waveforms. Therefore, the measured waveforms are linearized following studies [130, 131] and variability are computed in individual walking conditions following [81]. Similar PCA applications for linear modelling and waveform reductions are summarised in Table 3.8.

**Table 3.8: PCA applications relevant to the current study for waveform reduction and/or linearity analysis.**

Study	PCA application
Sklavos. S., et. al. [130, 131]	PCA applied to linearize waveforms collected from eye muscles activations and thereafter modelled in time and frequency domains as transfer functions.
Tan. M. H., et. al. [132]	PCA applied to estimation linear time invariant single input single output transfer function named as system identification process.
Maslivec. A., et. al. [81]	PCA applied to determine variability in each of pelvic, trunk and head signals (angular displacement) for young and old groups.
Soares. D. P., et. al. [113]	PCA model was constructed using control subjects data and applied to simulated conditions. The waveforms reconstructed for each of the six gait parameters in each walking condition.
Soares. D. P., et. al. [133]	PCA model constructed for each of GRF and COP data collected from using control subjects and applied to transfemoral amputees.
Yli-Ollila. H., et. al. [134]	Electrocardiogram repeated signals collected from radial and longitudinal axes of the carotid artery and PCA applied to each axis and subject's data and output waveforms reduced in noise.
Downes. T. D., et. al. [135]	Data collected from an array of bolometers and PCA applied to remove correlated data (noise removal) and transfer functions estimated from reduced signals of interest.
Xu. S., et. al. [136]	PCA used to reduce noise in current waveforms while measuring electrolyte impedance with the triangular wave input voltage.
Patel. R., et. al. [137]	Artefacts removed from EEG sensor waveforms collected from scalp applying PCA.
Lankinen. K., et. al. [138]	PCA applied to remove artefacts from MEG signals collected from human brain using sixteen subjects repeated trials.

PCA helps to model the data with linear equations of varying degrees by removing the redundancies. PCA was implemented in Matlab with the following mathematical interpretations.

$$X = \begin{bmatrix} t_{11} & \cdots & t_{1p} \\ \vdots & \ddots & \vdots \\ t_{n1} & \cdots & t_{np} \end{bmatrix} \quad (3.1)$$

$$[\text{coeff, score, latent, tsquared, explained, mu}] = \text{pca}(X) \quad (3.2)$$

where

**X**: input data matrix with  $n$  rows and  $p$  columns, rows present samples or observations, columns present the variables or trials.

**coeff**: coefficients or loadings is  $[p \times p]$  square matrix and each column presents a principal component (PC),  $\text{coeff}(i, j)$  presents loading variable  $i$  in principal component  $j$ , the first column represents maximum variance.

**score**: input data 'X' transformed to PC space with same matrix size  $[n \times p]$ ,  $\text{score}(i, j)$  present the row  $i$  of input matrix decomposed over the principal component  $j$  such that:

$$X(i, :) = \text{score}(i, 1) \times \text{coeff}(:, 1) + \text{score}(i, 2) \times \text{coeff}(:, 2) + \dots + \text{score}(i, p) \times \text{coeff}(:, p) \quad (3.3)$$

**latent**: variance explained by each principal component.

**explained**: percentage of variance explained by each PC, helps to decide how many PCs to keep.

**tsquared**: Hotelling's T-squared statistic gives a measure of each observation's distance from the centre of the entire dataset, useful to identify outliers.

**mu**: presents the estimated mean of each variable in X.

The output waveforms are reconstructed (Eq. 3.4) by multiplying a coefficient matrix with a selected number of principal components (coefficients) and the adding mean of the input matrix.

$$\text{reconstructed} = \text{score} \times \text{coeff}' + \text{repmat}(\text{mu}, n, 1) \quad (3.4)$$

The criteria of retaining principal components reported earlier as the number of PCs which explain variances  $>80\%$  in accumulation should be used in reconstructing the output waveforms [139].

### 3.6.2 Modelling in Time and Frequency Domains

Considering modelling approaches, a transfer function (TF) is either modelled using physical laws of body's dynamics assuming the lower limb motion as a rigid inverted pendulum structure [21, 93, 140, 141] or modelled empirically using resultant data from human experiments [34, 80, 92]. In this study, the second approach is adopted in which the data extracted from human trials (GRF) are fitted to the empirical models. The second modelling approach is further reported in two ways, firstly, parameters are estimated from time/frequency data and fitted to an empirical models [2, 92], secondly, curve fitting tools are applied to the time series data and transfer functions are obtained after Laplace transformation [34], or system identification tools are used to fit a frequency domain model (TF) directly to the experimental data [80]. In the

first empirical modelling approach, an oversimplified fixed 2<sup>nd</sup> order model fitted with constants from experimental data is used with limitations of missing system's dynamics and best-fit assessment. In the current study, both CoP-velocity and CoM-vibrations are modelled using curve-fitting tools applying system identification approach in Matlab. A hierarchical method of model identification is adapted from [142] and illustrated in Figure 3.13.

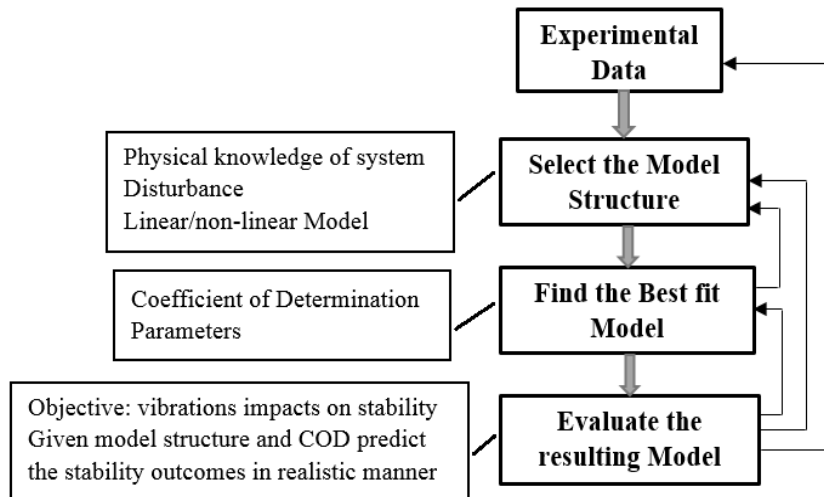


**Figure 3.13: Hierarchical approach of empirical modelling, applied to the CoM-vibrations data from imitated walking conditions.**

The selection of the appropriate model mainly depends on its application and the prior knowledge of the physical system. Further, the selection of best fit model versus a number of parameters was reported to be optimised, however, there were no fixed criteria reported previously. These criteria of model estimation are reported earlier in a webinar [143] and a manuscript [142]. Considering the stability viewpoint, any compromise in the best fit model over the number of parameters may induce lead/lag in either magnitude or time axis in the model's outputs. Later, these time/magnitude difference from the actual data revealed an error in the stability margins to be quantified ultimately.

In control engineering theory, almost all physical linear system models come out with Laplace solutions in the form of exponential, sinusoids, or combination of both. Hence, the experimental waveforms are modelled using least square regression algorithms and best fit models are determined based on the inherent shape of signals (impulse, sinusoid) and root means square error (RMSE). A best-fit model is described by the coefficient of the determinant ( $R^2$ ) in percentage. These models are similar to the models built in motion analysis software and used to compute various lower limbs trajectories. The mean data of each subject in each walking condition is modelled as a function of time. These time domain algebraic equations are transformed into the frequency domain by Laplace transformation. Each plant model

in the frequency domain is named as transfer function (ratio of output polynomials to unit input in the frequency domain). Further modelling details are provided in subsequent chapters for individual signals and walking conditions.

### 3.6.3 Nyquist and Bode (N&B) stability methods

Nyquist and Bode's methods are control engineering techniques in which a plant (system) is first modelled, observing its stability margins, a controller is designed that either stabilise an unstable plant or brings a plant's performance close to desired specifications. The plant model presents characteristics of a physical system mathematically and relates outputs in response to inputs. In this study, the lower limb is modelled as a plant (Figure 3.14) and its output responses are measured by resultant CoP or GRF signals assuming unit impulse inputs. The GRF (CoM-acceleration) also acted as somatosensory feedback to neuromotor, hence, is presented as inputs in the subsequent chapters. In this study, N&B methods are employed to quantify the stability margins of a plant. In simple words, these methods provide a mathematical way of scaling the bipedal stabilities using fixed reference thresholds.

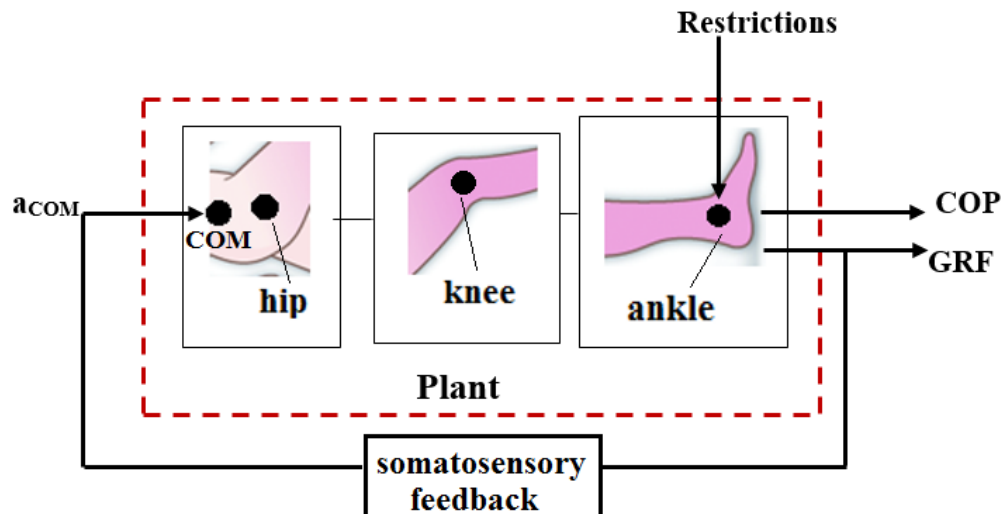


**Figure 3.14: Lower limb modelled using plant outputs responses and unit impulse inputs.**

Theoretically, a plant model is Laplace solution of a time domain differential equation called transfer function (TF). There are two examples of plant TFs described in Table 3.8 in support of the ongoing discussion. The roots of denominator polynomial of a TF are used in s-plane (frequency domain plane in which signals presented by complex numbers) to differentiate whether a system is stable (if lying in left half) or unstable (if lying in the right half). The existence of a single denominator root on right half or imaginary axis of s-plane makes the system unstable. However, the exact magnitude of stability of a plant is not predictable from the simple location of roots and quantified further applying Nyquist and Bode methods. In N&B methods, a unit impulse input is provided in the feedback and stability margins are computed. A range

of frequencies are put into a TF ( $s = j\omega$ ) and TF plotted on a logarithmic scale as gain (decibel) and phase (degree) plots.

In the gain plot, a zero decibel (0dB) axis is a reference, and in phase plot, a  $\pm 180^\circ$  and its multiple ( $\pm 2k\pi$ ) are reference axes. The points where gain plot cuts '0dB' and phase plot cuts ' $\pm 180^\circ \pm 2k\pi$ ' are critical to quantify stabilities. At these cut-off frequencies, gain and phase plots differences with respective references (0dB,  $\pm 180^\circ \pm 2k\pi$ ) provide the gain margins (GM) and phase margins (PM) respectively. The mathematical derivation of cut-off references (0dB,  $\pm 180^\circ \pm 2k\pi$ ) is discussed later. GM and PM are defined as:

**Gain Margin (GM)** - Gain margin presents the difference of system's gain from 0dB at a frequency where the respective phase plot cuts  $\pm 180^\circ \pm 2k\pi$ . It presents the amount of open-loop gain that can be increased or decreased before a closed-loop system becomes unstable if originally stable or becomes stable if originally unstable.

**Phase Margin (PM)** - Phase margin presents the difference of system's phase from  $\pm 180^\circ \pm 2k\pi$  at a frequency where the gain plot cuts 0dB. It presents the amount of open-loop phase that can be increased or decreased before a closed-loop system becomes unstable if originally stable or becomes stable if originally unstable. Alternatively, the PMs are used to quantify the time delay ( $-\Delta\theta_{max}\omega$ ) tolerances before a system becomes unstable [144].

The minimum absolute values of these margins are critical and used to specify the system's stability without controlling it. In the phase plot, the minimum value of the phase margin is measured between  $+180^\circ$  and  $-180^\circ$  axes. In the current study, the minimum values of GMs and PMs are evaluated and compared for lower limb stability analysis. The Nyquist and Bode plots are implemented in Matlab using built-in functions and for theoretical understanding, examples are illustrated in Table 3.9.

Another related concept is minimum and non-minimum phase TFs. A non-minimal phase system has one or more roots (poles/zeros) on the right half of s-plane (Example 2 in Table 3.9). Nyquist and Bode's methods are equally applicable for minimal phase systems, however, for non-minimal phase system, results from Bode methods are also recommended to be confirmed from Nyquist methods which are considered more authenticated for distinguishing stable/unstable regions [100]. However, Bode plots are simpler with its easy graphical representation with distinct gain and phase plots, hence, more widely used in control engineering.



**Table 3.9: Examples of Transfer functions minimum phase (MP) versus non-minimum phase (NMP).**

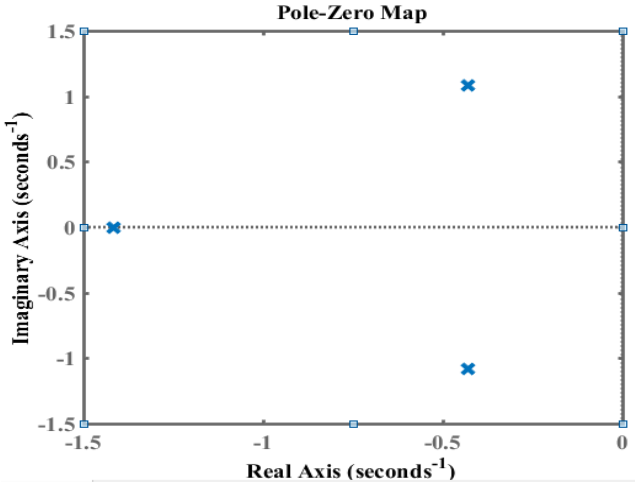
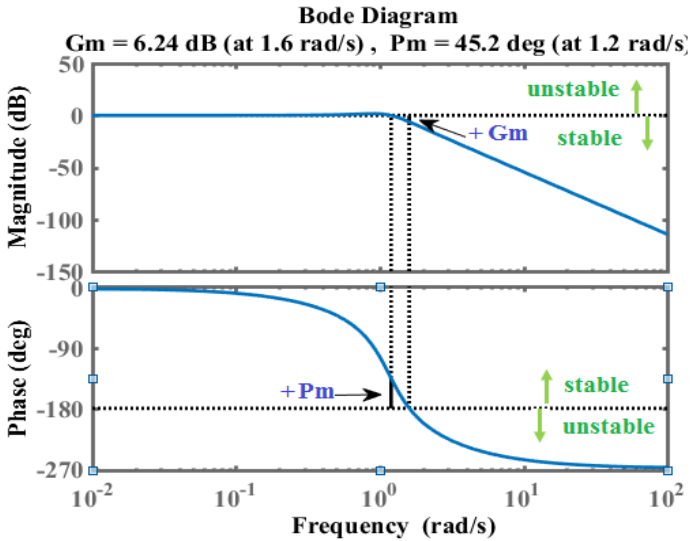
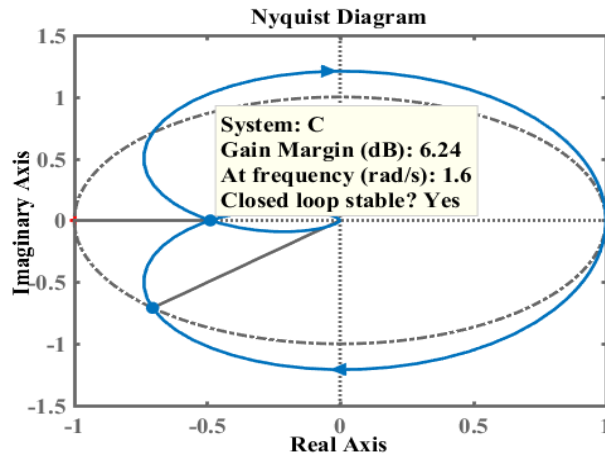
Transfer Functions	Stability Analysis
Third order TF minimum phase	<p>1). <math>C(s) = (1.9)/(s + 1.4)(s^2 + .8s + 1.3)</math> where <math>s</math> is frequency operator equivalent to <math>j\omega</math></p> <p>2). Location of denominator root (poles) in s-plane:  <math>-0.4294 + 1.0811i</math>, <math>-0.4294 - 1.0811i</math>, <math>-1.4174 + 0.0000i</math>                      all poles on left half implies system <math>C(s)</math> is stable.                      all roots on left half also implies minimum phase system.</p>  <p>3) bode(C) shows minimum stability margins for a stable system</p>  <p>nyquist(C) illustrates equivalent plot as</p>

Table 3.9 Continue



**Note:**  
**(stability criteria)**

Most of the control engineering texts used polarity concept i.e.  $\pm GM$  to distinguish stable (+) and unstable (-) system, whereas Yazdan Bavafa-Toosi [145, 146] settled these subtleties such that:

Stable MP system	GM: positive/negative, PM: positive
Unstable MP system	GM: positive/negative, PM: negative
Stable NMP system	GM: positive/negative, PM: positive/negative
Unstable NMP system	GM: positive/negative, PM: positive/negative

The widely used software Matlab functions simulate this criteria correctly. A system can be stable with positive/negative margins, for a stable system these present distance from unstable region, and for unstable system these present distance from stable region. The cut-off point is  $(0dB, \pm 180^\circ \pm 2k\pi)$ .

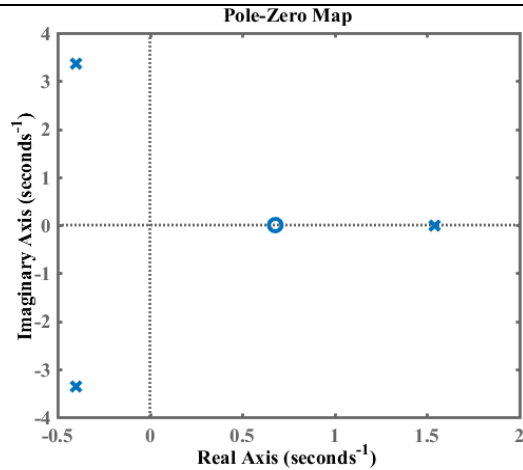
Third order TF non-minimum phase

1).  $C(s) = 26(s - 0.6)/(s - 1.5)(s^2 + 0.8s + 11.4)$  where  $s$  is frequency operator equivalent to  $j\omega$

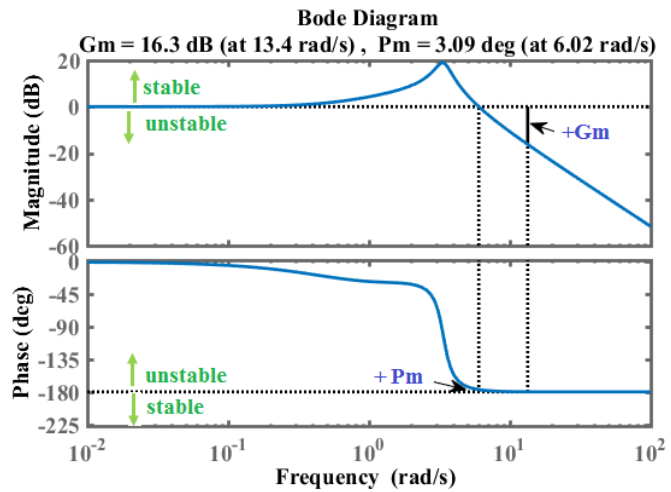
2). Location of denominator root (poles) in s-plane:  
 $-0.4016 + 3.3523i$  % left half  
 $-0.4016 - 3.3523i$  % left half  
 $1.5408 + 0.0000i$  % right half

Location of numerator root (zeros) in s-plane:  $0.6$  % right half  
 one pole on right half implies system  $C(s)$  is unstable.  
 one pole and one zero on right half implies non-minimum phase system.

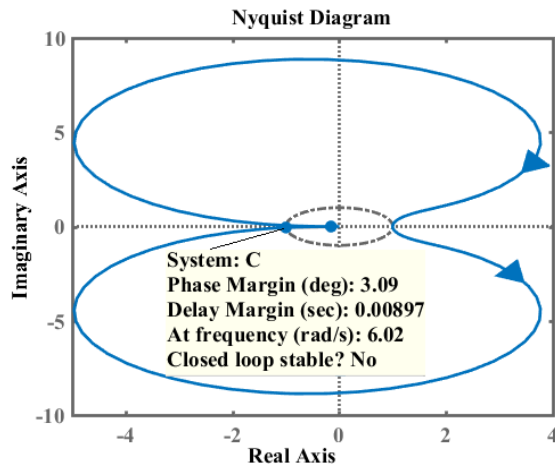
Table 3.9 Continue



3) bode(C) shows minimum stability margins for an unstable system



nyquist(C) illustrates equivalent plot as



Stability measures the tendency of a system to return to equilibrium after being disturbed (Figure 3.15). Stability margins define how far a system is from point of instability for a stable system. For an unstable system, these margins provide

magnitude differences to get in a stable region. Therefore, the cut-off point is (0dB,  $\pm 180^\circ \pm 2k\pi$ ) also referred to as (-1, 0j) The mathematical derivation of this point is illustrated in Figure 3.16.

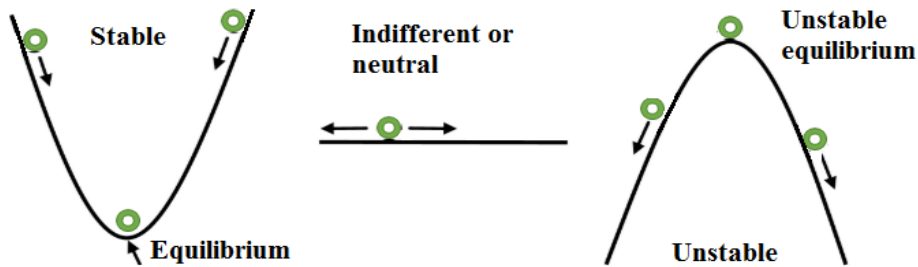


Figure 3.15: Stable and unstable equilibrium conditions.

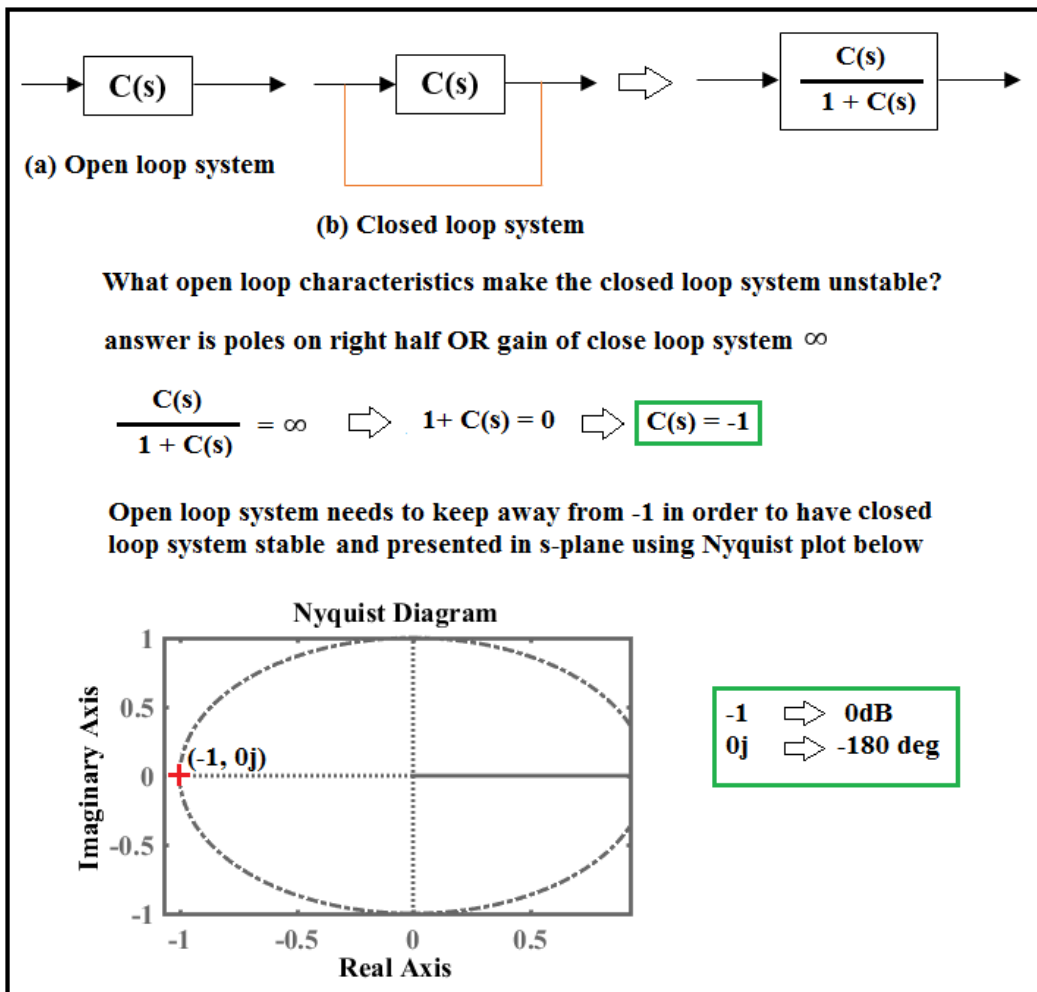


Figure 3.16: Mathematical interpretation of critical point of instability (-1, 0j).

Considering lower limb biomechanics, the application of N&B methods are categorised into three types. Firstly, these methods have been widely used in the design and control applications of biomedical robotics e.g. orthotics, prosthetics and exoskeletons [141, 147-149]. These devices are designed based on spring-mass-damper lower limb models and gait dynamics from real subjects are programmed to mimic lower limb trajectories. Secondly, N&B methods are moderately applied in

muscles biomechanics [150-152]. Thirdly, these methods are mildly applied to analyse gait specific aspects [92, 94-97, 153]. This study is an extension to third application and provides an alternative technique to quantify gait transitional stabilities. A brief overview of these applications is presented in Table 3.10.

**Table 3.10: Nyquist and/or Bode methods in lower limb biomechanics modelling and stability analysis.**

Study	N&B method applications
Morgan. D. K., et. al. [34, 35, 94]	N&B method applied to quantify knee stability using knee joint angles from healthy and cruciate ligament reconstructed
Ardestani. M.M. et. al. [36]	Bode method applied to quantify knee stability using knee power output from total knee arthroplasty simulations
Hur. P., et. al. [37]	N&B method applied to evaluate postural control in the presence of impulsive perturbations
Mahmood. I., et. al. [95-97]	N&B applied for stability analysis of gait transitional phases for level walk, inclined walk and rotational foot impairments
Alshabi. M., et. al. [153]	Two models simulated to present humanoid bipedal dynamics and Bode pots showing the responses of seat, head and lumbar spine segments.
Elhasairi. A., et. al. [141]	A linear inverted pendulum model developed for lower limb motion and controller designed for standing balance of humanoid robot.
Ficanha. M. E., et. al. [147]	A compliant cable driven ankle-foot plant model developed and controlled by applying N&B methods.
Karavas. N., et. al. [148]	A knee exoskeleton plant designed and controlled using Bode method
Rahman. S. M. M., et. al. [149]	An AFO modelled using a spring-mass-damper system and controller design applying Bode methods
Orizio. C., et. al. [152]	Torque output modelled as gain and phase plots for two study groups in response to electrical stimulation applied tibial anterior
Itoh. Y., et.al. [150]	Skeletal elbow muscles modelled in the frequency domain (TFs) and contractile properties evaluated using Bode plots
Orizio. C., et. al. [151]	MMG force and frequency response from cat medial gastrocnemius muscles are modelled as gain and phase plots
Hidler. J. M., et. al. [92]	For a spastic gait, ankle plantarflexion motion characterised in frequency domain applying Bode methods

### 3.6.4 Stable and Unstable Gait

There is no strict definition reported in literature [10, 11, 88] for a stable or unstable gait, because, a human walk can be unstable (probable to fall) during either portion of a gait cycle divided into heel rocker/loading, ankle rocker and toe rocker/unloading phase of stance as illustrated in Figure 3.17. However, prior studies applied principles of mechanics in relation to human gait to define stable/unstable notions for a normal or healthy gait. Considering the heel rocker (loading) phase, the foot area of contact increases, ankle-foot joint decelerates, and body's CoM sways within BoS, hence loading phase reported as a stable gait phase. In comparison, during forefoot rocker (unloading) phase, the foot area of contact decreases, ankle-foot accelerates to generate peak push-off, and body's CoM sways outside the BoS implied unloading as an unstable gait phase.

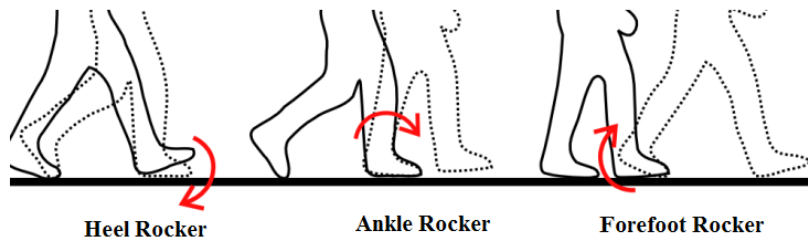


**Figure 3.17 Stance phase of a gait cycle divided into sub-phases. adopted from [58]**

Further, each of the stability assessment methods used its own algorithm to scale walking stability. A decrease in testing group thresholds (whether it quantifying stable/unstable phase) compared with outcomes from a control group is reported as a potential measure of unstable gait or risk of fall in more severe cases. This study discussed stability evaluations for symmetrically repeated walking conditions.

### 3.7 Comparison between past and proposed stability measures

The objective of current (N&B) and earlier mentioned (Chapter 2) stability methods is to scale the magnitude of balance/imbalance for applications like before/after an impairment, before/after rehabilitation, or with/without gait assistive devices. Considering the fact, the methods reported for such evaluations are categorised here based on discrete and continuous time series input waveforms as illustrated in Figure 3.18. Considering discrete events based evaluations, the extrapolated-CoM and BoS difference method i.e. MoS quantify stable response at HC (CoM within BoS) and unstable response at TO (CoM outside BoS) events. These two events also exhibit start and end points of loading and unloading inner gait phases and provide an estimation of stability trends being followed thereafter. The transitional stability evaluation methods proposed in current research (N&B methods) also reinforced the



### 3.8 Effect of extreme walking speeds on transitional stability

The N&B methods introduced in this study are used to quantify gait transitional stability as a gain margin (amplitude) and phase margin (time difference). In order to understand the effect of walking speed on these two quantitative outcomes, an experiment was also conducted using a single subject (to reduce inter-subject variances). A subject was asked to walk very slow (with little/no foot lift), slow, normal, fast, and very fast self-selected walking speeds (Table 3.11). A set of five trials was recorded for each of the walking speeds and the aforementioned stability evaluation criteria were applied. The results from neuromotor output signals i.e. CoP-velocity are discussed in Chapter 4 (section 4.4.6). Similarly, the outcomes from neuromotor inputs i.e. CoM-acceleration are discussed in Chapter 5 (section 5.4.10) for the forward direction of motion and presented in Chapter 6 (section 6.4.4) for the vertical direction.

**Table 3.11 Trials for walking speed effect on gait transitional stability.**

<b>Preferred Speed</b> (5 trials per speed)	<b>Mean Speed</b> m/s	<b>Double limb support time</b> sec (Std.)
<b>Very Slow</b>	0.258	1.605 (0.344)
<b>Slow</b>	0.51	0.673 (0.114)
<b>Normal</b>	0.927	0.346 (0.062)
<b>Fast</b>	1.231	0.249 (0.023)
<b>Very Fast</b>	1.466	0.193 (0.04)

### 3.9 Statistical Analyses

In each of the subsequent chapters, the hypotheses are evaluated based on statistical comparison. The gait-related measurements included spatiotemporal parameters, peak angles/ROMs, moments, gain margins, phases margins, the margin of stability, and correlation coefficients wherever applied. All statistical analysis was performed using SPSS software (IBM, version 23). Initially, normality in each of the data set is verified applying Shapiro-Wilk test with normal distribution outcome if  $p > 0.05$  otherwise non-normal. For the normal distribution, a T-test applied in pairwise (in section 3.4.4) and for non-normal distribution, Wilcoxon signed rank test was applied pairwise (Chapter 4-7). A parameter is considered statistically significant if  $p < 0.05$ . The



normal and imitated impairments are compared in pairwise as mentioned in Table 3.12.

**Table 3.12: Statistically comparative walking conditions.**

<b>Groups</b>	<b>Reference conditions</b>	<b>To be compared with</b>
Forward	AFO free-mode	DRT, DPRT, DRR, DPRR
	Normal walk	AFO-free mode, DRT, DPRT, DRR, DPRR
Rotational	Normal walk	Everted and Inverted foot walks
Walking Speed	Normal walk	Slow and Fast walks

DRT: dorsiflexion resistive torque, DPRT, dorsi-plantarflexion resistive torque, DRR: dorsiflexion range-of-motion restriction, DPRR: dorsi-plantarflexion range-of-motion restriction.

### 3.10 Summary

A detailed description of the experimental equipment and analytical procedures applied in this research were explained. Wearable ankle-foot orthoses were designed for imitating forward and rotational ankle-foot impairments. In the forward direction, moderate to severe range impairments were imitated using adjustable ankle-foot orthosis. These uniformly restricted impairments offer lesser variances in group-based studies and support in establishing new stability assessments. The experiments were performed in the motion capture lab using eleven healthy subjects for level ground and inclined walking daily living activities. Lower limbs kinematic and kinetic data were computed using Visual 3D motion analysis software. The peak angles and moments of imitated impairments were validated with earlier published patients data. The CoP and GRF (CoM-acceleration/mass) were earlier reported as two major predictors for neuromotor balance control, hence, modelled in this study for evaluating loading and unloading phases stabilities. The theoretical aspects of analytical procedures (PCA, system identification) were discussed in the context of the current study and similar applications reported earlier. Finally, the Nyquist and Bode methods of evaluating gait stability margins were explained with examples. The hierarchical layout of experimentation and data collection are summarised in the block diagram in Figure 3.17.

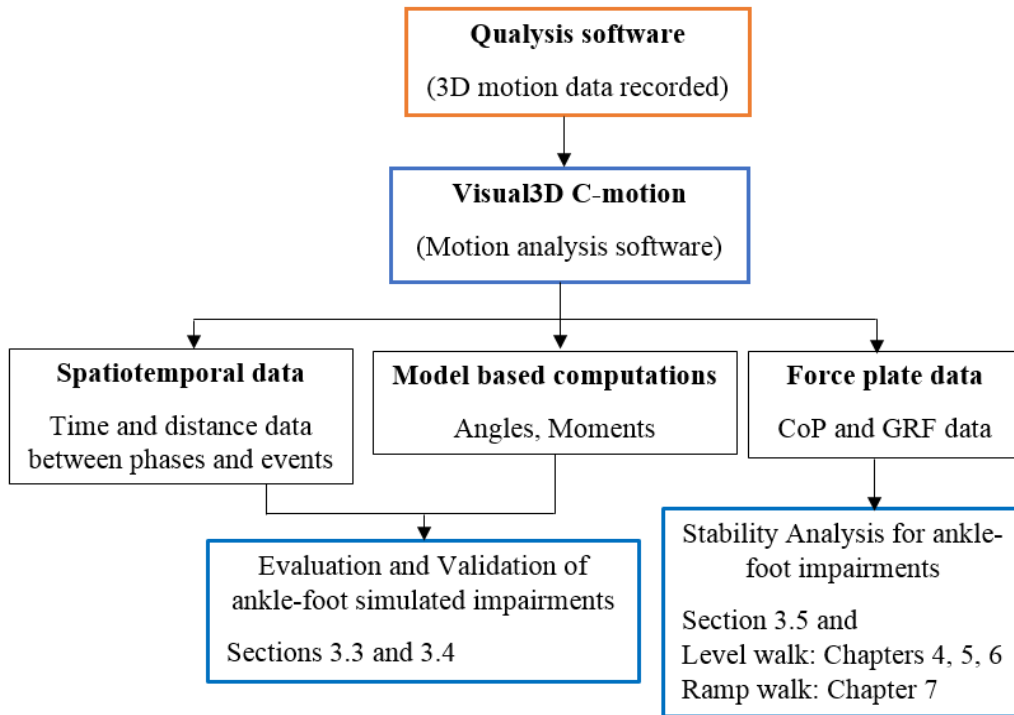


**Figure 3.19: Hierarchical layout of biomechanical data collection.**

## **CHAPTER 4**

# **GAIT TRANSITIONAL STABILITY ASSESSMENT USING COP IMPULSIVE RESPONSES FOR LEVEL WALK**

### **4.1 Introduction**

This chapter introduces the control engineering methods for evaluating gait dynamic stability during weight loading and unloading transitional phases while performing a level ground walk. Various ankle-foot impairments were imitated using an adjustable ankle-foot orthosis (AFO) and wedged foot insoles and experiments were recorded using motion capture system. The rate of change in the centre of pressure (CoP) waveforms was modelled in time and frequency domains. The Nyquist and Bode stability methods were implemented using frequency models of loading and unloading phases. The stability margins were evaluated for the aforementioned simulated impairments and compared statistically in three groups i.e. forwards impairments, rotational impairments, and self-selected walking speeds. The extrapolated-CoM stability method was applied to compare the results from stability margins, and gait kinematic/kinetic parameters were also quantified to explain the interlimb joints compensations.

The experimental protocol was approved by the ethical review board of the University of Leeds. Each subject signed an informed consent form. In addition, a separate consent about video/photographic data was also signed by each subject.

### **4.2 Hypotheses**

The objective of this chapter is to introduce, implement, and validate Nyquist and Bode methods to evaluate gait transitional stabilities. The following hypotheses are investigated for quantifying gait stability margins using neuromotor control patterns illustrated by neuromechanical outputs (i.e. CoP) shown in Figure 1.

Firstly, whether the neuromotor control generates a strong intralimb interaction to compensate unilateral/bilateral ankle-foot deficiencies?

Secondly, if the intralimb interaction exists then to what extent interlimb stability margins vary with forwarding and rotational ankle-foot deficiencies, and self-selected individuals walking speeds?

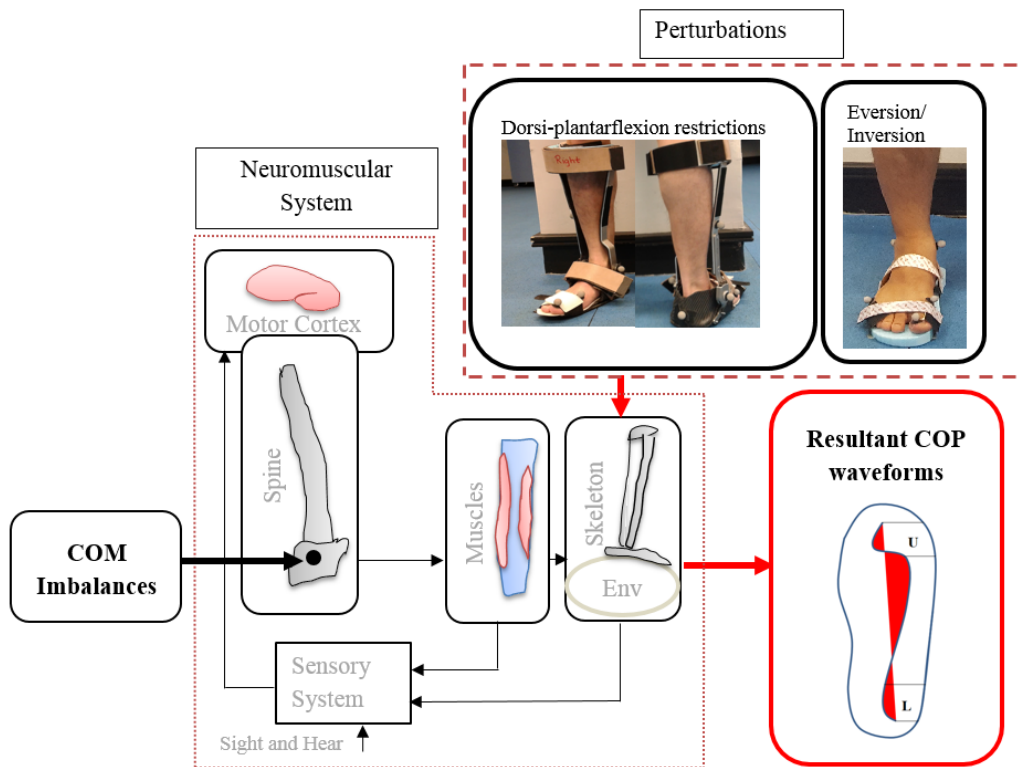


**Figure 4.1: Neuromuscular control loop shown with restricted ankle-foot motions. The neuromotor response to the imbalances in the body’s CoM with resultant effect measured from CoP trajectory. Wearable orthoses used to restrict ankle-foot motion in the forward and lateral directions. The CoP trajectories showing greater variations during loading (L) and unloading (U) phases.**

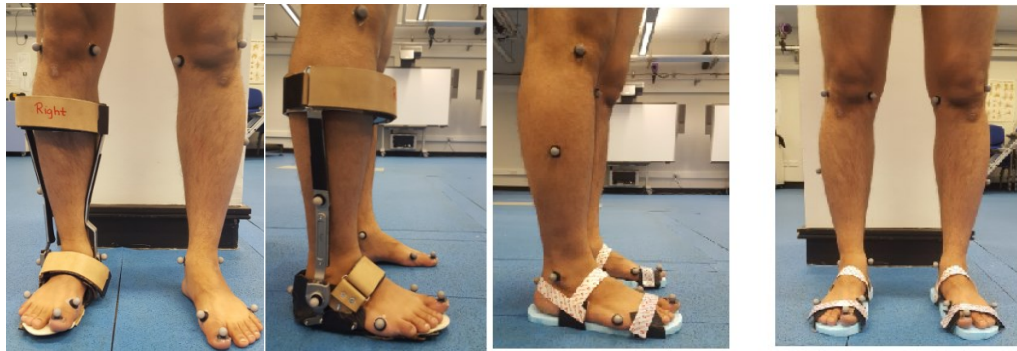
### 4.3 Methods

The detailed methods are already described in Chapter 3, here, the implementation of these methods for specifically centre-of-pressure (CoP) waveforms are defined.

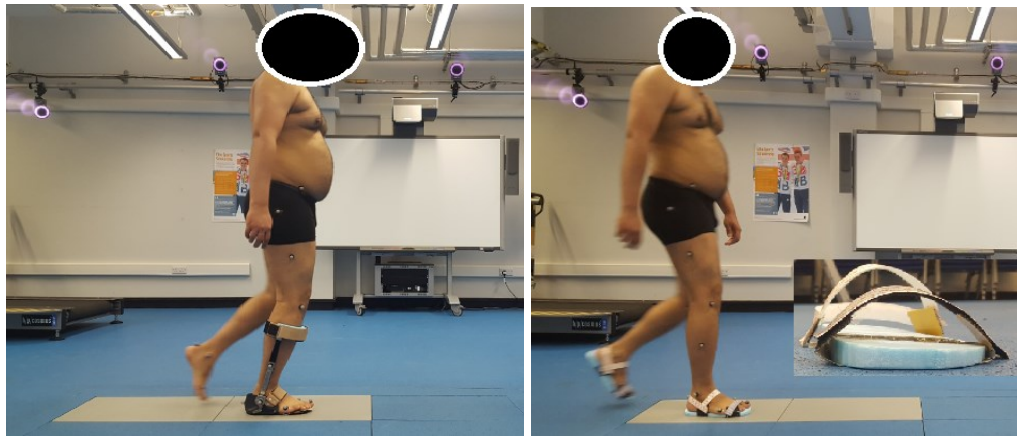
#### 4.3.1 Subjects and Trials

In total eleven healthy subjects (age  $30 \pm 1$ yr, weight  $74 \pm 3$ kg, and height  $1.72 \pm 2.5$ m) participated in this study and each subject performed five trials with each of the ten simulated walking conditions (details in Chapter 3 section 3.4.1). The demographic data of each individual subject is provided in Appendix D. The simulated walking conditions were mainly categorised into three groups i.e. anterior-posterior/forward restrictions (AFO), medial-lateral/rotational restrictions (Foot-insoles), and preferred walking speeds (slow, normal, and fast). The experimental trials are performed in the motion capture lab with a dominant foot of each subject for a level walk as shown in Figure 4.2. The motion capture data was exported to Visual-3D motion analysis software and CoP raw waveforms were exported to Matlab for further analyses (details in section 3.4.3). Following the prior studies [31], the exponential waveforms

were windowed such that the first 20% of stance (100 samples) starting from HC presented loading phase and last 20% of stance (100 samples) towards TO presented unloading phase.



(a) Adjustable Ankle-foot orthosis and wedged insoles



(b) Experimental trials recorded for imitated ankle-foot impairments

**Figure 4.2: Ankle-foot impairments imitated using wearable orthoses. (a) AFO and wedged insoles are illustrated, (b) Experimental trials recorded in motion capture lab.**

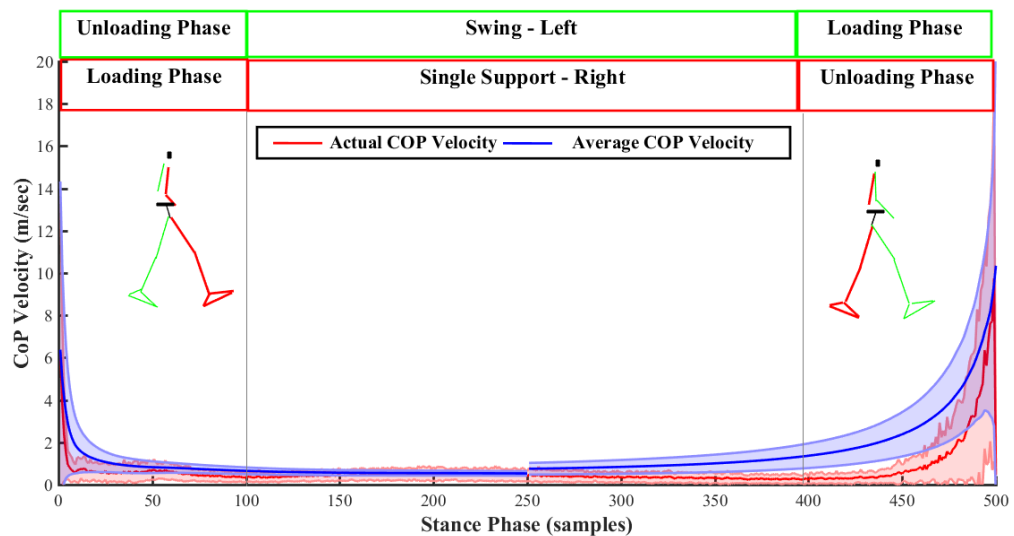


**Figure 4.3: The CoP-velocity (actual and averaged) impulsive responses for loading and unloading phases, each present ~20% of stance.**

### 4.3.2 CoP-velocity waveforms and Pre-processing

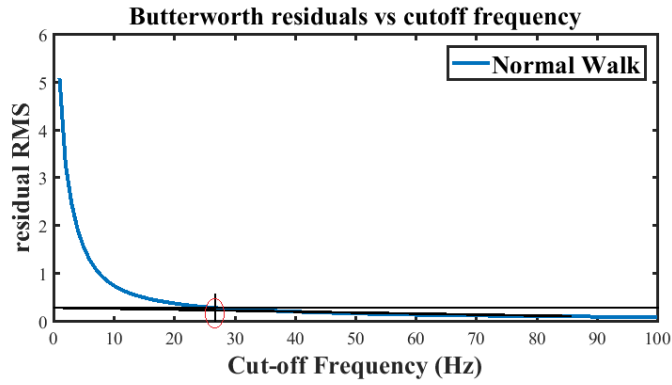
The randomly sampled CoP-displacement and time samples data was imported in Matlab-2017a where a finite difference algorithm was implemented adopting from [154]. Following prior studies [31, 155, 156], the absolute movement of CoP between two consecutive samples was divided by respective time difference using Equation 4.1 to compute actual CoP-velocity. The time derivative of raw CoP-waveforms also introduced noise in the output signals. The signal-to-noise ratio was improved by computing the cumulative average of CoP-velocity waveforms w.r.t time using Equation 4.2.

$$V_{COP\_actual} = \frac{d_{xi}}{d_{ti}} = \frac{|x_{i+1}-x_i|}{|t_{i+1}-t_i|} \quad (4.1)$$

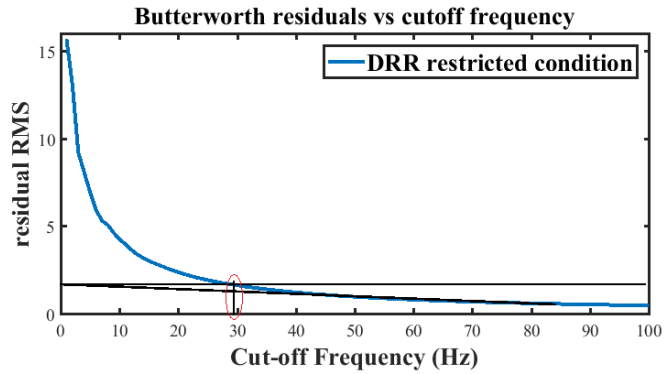
$$V_{COP\_average} = \frac{d_{xi}+d_{x\_sum}}{d_{ti}+d_{t\_sum}} \quad (4.2)$$

The randomly sampled mean CoP-velocity waveforms are further interpolated by fitting the splines and resampled the stance phases to 500 samples, shown in Figure 4.3, which was originally captured at 1000Hz using force platforms. Previously CoP waveforms were filtered from 10-30Hz cut-off frequencies using 2<sup>nd</sup> to 4<sup>th</sup> order low pass Butterworth filters [129, 157, 158]. The optimum specifications of a low pass filter were selected using residual analysis method [51, 159]. Applying this method, the mean CoP-velocity signals were filtered over a range of cut-off frequencies (10-40Hz) and root-mean-square error was computed between filtered and unfiltered data. The characteristics of the filter are reflected by a transient region of residual versus frequency plots as shown in Figure 4.4.

The cut-off frequency was estimated where the residual plot crossed the intercept of the tangent line with the ordinate. Further, the order of Butterworth filter was selected low to minimise the initial time delays in the filtered CoP-velocity waveforms. A first order low pass IIR Butterworth filter was determined optimum with cut-off frequency 30Hz. Thus, the averaged CoP-velocity waveforms are filtered using computed specifications and a comparison between raw and filtered waveforms are shown in Figure 4.5. The resultant waveforms showed two distinct impulses such that the first showed exponentially decaying behaviour starting from heel contact and decayed towards mid-stance, and the second showed exponential rise starting from terminal stance phase and ended at toe-off. These impulsive responses were also modelled in previous studies to predict dynamic stability and neuromotor control [96, 97]. All other gait parameters (angles, moments, extrapolated CoM and CoP displacements) were filtered in Visual-3D motion analysis software using 4<sup>th</sup> order Butterworth filter at 6Hz [125, 126].



(a) residual plot for a normal walk



(b) residual plot for an AFO restricted walk

**Figure 4.4: The residual analysis performed for optimum cut-off frequency selection. (a) normal/preferred speed walk, (b) with dorsiflexion ROM restriction ‘DRR’.**

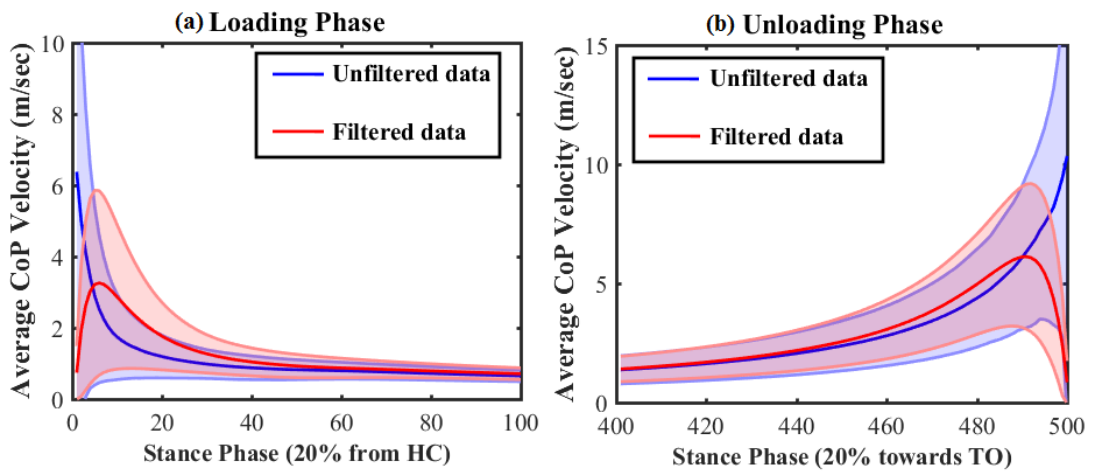


**Figure 4.5: The averaged CoP-velocity impulsive responses filtered (1<sup>st</sup> order, 30Hz) and unfiltered waveforms. (a) Loading phase data, (b) unloading phase data from normal speed trials.**

### 4.3.3 Linearity in Measured Waveforms

The basic requirement for applying control engineering theory is the representation of CoP-velocity waveforms as linear models or transfer functions. Following prior studies [130-132], the principal component analysis (PCA) was employed to prove the linearity of waveforms to be modelled. Also, the data from healthy subjects showed artefacts with potential sources such as varying force exertion by the individual subject against restrictions, self-selected walking speed, foot length/width, body weight etc.

The detailed theory and related applications of PCA were already explained in Chapter 3 (section 3.6.1), here, the PCA is applied to reduce the dimensions in CoP-velocity waveforms to ensure the linearity in the data following previous applied EEG wavelets analysis [160, 161]. An input matrix of size (100 x 55) was used for each of the simulated condition, where the rows present 100 samples/trial and columns present (5 x 11 = 55) trials from all eleven subjects. The PCA is performed in the Matlab-2017a, the first principal component (PC1) explains maximum (>80%) variances for each walking condition and respective variances are presented in Tables 4.1, 4.2, 4.4, 4.6, 4.7, and 4.8. The PCA output is in the form of scores (input data transformed to PCA coordinates) and coefficients (PCs) matrices. For respective walking conditions, the output waveforms were reconstructed by multiplying score matrix with the transpose of first PC and resultant matrix added with an estimated mean of each variable in the input matrix. As an example, the input and output waveforms (mean  $\pm$ Std.) are shown for the normal speed trials in Figure 4.6. The mean of each subjects' trials was computed [31] and used in the subsequent section for further modelling and analysis.

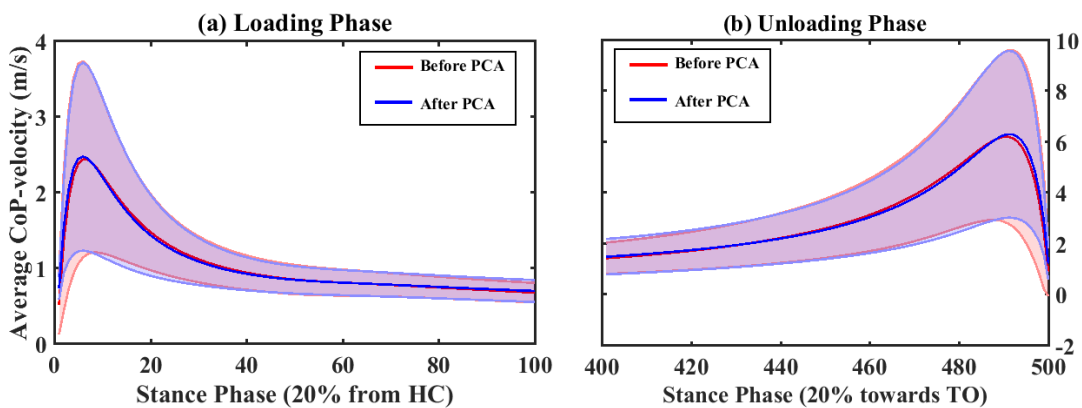


**Figure 4.6: The CoP-velocity impulses as a linear combination of PCA models after removing artefacts and reducing the dimension. (a) Loading phase data, (b) Unloading phase data from normal walk trials.**



#### 4.3.4 Time and Frequency Domain Models

The stability is quantified using impulsive CoP-velocity waveforms that count decay from maximum amplitude to steady state point for a loading phase and rise from a steady state value to maximum threshold near the end of stance for unloading phase. The initial sharp rise ( $t=0$ ) and final sharp decay ( $t \sim 500$  samples) in CoP-velocity waveforms are resulted from filtering delays and are not part of raw waveforms as shown in Figure 4.3, hence, the initial few samples are ignored while modelling loading and unloading phases impulsive responses. The least-square regression algorithm is implemented using Matlab curve-fitting toolbox and the sum of two first-order exponents (Equation 4.3) are found the best fit model for both loading and unloading phases impulses with different coefficients. The criteria of best-fit regression models are determined from the maximum coefficient of determinant values ( $R^2$ ) and mentioned in Tables 4.1, 4.2, 4.4, 4.6, 4.7, and 4.8 for respective walking conditions.

$$f(t) = ae^{-bt} + ce^{-dt} \quad (4.3)$$

Where ' $a$ ' and ' $c$ ' present initial gains, ' $b$ ' and ' $d$ ' present time constants. The CoP-velocity waveforms (Equation 4.3) are transformed to the frequency domain by Laplace transformations and presented in generalised form as a second order transfer function (TF) in Equation 4.4.

$$F(s) = \frac{s(a+c)+(ad+bc)}{s^2+s(b+d)+bd} \quad (4.4)$$

Where ' $s$ ' = Laplace operator, and  $F(s)$  = system's TF or plant model. Applying engineering control theory, the roots of the numerator polynomial of a TF presents zeros and denominator roots of a TF presents poles of the modelled system. These poles and zeros are used to define the stability of a system in the frequency domain (section 3.6.3). Further, a system is said to be minimum-phase if all its poles and zeros are on the left half of s-plane, otherwise called nonminimum-phase. Overall, the loading phases TF(s) showed poles on the left half of s-plane, implied stable open loop response, and respective unloading phases TF(s) showed their poles on the right half of s-plane, implied unstable and non-minimum phase systems (Figure 4.7). These models or TF(s) helped to define a model stable/unstable, however, the extent of stability or instability from some reference point was required to be quantified further in terms of stability margins.

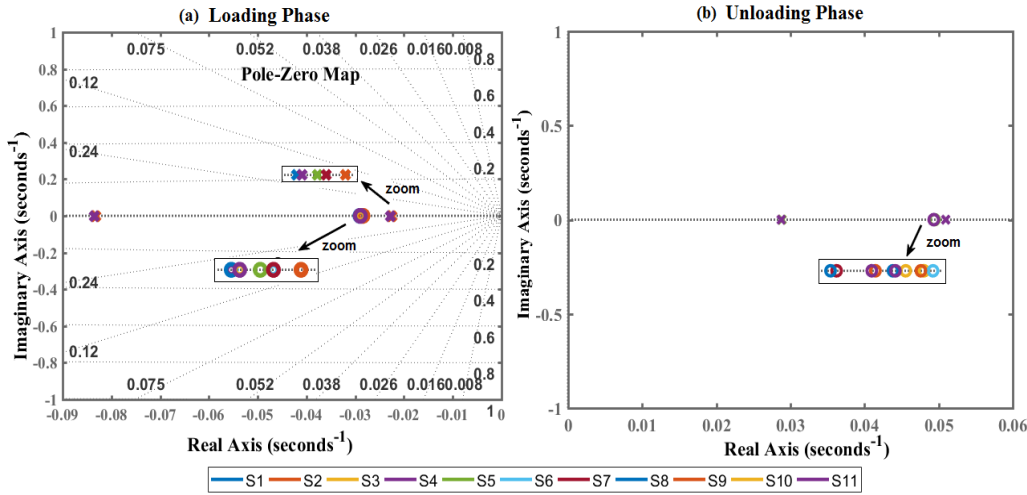


**Figure 4.7: The pole-zero map of frequency models (11 subjects) in the s-plane. (a) Loading phase with poles on the left half shows a stable and minimal phase system, (b) Unloading phase with poles on the right half of s-plane show unstable and non-minimum phase system.**

### 4.3.5 Nyquist and Bode Stability Methods

The final step was the analysis of the modelled linear transfer functions for the loading and unloading gait phases. The details of these algorithms, stability criteria and their applications in the field of biomechanics were described in Chapter 3 (section 3.6.3). A recent study successfully applied these methods for quantifying knee dynamic stability using knee angle waveforms in subjects having anterior cruciate ligament (ACL) reconstruction problem [34, 94]. These methods are implemented in this work to quantify whole-body stability analysis using the aforementioned impulsive CoP-velocities and for various walking conditions [96, 97]. As an example, the TF's Nyquist plot and equivalent Bode plots are illustrated in Figures 4.8 and 4.9 for the loading phase. The stability outcomes are quantified as gain margin (GM) and phase margin (PM) for the individual subject in all walking conditions.

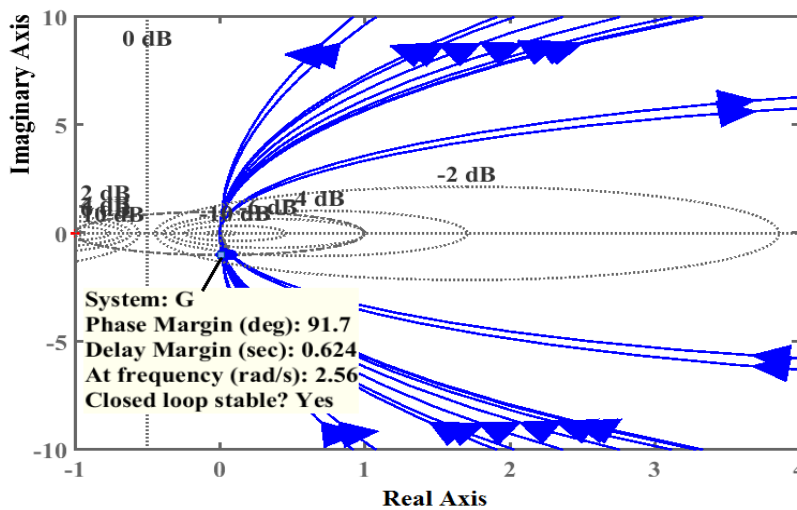


**Figure 4.8: Nyquist plots loading phases of normal walk trials (11 subjects).**

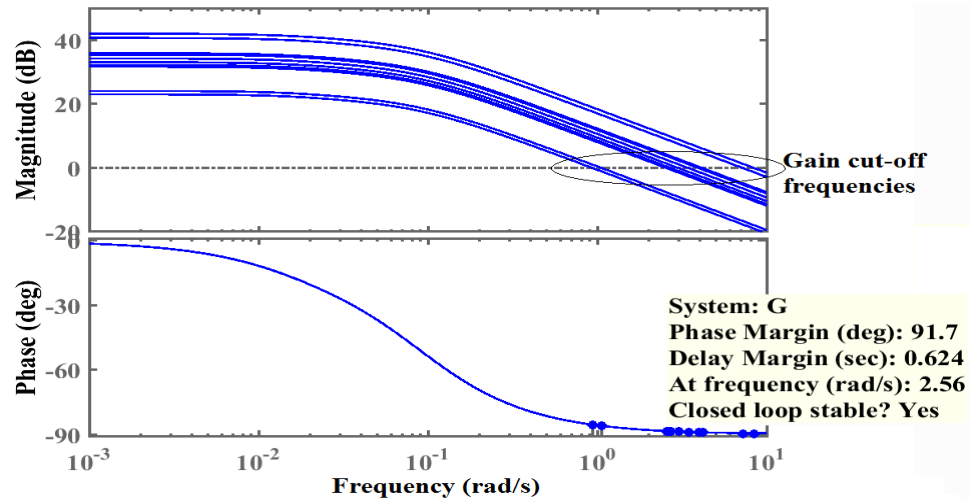


**Figure 4.9: Bode plots for loading phases of normal walk trials (11 subjects).**

The unstable models for the unloading phases are further stabilised using controller design technique to illustrate the controllability effect of imbalances generated during the human walk.

#### 4.3.6 Extrapolated CoM and Gait parametric variability Methods

For comparing the stability outcomes from Nyquist and Bode methods, the margins of stability (MoS) were also computed using extrapolated CoM method [12], and variability in gait kinematic and kinetic parameters method [162, 163]. However, a direct validation with any of these two stability methods was not possible due to the limitations mentioned in the discussion section of this chapter. The details of extrapolated-CoM method and stability criteria are discussed in Chapter 2 (section 2.4.5). Applying this method, the MoS(s) are quantified at heel contact (HC) and toe-off (TO) gait events for all walking conditions. Gait parametric variability method is also discussed earlier in Chapter 2 (section 2.4.1) and implemented here. Gait spatiotemporal, peak angles and peak moments are evaluated from lower limb joints (ankle, knee, and hip) using Visual-3D motion analysis software. The computational details are presented in Chapter 3 (section 3.4.3).

#### 4.3.7 Body mass index (BMI) impact on transitional stability

In this chapter, the impact of subjects BMI on walking stability also evaluated using normal speed, walking group. For individual subjects, body mass and height data are mentioned in Appendix D (Table B.1). Considering the outliers in BMI values, subjects are grouped into low (two), medium (five) and high (two) ranges. The outcomes are discussed in the results section.

#### 4.3.8 Statistical Analysis

The stability margins from Nyquist and Bode method, MoS(s) from extrapolated CoM method, and variability in discrete gait kinematic/kinetic parameters were compared statistically in respective groups (details Chapter 3, section 3.7). To

understand the intralimb interaction between loading phase of dominant foot and unloading phase of an opposite limb or vice-versa, the Spearman's correlation was determined using CoM-velocity time domain waveforms. A parameter was considered statistically significant if  $p < 0.05$ .

## 4.4 Results

### 4.4.1 Stability Margins from Nyquist and Bode Methods

The gain and phase margins were used to quantify the stability of simulated walking conditions. The Nyquist and Bode methods illustrated significant increase/decrease in stabilities in respective walking groups. The Nyquist plots are also shown in Figures 4.10 and 4.11 using mean waveforms of forwarding AFO restricted impairments for both loading and unloading phases. All walking groups and conditions showed overall stable responses with infinite GM(s) and finite PM(s) during loading phases mentioned in Tables 4.1, 4.4, 4.7 and Figure 4.10 in respective walking groups. However, the respective unloading phases showed unstable responses quantified as GM(s) and PM(s) in Tables 4.2, 4.6, 4.8 and Figure 4.11. The Spearman's correlation coefficients showed significant correlation -0.462 to -0.842 ( $p < 0.001$ ) between restricted foot loading and unrestricted foot unloading phases or vice-versa. The Spearman's correlation coefficients and their significance levels are given in Tables 4.3 and 4.5.

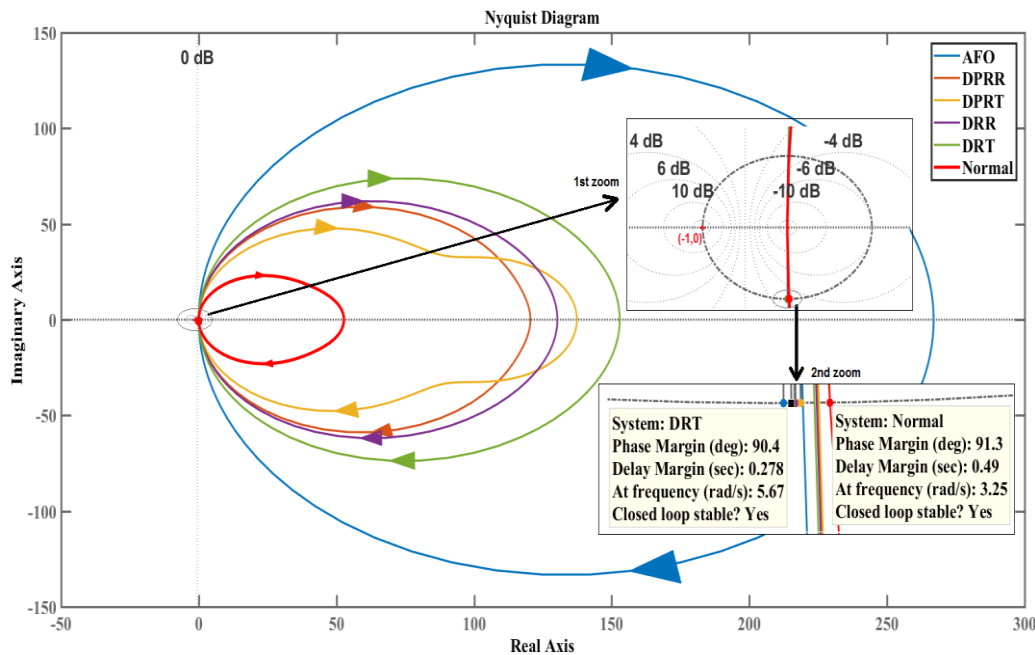


**Figure 4.10: Nyquist plots loading phase AFO conditions, stability margins calculated w.r.t unity circle passing through the point (-1, 0). Loading phases transfer functions cut unit circle (1<sup>st</sup> zoom) at points (2<sup>nd</sup> zoom) and differences of these points from (-1,0) give stability margin.**

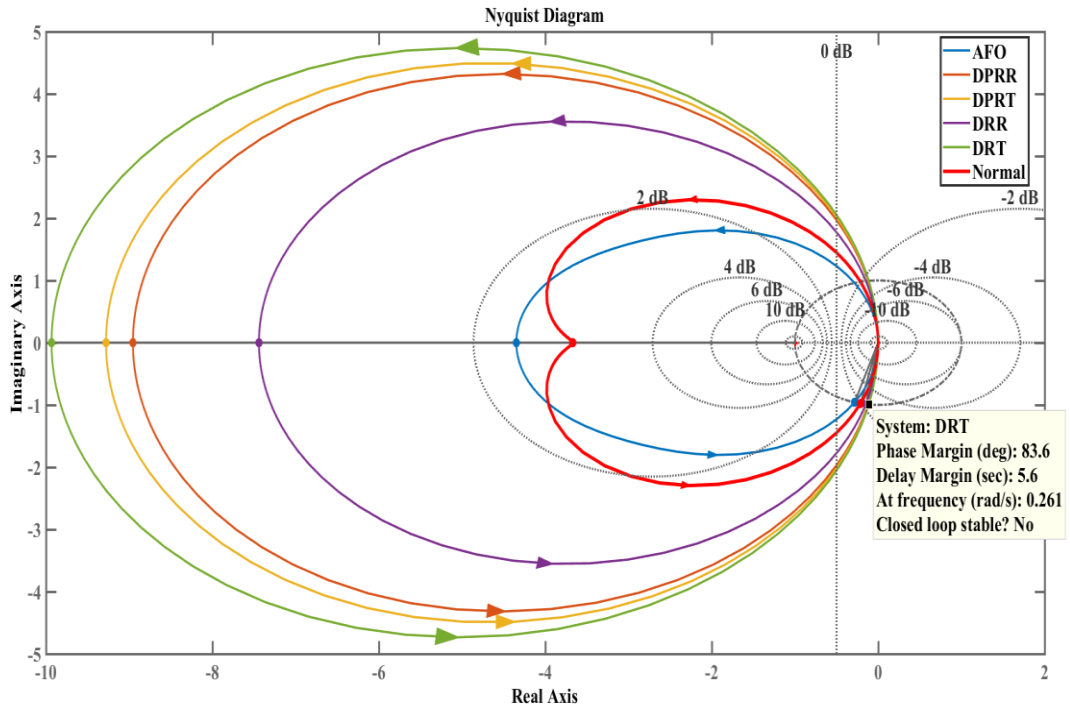


**Figure 4.11: Nyquist plots for AFO restricted conditions, stability margins calculated w.r.t unity circle passing through the point (-1, 0). Unloading phases transfer function plots and stability margins computed from (-1,0).**

A within-group comparison of GM/PM showed no significant difference between AFO free-mode walk and restricted conditions during loading phases (Table 4.1, Figure 4.12a), whereas during unloading phase, both the stiffness (DPRT, DRT) and range-of-motion (DPRR, DRR) restrictions showed significant increase ( $p < 0.05$ ) in instability with negative increase in GM(s) and positive increase ( $p < 0.05$ ) in PM(s) (Table 4.2, Figures 4.12b and 4.12c). The restricted AFO walking conditions were also compared with a normal walk (without wearing AFO) to understand the effect of wearable orthoses on gait dynamic stability with/without clinically prescribed adjustments. The results showed that the stability margins (PMs) significantly decreased ( $p < 0.05$ ) during loading phases in both restricted and free-mode AFO walks. During unloading phase, only dorsi-plantarflexion ROM restriction (DPRR) showed an increase ( $p < 0.05$ ) in instability as compared to a normal walk, however, a walk with AFO free mode also showed a decrease ( $p < 0.05$ ) in instability.

**Table 4.1: Quantified and compared stability margins for loading phases of AFO restricted conditions.**

Walking Condition	Gain Margin (decibel)	Phase Margin (degree)	% Variance Explained (PC1)	Coefficient of Determinant (R <sup>2</sup> )
Normal (without AFO)	∞	91.7 1.27	96.9	99.19
AFO (free mode)	∞	<b>90.66</b> 0.49	97.5	99.96
DPRR	∞	<b>90.71</b> 0.5	96.2	99.91
DPRT	∞	<b>91.28</b> 1.73	94.3	99.31
DRR	∞	<b>90.54</b> 0.27	97	99.85
DRT	∞	<b>90.56</b> 0.31	96.2	99.8

Bold values showing p<0.05 when compared with a normal walk, \* for p<0.05 compared with AFO free-mode walk.

**Table 4.2: Quantified and comparison of stability margins for unloading phases of AFO restricted conditions.**

Walking Condition	Gain Margin (decibel)	Phase Margin (degree)	% Variance Explained (PC1)	Coefficient of Determinant (R <sup>2</sup> )
Normal (without AFO)	-15.78 3.14	80.07 3.18	96.6	99.84
AFO (free mode)	<b>-9.22</b> 4.09	<b>67.51</b> 9.52	97.2	99.82
DPRR	<b>-17.98*</b> 3.14	<b>81.75*</b> 2.91	97.4	99.86
DPRT	-15.73* 2.84	80.57* 3.54	96.65	99.87
DRR	-16.4* 3.7	80.33* 3.83	96.2	99.9
DRT	-15.91* 2.62	80.41* 2.66	96.75	99.86

Bold values showing p<0.05 when compared with a normal walk, \* for p<0.05 compared with AFO free-mode walk.

**Table 4.3: Spearman correlation coefficients illustrate intralimb interaction between loading and unloading phases of AFO restrictions.**

<b>Walking Conditions</b>	<b>AFO</b> (p-value)	<b>DPRR</b> (p-value)	<b>DPRT</b> (p-value)	<b>DRR</b> (p-value)	<b>DRT</b> (p-value)
Unrestricted Unloading & Restricted Loading	-0.462 (0.001)	-0.720 (0.001)	-0.711 (0.001)	-0.859 (0.001)	-0.651 (0.001)
Restricted Unloading & Unrestricted Loading	-0.882 (0.001)	-0.749 (0.001)	-0.752 (0.001)	-0.786 (0.001)	-0.830 (0.001)

p-value showing the statistical significance level of correlation between two conditions.

**Table 4.4: Quantified and compared Stability margins for loading phases of rotational foot impairments.**

<b>Walking Condition</b>	<b>Gain Margin</b> (decibel)	<b>Phase Margin</b> (degree)	<b>% Variance Explained</b> (PC1)	<b>Coefficient of Determinant</b> (R <sup>2</sup> )
anterior-posterior stability margins				
Normal (without restriction)	∞	91.7 1.27	96.9	99.19
Eversion	∞	<b>90.75</b> 0.32	97.7	99.38
Inversion	∞	<b>90.59</b> 0.21	97.2	99.52
medial-lateral stability margin				
Normal (without restriction)	∞	93.34 3.79	97.9	99.28
Eversion	∞	<b>91.14</b> 0.40	97.5	99.47
Inversion	∞	<b>91.0</b> 0.38	97.6	99.51

Bold values showing p<0.05 when compared with a normal walk.

**Table 4.5: Spearman correlation illustrate intralimb interaction between loading and unloading phases of rotational impairments and walking speed groups.**

<b>Walking Conditions</b>	<b>Normal</b> (p-value)	<b>Eversion</b> (p-value)	<b>Inversion</b> (p-value)	<b>Slow</b> (p-value)	<b>Fast</b> (p-value)
Anterior-posterior (symmetric restrictions)	-0.809 (0.001)	-0.834 (0.001)	-0.779 (0.001)	-0.864 (0.001)	-0.778 (0.001)
Medial-lateral (symmetric restrictions)	-0.842 (0.001)	-0.812 (0.001)	-0.791 (0.001)	NA	NA

p-value showing the statistical significance level of correlation between two conditions.

**Table 4.6: Quantified and compared stability margins for unloading phases of rotational foot impairments.**

<b>Walking Condition</b>	<b>Gain Margin</b> (decibel)	<b>Phase Margin</b> (degree)	<b>% Variance Explained</b> (PC1)	<b>Coefficient of Determinant</b> (R <sup>2</sup> )
anterior-posterior stability margins				
Normal (without restriction)	-15.78 3.14	80.07 3.18	96.6	99.84
Eversion	-14.33 2.58	78.41 3.71	97.7	99.87
Inversion	<b>-12.58</b> 3.21	<b>75.46</b> 5.61	97.7	99.77
medial-lateral stability margins				
Normal (without restriction)	-12.45 2.52	75.65 3.98	97.6	99.74
Eversion	-11.40 3.26	73.22 6.44	98.7	99.73
Inversion	-11.27 3.26	72.89 7.07	98.5	99.79

Bold values showing  $p < 0.05$  when compared with a normal walk.

Considering medial-lateral/rotational impairments, the stability margins were compared both in forwarding and lateral directions. In the forward/posterior direction, both the eversion and inversion simulated conditions showed a decrease ( $p < 0.05$ ) in



stability with a decrease in GM(s) during loading phases compared to a normal walk (Table 4.4, Figure 4.13a). During unloading phase, the everted foot GM and PM showed insignificant change, however, the inverted foot showed a decrease ( $p < 0.05$ ) in instability both in GM and PM compared to a normal walk (Table 4.6, Figures 4.13b and 4.13c). Also, in the medial-lateral direction, the loading phase margins (PM) significantly decreased ( $p < 0.05$ ) in both eversion and inversion and GM/PM showed statistically insignificant differences during unloading phase compared to a normal walk.

**Table 4.7: Quantified and compared stability margins for loading phases of the level walk at self-selected walking speeds.**

Walking Speed	Gain Margin (decibel)	Phase Margin (degree)	% Variance Explained (PC1)	Coefficient of Determinant ( $R^2$ )
Preferred/Normal	$\infty$	91.7 1.27	96.9	99.19
Slow	$\infty$	<b>91.03</b> 0.45	96.9	99.9
Fast	$\infty$	91.53 0.86	97	99.74

Bold values showing  $p < 0.05$  when compared with a normal walk.

**Table 4.8: Quantified and compared stability margins for unloading phases of the level walk at self-selected walking speeds.**

Walking Speed	Gain Margin (decibel)	Phase Margin (degree)	% Variance Explained (PC1)	Coefficient of Determinant ( $R^2$ )
Preferred/Normal	-15.78 3.14	80.07 3.18	96.6	99.84
Slow	-15.91 2.51	80.42 3.18	98.3	99.79
Fast	<b>-10.79</b> 4.01	<b>71.38</b> 8.12	96.8	99.85

Bold values showing  $p < 0.05$  when compared with a normal walk.

The walking speeds trials were performed for subjects self-selected speed such that the walking speeds varied ( $p < 0.001$ , t-test pairwise) significantly with (mean  $\pm$  Std.)  $0.86 \pm 0.13$  m/s for slow walk,  $1.13 \pm 0.14$  m/s for normal/preferred speed walk, and  $1.35 \pm 0.13$  m/s for a fast speed walk. In this group, a slow speed walk showed a decrease ( $p < 0.05$ ) in stability (PM) as compared to a normal speed walk during the loading phase (Table 4.7, Figure 4.11a). During unloading phase, the fast walk

showed a decrease ( $p < 0.05$ ) in stability (GM and PM) and slow speed walk showed no difference compared to a normal speed walk (Table 4.8, Figure 4.11b and 4.11c).

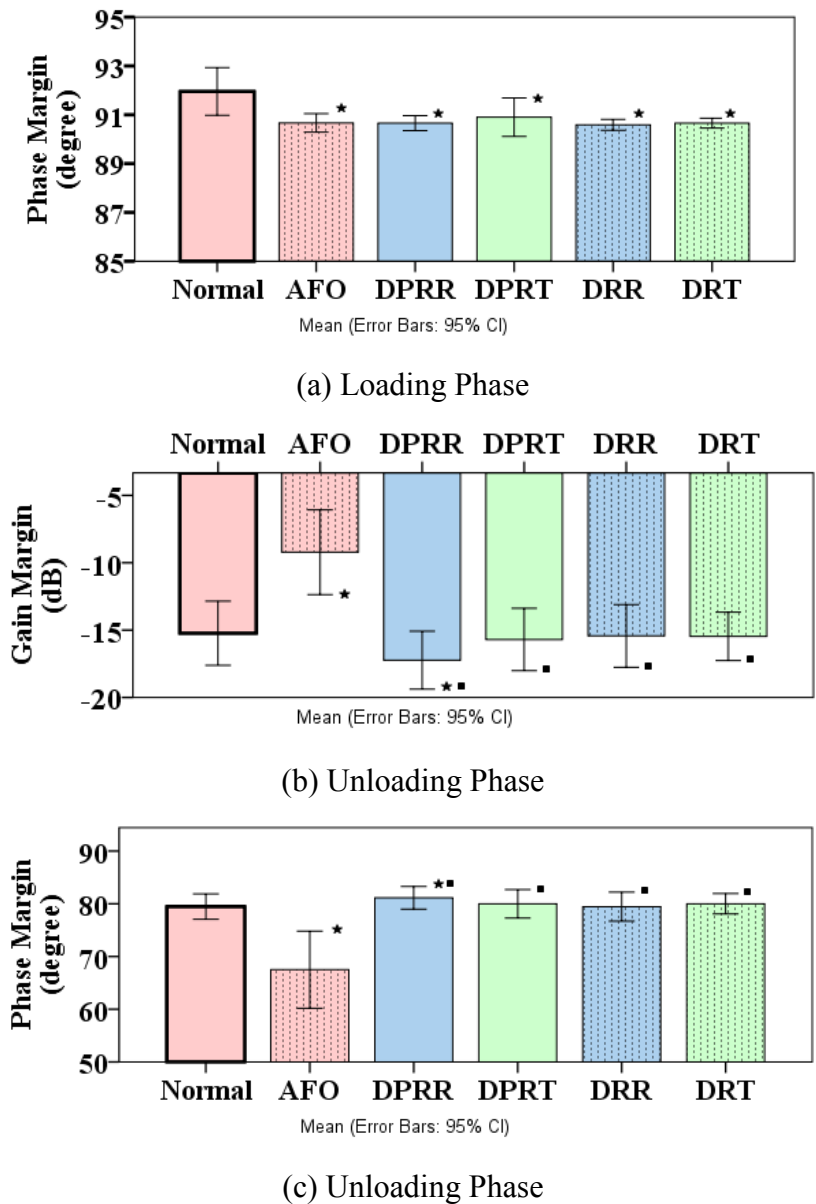
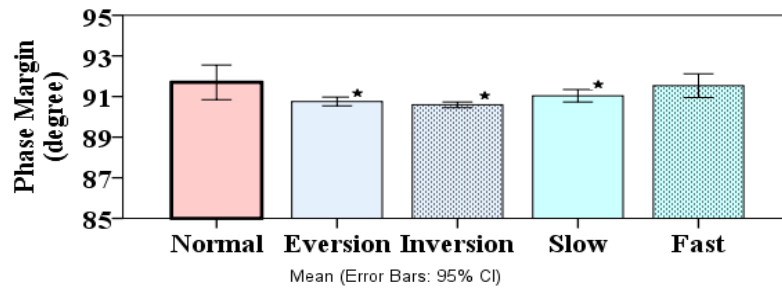
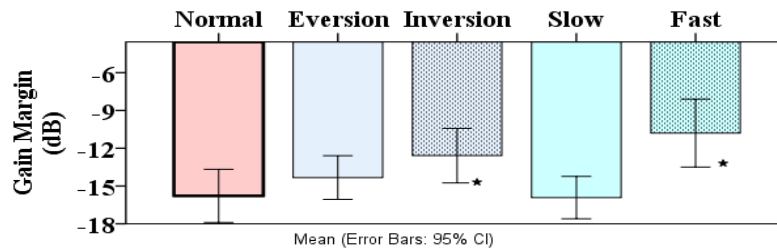


**Figure 4.12: Comparison of stability margins for forwarding direction ankle-foot impairments (mean 95% of CI), ‘★’ presents significant difference with a normal walk, ‘■’ present significant difference with AFO free-mode walk. (a) Phase margins during loading phases, (b) Gain margins during unloading phases, (c) Phase margins during unloading phases.**

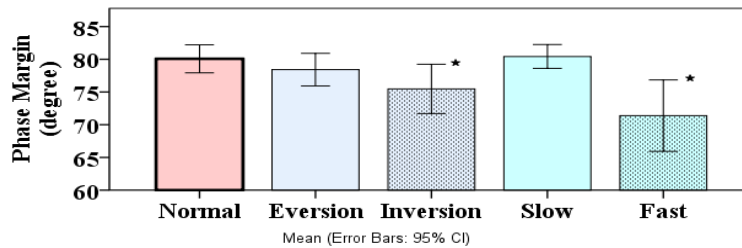
**Note:** for a loading phase, TF’s the GMs are infinite for all conditions, hence, a plot showing only PMs for loading phases.



(a) Loading Phase



(b) Unloading Phase



(c) Unloading Phase

**Figure 4.13: Comparison of stability margins for rotational restrictions and walking speed groups (mean 95% of CI). ‘★’ present a significant difference with a normal walk. (a) Phase margins during loading phases, (b) Gain margins during unloading phases, (c) Phase margins during unloading phases.**

#### 4.4.2 Margins of stability using Extrapolated-CoM (XCoM) Method

Stabilities were also quantified for aforementioned simulated conditions using extrapolated CoM and CoP differences at HC and TO gait events. The AFO restrictions showed no significant difference in MoS(s) compared to an AFO free-mode walk, however, decreased significantly when compared to a normal walk at both HC and TO (Table 4.9). In walking speed group (Table 4.10), there is no significant difference found at HC between self-selected slow, fast, and preferred/normal speed walk, however, both walks showed a decrease in MoS(s) significantly. Considering rotational/medial-lateral restrictions in Table 4.11, the everted foot showed a decrease ( $p < 0.05$ ) in stability at HC with decreased MoS(s) in both forward and lateral directions. The inverted foot also showed a decrease in stability at HC with decreased MoS(s) in the forward direction and increase in MoS(s) in the medial-lateral direction. AT TO event, the MoS(s) were decreased ( $p < 0.05$ ) in the forward direction, however,

in the medial-lateral direction, only inverted foot showed a decrease in stability ( $p < 0.05$ ) with increased MoS(s).

**Table 4.9: Comparison of the margin of stability for forwarding ankle-foot impairments applying extrapolated-CoM method.**

Walking Condition	MoS at HC (meter)	MoS at TO (meter)
Normal (without AFO)	0.296	0.292
	0.032	0.026
AFO (free mode)	<b>0.279</b>	<b>0.240</b>
	0.039	0.030
DPRR	<b>0.269</b>	<b>0.245</b>
	0.032	0.029
DPRT	<b>0.279</b>	<b>0.243</b>
	0.03	0.024
DRR	<b>0.278</b>	<b>0.251</b>
	0.023	0.036
DRT	<b>0.279</b>	<b>0.253</b>
	0.025	0.024

Bold values showing  $p < 0.05$  when compared with a normal walk, \* for  $p < 0.05$  compared with AFO free-mode walk.

**Table 4.10: Comparison of margins of stability for self-selected walking speeds applying extrapolated-CoM method.**

Walking Condition	MoS at HC (meter)	MoS at TO (meter)
Preferred / Normal	0.296	0.292
	0.032	0.026
Slow	0.289	<b>0.261</b>
	0.04	0.03
Fast	0.301	<b>0.304</b>
	0.025	0.024

Bold values showing  $p < 0.05$  when compared with a normal walk.

**Table 4.11: Comparison of margins of stability for rotational impairments applying extrapolated-CoM method.**

<b>Walking Condition</b>	<b>MoS at HC (meter)</b>	<b>MoS at TO (meter)</b>
anterior-posterior stability margins		
Normal (without restriction)	0.296 0.032	0.292 0.026
Eversion	<b>0.273</b> 0.021	<b>0.268</b> 0.031
Inversion	<b>0.273</b> 0.027	<b>0.270</b> 0.023
medial-lateral stability margin		
Normal (without restriction)	0.0494 0.008	0.0606 0.011
Eversion	<b>0.0316</b> 0.011	0.0566 0.014
Inversion	<b>0.0606</b> 0.013	<b>0.079</b> 0.013

Bold values showing  $p < 0.05$  when compared with a normal walk.

#### **4.4.3 Variability in Gait kinematic and kinetic parameters**

Forwards restrictions - the peak values of gait kinematic and kinetic parameters were evaluated in Chapter 3 (Table 3.5). During the loading phase, the ankle joint angles were not affected by the AFO resistive torque (DPRT, DRT) and ROM restrictions (DPRR, DRR), however, the peak knee flexion angle increased in all restricted conditions. Considering joints kinetics, peak moments such as ankle plantarflexion, knee flexion, and hip flexion were increased significantly for resistive torque conditions. During the unloading phase, the peak ankle dorsiflexion angles and moments were reduced significantly ( $p < 0.05$ ) for all AFO conditions. Also, the peak ankle plantarflexion angle significantly decreased ( $p < 0.01$ ) for all AFO resistive torque conditions.

Rotational Restrictions - the eversion and inversion restrictions were evaluated both in anterior-posterior (AP) and medial-lateral (ML) directions (Chapter 3, Table 3.5). During the loading phase, there was a significant decrease ( $p < 0.01$ ) observed in initial

plantarflexion angle and peak plantarflexion moment both in eversion and inversion. The peak knee flexion angles and moments were decreased by 28% for everted and 19% for the inverted foot. In the unloading phase, parameters such as peak dorsiflexion angle, peak dorsiflexion moment, and knee extension moment were significantly decreased ( $p < 0.01$ ) for the inverted foot. The peak plantarflexion angles and hip extension moments were decreased ( $p < 0.05$ ) for both inversion and eversion. The slow and fast walking speeds showed significant differences ( $p < 0.01$ ) in the knee and hip angles/moments. The ankle joints moments were significantly decreased in the slow walk and increased in the fast walk.

#### 4.4.4 BMI effect on stability

For a normal healthy walk, overall results illustrated no significant impact of BMI on stability for both loading and unloading phases as illustrated in Figure 4.14 for both loading and unloading phases. However, during the loading phase, a trend in a decrease in stability was observed with increase in BMI low to high.

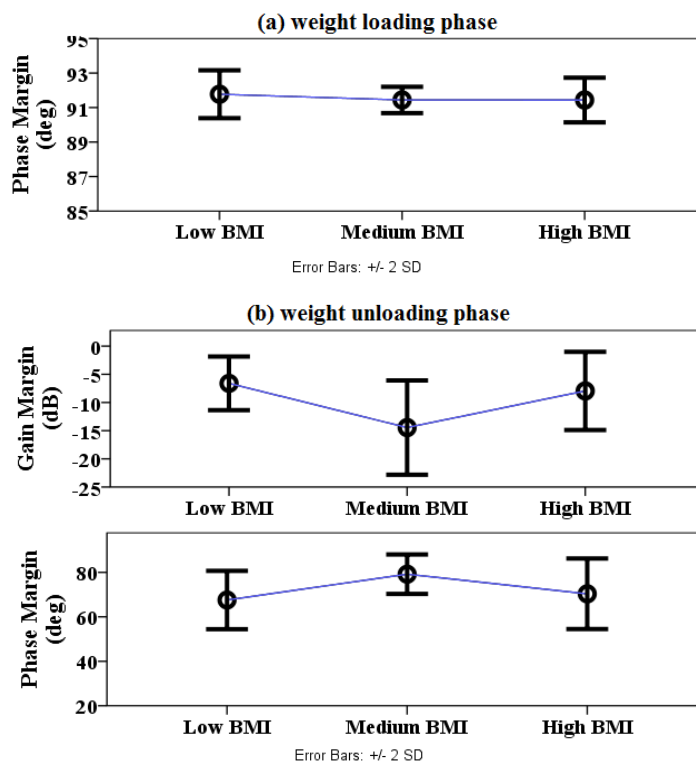


**Figure 4.14 Effect of body mass index (BMI) on gait transitional stability. BMI categorised into subgroups i.e. low ( $21.1 \pm 1.9$ ), Medium ( $25.22 \pm 0.6$ ), High ( $27.85 \pm 0.35$ ), stability margins shown for (a) loading phase, (b) unloading phase.**

#### 4.4.5 Controller design for unstable gait transitions

The controllability of unstable human gait phases is also illustrated by the controller design approach applying linear control theory (Figure 4.15). The results illustrated that an unstable unloading phase models (TF) can be made stable by a proportional-

integral-derivative (PID) controller. An example of a system model and controller parameters is mentioned in Table 4.12 for a normal speed walking trial.

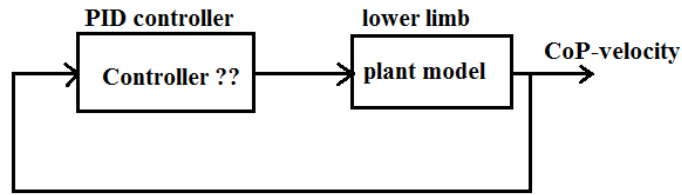
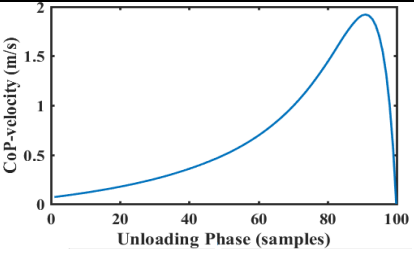
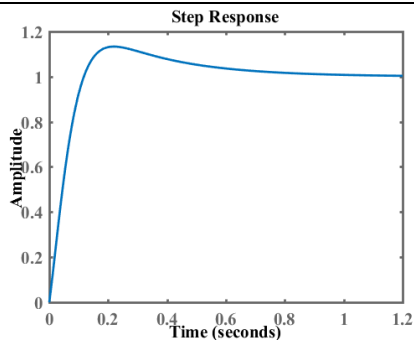


Figure 4.15 Controller design to stabilize the unstable gait phases.

Table 4.12 Controller design outcomes.

Plant/Controller	Model Response
unstable plant model (unloading phase) $0.08 s - 0.0012 / s^2 - 0.054 s + 0.00074$	
PID controller $K_p + K_i * 1/s + K_d * s/T_f * s + 1$ where $K_p = 208, K_i = 654, K_d = -2.48,$ $T_f = 0.0286$	

#### 4.4.6 Effect of walking speed on transitional stability

Results for varying walking speed trials with methods described in Chapter 3 (section 3.8) illustrated an increasing trend in stability (PM) for a walk at very slow speed and an increasing trend from slow to very fast speed during weight loading gait transition. During respective unloading phase, there is no trend observed in terms of gain margins (amplitudes), however, there was a decrease in instability observed from normal speed to very slow walk as illustrated in Figure 4.16.

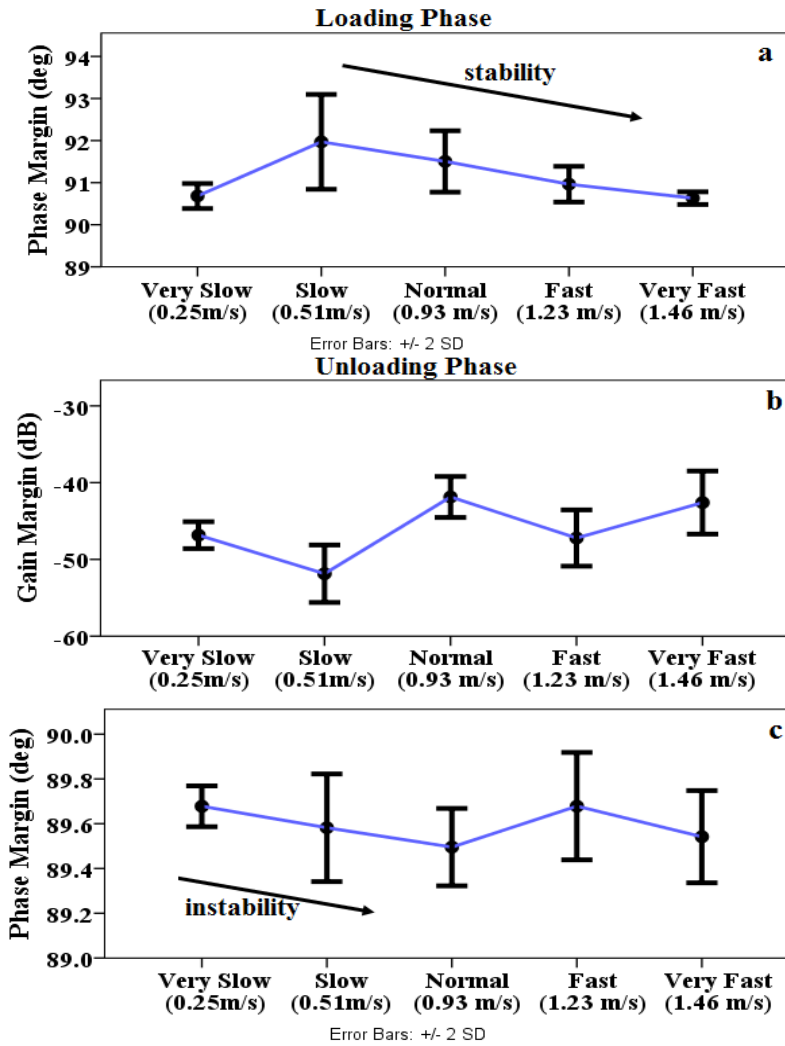


Figure 4.16 Stability trends with the effect of walking speeds.

## 4.5 Discussion

Nyquist and Bode stability methods were introduced in this chapter to quantify gait dynamic stabilities during transition phases which were remained unquantified in most of the prior stability assessments. The CoP-velocity waveforms were collected from unimpaired subjects for various simulated walking conditions and modelled to quantify stabilities. The results showed significant differences between normal and orthoses restricted simulated walks in both loading and unloading of stance phases, also compared by applying a prior extrapolated CoM method and explained by variability in lower limb joints angles and moments. The CoP-velocity showed impulsive behaviours during loading and unloading phases and also demonstrated earlier by heel/toe marker velocity waveforms [164] and lower limb muscles activation patterns during start and end of stance phase [33]. The time-dependent models and their frequency domain Laplace transformations were consistent from a prior study in which knee stability was assessed using Nyquist and Bode stability



methods and using knee angles waveforms [34]. In another study, similar modelling technique was adopted using ocular position traces as exponentially decaying time waveforms and further PCA was used to linearize the waveforms to be modelled and transformed to the frequency domain [131]. The modelling and analysis in this study are consistent with prior studies, however, the assessment of whole body gait stability margins using Nyquist and Bode methods and CoP-velocity waveforms is novel in this study.

Stability margins quantified using Nyquist and Bode methods showed loading phases as stable gait phases (minimal phase, GM:  $\infty$ , PM: positive) w.r.t the cut-off thresholds (0dB,  $\pm 180^\circ \pm 2k\pi$ ), and respective unloading phases showed unstable responses (non-minimal phase, GM: negative, PM: positive). Further, the gain margins of unloading phases were found far less than the loading phases. An earlier study also supported these findings such that the CoM remained within BoS at HC and showed stable MoS(s), whereas CoM sways outside the BoS at TO and illustrated a decrease in stability or unstable state [28]. The loading and unloading phases of opposite limbs took place in parallel but out of phase during double limb support [27]. The stability margins quantified here also explained an intralimb interaction such that the loading phases with greater stability margins were used to compensate the instabilities of opposite limbs unloading phases in parallel. That intralimb interaction was also reported earlier in elderly adults which used their leading limb to compensate work done by trailing limb [163]. Further, Spearman's correlations between opposite limbs' CoP-velocities also illustrated strongly negative correlations between loading and unloading phases of equal window sizes (20% of gait cycle from HC, and 20% towards TO). This suggests that with an exponential decrease in CoP-velocity, the opposite limb's CoP-velocity exponentially increases in parallel but with different rate and magnitude. This finding also reinforces intralimb stability interactions exhibited by the aforementioned stability margins (GM, PM) during the double-limb support phase of gait transitions. The first hypothesis in this study about intralimb stability interactions holds true using stability methods introduced in this chapter.

The level walk by wearing AFO illustrated the decrease in stability for all restricted/unrestricted conditions during loading phases compared to a normal walk. During respective unloading phases, a total ROM restriction (DPRR) showed an increase in instability compared to a normal walk. Most of the prior studies were conducted to assess gait performance with/without AFO(s) using spatiotemporal parameters, static balance, or verbal information from the subjects regarding stability [7, 8]. To our knowledge, there was no prior study quantified gait stability with the effect of AFO(s) while performing dynamic activities despite the assistive orthoses being widely prescribed clinically for lower limb impairments.

A comparison was performed between AFO free-mode and restricted walking conditions to understand the impact of clinically prescribed AFO adjustments on dynamic stabilities. Comparing with AFO free-mode walk, the restricted AFO conditions did not show significant variations towards loading phase stabilities, which showed the robustness of neuromotor control (adaptive behaviour). Earlier studies also revealed that people with lower-limb injuries adopted more proactive gait patterns during early stance phase [34], and unimpaired subjects with stronger somatosensory and visual acuity exhibited less instability in forwarding direction [25]. However, during unloading phases, the stiffness based AFO restrictions (DRT, DPRT) showed an increase in instability with an increase in GM/PM(s) comparative to an AFO free mode walk. That increase in instability got more prominent in total ROM restrictions (DRR, DPRR). That was the result of a reduction in ankle peak dorsiflexion and peak plantarflexion angles near to unloading phase which was also responsible to destabilise the gait during push-off [31]. This reduction in push-off was also reported earlier in AFO restricted ankle-foot motions [111, 112]. Surprisingly, a walk with AFO in free-mode showed a decrease in instability as compared to normal walk (without AFO), however by adjusting the moderate stiffness in DRT, DPRT conditions, the AFO increased instability to the level of a normal walk. That implies moderate range adjustments of AFO are essential to gain stability margins like healthy subjects, however, a more severe ROM restriction (DPRR) introduced more instability during the unloading phase. These findings support the second hypothesis in this study, the wearable AFO significantly affected walking stabilities during loading phases with/without applying restrictions when compared to a normal walk (without AFO). During unloading phases, only a total ROM restricted walk (DPRR) and a free-mode AFO walks got altered in stability, hence the second hypothesis also holds true conditionally for unloading phase.

Considering rotational/medial-lateral restrictions, the loading phases showed a decrease in stability margins observed in both anterior-posterior and medial-lateral directions. That was due to the reduced area during foot contact (HC) with the floor in these conditions [108]. These findings were also consistent with event-based MoS(s) evaluated using extrapolated-CoM method. Both rotational restrictions were decreased in stability during loading phases consistent to a prior study where the subjects showed an increase in MoS(s) in response to lateral perturbations [5]. However, the inverted foot was found least stable in this group with decreased PM(s) both in AP and ML directions. Previously, the inverted ankle sprain was described as the most sensitive sports injury and had a chronic contribution towards gait instability [165].

During unloading phases, N&B methods showed a decrease in inverted foot instability in the forward direction (AP). The peak dorsi-plantarflexion angles and moments were also decreased during inversion ( $p < 0.01$ ) more than eversion. That was also reported previously in patients with lateral ankle sprains who were observed reluctantly to put body weight at forefoot [166]. The MoS(s) applying extrapolated-CoM method also showed a decrease in CoM sway at TO event compared to a normal walk. That was consistent with findings from Nyquist and Bode stability margins. In the medial-lateral direction, Nyquist and Bode stability methods showed decreasing trends in instability for both inversion and eversion, however, remained statistically insignificant compared to MoS(s) computed using XCoM method. The main reason might be the consideration of CoM variations along with CoP in XCoM method which increased the sensitivity of measurement using another dynamic variable while quantifying MoS(s). Applying Nyquist and Bode methods, the second hypothesis that the rotational impairments significantly affect gait transitional stabilities holds true with a decrease in stabilities during loading phases both in AP and ML directions and a decrease in AP instability only for the inverted foot during unloading phase.

The effect of walking speed on gait dynamic stability has been reported with inconsistent outcomes e.g. slow speed walk was reported to be more stable in one study and negated by in another [167-169]. The stability margins quantified here at self-selected walking speed showed that a normal/preferred speed walk is more stable (PM) than a slow walk and has no difference with fast speed during the loading phase. This finding was also supported by prior studies [170, 171] with conclusions such as preferred walking speed showed the best compromise for frontal plane stability during single limb support and smooth weight transfer during double limb support. The self-selected normal walking speed also reported for the conservation of transformation energies (kinetic to potential and vice versa) during gait transitions [30, 172]. During respective unloading phases, a decrease in instability at fast speed walk made it preferred over slow and normal speed walks which did not show any mutual difference in stability margins. That was consistent with findings in a prior study in which fast speed walk (treadmill) was reported to have increased in stability resulted from local dynamic stability method quantified using acceleration (accelerometer mounted on the sternum) and markers based data collected for a fixed number of strides [164, 173]. The experiments in this study are performed at individuals' self-selected walking speeds, however, a treadmill-based constant speed trial might be able to illustrate the differences further. Applying Nyquist and Bode stability measures, the conclusions may be drawn that the preferred and fast walking speeds are equally stable during loading phases and fast speed decreased in instability during the unloading phase of double limb support.

Gait stability margins from Nyquist and Bode methods were also compared with MoS(s) computed using extrapolated-CoM and CoP interaction. However, a direct validation between these two methods was rather confusing as the former technique used to quantify gait phases and the latter quantified MoS(s) at discrete gait events (HC and TO). The stability quantification using CoP waveforms alone with Nyquist and Bode methods provided redundancy of measurement and decreased the dependability compared to interaction between two dynamic variables (CoM and BoS/CoP) in extrapolated-CoM method. The Nyquist and Bode methods illustrated the potential of CoP waveforms to quantify gait dynamic stabilities alone. Further, the criteria of quantifying gait dynamic stability were reported previously with discrepancies. For example, increased variabilities in spatiotemporal features, or CoM sways [28, 40] were reported to present poor balance control, in contrast, the decreased variabilities in CoM sway w.r.t BoS, temporal parameters, or joint angles [28, 34] were also used to quantify poor stability. Further, the time-dependent rate of change in two interactive variables (CoM and CoP) was ignored while computing MoS (meters) implied that no conclusion could be strictly quantified about the time-dependent gain/loss in stability applying extrapolated-CoM method.

Comparing with all prior methodological choices, the Nyquist and Bode methods used distinct cut-off thresholds (gain: 0dB, phase:  $\pm 180^\circ \pm 2k\pi$ ) [100, 101, 145] with reference to which stability margins were quantified for both healthy individuals and impaired subjects, and thereafter the stability margins were compared statistically among investigating groups. All prior stability assessment techniques (XCoM, Lyapunov exponent, ICC, parametric variability) [10, 11] relied on outcomes from control subjects in order to define stability/instability during a gait cycle. That dependence on control subjects made the stability definition non-standardised and varied from one study group to another. Further, prior methods measured walking stabilities either at discrete gait events (e.g. HC and TO in XCoM method) or used whole time series waveforms of a kinematic parameter (e.g. Lyapunov exponent method) which were deficient to quantify stabilities during gait transitions (loading, unloading) i.e. changeover between single to double support and vice-versa [164]. Comparatively, the window based stability quantification in this study provided detailed assessment during these transitions. The Nyquist and Bode methods were also capable of quantifying multiple stability changeovers (between stability and instability) over the considered span of a gait phase, however, the least stability margins were considered critical and hence used in this chapter.

There are also few limitations of the current study e.g. CoP-velocity gave good stability measure for gait transient phases (double-limb-support) and remained steady state during mid/terminal-stance phase (single-support phase) consistent with lower

**Table 4.13: Summary of discussion regarding the first hypothesis.**

<b>Intralimb interaction</b>	<b>Spearman Correlation (min to max)</b>	<b>Hypothesis 1</b>
Intact limb unloading and impaired limb loading	negative (p<0.001) forward impairments (-0.462 to -0.842) rotational impairments (-0.779 to -.834)	hold true
Intact limb loading and impaired limb unloading	negative (p<0.001) forward impairments (-0.749 to -0.882) rotational impairments (-0.791 to -0.812)	hold true

**Table 4.14: Summary of discussion regarding the second hypothesis.**

<b>Comparative conditions</b>	<b>Stability Margins (N&amp;B methods)</b>	<b>Margin of stability (MoS*) from Extrapolated-CoM method</b>	<b>Hypothesis 2</b>
<b>Loading Phases</b>			
Difference of a normal walk by wearing AFO (free mode)	stability decrease	MoS decreases at HC	holds true
Impact on AFO (free mode) walk by restricting ankle-foot motions	no difference	no difference in MoS(s) at HC	not hold true

<b>Table 4.14 Continue</b>	<b>Stability Margins (N&amp;B methods)</b>	<b>Margin of stability (MoS*) from Extrapolated-CoM method</b>	<b>Hypothesis 2</b>
Difference of rotational restriction with a normal walk	stability increase in eversion and decrease in inversion	MoS decreases at HC	holds true
Difference of walking speeds with a normal walk	stability decrease in slow walk	no difference in MoS(s) at HC	holds true
<b>Unloading Phases</b>			
Difference of a normal walk by wearing AFO (free mode)	instability decrease	MoS decreases at TO	holds true
Impact on AFO (free mode) walk by restricting ankle-foot motions	instability increased	no difference in MoS(s) at TO	holds true
Difference of rotational restriction with a normal walk	instability decrease in inversion	MoS decreases at TO	holds true
Difference of walking speeds with a normal walk	instability decrease in fast walk	MoS increased at fast speed and decreased at slow speed	holds true

\*MoS presents stability at heel contact (HC) and instability at toe-off (TO).

limb muscles activations during stance phase. However, the CoP signals provide no stability information for the swing phases. The CoP-velocity provided whole-body stability measure (centroid of reaction forces) whereas to understand the detailed inter/intralimb interactions, the variability in lower limb joints angles and moments are further required to evaluate. Also, the signals pre-processing such as computing the derivative and mean velocity of CoP waveforms, filtering the noise, and ensuring the linearity of modelled waveforms added more computational steps compared to prior stability assessment methods.

Clinically, these methods can be implemented to compute stability margins for ankle-foot abnormalities e.g. foot drop, Charcot-Marie-tooth, Equinus, everted/inverted feet with a varying degree of impairments and in different age groups. These impairments might affect the ankle or foot performance either in loading, unloading, or both phases, thus a window based gait stability analysis proposed in this study provides a way to quantify stability in either phase. The simulated impairments approach was used for implementing Nyquist and Bode stability methods that reduced variability within the group, however, investigation with real patients is proposed as a part of future work. The aforementioned discussion is summarised in Tables 4.13 and 4.14.

## **4.6 Summary**

In this chapter, the body's CoP waveforms were used to predict neuromotor balance control for various imitated ankle-foot impairments. The impulsive nature CoP-velocity waveforms were modelled in time and frequency domains and analysed further by implementing control engineering theory i.e. Nyquist and Bode stability methods. These techniques quantified gait dynamic stabilities as gain margins and phase margins for each of the walking conditions. The results showed significant differences of the normal walk with forwarding impairments imitated by wearing an ankle-foot orthosis (AFO), with foot rotational impairments imitated with foot insoles, and walking at different speeds during loading and unloading gait transitions. Summarising results, these methods illustrated a decrease in gait dynamic stabilities for imitated impairments, also compared by applying extrapolated CoM and CoP interaction method. The Nyquist and Bode methods illustrated alternative stability assessment techniques with certain advantages over prior methods. These included distinct cut-off thresholds to define stable/unstable margins, stability quantification for transitional phases of stance and provided redundancy of measurements using CoP signals alone. The proposed methods are introduced in this chapter as a pilot study and have potential applications towards the assessment of the ankle-foot abnormalities/injuries, rehabilitation effectiveness, and stability evaluations with wearable orthoses/exoskeletons/prostheses.

## **CHAPTER 5**

# **SOMATOSENSORY FORWARD COM-OSCILLATIONS IMPACTS ON GAIT TRANSITIONAL STABILITIES**

### **5.1 Introduction**

This chapter evaluates the body's CoM fluctuations impact on gait dynamic stability as a sensory feedback to the neuromotor control in anterior-posterior (forward) direction. The wearable orthoses were designed to imitate walking deficiencies grouped into forwarding ankle-foot impairments, rotational impairments, and self-selected walking speeds. The resultant  $GRF_{AP}$  data was collected as an accumulated response from the leg muscles. The rate of change in CoM-acceleration ( $GRF_{AP}/mass$ ) illustrated two major impulses at HC and TO. These impulsive CoM-oscillations were modelled in time and frequency domains and analysed by applying engineering control theory. The balance control stability margins were quantified as gain margins (GM) and phase margins (PM) applying Nyquist and Bode stability methods. The results were compared with previous methods such as lower limb kinematic/kinetic peaks, variability in time series CoM-oscillations, and correlations. Lastly, stability margins quantified from CoP as an output neuromotor response are compared with CoM-oscillations as a somatosensory input to the neuromotor.

The experimental protocol was approved by the ethical review board of the University of Leeds. Each subject signed an informed consent form. In addition, a separate consent about video/photographic data was also signed by each subject.

### **5.2 Hypotheses**

It was reported earlier that the spine motor activity fluctuated with body's CoM and generate two major bursts of activity around heel contact (HC) and toe-off (TO), also exhibited by most of the leg muscles [33]. In this chapter, these fluctuations in CoM are modelled as somatosensory feedback to the neural system as illustrated in Figure 5.1 and investigated following balance control aspects:

Firstly, what is the impact of anterior-posterior CoM-vibrations on gait transitional stabilities with forward and rotational ankle-foot impairments, and with variations in preferred walking speeds?

Secondly, whether ankle-foot orthosis increase/decrease gait transitional stability by tuning the device to clinically applied adjustments?



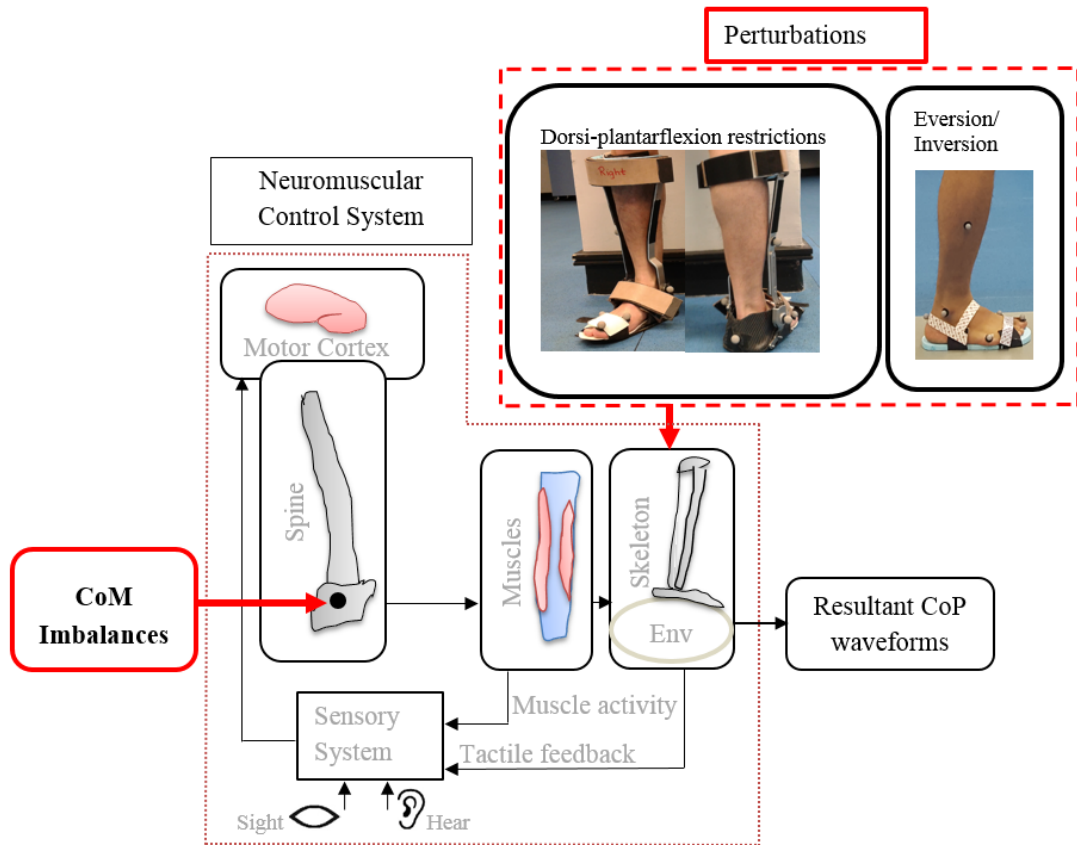


**Figure 5.1: Neural postural control loop showing the sensory feedback provided to the brain by proprioception, hear, and sight senses and an error signal generated in the brain used to reweight muscles activation to provide stabilizing toques to the lower limb joints. The resultant imbalances measured from body CoM-vibrations in the direction of motion.**

## 5.3 Methods

### 5.3.1 Experimental Protocol

A total of ten healthy subjects (age:  $30 \pm 1$ yr, weight:  $71.6 \pm 8$ kg, height:  $1.69 \pm .5$ m) were inducted in this study. It was ensured that the subjects did not have any prior neuromuscular or anatomical impairments. The trials were recorded using a motion capture system and force platforms with details described in Chapter 3 (section 3.4). The rotational/wedged insoles [110, 113, 174] and AFO restricted walking imitations were followed from earlier studies [15, 111, 112] (details in section 3.3). Five trials were used from each subject for further analysis. In total, ten walking conditions are simulated divided into three groups i.e. walking speed, rotational, and forward ankle-foot impairments (details in Table 3.4).

### 5.3.2 Data Processing

The force plates data was exported to Visual-3D motion analysis software in the form of C3D files. The events detection algorithm was applied and stance phases ground reaction force (GRF) data were exported in Matlab-9.2 for further analysis. The anterior-posterior (AP) component of GRFs was processed in subsequent steps. Firstly, the finite difference algorithm was implemented and time-dependent change in the anterior-posterior component of GRFs was computed. Then, the randomly sampled data was equalised by interpolating such that each trial was equivalent to 500 samples of the stance phase. Secondly, the rate of change in GRFs was normalised by subjects body weight to get the anterior-posterior rate of change in CoM-acceleration. Thirdly, the root means square (RMS) of resultant CoM-oscillations were determined. The RMS value of CoM-vibration waveforms was computed to capture actual power density spectrum following earlier studies [2, 9, 175]. Both the raw and RMS data is shown in Figure 5.2 for normal walk trials.

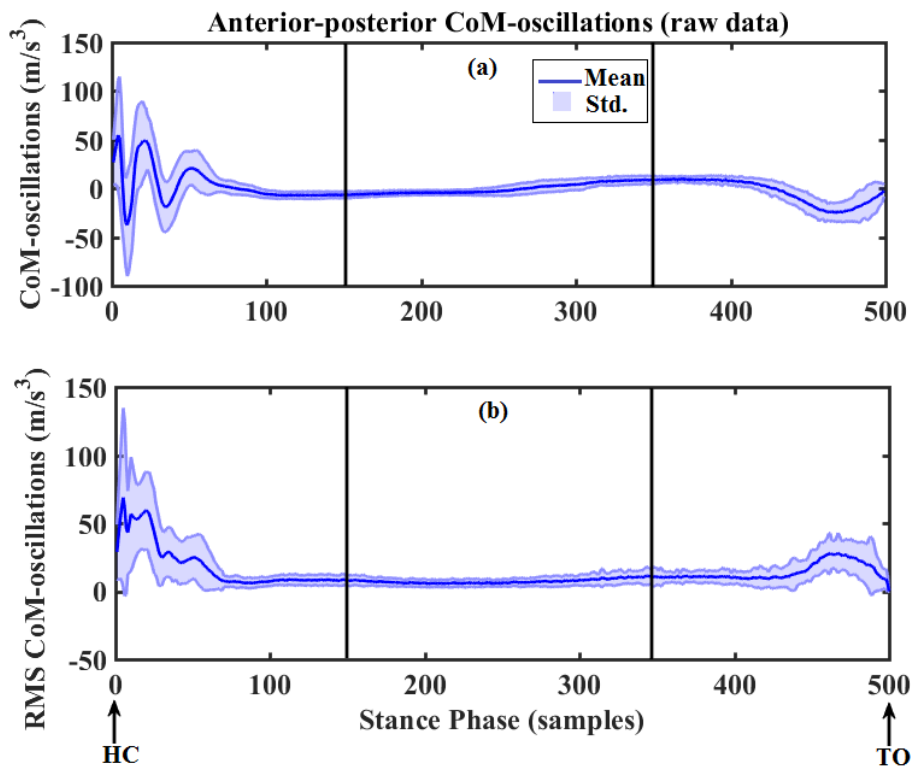


**Figure 5.2: (a) The impact forces illustrate maximum magnitudes and oscillatory response during heel impact and relatively low magnitude oscillations during unloading phases. (b) The RMS value showing the power density spectrum of CoM-vibrations.**

Finally, the resultant waveforms were filtered. Previously, GRF/CoM-acceleration and jerk data were reported to be filtered at 10 Hz cut-off using lowpass filters [158, 175]. In this study, the cut-off frequency is further confirmed by applying residual analysis methods [159] to the CoM-vibrations data. Applying this algorithm, the

residual RMS plot is shown in Figure 5.3. The cut-off frequency was the one where the averaged residual crossed the intercept of the tangent line with the ordinate. A 2<sup>nd</sup> order lowpass Butterworth filter was found to be optimal with cut-off frequency 10Hz.

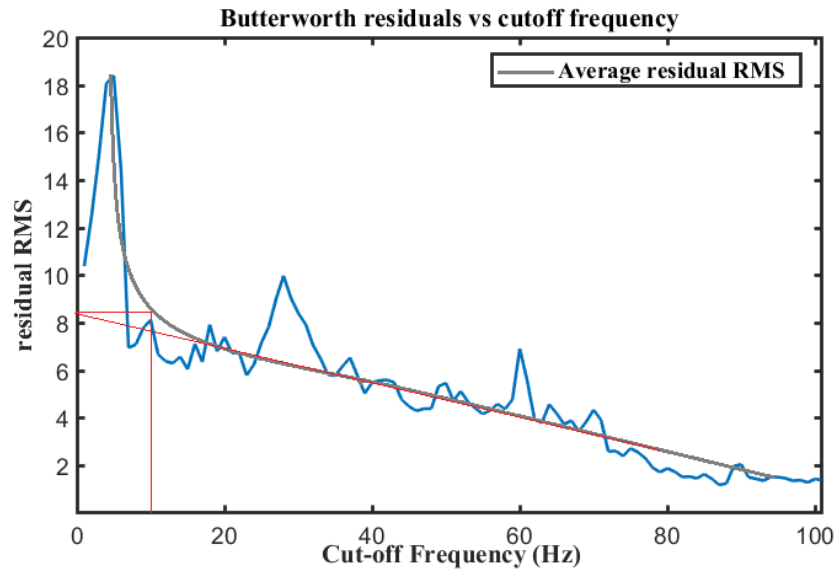


**Figure 5.3: Residual analysis to estimate the cut-off frequency of filtering, performed using CoM-vibrations data from an unrestricted normal walk.**

### 5.3.3 Time and Frequency domain Modelling

The rate-dependent CoM-acceleration waveforms showed oscillatory response with initially decaying amplitudes from HC towards mid-stance and thereafter rising magnitudes from mid-stance towards TO as illustrated earlier in Figure 5.2(b). These transitions in amplitudes took place in first ~30% of stance and then became a steady state and then rise in amplitude during last ~30% of stance phase. Hence, the CoM oscillations were windowed accordingly following earlier vertical GRF based windowing approach [31]. The shape of these CoM-oscillations observed closer to sinusoidal models compared to exponential CoP-velocity waveforms as modelled in Chapter 4. A decay or rise in rate in CoM-acceleration were modelled and analysed here to quantify gait dynamic stabilities in the forward direction of motion.

The CoM-oscillatory waveforms showed artefacts resulted from variations in subjects height/mass, walking patterns, instrumentation noises, orthoses adjustments, brace fittings, and derivative of measured CoM-acceleration waveforms. These artefacts induce non-linearity and hence removed applying principal component analysis (PCA) [130-132]. The theoretical background and related application of PCA method are already discussed in Chapter 3 (section 3.6.1). Applying the concept, the input data sets were used for each of the walking conditions such that each input matrices ( $150 \times 50$ ) were used whereas 50 trials included five trials per subject of total of ten subjects (subjects  $\times$  trials:  $10 \times 5$ ) and each trial contains 150 samples for respective loading and unloading phases. The output waveforms were reconstructed using

$X=ZU^t$  ( $Z$ : score matrix,  $U$ : coefficient matrix,  $X$ : output matrix) and resultant matrix added with estimated mean of the input matrix. The principal components (PCs) those presented maximum variances were used for further analysis. The criteria used to select the number of PCs were described earlier as the PCs which explained  $>80\%$  variance should be included to reconstruct the outputs [29]. In this study, the principal components (PCs) those meet these criteria are used to reconstruct CoM-vibration waveforms as shown in Figure 5.4 and 5.5 for respective walking conditions and gait phases. Further, the variability in the first principal component (PC1 score in %age) was used to compare time series waveforms in respective walking groups following earlier studies [81, 113]. A low magnitude of variance explained by PC1 implied more instability as more components required to describe maximum variance ( $>80\%$ ) compared to a walking condition that exhibited higher variances [81].

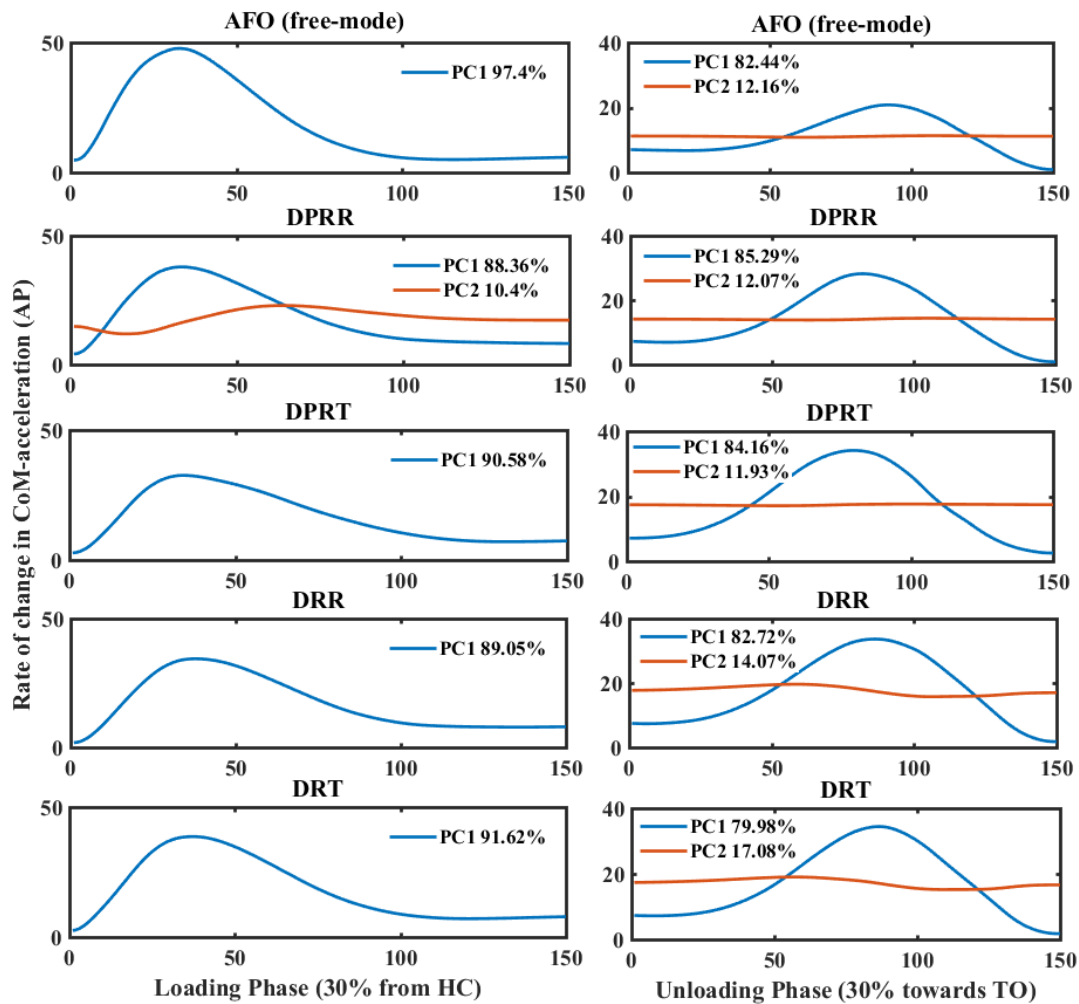


**Figure 5.4: Principal component analysis illustrates the resultant waveforms for AFO restricted conditions, waveforms plotted with  $90\pm 1\%$  variance explained by PC1. For conditions with low values, the PC2 was also plotted.**

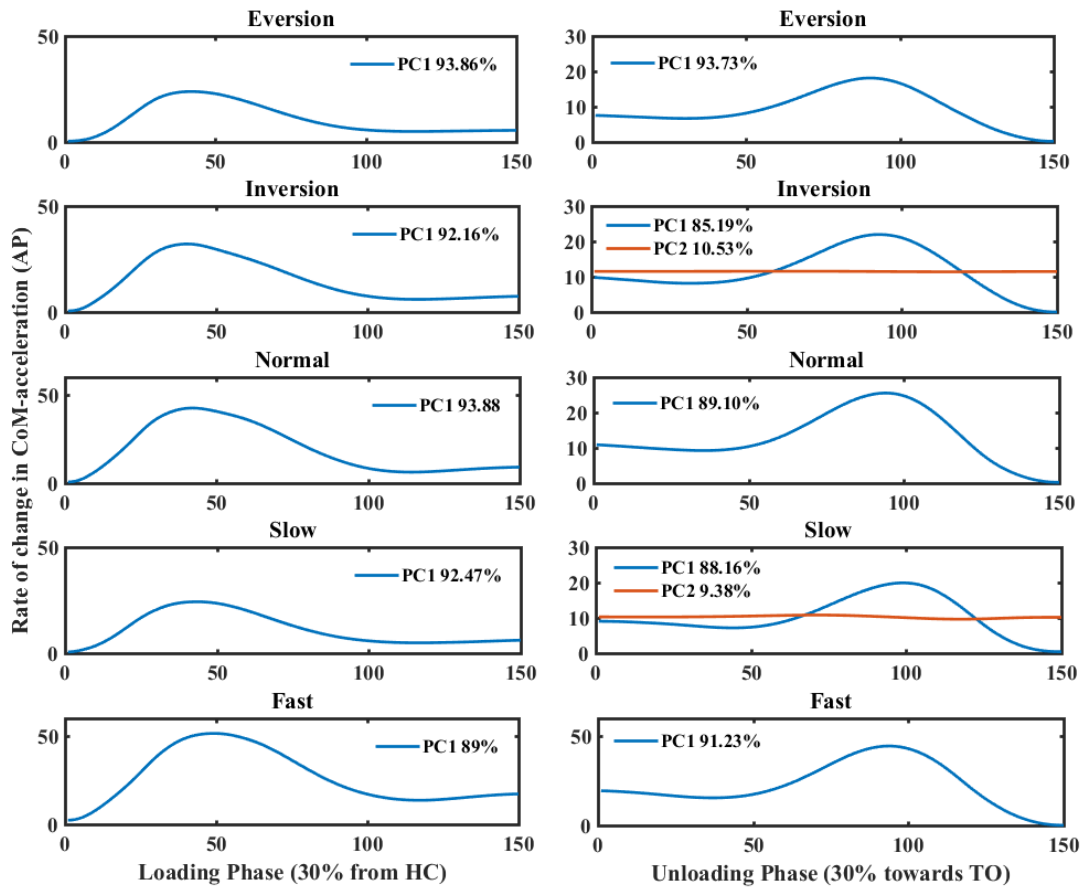


**Figure 5.5: Principal component analysis illustrate the resultant waveforms for rotational restrictions and walking speed groups, and waveforms plotted with  $90\pm 1\%$  variance explained by PC1. For conditions with lower values, the PC2 also plotted.**

The reconstructed time series CoM-vibrations showed decaying oscillations during loading and rising but relatively low magnitude growing oscillations during unloading phases. These vibrations were modelled using system identification approach. A detail about gait-related modelling techniques is described in Chapter 3 (section 3.6.2). Using that information, initially, the sum of exponential models are implemented to CoM-oscillation waveforms using the curve-fitting toolbox and these models are found far away from best fit as shown in Figure 5.6. The other best fit model was polynomial of degree seven however intuitively that resulted in a higher order TFs due to factorial involved in the Laplace transformations. Then the sum of three sinusoids was found the best fit with the coefficient of determination  $R^2 > 99\%$ . The other curve-fitting models such as Gaussian, Fourier were unsuitable for stability analysis due to the complexity of the models and Laplacian transformations. The exponential or sinusoids models were more appropriate because of inherent oscillatory responses, less number of coefficients, and simplified TFs for stability analysis.

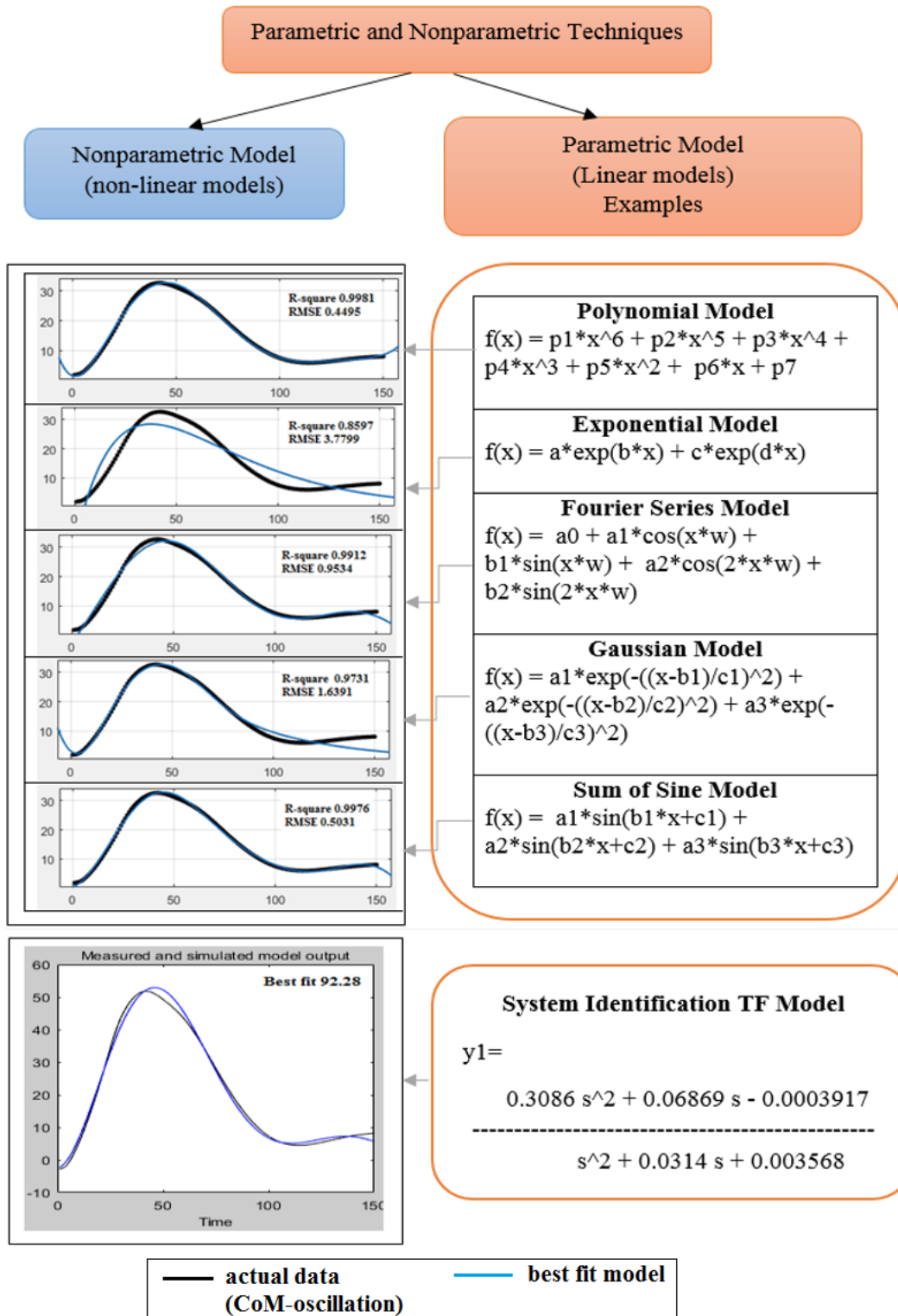


**Figure 5.6: Various empirical linear models simulated for loading phases CoM-vibrations, the best fit model selected based on the coefficient of the determinant ( $R^2$ ) and root mean square error (RMSE).**

Other alternative i.e. system identification toolbox (SIT) was also applied to model linear TFs from the time series waveforms. The best fit models (TFs) using SIT are obtained in varying orders of the numerator and denominator polynomials and with a smaller coefficient of determinants ( $R^2$ ) than curve-fitting as illustrated in Figure 5.7.

Considering stability analysis, the model orders are required to be consistent for all walking conditions to be compared statistically. Because, the varying order of TFs implied the stability margins quantified from these models are at different scales, hence, a statistical comparison with such outcomes is inappropriate. Furthermore, this approach did not converge (miss fit) to unloading phases time series waveforms.

Model	Transfer Function Example
Polynomial Model	$F = \frac{-0.2193 s^{25} + 0.1856 s^{24} - 0.01621 s^{23} + 0.0007327 s^{22} - 1.854e-05 s^{21} + 2.117e-07 s^{20}}{s^{27}}$
Sum of Sine	$F = \frac{0.3965 s^5 + 0.2938 s^4 + 0.08111 s^3 + 0.001777 s^2 + 0.0004973 s + 8.698e-06}{s^6 + 0.01182 s^4 + 3.645e-05 s^2 + 9.199e-09}$

**Figure 5.7: Equivalent transfer functions illustrated for the polynomial and sinusoidal models.**

Among the aforementioned modelling approaches, the sum of sine models was determined to appropriate under the assumption that no further reduction is applied to the output TFs. These time domain sinusoid models were converted to the frequency domain after Laplace transformations. The TFs computed from sinusoids showed all their poles on the imaginary axis as shown in Figure 5.8, which implied an unstable system’s responses for both loading and unloading phases.

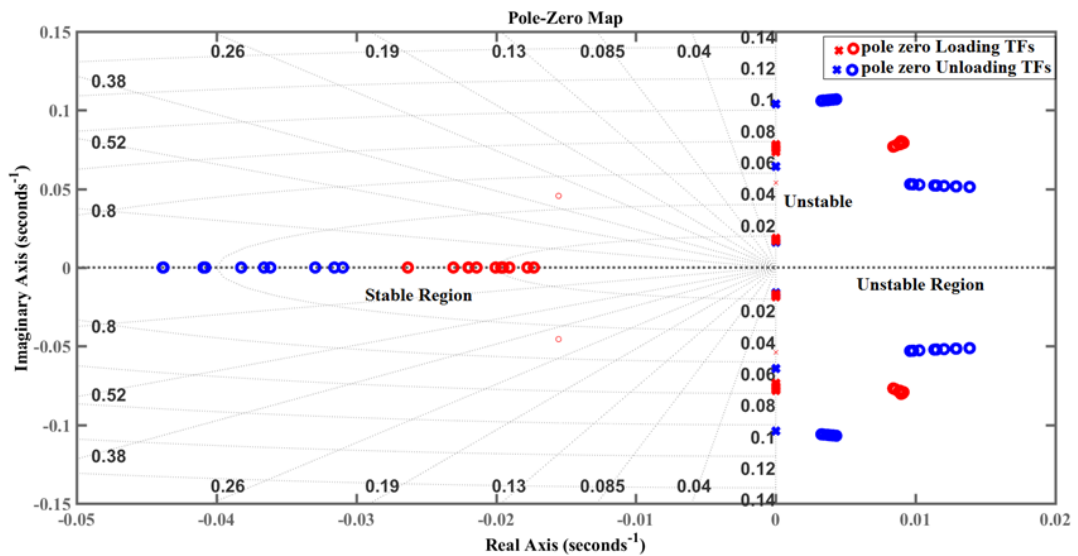


**Figure 5.8: Pole-zeros map showed for both loading and unloading transfer functions (TFs) using unrestricted normal walk trials.**

Applying engineering control theory, both loading and unloading phase TFs showed zeros (roots of numerator polynomials) on the right half of s-plane which mean TFs presented non-minimum phase system. This was consistent with prior flexible system models [176]. The Nyquist and Bode stability methods are implemented and stability

margins are quantified as gain margin (GM) and phase margin (PM) as shown in Figure 5.9. The basic theory of these algorithms is already discussed in Chapter 3 (section 3.6.3).

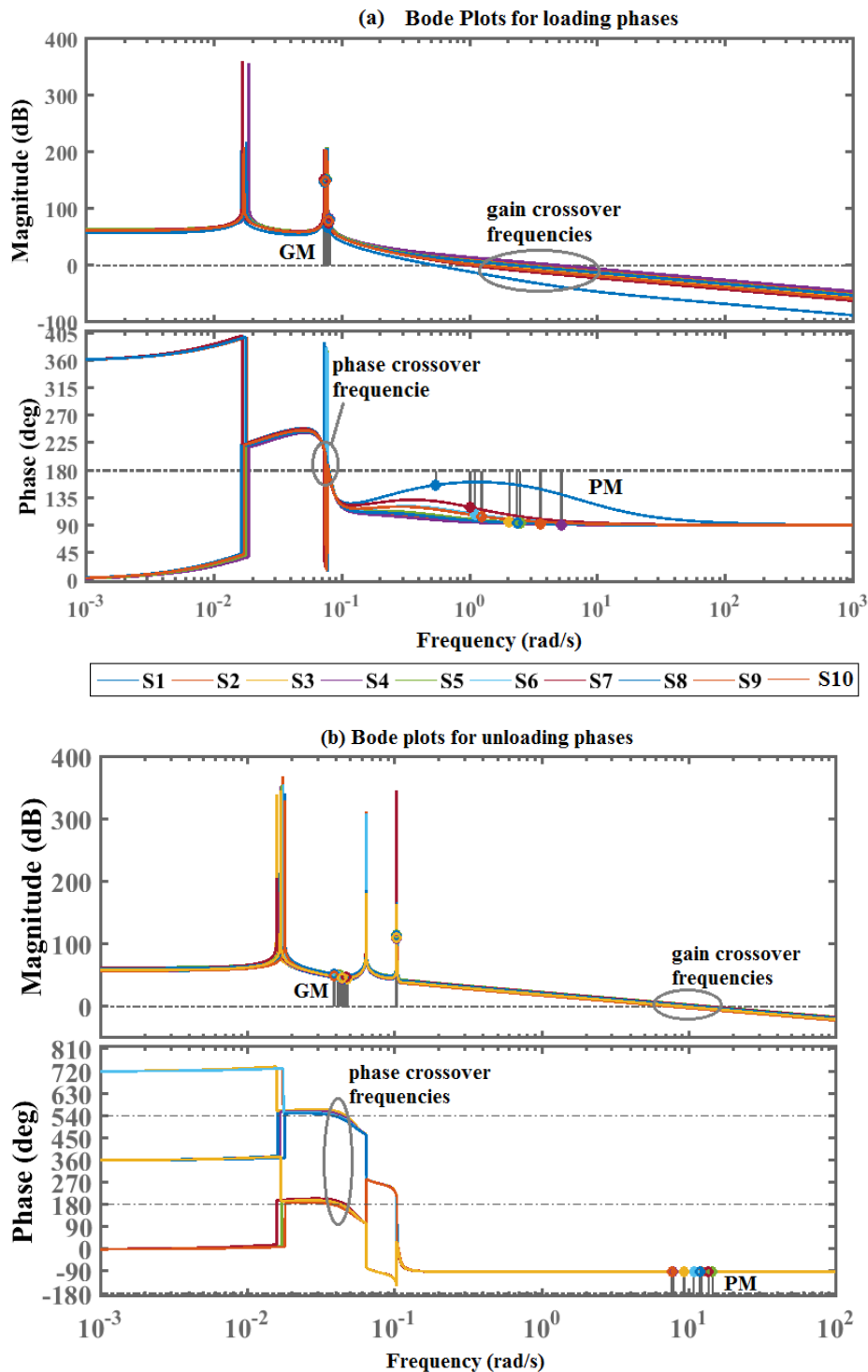


**Figure 5.9: Bode plots examples illustrated for the loading and unloading phases transfer functions using normal walk mean trials (S: subjects). The critical stability margins quantified for: (a) minimum phase margins at 0dB gain crossover frequencies, (b) minimum gain margins at  $\pm 180^\circ \pm 2k\pi$  phase crossover frequencies.**



### 5.3.4 Correlation Coefficients

The correlation coefficient method explained in Chapter 2 (section 2.4.2) and applied here using CoM-vibrations data for respective transitional phases in support to the outcomes from Nyquist and Bode stability methods. The motivation behind was that the impaired subjects showed inconsistent and more frequent movements with a decrease in correlation between two conditions to be compared. The correlation is examined here such that the normal walk is compared with each of the restricted walking conditions.

### 5.3.5 Statistical Analysis

The stability margins quantified here using Nyquist and Bode methods, correlation coefficients, were compared statistically (Wilcoxon-signed rank test,  $p < 0.05$ ) in respective walking conditions and groups (details in Chapter 3 section 3.7).

## 5.4 Results

The results from Nyquist and Bode methods are also compared with earlier methods using same rate dependant CoM-acceleration data as illustrated in Figure 5.10.

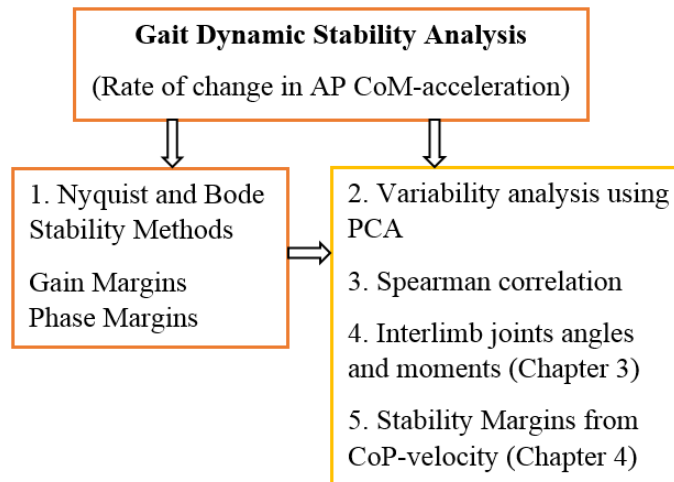


**Figure 5.10: Flow diagram illustrating the comparison between stability outcomes quantified by applying different methods.**

### 5.4.1 Modelling Results

The results regarding best fit models are mentioned in Tables 5.1 and 5.2. The alternative best fit models for CoM-vibrations data and their Laplace transforms are already described earlier in Figure 5.7. The CoM-vibrations damped responses as the limb moved towards mid-stance. The pole-zero map of these TFs showed unstable response with all poles located at the imaginary axis. The unloading phases showed relatively low magnitude CoM-vibrations while moving the terminal stance towards the unloading phase. Likewise the loading phases, the unloading phase TFs showed

all their poles also located on imaginary axes of the s-plane and hence showed unstable responses. The exact quantification of stability margins was determined using GMs and PMs for the individual walking conditions.

#### 5.4.2 Loading Phases Stability Margins

Considering the AFO restriction group in Table 5.1 and Figure 5.11, an AFO free-mode walk showed maximum instability in this group in terms of GMs. Comparing with AFO free-mode walk, the stiffness based AFO restrictions (DPRT, DRT) and range of motion AFO restriction (DRR) showed a significant decrease ( $p < 0.05$ ) in instability whereas the combined dorsi-plantarflexion ROM restriction (DPRR) remained unaffected. Comparing phase margins, there was no significant difference observed between AFO free-mode and restricted walking conditions. A comparison between with AFO and without AFO (normal) walks showed that all AFO walking conditions increased in instability (GMs,  $p < 0.05$ ) compared to a normal/preferred speed walk, however, there was no significant difference found in PMs.

**Table 5.1: Stability margins (mean $\pm$  Std.), variances, and coefficient of determinant quantified for loading phases of AFO restricted conditions.**

Walking Condition	Gain Margin (decibel)	Phase Margin (degree)	% Variance Explained (PC1)	Coefficient of Determinant (R <sup>2</sup> )
Normal (without AFO)	-148.66 6.75	78.36 12.90	93.88	99.76
AFO (free mode)	<b>-169.24</b> 9.31	77.22 14.40	97.4	99.98
DPRR	<b>-164.38</b> 6.25	81.68 6.84	88.36	99.97
DPRT	<b>-155.08*</b> 5.50	78.98 14.71	90.58	99.96
DRR	<b>-154.73*</b> 3.23	78.87 13.93	89	99.76
DRT	<b>-155.23*</b> 4.33	81.61 8.18	91.62	99.92

Bold values showing  $p < 0.05$  when compared with a normal walk, \* for  $p < 0.05$  compared with AFO free-mode walk.

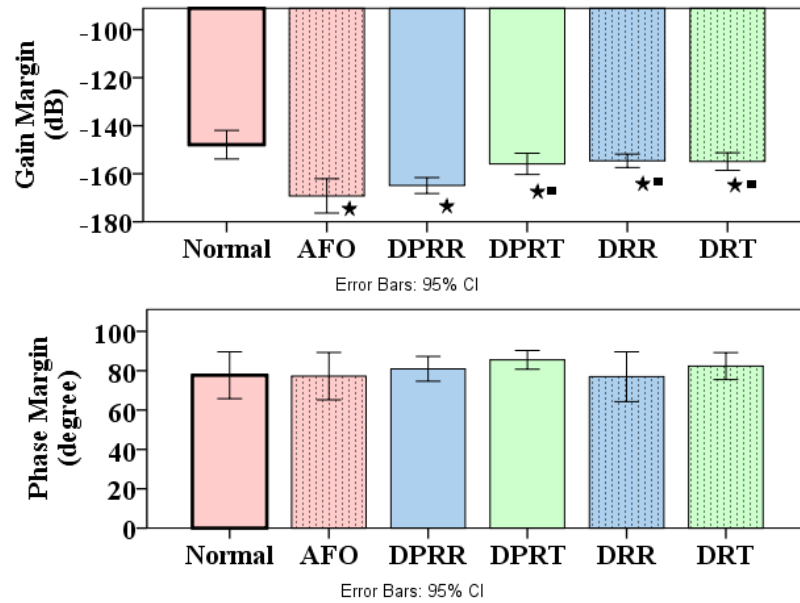


**Figure 5.11: Stability margins comparison for loading phases of AFO restricted conditions using Bar plot (mean ± 95 CI), ‘★’ illustrate the significant difference with a normal walk, ‘■’ illustrate the significant difference with an AFO free-mode walk.**

Considering rotational impairments in Table 5.2 and Figure 5.12, the everted foot showed a decrease in GMs ( $p < 0.05$ ) and an increase in PMs ( $p < 0.05$ ) compared to a normal walk, and an inverted foot condition showed no difference at all. Lastly, the self-selected walking speed group in Table 5.3 and Figure 5.13 showed stability margins ( $p > 0.05$ , GMs, PMs) while compared between normal and fast speed walks, however, the slow speed showed a decrease in instability ( $p < 0.05$ , GMs) and increase in instability ( $p < 0.05$ , PMs) compared to a normal speed walk. Overall, during loading phases, the anterior-posterior CoM-oscillations showed significant differences in w.r.t GMs and showed statistically insignificant differences w.r.t PMs.

**Table 5.2: Stability margins (mean ± Std.), variances, and models coefficient of determinant quantified for loading phases of rotational foot restrictions.**

Walking Condition	Gain Margin (decibel)	Phase Margin (degree)	% Variance Explained (PC1)	Coefficient of Determinant (R <sup>2</sup> )
Preferred/Normal	-148.66 6.75	78.36 12.90	93.88	99.76
Eversion	<b>-133.11</b> 3.91	<b>89.37</b> 2.27	93.86	99.9
Inversion	-142.53 7.56	85.06 3.59	92.16	99.74

Bold values showing  $p < 0.05$  when compared with a normal walk.

**Table 5.3: Stability margins (mean± Std.), variances, and models coefficient of determination quantified for loading phases of self-selected walking speeds.**

Walking Speed	Gain Margin (decibel)	Phase Margin (degree)	% Variance Explained (PC1)	Coefficient of Determinant (R <sup>2</sup> )
Preferred/Normal	-148.66 6.75	78.36 12.90	93.88	99.76
Slow	<b>-141.30</b> 3.46	<b>87.48</b> 2.42	92.47	99.86
Fast	-146.57 3.77	83.51 11.70	89	99.94

Bold values showing  $p < 0.05$  when compared with a normal walk.

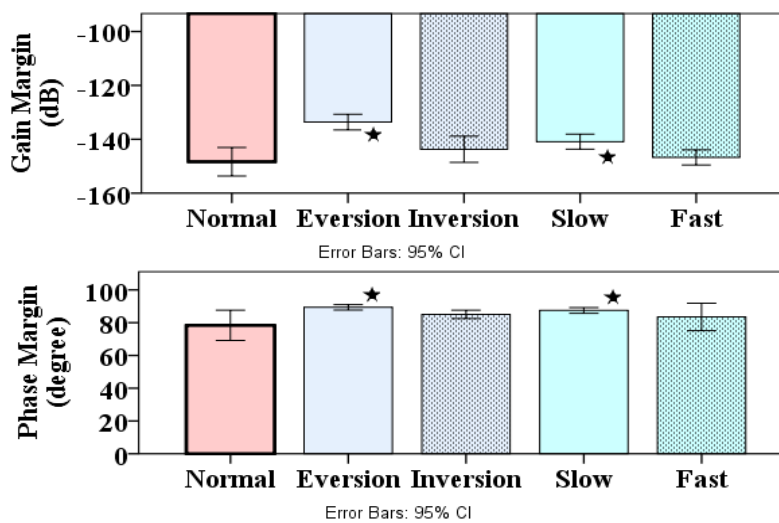


**Figure 5.12: Stability margins comparison for loading phases of rotational impairments and walking speed groups using Bar plots (mean ± 95 CI), ‘★’ illustrate significant difference w.r.t a normal walk.**

### 5.4.3 Unloading Phases Stability Margins

Considering AFO restrictions in Table 5.4 and Figure 5.13, the AFO restricted walking conditions showed a decrease ( $p < 0.05$ ) in instability (GMs) for combined dorsi-plantarflexion ROM restriction (DPRR) and increased in instability (GMs) for dorsiflexion restrictions alone (DRR, DSR) compared to an AFO free-mode walk. Comparing with a normal walk (without orthoses), all AFO walking conditions showed an increase in instability ( $p < 0.05$ , GMs) except a combined dorsi-plantarflexion ROM restriction (DPRR) which was reduced in instability ( $p < 0.005$ , GMs). The phase margins showed statistically insignificant variations during unloading phases. The only difference was found between AFO free-mode and total restriction ‘DPRR’ condition where the ‘DPRR’ restriction showed a decrease in instability ( $p < 0.008$ , PMs). Comparing with a normal walk (without orthoses), the AFO free-mode walk showed an increase in instability and ‘DPRR’ condition showed a decrease in instability ( $p < 0.005$ , PMs).

**Table 5.4: Stability margins (mean± Std.), variances, and models coefficient of determination quantified for unloading phases of AFO restricted conditions.**

Walking Condition	Gain Margin (decibel)	Phase Margin (degree)	% Variance Explained (PC1)	Coefficient of Determinant (R <sup>2</sup> )
Normal (without AFO)	-111.96 2.33	89.963 0.009	89.1	99.98
AFO (free mode)	<b>-114.16</b> 2.33	<b>89.976</b> 0.009	82.44	99.97
DPRR	<b>-90.52*</b> 3.93	<b>89.926*</b> 0.019	85.29	99.91
DPRT	<b>-119.42</b> 5.79	89.955 0.023	84.16	99.98
DRR	<b>-161.75*</b> 16.11	89.941 0.043	82.72	99.98
DRT	<b>-151.77*</b> 2.93	89.955 0.361	80	99.96

Bold values showing  $p < 0.05$  when compared with a normal walk, \* for  $p < 0.05$  compared with AFO free-mode walk.

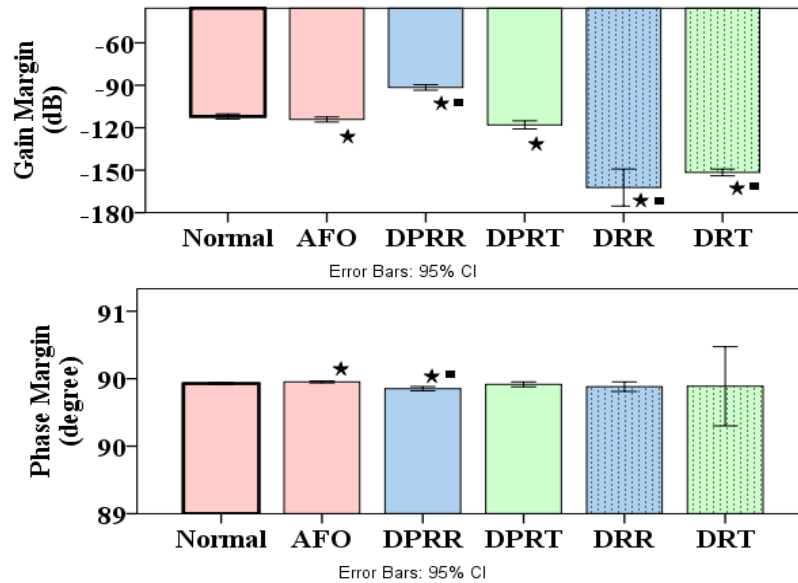


**Figure 5.13: Stability margins comparison for unloading phases of AFO restricted conditions using Bar plot (mean ± 95 CI), ‘★’ illustrate the significant difference with a normal walk, ‘■’ illustrate the significant difference with an AFO free-mode walk.**

Among the rotational impairments in Table 5.5 and Figure 5.14, an inverted foot walk showed a significant increase in instability ( $p < 0.005$ , GMs, PMs) compared to a normal walk. However, an everted foot walk showed a small but significant decrease in instability ( $P < 0.05$ , PMs) compared to a normal walk. In walking speed group Table 5.6 and Figure 5.15, the fast walk showed a decrease in instability in terms of GMs, and slow walk showed a decrease in instability in terms of PMs. Overall, during

unloading phases, the stability margins showed greater variations in gain margins for all walking conditions, and small but significant variations in phase margins in walking conditions i.e. ‘DPRR’, eversion/inversion rotational impairments, and slow walking speed.

**Table 5.5: Stability margins (mean± Std.), variances, and models coefficient of determination quantified for unloading phases of rotational foot restrictions.**

Walking Condition	Gain Margin (decibel)	Phase Margin (degree)	% Variance Explained (PC1)	Coefficient of Determinant (R <sup>2</sup> )
Preferred/Normal	-111.96 2.33	89.963 0.009	89.1	99.98
Eversion	-104.03 9.46	<b>89.899</b> 0.11	93.43	99.9
Inversion	<b>-115.37</b> 2.16	<b>90.101</b> 0.308	85.2	99.9

bold values showing p<0.05 when compared with a normal walk.

**Table 5.6: Stability margins (mean± Std.), variances, and models coefficient of determination quantified for unloading phases of self-selected walking speeds.**

Walking Speed	Gain Margin (decibel)	Phase Margin (degree)	% Variance Explained (PC1)	Coefficient of Determinant (R <sup>2</sup> )
Preferred/Normal	-111.96 2.66	89.963 0.009	89.1	99.98
Slow	-114.72 3.75	<b>89.917</b> 0.023	88.16	99.94
Fast	<b>-114.87</b> 2.66	89.973 0.012	91.23	99.99

bold values showing p<0.05 when compared with a normal walk.

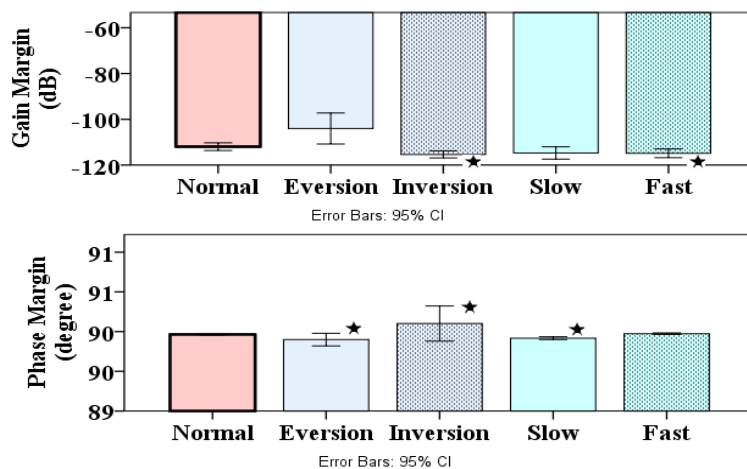


**Figure 5.14: Stability margins comparison for unloading phases of rotational impairments and walking speed groups using Bar plots (mean ± 95 CI), ‘★’ illustrate significant difference w.r.t a normal walk.**

#### 5.4.4 Variability in Principal Components

The variability in CoM-vibration time series waveforms is quantified by the first principal component (PC1, >80% variance) in Tables 5.1 and 5.2 for respective walking conditions. The results illustrated that the variability (data explained by PC1 in percentage) increases in AFO restricted conditions expressed by low percentages of PC1's when compared to a normal walk. The PCA results for rotational impairments showed no noticeable differences for the loading phases, however, during respective unloading phases, the inverted foot increased 3.9% and everted foot decreased 4.33% in variabilities compared to a normal walk. Similarly, in walk speed group, both the slow and fast walks were increased in variability explained by PC1's in loading phases. In the respective unloading phase, only fast walk showed a decrease in variability.

#### 5.4.5 Spearman Correlations

The results from Spearman's correlation coefficient in Table 5.7 showed a relatively low correlation between normal and AFO free-mode walk compared with other AFO restricted walking conditions during loading phases. During unloading phases, the correlation was relatively decreased for moderate stiffness DPRT condition and remain consistent for the rest of AFO walking conditions. The results for rotational restrictions and walking speed groups in Table 5.7 showed equally strong correlations between normal walk and eversion, inversion, slow and fast speed walks. However, that correlation was relatively weak for a fast walk during the unloading phase. Unlike to CoP-velocity (Chapter 4), there is no intralimb interaction found in CoM-oscillations.

**Table 5.7: Spearman's correlation between normal walk and AFO restricted conditions, rotational restrictions and walking speed groups.**

Correlation between	AFO restricted impairments				
	AFO (p-value)	DPRR (p-value)	DPRT (p-value)	DRR (p-value)	DRT (p-value)
Loading phase	0.736 (0.001)	0.872 (0.001)	0.929 (0.001)	0.875 (0.001)	0.867 (0.001)
Unloading phase	0.820 (0.001)	0.883 (0.001)	0.778 (0.001)	0.896 (0.001)	0.823 (0.001)
Correlation between	Rotational restrictions and walking speed				
	Eversion (p-value)	Inversion (p-value)	Slow (p-value)	Fast (p-value)	
Loading phase	0.830 (0.001)	0.849 (0.001)	0.890 (0.001)	0.943 (0.001)	
Unloading phase	0.884 (0.001)	0.837 (0.001)	0.978 (0.001)	0.744 (0.001)	

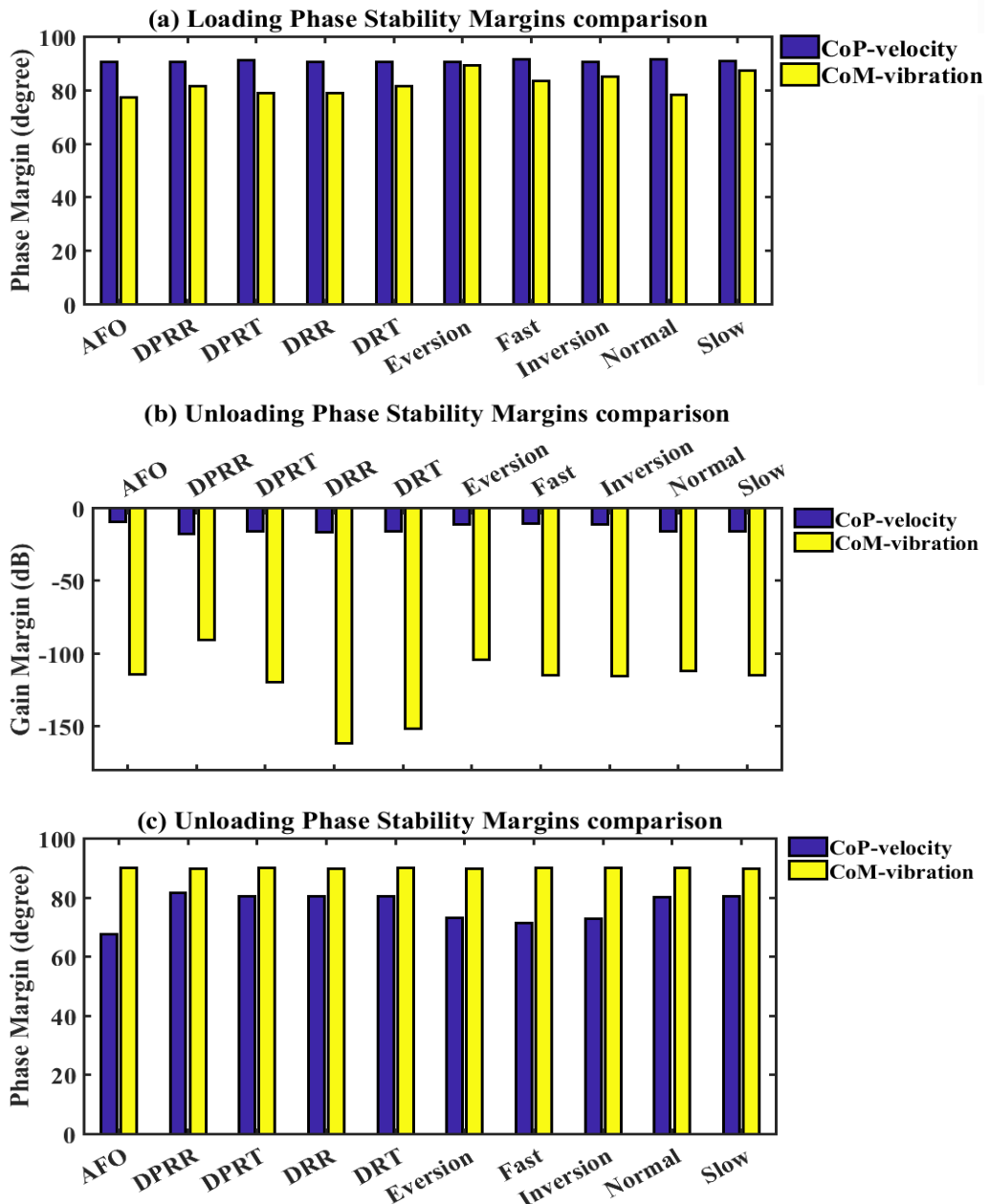
#### **5.4.6 Comparison between CoP and CoM stability outcomes**

The results from CoM-oscillations illustrated unstable (GMs, PMs) proprioceptive inputs to the neuromotor control, whereas in Chapter 4, the output stability response of the neuromotor was quantified by CoP-velocity waveforms. From Chapter 4, the loading phase margins showed stable responses with infinite GMs and  $90\pm 2^\circ$  PMs. The stability margins from these inputs and outputs are compared here using bar plots in Figure 5.15 for respective loading and unloading phases. Here, the results in Figure 5.15(a) illustrated that the stability margins from outputs (CoP-velocity) were greater in magnitude than the input instabilities quantified from CoM-vibrations. During respective unloading phases in Figure 5.15 (b) and (c), both the inputs (CoM-vibration) and outputs (CoP-velocity) were demonstrated unstable margins, however, the instabilities quantified from outputs (CoP-velocity) were significantly less than the instability generated by inputs (CoM-vibration). Summarising, the margins from inputs (CoM) showed an increase in instabilities in overall, and from outputs (CoP) showed stable responses for the loading phases and decrease in instabilities for the respective unloading phases.

#### **5.4.7 Spatiotemporal, kinematic and kinetic parameters**

Lastly, the stability margins quantified from Nyquist and Bode stability methods were further explained by variability in interlimb hip, knee, and ankle joints angles and moments. The results from lower limb joints angles, moments, and spatiotemporal parameters are summarised in Chapter 3 (Table 3.5). Considering AFO walking conditions, the peak dorsiflexion angles and moments decreased ( $p<0.05$ ) for all AFO restricted conditions comparing with AFO free mode walk. Peak plantarflexion ankle angle reduced ( $p<0.05$ ) only for plantarflexion restricted AFO conditions (DPRR, DPRT) and peak plantarflexion ankle moments increased for resistive torque based conditions (DPRT, DRT). The rotational impairments showed an increase in step length and walking slow speed walk showed a decrease in step length compared to a normal speed walk. The initial plantarflexion ankle angle decreased ( $p<0.05$ ) for both eversion and inversion compared to a normal walk. The peak dorsiflexion ankle angle decreased in the inverted foot and peak plantarflexion angles decreased for both of the rotational impairments. The respective peak ankle moments also decreased for both of the rotational impairments. The slow speed walk showed a decrease ( $p<0.05$ ) in peak knee/hip flexion angles and moments both in stance and swing phases. The fast speed trials showed an increase in knee and hip joints angles ( $p<0.05$ ), and an increase in the ankle, knee, and hip joints moments.

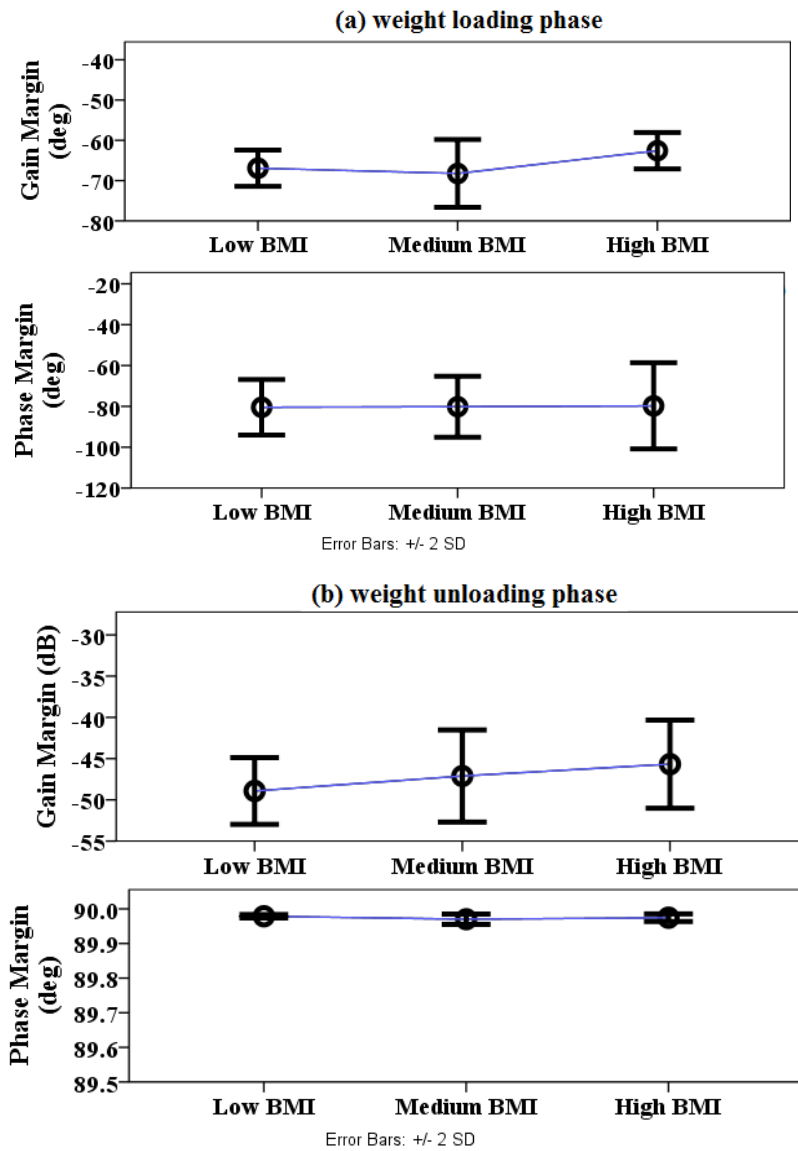




**Figure 5.15: Stability margins quantified from input CoM-vibrations TFs compared with outcomes from respective output CoP-velocity TFs. (a) Loading phases phase margins, (b) Unloading phases gain margins, (c) Unloading phases phase margins.**

### 5.4.8 Body mass index (BMI) impact on transitional stability

Like in the previous chapter (section 4.3.7), the BMI effect on stability outcomes also evaluated using forward CoM-acceleration in this chapter. The BMIs illustrated no significant impact for three ranges (low, medium, and high) within healthy subjects within normal walking speed groups. However, the trend in mean stability margins illustrated a slight increase in instability with an increase in BMI as illustrated in Figure 5.16 for loading and unloading phases margins.

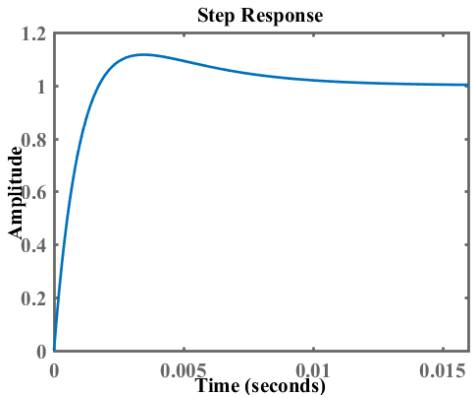
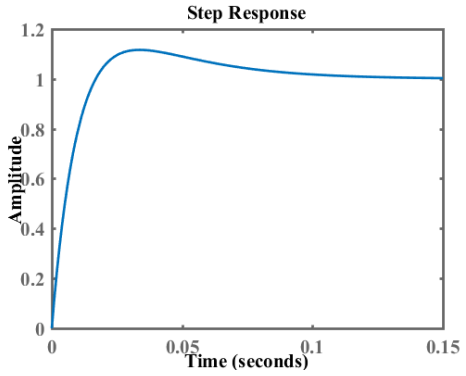


**Figure 5.16** Effect of body mass index (BMI) on gait transitional stability. BMI categorised into subgroups i.e. low ( $21.1\pm 1.9$ ), Medium ( $25.22\pm 0.6$ ), High ( $27.85\pm 0.35$ ), stability margins shown for (a) loading phase, (b) unloading phase.

#### 5.4.9 Controller design for unstable gait transitions

Following the methods described in Chapter 4 (section 4.3.5), the results illustrated that the unstable gait transitional phases (models) can be made stable using controller design approach. The outcomes show that the unstable human gait transitions are controllable as explained by examples in Table 5.8 for both loading and unloading phases.

**Table 5.8 Controller design for unstable CoM-oscillations models.**

<b>Loading Phase</b>	<p>Unstable plant model</p> $\frac{-4.166 s^5 + 1.175 s^4 + 0.078 s^3 + 0.0074 s^2 + 0.00067 s + 1.788e-05}{s^6 + 0.0112 s^4 + 3.361e-05 s^2 + 1.002e-08}$ <p>PI Controller</p> <p><math>K_p + K_i * 1/s</math> where <math>K_p = -298</math>, <math>K_i = -7.42e+04</math></p> 
<b>Unloading Phases</b>	<p>Unstable plant model</p> $\frac{10.63 s^5 + 0.049 s^4 + 0.14 s^3 + 0.0021 s^2 + 0.00024 s + 1.127e-05}{s^6 + 0.01466 s^4 + 4.563e-05 s^2 + 1.108e-08}$ <p>PI controller</p> <p><math>K_p + K_i * 1/s</math> where <math>K_p = 12</math>, <math>K_i = 307</math></p> 

**5.4.10 Effect of walking speed on transitional stability**

Results for varying walking speed trials illustrated increasing trends in instability (GMs and PMs) from very slow to very fast speed during weight loading gait transition. During respective unloading phase, a similar (increasing) trend was observed in terms of gain margins (amplitudes), however, a decrease in instability was observed at very slow speed alone compared with other walking speeds as illustrated in Figure 5.17.

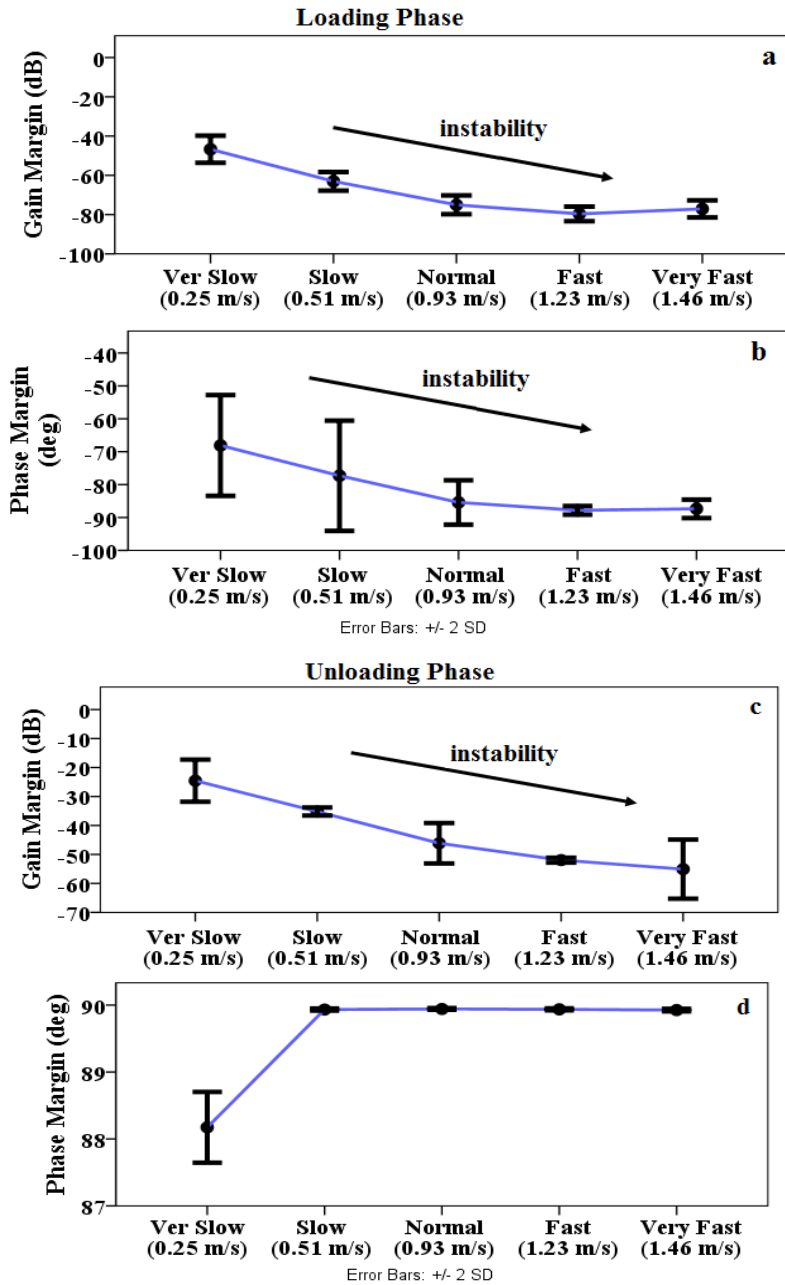


Figure 5.17 Walking speed effect on transitional stability. (a, b) Loading Phases, (c, d) Unloading Phases.

## 5.5 Discussion

The objective in this chapter was to quantify the impact of anterior-posterior CoM-vibrations on gait transitional stabilities during a level walk. The motivation behind this study is that the neuromotor responds to impact forces at HC and TO events and activates leg muscles to generate joints moments. This proprioception feedback (impact forces) is modelled and analysed here for the loading and unloading gait transitions and using the rate of change in CoM-acceleration. The results from three simulated walking groups illustrated that the CoM-vibrations significantly affected gait transitional stabilities. The walking conditions grouped into AFO restrictions

wedged insoles, and self-selected speeds showed significant differences in gain margins for both loading and unloading of stance phases. Relatively, the phase margins showed significant differences mainly in rotational impairments and at slow walking speed. The discussion section is also summarised in Table 5.9.

### **5.5.1 Methodological Considerations**

The rate of change in anterior-posterior CoM-acceleration ( $GRF_{AP}/mass$ ) gives a measure of resultant somatosensory feedback to whom neuromotor responds to control the balance during gait transitions i.e. loading and unloading phases. The central nervous system receives the body orientation feedback from visual (10%), vestibular (20%) and proprioception (70%) [53], based on these generates the error signals w.r.t the reference thresholds, and thus reweight the muscles actuation and sensory information in the repeated loops [80]. The resultant anterior-posterior inputs are modelled here using CoM-acceleration and outputs were modelled in Chapter 4 using CoP waveforms. Both the rate of change in CoP and CoM-acceleration illustrated stance phase transitions by impulsive waveforms and modelled in this study to understand neuromotor balance control. The initial CoM-vibrations were observed just after heel contact and gained steady state towards mid-stance, and the second impulse got prominent from terminal stance and ended towards the push-off phase. A phase/gain shift in these CoM impulses was used to quantify the impact of wearable devices on gait stability. The wearable orthoses introduced small restrictions to the ankle-foot joint motions and hence destabilised the response compared to normal (unrestricted) walk. These simulated restrictions also resemble with real-life ankle-foot impairments such as foot drop (DRT, DRR), Charcot-Marie tooth (DPRT, DPRR), eversion and inversion walking feet. Various simulated restrictions were induced in the ankle-foot joint to understand the neuromotor control and sensory inputs.

The stability margins were quantified by applying control engineering methods. These stability analysis methods were sensitive to best fit empirical model in order to predict precise stability margins. A slight deviation of the model from experimental data resulted in a change in amplitude (gain) and/or time delays (phase). Implies, the corresponding frequency domain gain and/or phase plots might have large deviations from the critical point of instability which used to quantify stability margins. Thus, the resultant gain or phase margins from fewer fit models (e.g. system identification models in this study) were not desirable for comparison between walking conditions which illustrated small differences in magnitudes.

For modelling the CoM-vibrations, the sinusoid models were selected based on inherent oscillatory nature of time series. There is care required while fitting the type and order of the model to the individual walking condition that the two walking

conditions to be compared statistically are required to have similar models types and orders. This is because the output margins would be scaled at different levels with the difference in model order/type and a comparison between two such walking conditions would result in an erroneous interpretation. The others fit models described in methods such as Fourier, Gaussian, polynomial enhanced the complexity of the models and thereafter stability analysis applying Laplace transformations. The high order TFs e.g. the one obtained from the polynomial models can be simplified to lower order models by cancelling the numerator and denominator common factors, however, the resultant models were the unpredictable w.r.t coefficient of the determinant ( $R^2$ ) comparative to lower order sinusoidal best fit models. On the other hand, the system identification tools modelled TFs, ease the further analysis, however, the lack of best fit made the stability outcomes questioned.

The principal component analysis (PCA) removed the artefacts from the oscillatory data and ensured the linearization by transforming the data to simplified uncorrelated components. The maximum variances explained by first principal components (PC1) and respective best fit coefficient of determination ( $R^2$ ) values elucidated the amount of data and efficiency of modelling algorithms to be used to quantify stabilities. The prior stability methods such as Lyapunov exponent and extrapolated-CoM also used time series data, however, these methods [12, 28, 85, 164] were deficient to interpret the efficiency of algorithms used to quantify stability margins.

Applying Nyquist and Bode methods, the stability margins were quantified here as GMs and PMs for respective walking conditions, and both metrics showed unstable outcomes considering the system's overall stability. The GM is used to define robustness w.r.t gain/magnitude/amplitude variations, and PM is used to define the stability of a system as a function of time. The PMs in loading phases showed greater standard deviations, that was due to subjects' less consistent and more frequent adjustments to stabilize trunk movements as also reported previously using tri-axial accelerometer data [11]. Both the loading and unloading phases TFs showed unstable responses overall. However, the output stability quantified in Chapter 4 using CoP waveforms, showed stable response in loading and relatively less unstable unloading phases stability margins. These results illustrated the neuro-mechanical control loop to maintain the balance within safe thresholds in the presence of orthoses restricted perturbations (stiffness, ROM, rotational). The contribution from the other sensory feedbacks i.e. visual and vestibular was not counted in this study.

Prior studies applied AP CoM-acceleration time series fitted to negative exponential models and quantified stabilities for transient activities such as sit-to-stand, bending forward, and stepping forward [2, 9]. The instabilities were estimated comparing model parameters i.e. time constant, static sway, and transitional sways from healthy

subjects with impaired subjects. Comparatively, the rate of change in CoM-acceleration provided more appropriate convergence for exponential models both in loading and unloading phases. However, the sinusoid models were found more appropriate convergent to capture actual oscillatory responses rather taking median or over smoothening the actual time series like in these studies. Further, there was no study found previously which used CoM-acceleration signals to quantify gait transitional stabilities for a level ground walk and with ankle-foot impairments. However, a recent study used variability in angular displacements of trunk, pelvis, and head to estimate stabilities following the criteria of decreased variability indicating increased segmental stability [81]. Applying this criterion to CoM-oscillations data in this study, the variabilities were quantified from the first principal components (PC1s) those illustrated greater variabilities in AFO restricted conditions with low PC1 values compared to a normal walk (94% loading, 89% unloading), and implied greater instabilities found in the AFO restricted conditions. However, these variances were computed using overall time series waveforms for either loading or unloading phases and gave no idea about critical point/points of instability as quantifiable from frequency domain analysis as GMs and PMs. Comparing with prior studies, the estimation of transient locomotor stabilities using CoM-acceleration time series for a level walk and with the effect of wearable orthoses is new in this study.

In Bode plots, two distinct gain versus frequency and phase versus frequency plots were obtained for the CoM-vibration data from each trial, from each plot stability margins were quantified w.r.t a critical cut-off point  $(-1, 0j)$ . In comparison, earlier stability methods such as Lyapunov exponent and extrapolated-CoM methods relied on more than one signals to quantify stabilities and predict stability margins by comparing waveforms between control and impaired subjects without any distinct criteria. To our knowledge, there was no prior study found that investigated CoM-oscillations impact on gait transitional stabilities.

### **5.5.2 Stability Margins**

In this study, the objective of neuromechanical modelling was to examine neuromotor deficits and therapies effectiveness in the presence of imitated impairments. The Nyquist and Bode methods were introduced here to quantify proprioception feedbacks impacts on gait stability. The gain margins quantified from AP CoM-vibrations showed a significant increase in instability by wearing AFO and that instabilities reduced by applying restrictions to the ankle-foot motion during loading phases. The Spearman's correlation coefficients also confirmed these findings by relatively less correlation (0.73) between normal and AFO free-mode walk and that correlation increased ( $>0.86$ ) by tuning AFO restrictions. Implied, the AFO metallic structure increased instability due to loading phase impacts in an anterior-posterior direction

which reduced in intensity by introducing stiffness or ROM restrictions to the ankle joint. That increase in instability (GMs) was due to reduced ankle-foot peak plantarflexion moments in loading phase which also inferred that the lower limb muscles were stiffed enough against initial dorsiflexion restrictions to provide further moments. The output GMs from CoP-velocity waveforms (Chapter 4) illustrated infinite magnitudes in loading phases of all walking conditions. The physical meaning of infinity GMs was that the bipedal loading phases were robust enough to accommodate large variations in stability. Relatively, the PMs from outputs (CoP) illustrated finite but significant variations compared to PMs quantified from inputs (CoM-acceleration). The contribution from visual and vestibular feedbacks are unknown here and speculated to have a contribution in margins quantified from outputs.

During respective unloading phases, a totally restricted condition 'DPRR' illustrated a decrease in instability (GMs and PMs). That was resultant of reduced ankle-foot push-off ability illustrated by both peak plantarflexion angle and peak dorsiflexion moment. The total restriction in 'DPRR' condition did not allow ankle joint for a further excursion of the moment which was increased in stiffness based restricted condition 'DPRT'. Comparatively, the alone dorsiflexion based restrictions (DRT, DRR) showed an increase in instability (GMs) despite no difference in ankle joint angles near push-off. Implied, the reduction in dorsiflexion motion during mid/terminal stance phase (just before push-off) had accumulative impacts on the push-off phase where there was no restriction applied to the ankle-foot motion. This was also confirmed by an increase in the ankle-foot moment during push-off in 'DRT' condition. The time series waveforms comparison using Spearman's correlation did not illustrate any noticeable decrease in correlations between unrestricted and restricted walking conditions. These findings demonstrated that AFO orthoses mainly impacted w.r.t gain margins during loading and unloading phases and these impacts reduced when AFO was tuned to moderate stiffness or total ROM restrictions.

In rotational impairments, the stability impact of foot forward rotation was modelled with imbalances imitated in eversion or inversion directions. The everted foot with its weak muscular strength showed a decrease in GM and an increase in PM. The initial ankle plantarflexion angle was also reduced in both of the rotational impairments and reduction was more prominent for everted foot consistent with previously reported medial wedges influence at the ankle joint [113]. However, the everted foot delayed in landing due to delay to medially initiated forefoot landing towards the ground. The PCA method did not explain any noticeable differences in variability of PC1 for rotational impairments during loading phases. During unloading phases, the inverted foot showed increased in instability (GM and PM), also confirmed by a prior study



[108], and results from ankle-foot peak plantarflexion angles and moments which were decreased prominently for the lateral wedges consistent to an earlier study [113]. The PCA based variability also confirmed this finding with more variability for the inverted foot (less %) explained by PC1 compared to a normal walk. These findings suggested that the CoM-oscillations impacted everted foot in the loading phase and inverted foot in unloading phases with an increase in instabilities.

The slow walking speed showed a decrease in GM and an increase in PM compared to a normal speed walk. These inconsistent patterns were also illustrated by Lyapunov exponents for slow speed stability analysis [167]. That was due to reduced heel impacts and time delays in foot landing while walking at slow speed. The spatiotemporal data also confirmed these finding with an increase in initial double limb support time and reduced step length, peak knee flexion angle and moment. During unloading phase, a fast speed walk increased in instability (GM and PM) consistent to a prior study [173], also shown by an increase in peak plantarflexion ankle moment, knee and hip extension moments after the push-off phase. The slow walk relatively exerted lesser push-off moments and showed a decrease in stability with reduced PMs. Both Spearman's correlation and PCA variability methods were unable to explain these finding. This is because these methods compared whole time series waveforms and unable to distinct critical stability margins as quantified here applying Nyquist and Bode stability methods. Summarising the walking speed group, the slow speed showed less instability in this group and fast walk shoed more instability during unloading phases.

A comparison between stability outcomes from CoP-velocity (output) and CoM-vibrations (input) signals illustrated, during loading phases, the outputs had stable margins compared to inputs margins (unstable). During respective unloading phases, both the inputs and outputs were quantified with unstable margins, however, the output instability margins were found lesser in magnitudes. This increase in output's stability during loading and decrease in output's instability during the unloading phase illustrated the neuromotor balance control ability in response to anterior-posterior input proprioception feedbacks. The main emphasis of this study is to establish the Nyquist and stability methods for gait transitional stability analysis, however, there are few limitations as well which are required to be addressed in future work. This study proposed Nyquist and Bode stability methods to quantify stability thresholds using the I/O's neuromechanical signals and with the effect of wearable orthoses and walking speeds. This pilot stability study is conducted using healthy subjects and imitated impairments to obtain uniform gait patterns, however, the actual patients are expected to have more variances with/without orthoses. The orthotic devices used in this study have the same material/structural characteristics (Styrofoam, carbon fibre,

**Table 5.9: Summary of discussion and hypothesis outcomes.**

<b>Comparative conditions</b>	<b>Stability Margins (N&amp;B methods)</b>	<b>Spearman Correlation, Interlimb joints variations, Variability (PCA)*</b>	<b>Hypothesis 1 &amp;2 **</b>
<b>Loading Phases</b>			
Difference of a normal walk by wearing AFO (free mode)	instability increase w.r.t GMs	relatively less correlation (0.73)	holds true**
Impact on AFO (free mode) walk by restricting ankle-foot motions	instability decrease w.r.t GMs	strong correlation (>0.86), peak plantarflexion moments decreased, peak hip flexion moment increased	holds true**
Difference of rotational restriction with a normal walk	instability decrease w.r.t GMs and increased w.r.t PMs in everted foot	initial peak plantarflexion angle and moment decreased,	holds true
Difference of walking speeds with a normal walk	instability decrease w.r.t GMs and increased w.r.t PMs in slow walk	initial double limb support time increased in slow, knee flexion angle and moment increased	holds true
<b>Unloading Phases</b>			
Difference of a normal walk by wearing AFO (free mode)	instability increased	strong correlation (0.83), knee flexion ROM and hip flexion moment decreased	holds true**

<b>Table 5.9 Continue</b>	<b>Stability Margins</b>	<b>Spearman Correlation, Interlimb joints variations, Variability (PCA)*</b>	<b>Hypothesis 1 &amp;2 **</b>
Impact on AFO (free mode) walk by restricting ankle-foot motions	instability increased for alone dorsiflexion impairments w.r.t GMs	strong correlation ( $>0.84$ ), peak plantarflexion angle and dorsiflexion moment (DPRT, DPRR) decreased	holds true**
Difference of rotational restriction with a normal walk	instability increased in inverted foot	more variability (PC1), peak dorsiflexion, knee and hip extension moments decreased in inverted foot	holds true
Difference of walking speeds with a normal walk	instability decreased for slow walk and increased for fast walk	peak plantarflexion moment increased in fast walk and relatively decrease in slow walk,	holds true

\*results mentioned wherever significant difference exists among three methods, \*\* H1: effect of forward impairment imitated using AFO, H2: AFO effect on walking stabilities.

aluminium) throughout the experiments, the other commercial or research-based AFO's may be examined further by applying these methods. The empirical models are investigated here using built-in modelling Matlab tools, however, the other non-built-in model's structures could be tried further to simplify the TFs. Lastly, the input and output signals are investigated here independently for simplicity which is required to integrate as a musculoskeletal multi-segmental control loop. The application of these methods can be extended further towards other real-time lower limb impairments and understanding the ageing effects on gait transitional stabilities.

## 5.6 Summary

The impact of anterior-posterior CoM-vibrations is quantified in this study as somatosensory feedback to the neuromotor balance control. The rate of change in CoM-acceleration showed decaying and rising oscillatory waveforms during loading and unloading of stance phases. Various system identification techniques were applied to model these transient waveforms in support of gait stability analysis. The sum of sinusoid models was determined best fit with reduced complexity and low order transfer functions after Laplace transformations. The modelled TFs showed unstable margins (GMs and PMs) applying Nyquist and Bode methods from control engineering theory. The results showed that the AFO significantly impacted gait stability with an increase in instability (GMs) compared to a normal walk. The insoles simulated rotational impairments showed an increase in loading phase instability (PM) for everted foot condition and an increase in unloading phase instability for an inverted foot walk. Among walking speed trials, a slow speed walk illustrated an increase in instability (PM) during the loading phase and a decrease in instability during the unloading phase.

The phase dependent time series CoM-oscillation waveforms were also compared using variabilities among walking conditions applying Spearman's correlation and principal component analysis (PCA) methods. The increased variability in time series waveforms supported the increase in instability in AFO restricted walking conditions. The lower limb joints angles and moments were also quantified to explain the stability outcomes. Summarising, the resultant CoM-oscillations were modelled to understand variability and robustness in somatosensory feedback and quantify their impacts on balance control in both healthy and impaired subjects gait transitions. The applications of the current study are for stability analysis in situations where biomechanical structures are worn to the lower limbs such as orthoses, prostheses or exoskeletons. The CoM-vibrations are further required to investigate in the vertical direction where the GRFs have maximum magnitudes and contribute a major proprioceptive input to the neuromotor.

## **CHAPTER 6**

# **VERTICAL COM-OSCILLATIONS IMPACTS ON GAIT STABILITIES AND CONTRACTILE DYNAMICS**

### **6.1 Introduction**

This chapter evaluates rigidly mounted ankle-foot orthoses impacts on gait transitional stabilities and lower limb contractile properties in the vertical direction. An adjustable AFO was tuned w.r.t stiffness and range of motions to imitate various ankle-foot impairments in the forward direction of motion. The experiments were performed utilising motion capture system and force platforms using eleven unimpaired subjects. The rate of change in vertical GRF (normalised with body mass) presented whole-body vertical vibrations (CoM-oscillations) and the frequency models of these impact forces during loading phase are used to characterise contractile properties of lower limbs i.e. damping factor, the natural frequency of oscillation, and peak gain. Further, the impact of vertical CoM-oscillations on walking stability was investigated during gait loading and unloading phases applying Nyquist and Bode stability methods from control engineering. The interlimb variations in joints angles and moments are used to explain the outcomes of the frequency domain methods.

The experimental protocol was approved by the ethical review board of the University of Leeds. Each subject signed an informed consent form. In addition, a separate consent about video/photographic data was also signed by each subject.

### **6.2 Hypotheses**

The rate-dependent variations in whole-body acceleration are modelled in the vertical direction as proprioception feedback to the neural system and investigated following balance control aspects:

Firstly, whether the heel strike generated CoM-vibrations have impacts on contractile dynamics of the body by wearing AFO or variations in self-selected walking speeds?

Secondly, what is the impact of whole-body vertical vibrations on stability margins with ankle-foot impairments and self-selected walking speeds in the forward direction of motion?

## 6.3 Methods

### 6.3.1 Experimental Protocol

The experiments were performed with eleven healthy subjects (age  $30 \pm 1$ yr, weight  $74 \pm 3$ kg, and height  $1.72 \pm 2.5$ m). The subjects were inducted with no prior history of neurological or neuromuscular impairment. Experiments were recorded using motion captured system and the detailed procedure was already explained in Chapter 3 (sections 3.3 and 3.4). An ankle-foot orthosis was used to induce perturbations into the ankle joint in the sagittal plane following earlier studies [15, 111]. The simulated ankle-foot restrictions and their operating ranges are summarised in Table 6.1.

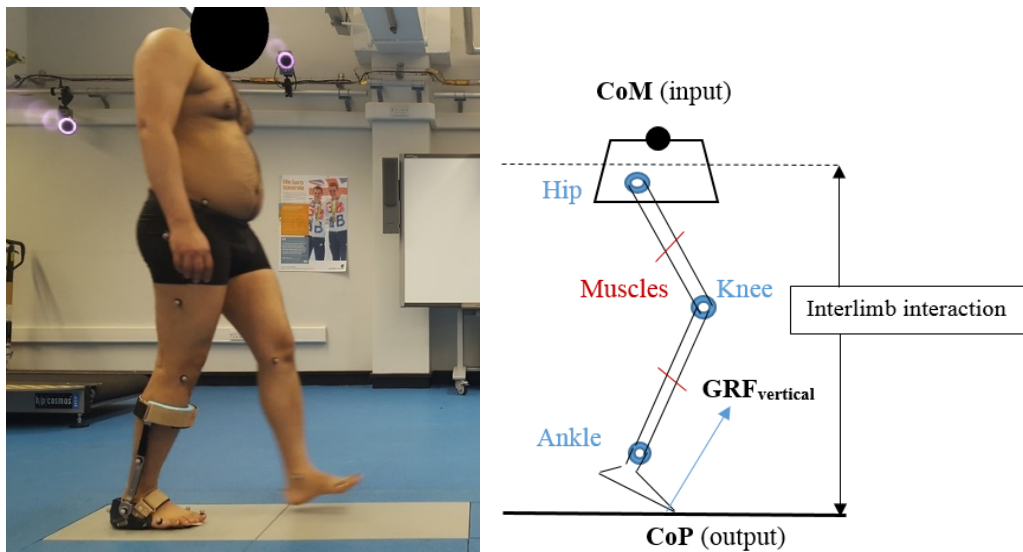


**Figure 6.1: (a) Experimental trials recorded in motion lab wearing Ankle-foot orthosis. Restrictions applied for dorsiflexion and/or plantarflexion ankle motions, (b) interlimb joints coordination and resultant responses measured using CoP (output) and GRF (CoM input).**

**Table 6.1: The AFO restrictions and their operating ranges.**

AFO Restrictions (dominant foot)	Abbreviation	Range
Normal (without AFO)	Normal	-
AFO restriction free	AFO	Free
Dorsiflexion resistive torque	DRT	$33 \pm 1$ Nm
Dorsiflexion range-of-motion restriction	DRR	$35^\circ \pm 5^\circ$
Dorsi-plantarflexion resistive torques	DPRT	$\pm 33 \pm 1$ Nm
Dorsi-plantarflexion range-of-motion restrict.	DPRR	$\pm 35^\circ \pm 5^\circ$

### 6.3.2 Data Processing

The lower-limb joints angles and moments were computed in Visual3D software and output waveforms were filtered at cut-off frequency 6 Hz using a 4<sup>th</sup> order Butterworth filter (details in Chapter 3). The vertical GRFs raw data was exported to Matlab-2017a and a finite difference algorithm was implemented to determine rate-of-change in vertical forces. The randomly sampled raw data was equalised by interpolating the waveforms such that each trial (stance phase) was equivalent to 500 samples. The resultant CoM-vibrations were determined by normalising the rate-of-change in GRFs with subjects' body mass. The root means square (RMS) of oscillatory CoM waveforms was computed to consider power density spectrum following prior studies [93, 104]. The raw data and RMS CoM-vibrations are shown in Figure 6.2. Lastly, the resultant CoM-vibrations were filtered and a residual analysis method was applied to select optimum cut-off frequency. In this method, a residual RMS spectrum is plotted as shown in Figure 6.3. The optimum cut-off frequency is the one where the tangent from the residual plot intercept the vertical axis and a horizontal line from that intercept cuts the residual plot. Thus the whole body vertical vibrations were filtered at cut-off frequency 18 Hz using 4<sup>th</sup> order Butterworth filter.

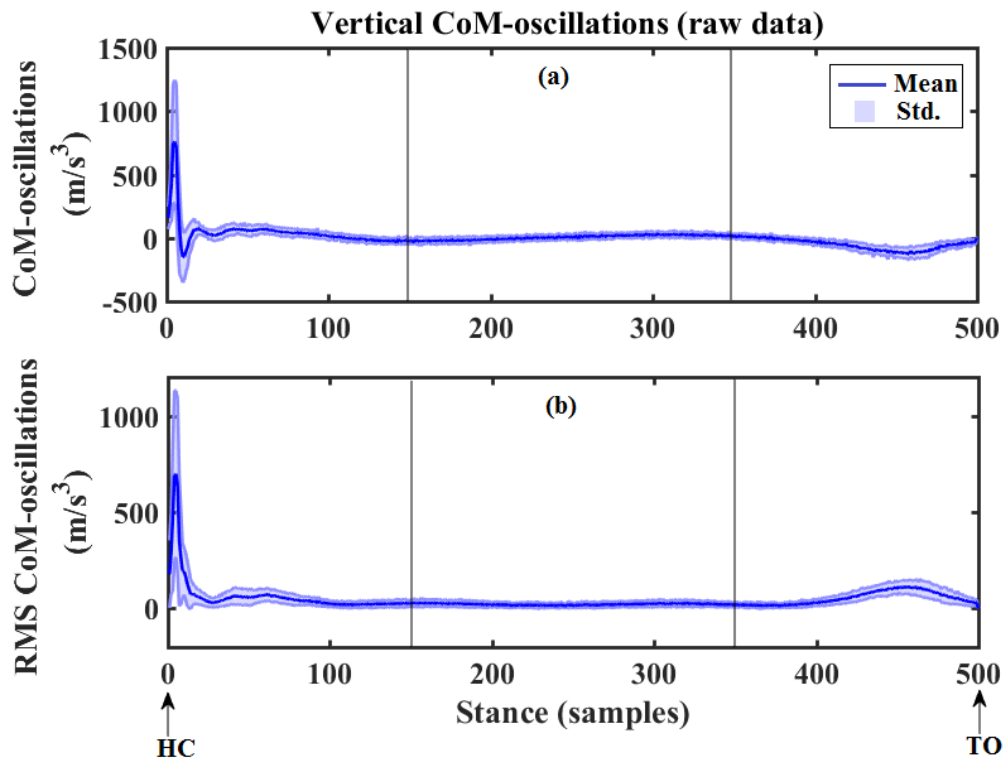


**Figure 6.2: The rate of change in CoM-acceleration showing the oscillatory response. (a) actual CoM-oscillations, (b) RMS CoM-oscillations.**

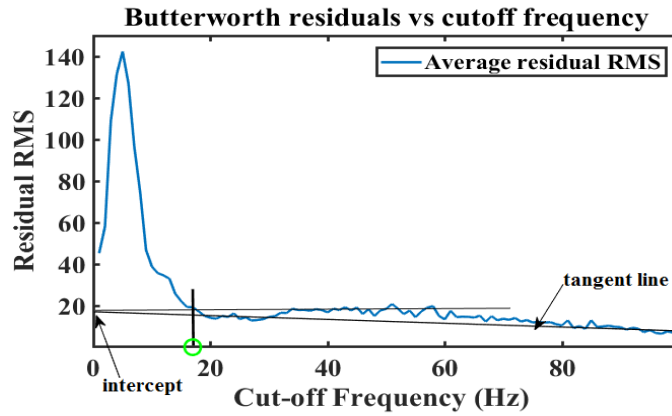


**Figure 6.3: Residual analysis method applied to select cut-off frequency.**

### 6.3.3 Modelling of whole-body vertical vibrations

The vertical CoM-vibrations showed two major impulses in loading and unloading phases of stance such that the first impulse showed an instant rise in magnitude at HC and then oscillatory decay towards mid-stance, conversely, the second impulse showed slow rise around terminal stance and decay instantly around TO as illustrated earlier in Figures 6.3. Observing these impulsive responses, a window size of 150 samples was selected from HC for loading phases, and 150 samples towards TO for unloading phases with reference to minimum steady-state values in mid/terminal stance phases. The derivative of acceleration waveforms induced noise in the output data. Further, the variations in subjects body weight, height, stiffness or ROM tunings in an orthosis, and subjects adaptations to AFO generated artefacts in the output waveforms.

In the modelling scenario, PCA is applied to specify whether a system can be defined as a linear model and also determine the order of that model [130]. The principal component analysis (PCA) was performed using input data of each of the walking conditions. The PCA was implemented to ensure linearity in the data and reduced the variability by removing artefacts. The input matrices of size  $(150 \times 50)$  were used whereas 50 trials included five trials per subject of total ten subjects (subjects x trials:  $10 \times 5$ ) and each trial contains 150 samples for respective stance phases. The PCA implementation theory is already explained in Chapter 3 (section 3.6.1). Thus the output waveforms were reconstructed using first principal components i.e. PC1 scores and coefficient vectors and adding estimated mean of the input matrix. The mean and standard deviation of output waveforms are illustrated in Figures 6.4 and 6.5 for unloading and loading phases of simulated walking conditions. The mean of each subject's data was computed for further analysis following an earlier study [31].



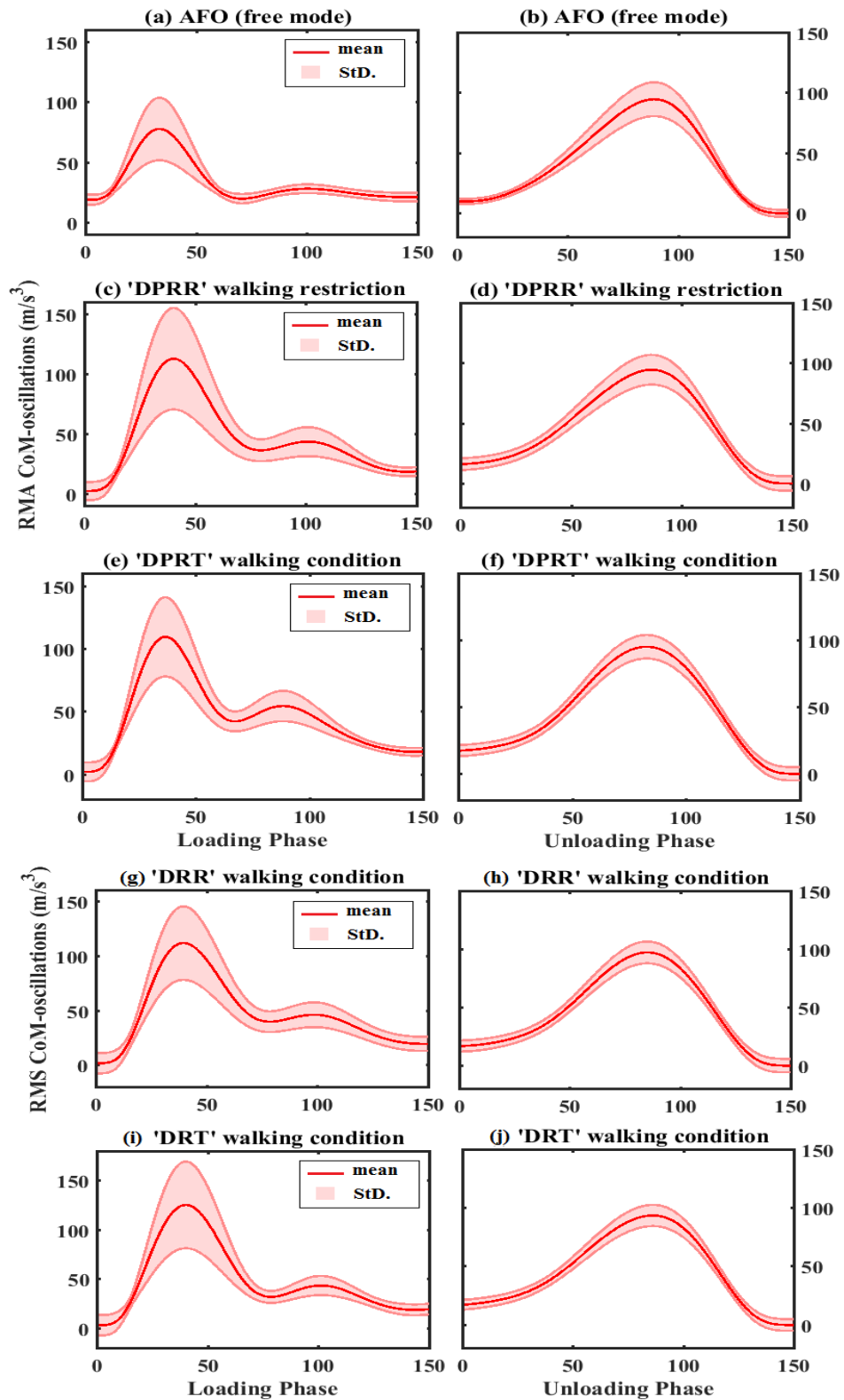


**Figure 6.4: CoM-oscillations illustrated for walking conditions with an ankle-foot orthosis. AFO free-mode walk: (a) loading phase, (b) unloading phase; (e) dorsi-plantarflexion ROM restrictions: (c) loading phase, (d) unloading phase; dorsi-plantarflexion resistive torques: (e) loading phase, (f) unloading phase; dorsiflexion ROM restriction: (g) loading phase, (h) unloading phase; dorsiflexion resistive torque: (i) loading phase, (j) unloading phase.**

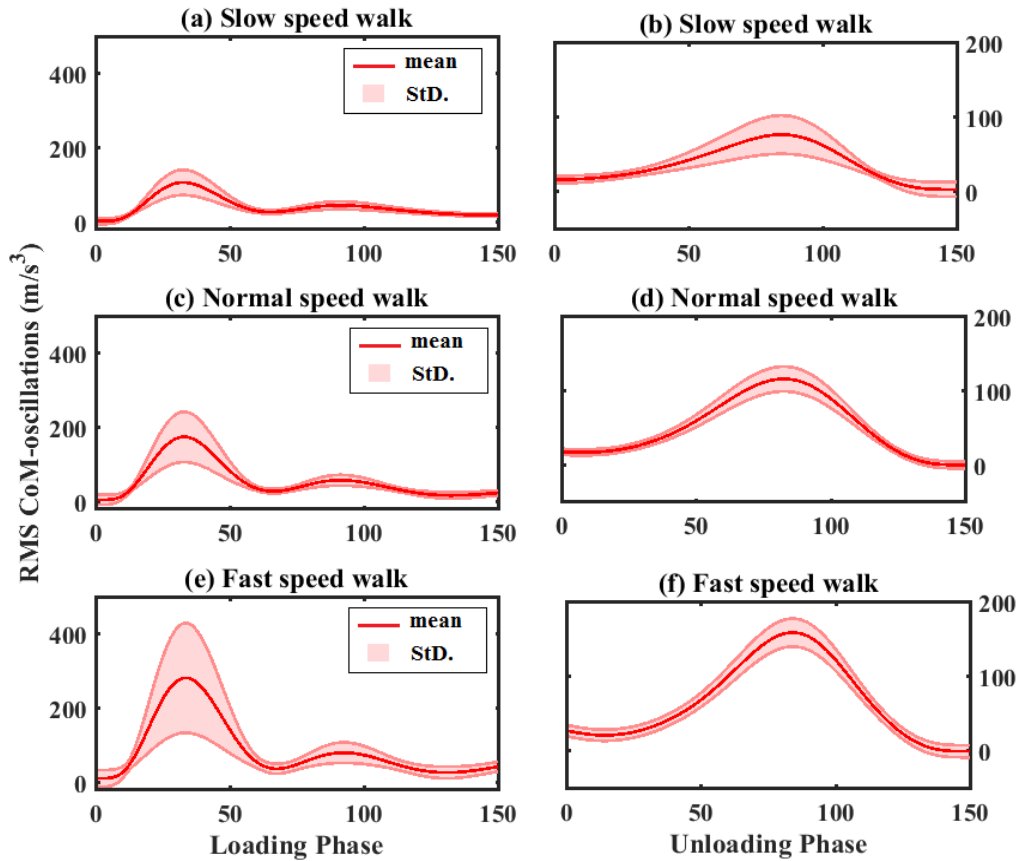
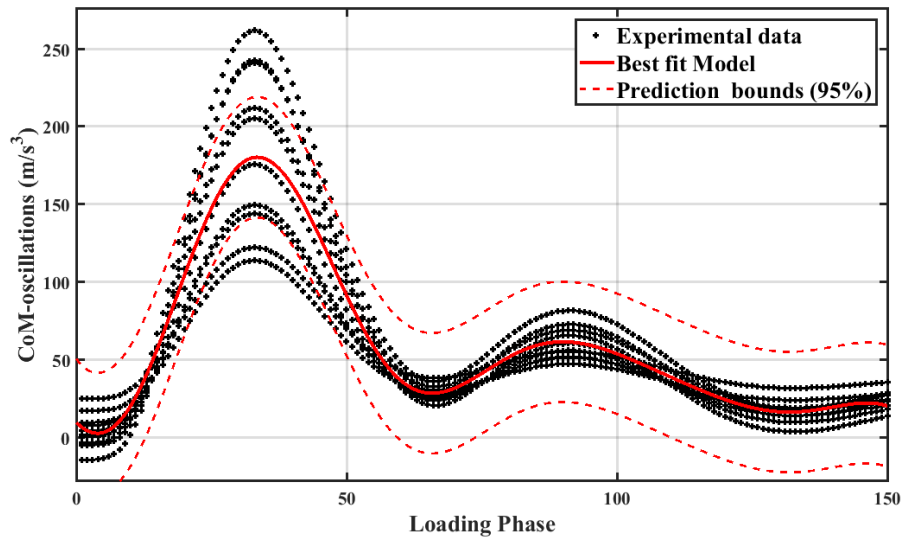
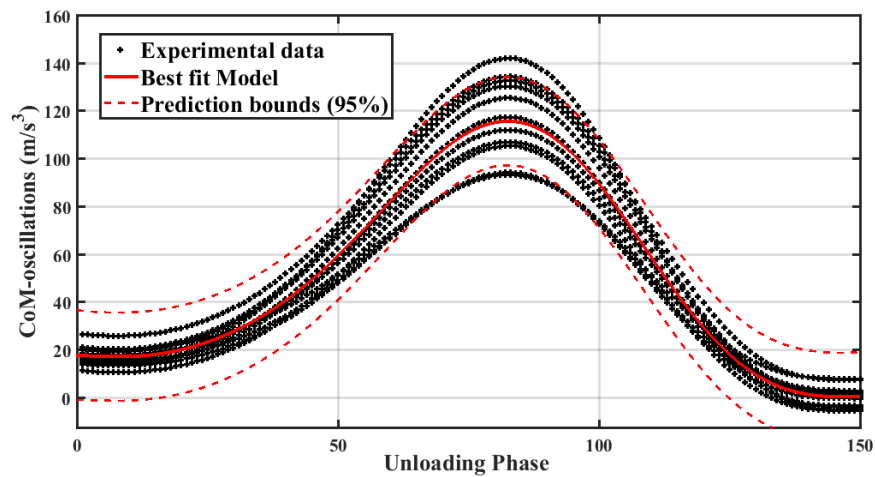


**Figure 6.5: CoM-oscillations (vibrations) illustrated for walking speed group. Slow speed walk: (a) loading phase, (b) unloading phase; Normal speed walk: (c) loading phase, (d) unloading phase; Fast speed walk: (e) loading phase, (f) unloading phase.**

The impulsive nature CoM-vibrations were modelled in time domain using the curve fitting toolbox in Matlab-9.2 which allows users to determine best fit linear models for a dynamic system just like the free vibrations identified earlier using system identification tools [177]. A best-fit model was quantified from the coefficient of determinants ( $R^2$ ). The oscillatory nature CoM-vibrations were determined the best fit with a sum of sinusoidal models  $R^2 > 99\%$ . For loading phases, the fourth sum of sine waves is found the best fit as illustrated in Figure 6.6(a), whereas, for respective unloading phases, the third sum of sine waves is found best fit as shown in Figure 6.6(b). The time domain models are converted to frequency domain after Laplace transformation and these frequency models are called transfer functions (TFs).



(a) Sum of four sine waves fitted to experimental data with  $R^2 > 99\%$ .



(b) Sum of three sine waves fitted to experimental data with  $R^2 > 99\%$ .

**Figure 6.6: Linear regression model fitted to CoM-vibrations (oscillations) data for normal walking trials. (a) Loading phase, (b) Unloading phase.**

A transfer function is a mathematical model that presents a system in the frequency domain as a ratio of Laplace of the output to input polynomials. These TFs are found to be a non-minimum phase (NMP) in nature with numerator polynomial roots (zeros) lying on the right half of s-plane as illustrated in Figure 6.7. The roots of denominator polynomials (poles) were lying on the imaginary axis of s-plane and showed unstable responses. However, the margins of instability are quantified by applying Nyquist and Bode methods. Following the control engineering approach, impulse inputs are provided to the modelled TFs and output response reproduced the oscillatory features of original time domain signals.

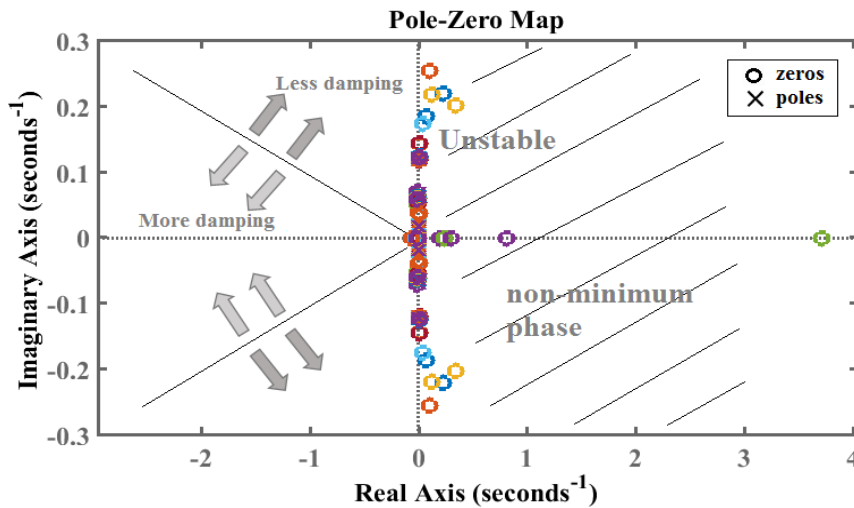


**Figure 6.7: Pole-zero map illustrated for Loading phases transfer functions, the poles lie on imaginary axis showing the unstable, undamped system and zeros on the right half showing the non-minimal phase system.**

### 6.3.4 Nyquist and Bode Stability Analysis

From engineering control theory, Nyquist and Bode stability methods are implemented in Matlab to compute stability margins. The examples of loading and unloading phases Bode plots are shown in Figure 6.8 and 6.9 for the normal speed walking trials. The detailed theory of these methods is explained in Chapter 3 (section 3.6.3).

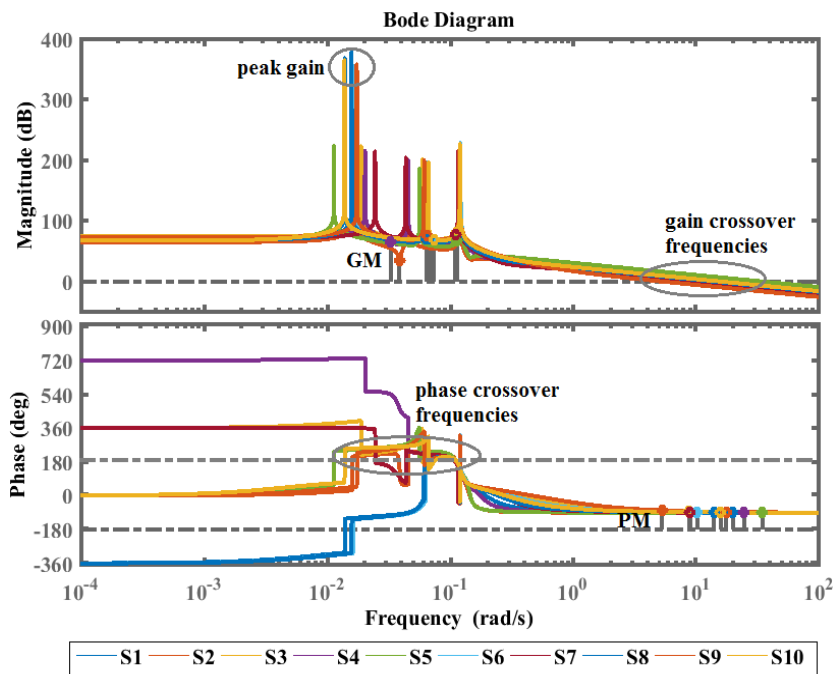


**Figure 6.8: Bode plots of loading phases showing the gain margins, phase margins, and respective cut-off frequencies for normal speed walking trials.**

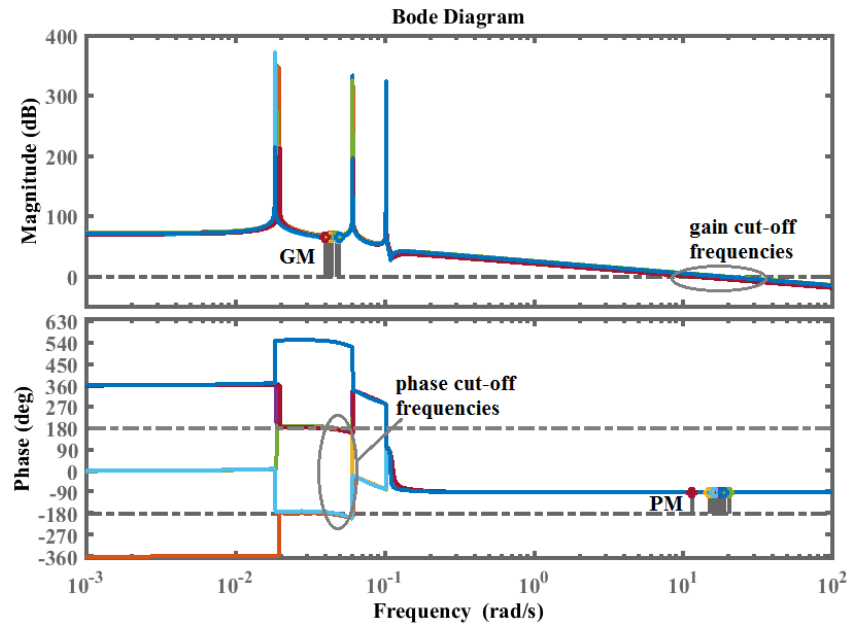


**Figure 6.9: Bode plots of unloading phases showing the gain margins, phase margins, and respective cut-off frequencies for normal speed walking trials.**

Lower limb semi-flexible structure has the capability to damp vertical vibrations generated due to heel impact. The vibrations natural frequency, peak gain, and damping factor are used to define contractile properties of the lower limb [92]. The contractile properties and stability margins are defined earlier in Chapter 2 (section 2.6) and computed here using Bode plots using built-in Matlab functions.

### 6.3.5 Statistical Analysis

The contractile properties and stability margins were compared statistically to understand the impact of walking speeds and AFO restrictions. The comparison is made by applying the Wilcoxon-signed rank test,  $p < 0.05$  in each group (details in Chapter 3 section 3.7).

## 6.4 Results

### 6.4.1 Stability margins and Contractile properties

The frequency models of whole body vertical vibrations were used to quantify damping ratio, peak gain, natural frequency, and stability margins. Comparing with normal and AFO free mode walking conditions in Table 6.2, the contractile properties showed small damping factors ( $\zeta$ ) in all walking conditions and peak gains decreased ( $p < 0.05$ ) only for dorsiflexion restricted walks (i.e. DRT, DRR) with large standard deviations. The walking speed group illustrated no significant difference in both peak gain and damping factor properties. The natural frequency of oscillations ( $\omega_n$ ) decreased 10% for AFO restrictions except for the ‘DPRT’ condition in which the

frequency ( $\omega_n$ ) increased compared to a normal walk. The natural frequency was also decreased ( $p < 0.05$ ) at a slow speed walk in walking speed group. A comparison between AFO free-mode walk and AFO restricted conditions showed that the alone dorsiflexion restricted walks decreased 8% in natural frequency ( $\omega_n$ ) and increased significantly in 'DPRT' condition, whereas, there was no difference found in peak gains.

**Table 6.2: Contractile properties of walking conditions during loading phases.**

Walking Condition	Damping Ratio ( $\zeta$ ) 1.0e-15 <sup>^</sup>	Natural Frequency (rad/s)	Peak Gain (decibel)
AFO walking restrictions			
AFO (free mode)	0.2782	0.1189 0.004	248 61.16
DPRR	0.3509	<b>0.1137*</b> 0.002	268.3 70.37
DPRT	0.4146	<b>0.1232*</b> 0.004	267.7 69.78
DRR	0.3106	<b>0.1094*</b> 0.003	<b>268.72</b> 71.88
DRT	0.4628	<b>0.1073*</b> 0.001	<b>228.63</b> 40.93
Walking speed group			
Slow	0.3826	<b>0.1184</b> 0.003	265 69.61
Normal	0.5172	0.1218 0.001	286 77.52
Fast	0.3118	0.1222 0.0004	285.72 73.32

Bold for comparison with a normal walk, \* for comparison with AFO free-mode walk.

The stability margins of AFO walking conditions are compared with a normal walk for loading phases in Table 6.3 and for respective unloading phases in Table 6.4.

During the loading phase, the AFO restrictions showed no significant differences in GMs compared to an AFO free mode walk, however, decreased significantly when compared to a normal walk. The PMs increased ( $p < 0.05$ ) for dorsiflexion restrictions (i.e. DRT and DRR) when compared with an AFO free mode walk. During unloading gait phases, the GMs of all AFO walking conditions significantly decreased ( $p < 0.008$ ) in total restrictions (i.e. DRR, DPRR), and significantly increased ( $p < 0.008$ ) in stiffness based restrictions (i.e. DRT, DPRT) compared to an AFO free mode walk. Similarly, a total dorsiflexion restriction i.e. ‘DRR’ showed a decrease ( $p < 0.003$ ) in GMs and stiffness based restrictions (i.e. DRT, DPRT) showed an increase ( $p < 0.003$ ) in GMs compared to a normal walk. All AFO walking conditions showed a decrease in PMs compared to a normal walk and increased in PMs compared to an AFO free-mode walk, though the differences are small, however, stand statistically significant.

**Table 6.3: Stability margins for loading phases of AFO restricted walking conditions.**

Walking Condition	Gain Margin (decibel)	Phase Margin (degree)	% Variance Explained (PC1)	Coefficient of Determinant (R <sup>2</sup> )
Normal (without AFO)	-71.943 5.70	91.196 1.407	90.28	99.78
AFO (free mode)	-66.911 10.21	90.118 0.094	88.73	99.69
DPRR	<b>-62.987</b> 3.34	91.304 1.149	85.2	99.88
DPRT	<b>-63.973</b> 3.04	91.889* 2.566	82.5	99.97
DRR	<b>-55.457*</b> 4.12	91.542* 1.815	77.71	99.94
DRT	<b>-66.414</b> 4.31	91.917* 2.565	85.11	99.99

Bold for comparison with a normal walk, \* for comparison with AFO free-mode walk.

**Table 6.4: Stability margins for unloading phases of AFO restricted walking condition.**

<b>Walking Condition</b>	<b>Gain Margin (decibel)</b>	<b>Phase Margin (degree)</b>	<b>% Variance Explained (PC1)</b>	<b>Coefficient of Determinant (R<sup>2</sup>)</b>
Normal (without AFO)	-66.065 1.14	90.027 0.011	92.16	99.9
AFO (free mode)	<b>-124.593</b> 1.19	<b>89.715</b> 0.151	94.47	99.9
DPRR	-68.964* 4.20	<b>89.815*</b> 0.134	89.17	99.9
DPRT	<b>-170.64*</b> 6.73	<b>89.932*</b> 0.048	93.97	99.97
DRR	<b>-35.945*</b> 5.41	<b>89.904*</b> 0.074	90.57	99.9
DRT	<b>-130.316*</b> 0.765	<b>89.81*</b> 0.086	91.77	99.9

Bold for comparison with a normal walk, \* for comparison with AFO free-mode walk.

The variations in interlimb joints angles and moments are compared in Chapter 3 (Table 3.5). Overall, peak dorsiflexion and peak plantarflexion ankle-foot angles significantly decreased ( $p < 0.05$ ) in their ROMs for restricted AFO conditions compared to an AFO free mode walk. The peak ankle dorsiflexion moments increased ( $p < 0.05$ ) for combined restrictions (DPRT, DPRR) and peak plantarflexion moments decreased ( $p < 0.05$ ) for all AFO restrictions. The knee flexion angles and moments were also increased ( $p < 0.05$ ) in loading phases of AFO restrictions. Comparing with a normal walk, the AFO restricted conditions decreased in ankle-plantarflexion ROMs, peak plantarflexion moments, and knee extension moments during unloading phases.

In the walking speed group, the self-selected walking speeds were obtained as slow ( $0.86 \pm 0.13$  m/s), normal ( $1.132 \pm 0.15$  m/s), and fast ( $1.356 \pm 0.14$  m/s). During loading phases, there is no significant difference found in stability margins of different walking speeds in Table 6.5. During unloading phases in Table 6.6, the fast walking speed showed an increase ( $p < 0.05$ ) in GMs and slow walking trials showed a decrease



( $p < 0.003$ ) in PMs compared to a normal walking speed. Generally, the results showed that the impulsive nature vertical vibrations generated by wearable AFO have a significant impact on lower limb contractile properties in terms of natural frequency and stability margins.

**Table 6.5: Stability margins for loading phases of walking speed group.**

<b>Walking Speed</b>	<b>Gain Margin (decibel)</b>	<b>Phase Margin (degree)</b>	<b>% Variance Explained (PC1)</b>	<b>Coefficient of Determinant (R<sup>2</sup>)</b>
Preferred/Normal	-71.943 5.70	91.196 1.407	90.28	99.78
Slow	-68.96 7.62	91.596 0.023	86	99.58
Fast	-76.89 5.44	91.154 1.28	86.27	99.99

Bold for comparison with a normal walk, \* for comparison with AFO free-mode walk.

**Table 6.6: Stability margins for unloading phases of walking speed group.**

<b>Walking Speed</b>	<b>Gain Margin (decibel)</b>	<b>Phase Margin (degree)</b>	<b>% Variance Explained (PC1)</b>	<b>Coefficient of Determinant (R<sup>2</sup>)</b>
Preferred/Normal	-66.065 1.14	90.027 0.011	92.16	99.9
Slow	-62.844 5.96	<b>89.948</b> 0.037	90.56	99.9
Fast	<b>-71.398</b> 5.42	90.052 0.028	90.78	99.99

Bold for comparison with a normal walk, \* for comparison with AFO free-mode walk.

#### **6.4.2 Body mass index (BMI) effect on transitional stability**

Following previous chapters (section 4.3.7), the effect of BMI on stability outcomes also evaluated here for vertical-CoM acceleration. The results illustrated no significant impact of BMI (grouped into low, medium and high) for normal walking speed stability outcomes as illustrated in Figure 6.10.

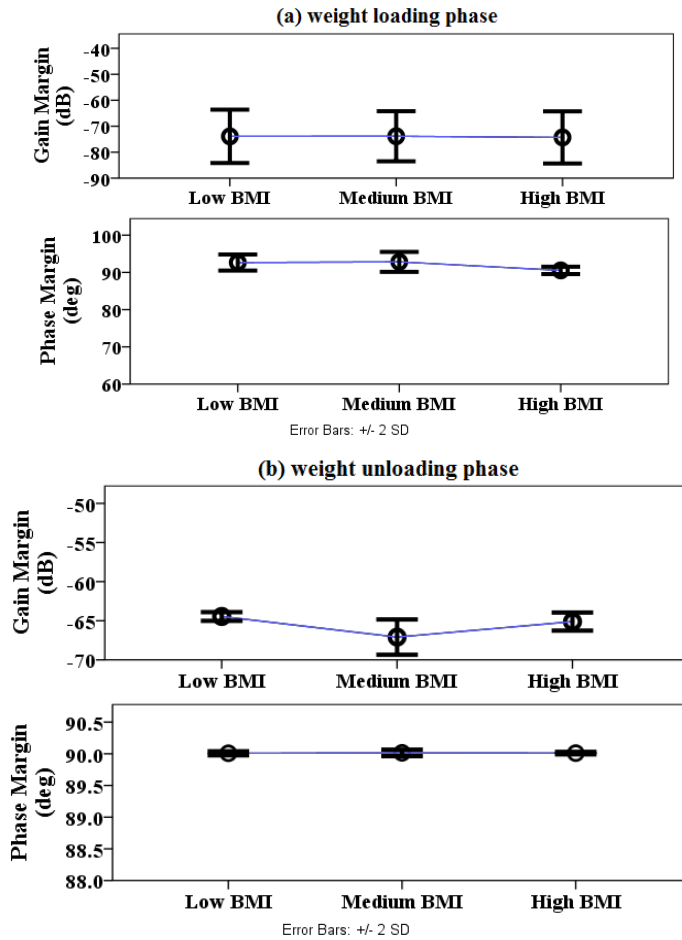


**Figure 6.10** Effect of body mass index (BMI) on gait transitional stability. BMI categorised into subgroups i.e. low ( $21.1 \pm 1.9$ ), Medium ( $25.22 \pm 0.6$ ), High ( $27.85 \pm 0.35$ ), stability margins shown for (a) loading phase, (b) unloading phase.

### 6.4.3 Controller design for unstable gait transitions

Following the methods described in Chapter 4 (section 4.3.5), the results illustrated that the unstable gait transitional phases (models) can be made stable using controller design approach. The outcomes showed that the unstable human gait transitions are controllable as explained below with examples for both loading and unloading phases.

Considering loading phase unstable TF,

$$17.32 s^7 - 6.626 s^6 + 1.717 s^5 - 0.088 s^4 + 0.024 s^3 + 0.00052 s^2 + 6.74e-05 s + 1.385e-06 / s^8 + 0.03403 s^6 + 0.0003464 s^4 + 9.333e-07 s^2 + 2.789e-10$$

PI controller ( $K_p + K_i * 1/s$ )

where  $K_p = 55.9$ ,  $K_i = 1.08e+04$

The feedback step response of plant and controller is illustrated in Figure 6.11 below.

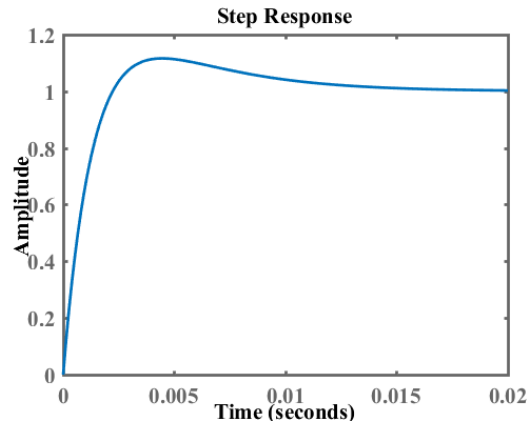


**Figure 6.11 Stable output response for unstable loading phase plant model.**

Similarly, for an unloading phase TF,

$$18 s^5 + 0.03 s^4 + 0.2062 s^3 - 0.0032 s^2 + 0.00084 s - 1.134e-06 / s^6 + 0.008559 s^4 + 1.22e-05 s^2 + 2.572e-11$$

PI controller design ( $K_p + K_i * 1/s$ )

where  $K_p = 15.6$ ,  $K_i = 882$

The feedback step response of plant and controller is illustrated in Figure 6.12 below.

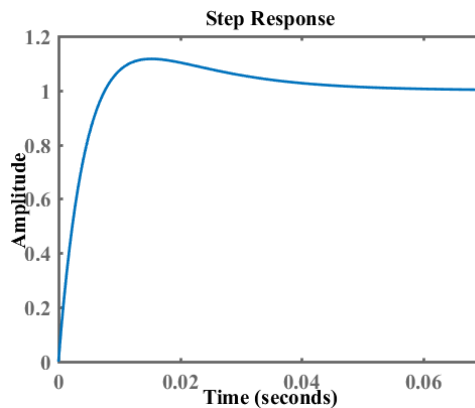


**Figure 6.12 Stable output response for unstable unloading phase plant model.**

#### **6.4.4 Effect of walking speed on transitional stability**

Results for varying walking speed trials illustrated an increase in instability (GMs) from slow to very fast speed during weight loading gait transition. During the respective unloading phase, a similar (increasing) trend was observed in terms of both GMs (amplitudes) and PMs as illustrated in Figure 6.13.

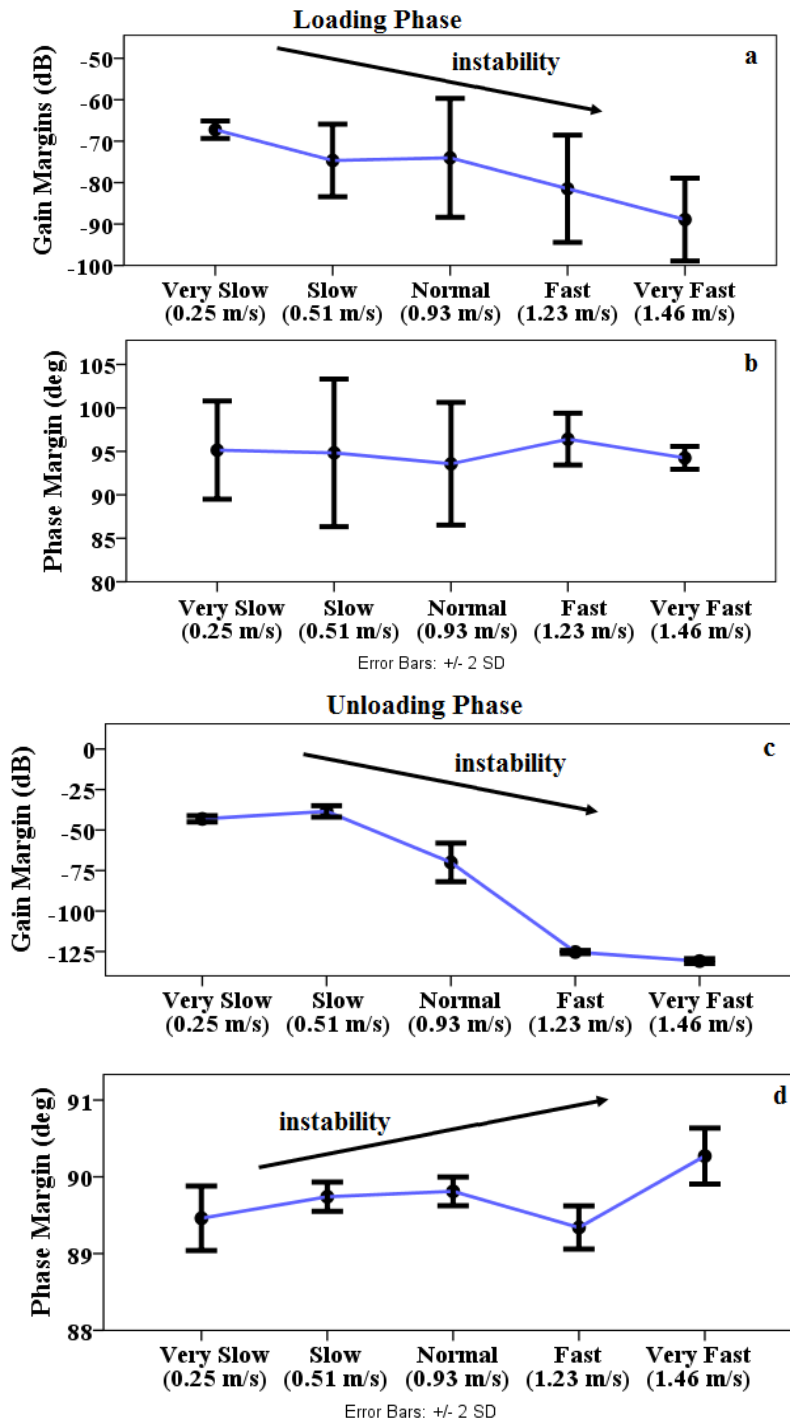


Figure 6.13 Walking speed effect on transitional stability. (a, b) Loading Phases, (c, d) Unloading Phases.

## 6.5 Discussion

The objective of this study was to evaluate the impact of ankle-foot orthosis and self-selected walking speeds on gait contractile properties and gait transitional stabilities. The rate-dependent variations in vertical CoM-acceleration were modelled in the frequency domain and analysed by applying Nyquist and Bode stability methods. The

results illustrated significant variations in natural frequency of oscillations in loading phases, and stability margins quantified for both loading and unloading phases.

### **6.5.1 Loading phases vibrations impact on contractile properties**

The impact forces are modelled here as somatosensory feedback to the neuromotor. Previously, the leg muscles activations were linked with CoM fluctuations (impact forces) where bursts of activity took place around heel contact and toe-off which was exhibited by most of the lower limb muscles [33, 99]. The lower limb GRFs data illustrated that the CoM-oscillations have maximum magnitudes in a vertical direction. Hence, these CoM-oscillations are modelled here as input feedback to the neuromuscular balance control. The empirical sinusoidal functions were found best-fit models for the CoM-vibrations waveforms with  $R^2 > 99\%$ . Previously the heel impact generated CoM-oscillations were investigated using spring-mass-damper (SMD) models [102, 103, 106, 178] fitted with contractile parameters to gain the amplitude of vertical GRFs obtained from human experiments. These rigid models did not consider soft tissue wobbling (move unsteadily) around bony parts which are reported to be critical during loading phases to damp CoM-oscillations [179]. Further, they did not explicitly count the ankle-foot flexible interaction with the ground rather a fixed rigid element was used. The loading rates quantified in these studies to characterise impact forces were assumed constant throughout the loading phase which actually varied over time. This study modelled loading phase CoM-vibrations from human body diffusing the concept of rigidity. Various clinically prescribed AFO adjustments are tuned and their impacts on contractile properties are investigated. Further, the mass and structural impacts of wearable rigid AFO are quantified assuming the non-rigid anatomy of the lower limbs.

The results in this study are compared in support to one of the possible arguments (i.e. increase/decrease/no change) which reported previously with inconsistent outcomes. For example, it was reported earlier that the leg geometry and changes in ankle-foot joint stiffness at heel contact altered the amplitude and frequency of external impact forces [180]. Considering that there were conflicting correlations (strong, small, no) reported previously between attenuation of impact forces and decrease in shoe stiffness [178]. This study supported a decrease in natural frequency of CoM-oscillations by applying stiffness or ROM based restrictions to the ankle-foot joint. However, the attenuation (damping) in these oscillations remains constant in this study as illustrated by constant peak gains and small magnitudes of damping factors (closer to zero). Previously, the SMD model based damping ratio was reported to vary  $0.02 < \zeta < 0.08$  with varying spring constants (stiffness) to match the model's output GRF with the experimental data [102]. The contractile properties evaluated in this study are compared with prior model based outcomes in Table 6.7.

**Table 6.7: Comparison of contractile properties using SMD models and empirical CoM-vibrations models for different walking speeds.**

<b>Studies</b>	<b>Damping Ratio</b> <b>‘<math>\zeta</math>’</b>	<b>Natural Frequency</b> <b>‘<math>\omega_n</math>’ (rad/s)</b>	<b>Peak Gain</b> <b>(dB)</b>	<b>Spring constant</b> <b>‘k’ (kN/m)</b>
control subjects [92]	0.64 – 0.9	2-3	48.5–50	-
control subjects* [102]	0.02 – 0.06	-	-	15 – 30
control subjects* [103]	0.04 – 0.08	-	-	40 – 80
control subjects* [181]	0.005 – 0.023	16-20	-	20 – 40
current study*	1.0e-15 x (0.52 – 0.31)	0.11 – 0.12	265-286	–

\*The variation in results from SMD models presented for walking speed 1.1-1.8 m/s and for current study 0.86-1.35 m/s.

The healthy subjects are capable to adapt ankle-foot restricted motions as illustrated by consistent damping factors and peak gains. Because, during loading phases, the breaking moments are required by the ankle-foot joint and thus the applied restrictions supported the foot in loading with unknown intensity. The peak ankle plantarflexion moments increased in ‘DPRT’ and ‘DPRR’ conditions which mean the leg stiffness increased in addition to required support in the loading phase compared to an AFO free mode walk. Further, the knee flexion angles and knee extension moments also increased during loading phases. This implied that the lower limb muscles activated more than their normal levels and an interlimb interaction contributed to regulate damping and impact forces against restricted ankle-foot motions. The constant vertical impact forces were also reported previously for running with varying stiffness shoe soles where the joints angles, angular velocities, and muscle activations varied in the lower limbs, the resultant GRF remained constant [106, 182]. Considering interlimb interaction, the net leg stiffness was reported previously as a combination of the knee, ankle, and metatarsal joints [103]. To decelerate the loading phase impact, the knee flexed maximum as illustrated in this study by a significant increase in the knee flexion angle and moment. Prior studies also reported that the knee joint provided additional power to make the walk possible with an impaired ankle joint [22, 30, 102]. From the results regarding the first hypothesis, it is concluded that the AFO and walking speeds did not affect contractile properties (peak gain and damping ratio),

whereas, the natural frequency of CoM-oscillations decreased for restricted ankle-foot conditions. The interlimb joints interaction plays a role to keep the contractile parameters constant. In this study, a commercially available Ultraflex AFO joint is used with built-in urethane elastomer springs [119], however, other elastic materials (silicon, nylon urethane, and delrine) can provide further insight towards orthoses impact on contractile dynamics.

### **6.5.2 Whole body vertical-vibrations impacts on Dynamic Stabilities**

The ankle-foot joint as an end-effector is the most sensitive joint to maintain postural stability [27]. In this study, the experimental results (gain and phase margins) demonstrated that transitions from the loading phase towards mid-stance had decelerating oscillations and from terminal-stance towards push-off showed rising magnitudes. The best fit frequency models showed poles on imaginary axes in s-plane, implying, unstable responses from all simulated walking conditions. The relative stabilities between imitating conditions were further quantified by applying control engineering methods. Prior studies [10, 11] evaluated gait dynamic stabilities in AP/ML directions and lacked to consider stabilities in a vertical direction despite the vertical GRFs were maximum in magnitudes. In this study, the Nyquist and Bode stability methods are introduced to analyse frequency models of vertical CoM-vibrations with the advantage of a distinct cut-off threshold ( $0\text{dB}$ ,  $\pm 180^\circ \pm 2k\pi$ ) from which the stability margins are quantified for both healthy and impaired subjects.

Comparing with a normal walk, the bipedal walk by wearing AFO with adjustable restrictions showed a decrease in instabilities in terms of GMs (amplitude), however, these instabilities were increased in terms of PMs (time delays), though the magnitudes were small. The results in this study can be used to explain this as, by wearing AFO, the lower limb joints ROMs reduced and hence CoM-oscillations were also decreased in magnitudes at a critical point of stability, however, these restrictions induced time delays in loading. An earlier study also reported that subjects with reduced lower limbs motions used to adopt more protective gait patterns [34]. The unrestricted AFO walk (free mode) showed a decrease in PMs (time delay) and hence in instability, which supported these findings. During unloading phases, greater push-off torque is exerted by the normal ankle to accelerate and lift the limb forward. The stability margins in this phase illustrated that the GMs were increased for AFO free-mode and stiffness based walking restrictions, and offered more instabilities compared to a normal walk. Opposite to the loading phases, the PMs (time delay) decreased during unloading phases of AFO restricted conditions which mean the push-off phases ended earlier compared to a normal walk PM. This earlier push-off exertion and increased GMs were also illustrated by the decrease in ankle plantarflexion and knee extension moments near the push-off, consistent with previously reported gait patterns

of elderly subjects with reduced lower limb movements [28, 163]. From these findings, it is concluded that both dorsiflexion alone and combined dorsiplantarflexion restrictions have effects on walking stabilities in unloading phases.

Comparing with AFO walk (free mode), overall the AFO restricted conditions showed no significant differences in GMs during loading, presenting robustness of neuromotor control. This was consistent with earlier studies where the CNS was reported to keep the GRFs constant by a periodic tuning of leg muscles [105]. The PMs of restricted AFO conditions increased during loading phases compared to free mode walk consistent with outcomes while compared above with a normal walk. During unloading phases, the total ROM based AFO restrictions (DRR, DPRR) decreased in instability (GMs) compared to stiffness based restrictions (DRT, DPRT). This is because total restrictions did not allow push-off exertion compared to a walk with moderate stiffness, hence, the amplitudes of the oscillations also reduced at a critical point of measurements. However, the PMs increased for all restricted conditions compared to an AFO free mode walk. That was also reported earlier in elderly people with spastic gait who took delays prior to step forward [164, 183]. This finding also illustrates that the walking conditions with dorsiflexion restrictions (without any plantarflexion resistance) accumulated delays in the mid/terminal part of stance phases and revealed during unloading phases which took place as the last phase of the stance.

The second hypothesis is concluded (Table 6.8) as the ankle-foot orthoses have significant effects on stability margins when tuned w.r.t stiffness and/or ROMs compared to a normal walk. That illustrates the sensitivity of the walking stability resulted from vertical vibrations. Overall, the instability decreased in terms of GMs (amplitudes at the critical point) and increased in terms of PMs (time delays at the critical point) in loading phases. During unloading phases, the resistive torque conditions showed more instability w.r.t both GMs and PMs. The whole body vertical-vibrations were modelled here just like the mathematical models used in Visual3D or OpenSim to compute gait biomechanics. This study provided one way to empirically model harmonic nature CoM-vibrations, however, there might exist other possibilities just like the multiple solutions to impulsive differential equations [184]. The Nyquist and Bode methods provided alternative techniques for gait stability assessments. The uniformly restricted walking conditions helped in establishing these methods. In future, the scope of this research is proposed to extend by including patients having ankle-foot impairments and quantifying stabilities using other lower limb orthoses.



**Table 6.8: Summary of discussion regarding second hypothesis.**

<b>Comparative conditions</b>	<b>Stability Margins (N&amp;B)</b>	<b>Interlimb joints variations</b>	<b>Hypothesis 2</b>
<b>Loading Phases</b>			
Difference of a normal walk with AFO free & restricted modes	no difference free mode, instability decreased tuning AFO restrictions	peak plantarflexion and knee & hip extension moments decreased in loading	holds true
Impact on AFO (free mode) walk by restricting ankle-foot motions	instability increased in terms of PMs	peak plantarflexion moments increased in DPRT, DRT, knee flexion increased in stance, hip flexion moment also increased	holds true
Difference of walking speeds with a normal walk	no difference	knee and hip flexion angles and moments increased at fast and decreased at slow	not holds true
<b>Unloading Phases</b>			
Difference of a normal walk with AFO free & restricted mode	instability increased w.r.t GM and decreased w.r.t PMs	peak plantarflexion and knee flexion ROM decreased, hip flexion moment decrease	holds true
Impact on AFO (free mode) walk by restricting ankle-foot motions	instability decreased for total restrictions and increased in stiffness restrictions	peak plantarflexion angle decreased and peak dorsiflexion moments decreased	holds true
Difference of walking speeds with a normal walk	instability decrease for slow speed and increased for fast speed	moments of all three joints increased at fast speed, and decreased at slow speed	holds true

## **6.6 Summary**

In this chapter, the whole body vertical vibrations impact on gait contractile properties and dynamic stabilities were investigated with the effect of ankle-foot orthosis and self-selected walking speeds. The results illustrated that overall the contractile properties remained constant except the natural frequency of oscillations, and an interlimb joints coordination played an important role to keep damping factor and peak gains constant. However, the stability margins by wearing AFO varied significantly from their normal thresholds both in loading and unloading phases. These findings signify the impact of vertical vibrations on gait transitional stabilities which has remained uninvestigated earlier. The methodological choice of Nyquist and Bode methods provided a way to quantify stability effects of vertical vibrations further to studying contractile properties. This study provides a guideline to analyse wearable devices impact in the vertical direction with other similar applications like orthoses, prostheses, exoskeletons, walking surfaces, footwear, and lower limb impairments.

## **CHAPTER 7**

# **EVALUATION OF GAIT TRANSITIONAL STABILITY FOR RAMP ASCEND AND DESCEND WALKS**

### **7.1 Introduction**

This chapter evaluates stability during loading and unloading gait transitions while performing ramp ascend and descend activities. The biomechanical signals i.e. CoP and CoM-acceleration are used to measure neuromotor balance control ability as output and input (O/I) responses respectively. Experiments were performed using a force platform and motion capture system for ramp ascend and descend activities. Various ankle-foot impairments were imitated using healthy subjects and adjustable orthoses. The rate of change in CoP signals was quantified in the anterior-posterior direction and rate of change in CoM-acceleration signals was computed in vertical and anterior-posterior directions. These impulsive nature O/I signals were modelled in time and frequency domains and analysed by applying Nyquist and Bode stability methods. Further, the contractile properties (peak gain, damping ratio, and natural frequency) were evaluated for ramp walk to understand the heel impacts generated vertical oscillations impacts. The interlimb joints angles and moments were also computed for the ramp walk to explain the stability strategies.

### **7.2 Hypothesis**

The objective is to quantify the body's balance control ability using resultant responses i.e. CoM-acceleration (GRF/mass) as proprioceptive input and CoP as an output as illustrated in Figure 7.1. The Nyquist and Bode methods are applied using these signals in order to investigate following hypotheses for a ramp walk.

Firstly, to what extent the neuromuscular balance control get affected during gait transitions for various types and degrees of imitated ankle-foot impairments?

Secondly, what is the impact of heel impact generated vertical vibrations on the contractile properties by wearing AFO for various clinically applied adjustments?

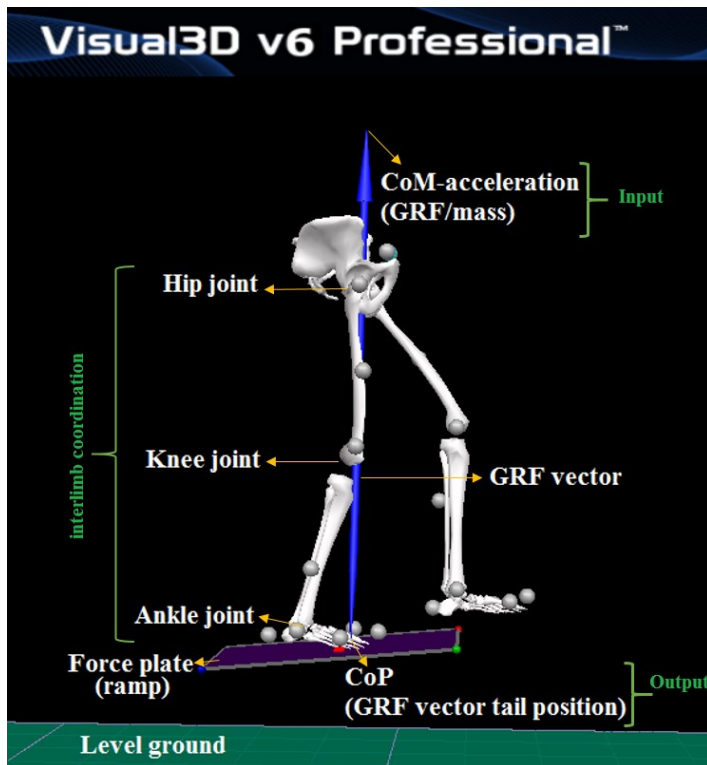


**Figure 7.1: Input, output neuromechanical responses and interlimb joints coordination illustrated for balance control.**

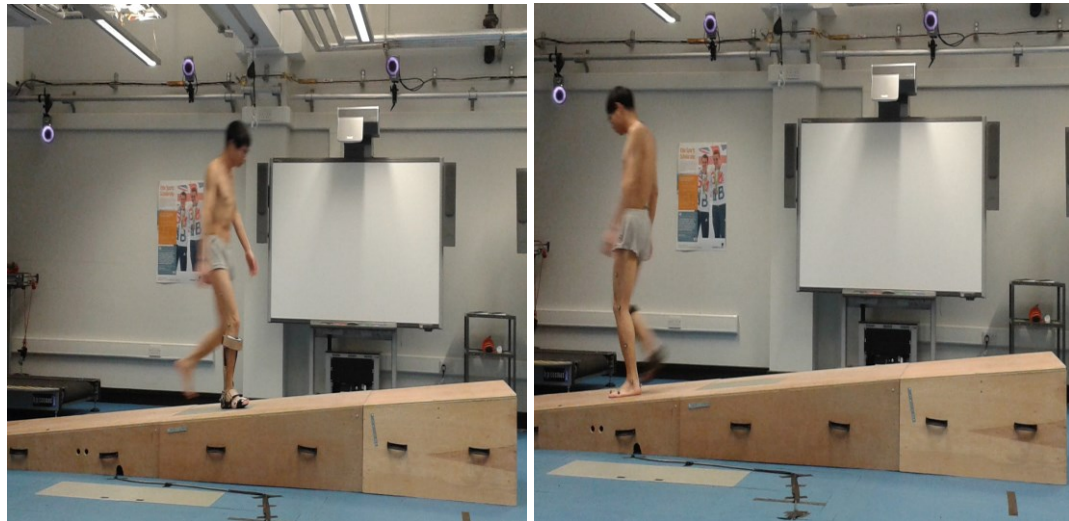
## 7.3 Methods

### 7.3.1 Experimental Protocol

A total of ten healthy subjects participated in this study (age  $30 \pm 1$  yr, weight  $74 \pm 3$  kg, and height  $1.72 \pm 2.5$  m) after confirming no prior anatomical or neuromuscular impairments. A wooden ramp platform with  $5^\circ$  slope and 8-meter track length was used to conduct the trials. The ankle-foot impairments were simulated in the forward (anterior-posterior) direction using an adjustable ankle-foot orthosis (AFO) and in rotational (media-lateral) direction using wedged insoles. The details of orthoses design, experimentation, and walking conditions (abbreviations) are discussed in Chapter 3 (section 3.3 and 3.4) and abstracted here to get an overview.

### 7.3.2 Data Collection

The experimental data collected using a motion capture system on an inclined surface as shown in figure 7.2. The subjects were asked to get familiar with each of imitated impairments and then the trials were recorded for the dominant foot on a ramp ascend and descend activities. The Qualysis software was used for the recording the motion data (markers positions, GRF, and CoP) which was extracted in the form of C3D files for further analysis. The detailed hierarchy of walking activities, gait transitions, walking condition, and measurement signals are illustrated in Figure 7.3.



(a) Ramp ascend

(b) Ramp descend

**Figure 7.2: Experimental data collection for imitated ankle-foot impairments in motion capture lab.**

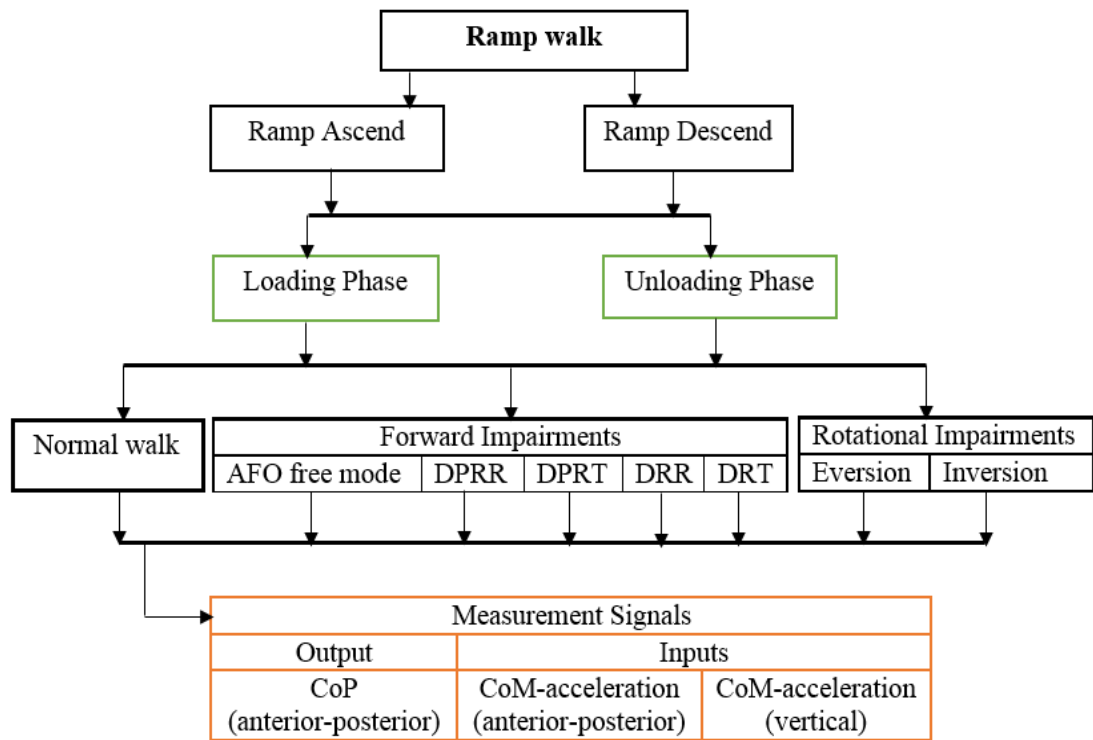


**Figure 7.3: Walking activities, gait transient phases, ankle-foot impairments and measurement signals hierarchy.**

### 7.3.3 Data Processing

The experimental data (C3D files) was exported to Visual3D motion analysis software (C-Motion) where the events detection algorithm was implemented to detect stance phases precisely between heel contact and toe-off events. The raw data were exported to Matlab-9.2 included anterior-posterior and vertical components of ground reaction forces (GRFs), and an anterior-posterior component of the centre of pressure (CoP).

The finite difference algorithm was implemented in Matlab-2017a to compute the rate of change in these three measured signals. The randomly sampled raw data was equalised by interpolating the waveforms such that each trial (stance phase) was equivalent to 500 samples. The rate of change in GRFs was further normalised with subjects body weight to determine the rate of CoM-accelerations. The mean CoP-velocities were computed to optimise the signals noise and root mean square (RMS) of CoM-oscillations were computed to get power density spectrums. The resultant waveforms are illustrated in Figure 7.4 for unrestricted normal walk trials.

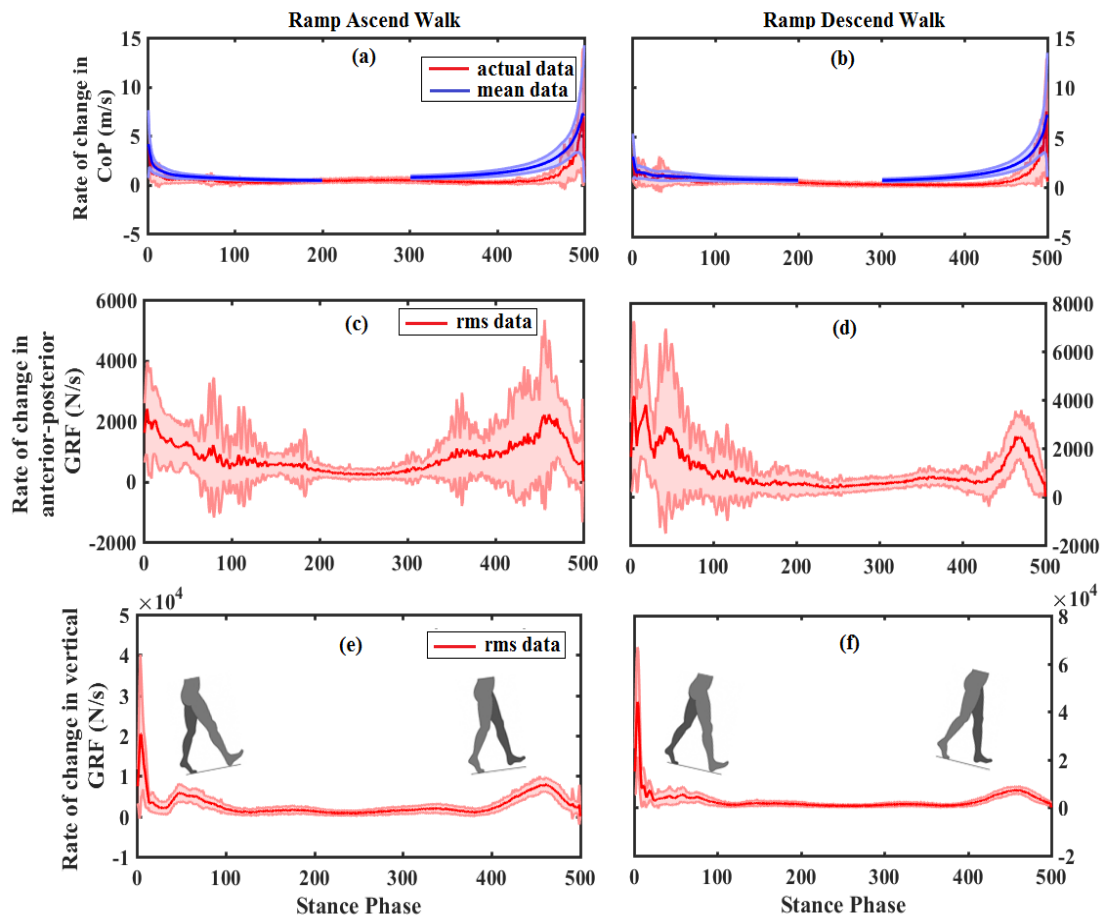


**Figure 7.4: Mean CoP-velocity and RMS CoM-vibrations raw data illustrate the impulsive responses during stance phase transitions.**

The mean CoP-velocity waveforms illustrated two major impulses first with the exponentially decaying response after HC and second exponentially rising response before TO. Similarly, the RMS CoM-vibration signals illustrated oscillations with decaying magnitudes just after HC and rising magnitudes towards TO. These impulsive and oscillatory waveforms present the weight loading and unloading transitions of stance phases. The measured signals were windowed to 150 samples observing the transient and steady-state responses for each of these transitional phases while performing ramp ascend and ramp descend walks.

The CoP-velocity and CoM-vibration waveforms were filtered. The filtering cut-off frequencies were selected by applying the residual analysis algorithm [159] for each of the three signals. In this method, the RMS value of residuals (filter and unfiltered waveforms) is plotted as illustrated in Figure 7.5. The tangent lines were drawn from decaying magnitudes of the respective residual plots those intercepted the respective vertical axes at certain points. From those intercepts, the lines parallel to respective horizontal axes were drawn. The points where horizontal lines cut the residual plots were used to define optimum cut-off frequencies for respective signals. Applying this method, the mean CoP-velocities were filtered using a 1<sup>st</sup> order Butterworth filter at 30Hz consistent with [76, 129]. This low order filter was selected to minimise the initial time delay in CoP-velocity impulses. The CoM-vibrations were filtered using 2<sup>nd</sup> order Butterworth filter at 10Hz for the anterior-posterior component [37, 158] and using 4<sup>th</sup> order Butterworth filter at 18Hz for vertical component [185].

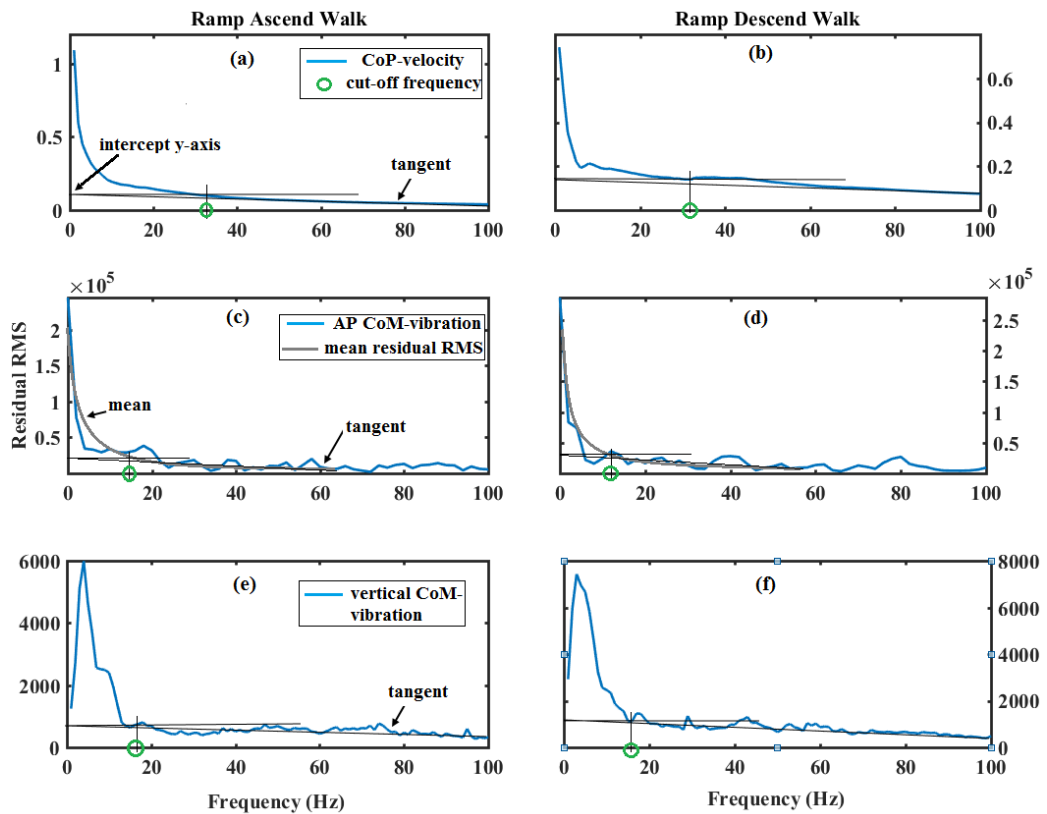


**Figure 7.5: Residual analysis method applied to select cut-off frequencies for three measurements signals.**

### 7.3.4 Time and Frequency domain Models

The time domain waveforms of three measured signals (CoP-velocity, CoM-vibrations: anterior-posterior and vertical) were obtained for loading and unloading gait transitions. The resultant waveforms were ensured w.r.t their linearity by applying principal component analysis (PCA). Because the measured immune with artefacts which induce non-linearity in the data due to varying anthropological parameters of

individual subjects, adaptation to restricted walks, and adjustments/fitting of wearable orthoses. The PCA was reported as a standard technique to overcome artefacts and ensure linearity in the data [130-132] (details in Chapter 3 section 3.6.1). Following earlier studies [81, 113, 161], the PCA was implemented for each walking conditions and each of the measured signals using input matrices of size (samples  $\times$  total-trials: 150  $\times$  50), where 50 columns present (subjects  $\times$  trials: 10  $\times$  5). Each principal component explains the variance in the data and the first few components explain maximum variances. Conventionally, the criteria for selecting PCs was being followed as to include the principal components those explain total variances  $>80\%$  [139]. In this study, the first principal component (PC1) or the first two PCs explained maximum variances ( $>80\%$ ) for most of the walking conditions, hence, used to reconstruct the output waveforms. PCA gives output in the form of score and coefficient matrices. For each walking condition, the output waveforms were obtained by multiplying scores (PCs) with coefficients and the adding mean of the input matrix. The output matrices were obtained equivalent to the size of input matrices (samples  $\times$  total-trials: 150  $\times$  50). The mean of each subject five trials was computed in respective walking conditions. Applying PCA, the output waveforms are illustrated in Figure 7.6 for ramp ascend activity and three measured signals of normal walking conditions.

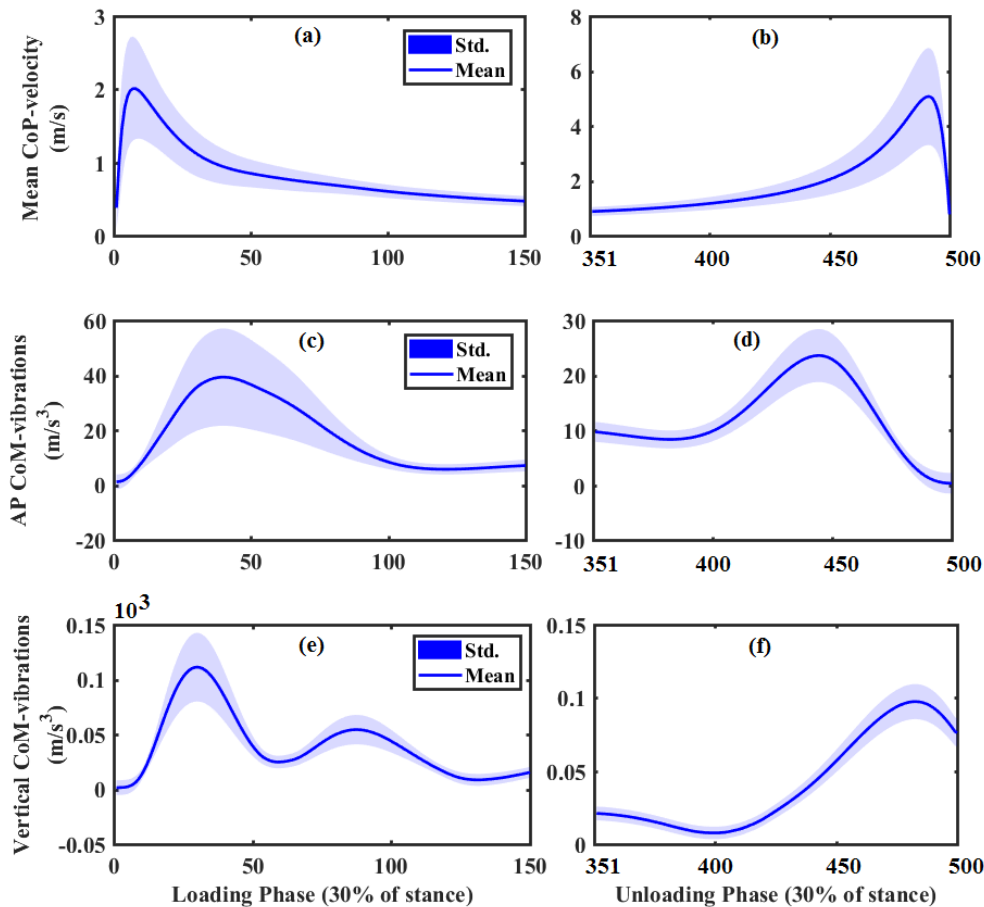


**Figure 7.6: PCA reconstructed waveforms illustrated using normal walk trials for a ramp ascend activity.**



Both the CoP-velocity and CoM-vibrations time series data was modelled empirically using the curve-fitting toolbox in Matlab-9.2. The prerequisite shapes of CoP-velocity and CoM-vibrations were found exponential and oscillatory respectively. Following that, a sum of two exponents was found best fit models for CoP-velocity waveforms and a sum of three/four sinusoids was found the best fit for CoM-vibrations waveforms. The best fit models were determined from the coefficient of the determinant ( $R^2$ ) which were obtained on an average  $99\pm 1\%$  for three measured signals. The orders of the best fit models were kept consistent within walking groups to be compared statistically. The time domain models were transformed into the frequency domain by Laplace transformation following prior studies [34, 130]. The equivalent frequency domain models are called transfer functions (TFs). The roots of a TF are used to define a stable or unstable system (details in Chapter 3 section 3.6.3). In this study, the loading phase TFs were modelled using CoP-velocity and showed stable responses (poles on the left side) for all walking conditions as shown in Figure 7.7. All other modelled TFs (walking conditions) showed unstable responses with poles on the right half of s-plane or on imaginary axes.

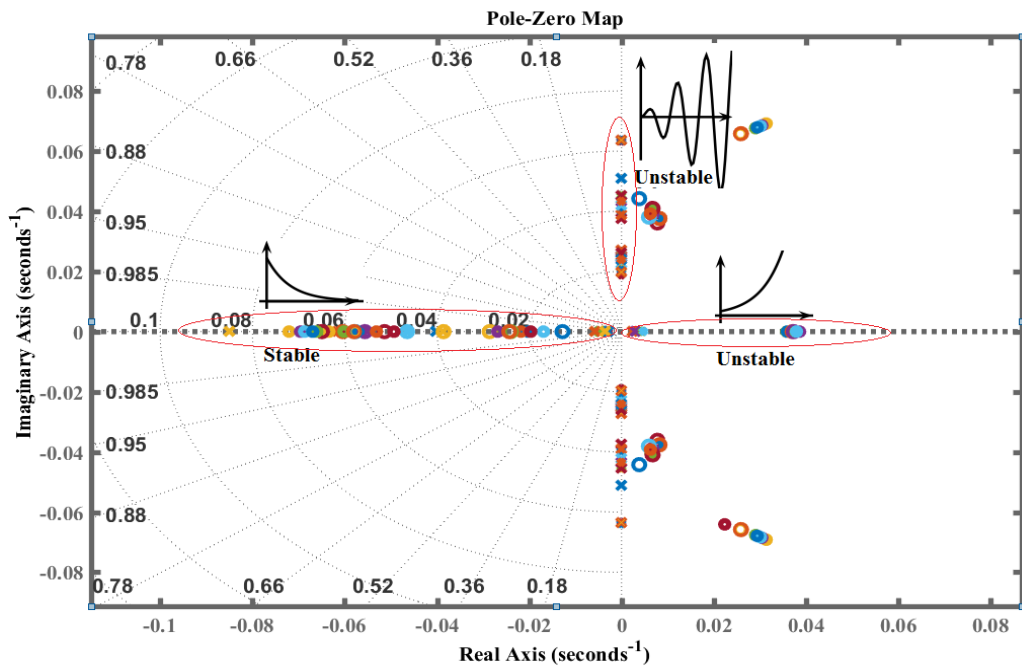


**Figure 7.7: Pole-zero map illustrating the stability of modelled I/O's TFs for normal walk data.**

### 7.3.5 Nyquist and Bode stability methods

The location of poles describes whether a system (TF) is stable or unstable, however, the relative stability margins are quantified further by applying Nyquist and Bode stability methods. These are mathematical techniques of analysing linear time-invariant (LTI) TFs and measures dynamic stability as gain margin and phase margins (details in Chapter 3 section 3.6.3). In this study, the loading phase CoP-velocity

models illustrated minimum phase responses and all other models (TFs) showed non-minimum phases. Hence, the non-minimum TFs were analysed by applying both Nyquist and Bode stability methods. The Nyquist and Bode methods were implemented in Matlab-9.2 using the command prompt. The relative stabilities were quantified as GMs and PMs for three measured signals and respective walking conditions.

Lastly, the contractile properties (peak gain, damping ratio, and natural frequency) were quantified using vertical CoM-vibrations generated from heel impacts during loading transitions. The gain plots of Bode method was used to quantify them. The peak gain defines the maximum gain magnitude (decibel), damping ratio defines the decay in oscillatory response, and natural frequency (Hz) presents the frequency of oscillations (details in Chapter 2 section 2.6). Here, the contractile properties were quantified for loading phases of ramp ascend and ramp descends activities applying Matlab commands to the modelled TFs.

### **7.3.6 Lower limb joints angles and moments**

The joints range-of-motions (angles) and moments are quantified at discrete peak points and definitions of these points are mentioned in Chapter 2 (section 2.2.4). The ankle and knee joints angles (ROMs) and moments were computed in the sagittal plane using Visual3D motion analysis software (detail in section 3.4.4). The angles and moment waveforms were filtered using a 4<sup>th</sup> order Butterworth filter at 6Hz [125, 126].

### **7.3.7 Statistical Analysis**

For statistical comparison, the imitated impairments were compared in respective groups and for each of ascend and descend activity (details Chapter 3 section 3.7). In this study, a non-parametric Wilcoxon-signed rank test was applied. A parameter was considered statistically significant if  $p < 0.05$ .

## **7.4 Results**

The results are divided into ramp ascend and descend activities. In each activity, stability margins are described for each of the three I/O signals. For each signal and activity, the walking conditions are compared statistically in three steps. Firstly, normal walk stability margins are compared with an AFO free mode walk. Secondly, an AFO free mode walk is compared with its restricted conditions (i.e. forward impairments). Thirdly, the rotational impairments are compared with a normal walk. Lastly, the variations in interlimb joints angles and moments are compared respectively.

### 7.4.1 Ramp Ascend activity

The CoP-velocity models illustrated stable responses during loading phases and unstable responses during unloading phases. During stable loading phases, stability margins quantified as infinite GMs and  $90^{\circ} \pm 1$  PMs for all walking conditions. A small but statistically significant difference found in PMs. Firstly, the AFO free mode walk decreased in stability compared to a normal walk. Secondly, the PMs illustrated the forward impairments increased ( $p < 0.05$ ) in stability compared to an AFO free mode walk. Thirdly, the rotational ankle-foot impairments decreased in stability (PMs,  $p < 0.05$ ) compared to a normal walk. In respective unstable unloading phases, firstly, an AFO free mode walk illustrated the significant increase in instability (GM and PM) compared to a normal walk. Secondly, both the GMs and PMs decreased ( $p < 0.05$ ) in forwarding impairments compared to an AFO free-mode walk. Thirdly, there was no difference observed in rotational impairments compared to a normal walk. The numerical values are mentioned in Tables 7.1 (a) and 7.2 for loading and unloading phases respectively.

**Table 7.1: Loading phases stability margins quantified using anterior-posterior CoP-velocity.**

Walking Condition	Gain Margin (decibel)	Phase Margin (degree)	% Variance Explained (PC1)	Coefficient of Determinant ( $R^2$ )
Normal (without AFO)	$\infty$	90.85 0.26	95.3	99.38
<b>Forward AFO restricted Impairments</b>				
AFO (free mode)	$\infty$	<b>90</b> 0.1	94.45	99.89
DPRR	$\infty$	90.6* 0.27	94.42	99.87
DPRT	$\infty$	90.61* 0.24	95.71	99.77
DRR	$\infty$	<b>90.56*</b> 0.107	97.14	99.86
DRT	$\infty$	<b>90.48*</b> 0.103	94.21	99.8
<b>Rotational Ankle-foot Impairments</b>				
Eversion	$\infty$	<b>90.61</b> 0.144	97.27	99.77
Inversion	$\infty$	<b>90.59</b> 0.26	97.37	99.86

Bold for comparison with a normal walk, \* for comparison with AFO free-mode walk.

**Table 7.2: Unloading phases stability margins quantified using anterior-posterior CoP-velocity.**

<b>Walking Condition</b>	<b>Gain Margin (decibel)</b>	<b>Phase Margin (degree)</b>	<b>% Variance Explained (PC1)</b>	<b>Coefficient of Determinant (R<sup>2</sup>)</b>
Normal (without AFO)	-46.09 3.22	89.69 0.11	95.77	99.93
<b>Forward AFO restricted Impairments</b>				
AFO (free mode)	<b>-109</b> 6.07	<b>90</b> 0.1	99.21	99.88
DPRR	-45.32* 3.37	89.65* 0.13	96.44	99.91
DPRT	-44.46* 1.44	89.63* 0.067	96.49	99.89
DRR	-44.51* 1.98	89.64* 0.084	96.04	99.93
DRT	-44.64* 0.84	89.66* 0.051	97.62	99.91
<b>Rotational Ankle-foot Impairments</b>				
Eversion	-44.81 1.69	89.66 0.069	97.7	99.93
Inversion	-45.33 1.81	89.66 0.051	97.43	99.93

Bold for comparison with a normal walk, \* for comparison with AFO free-mode walk.

In the anterior-posterior direction, the CoM-vibrations were modelled using sinusoidal best fit models (99.5±0.5%). These models quantified unstable margins for both loading and unloading gait transitions in all walking conditions. During loading phases, firstly, the GMs (p<0.05) increased and PMs decreased in AFO (free mode) compared to a normal walk. Secondly, a total AFO restriction ‘DPRR’ showed a decrease in instability (GMs, p<0.05) and a moderate restriction ‘DPRT’ showed an increase in instability (GMs, p<0.05) compared to an AFO free mode walk. Thirdly, compared with a normal walk, rotational impairments increased in GMs and decreased in PMs (p<0.05) compared to a normal walk. During respective unloading phases, firstly, an AFO free mode walk increased in instability (GMs, p<0.05) comparing with a normal walk. Secondly, alone dorsiflexion based restrictions (DRR and DRT) decreased in GMs (p<0.05) and increased in PMs (p<0.05) compared to an AFO free mode walk. A moderate dorsi-plantarflexion forward impairment ‘DPRT’ increased in instability (GM, p<0.05) compared to an AFO free mode walk. Thirdly, an inverted foot rotational impairment decreased in instability (GMs, p<0.05) and increased PMs compared to a normal walk. The numerical values are mentioned in Tables 7.3 and 7.4 for loading and unloading phases respectively.

**Table 7.3: Loading phases stability margins quantified using anterior-posterior CoM-vibrations.**

<b>Walking Condition</b>	<b>Gain Margin (decibel)</b>	<b>Phase Margin (degree)</b>	<b>% Variance Explained (PC1)</b>	<b>Coefficient of Determinant (R<sup>2</sup>)</b>
Normal (without AFO)	-51.3 6.33	86.07 1.6	88.94	99.77
<b>Forward AFO restricted Impairments</b>				
AFO (free mode)	<b>-62.91</b> 2.09	<b>78.17</b> 10.43	90.5	99.94
DPRR	-56.9* 5.4	87.42* 2.23	96.8	99.82
DPRT	<b>-84.34*</b> 7.6	81.44 16.02	92.51	99.79
DRR	-57.89 9.95	79.78 11.82	98.99	99.8
DRT	-57.25 10.76	83.96 6.08	98.74	99.77
<b>Rotational Ankle-foot Impairments</b>				
Eversion	<b>-66.88</b> 3.92	<b>79.72</b> 8.53	96.94	99.85
Inversion	<b>-61.45</b> 6.77	<b>77.16</b> 9.58	95.86	99.82

Bold for comparison with a normal walk, \* for comparison with AFO free-mode walk.

**Table 7.4: Unloading phases stability margins quantified using anterior-posterior CoM-vibrations.**

<b>Walking Condition</b>	<b>Gain Margin (decibel)</b>	<b>Phase Margin (degree)</b>	<b>% Variance Explained (PC1 + PC2)</b>	<b>Coefficient of Determinant (R<sup>2</sup>)</b>
Normal (without AFO)	-39.2 3.46	89.8 0.09	86.97	99.96
<b>Forward AFO restricted Impairments</b>				
AFO (free mode)	<b>-128.68</b> 4.04	89.46 0.68	87.1	99.99
DPRR	<b>-125.52</b> 13.46	89.9 0.13	80.33	99.99
DPRT	<b>-148.39*</b> 13.64	89.93 0.19	78.24+15.52	99.84
DRR	-46.92* 37.04	<b>90.07</b> 0.27	71.33+17.3	99.97
DRT	<b>-47.76*</b> 15.76	<b>90.01</b> 0.06	66.15+16.69	99.99
<b>Rotational Ankle-foot Impairments</b>				
Eversion	-40.66 3.76	89.8 0.07	86.15	99.98
Inversion	<b>-26.24</b> 1.45	<b>90</b> 0.1	83.1	99.25

Bold for comparison with a normal walk, \* for comparison with AFO free-mode walk.

In the vertical direction, the CoM-vibrations were modelled using sinusoid functions and illustrated unstable margins for both of the gait transitions. During loading phases, firstly, an AFO free mode showed a decrease in instability (GMs, PMs,  $p < 0.05$ ) compared with a normal walk. Secondly, the forward AFO restricted impairments (DPRR, DRR, and DRT) showed an increase in instability (GMs, PMs,  $p < 0.05$ ) compared to an AFO free mode walk. During unloading phases, firstly, the AFO free mode showed an increase in instability (GMs,  $p < 0.05$ ) compared with a normal walk. Secondly, The dorsi-plantarflexion combined restrictions (DPRR and DPRT) showed a decrease in instability (GMs,  $p < 0.05$ ) whereas the alone dorsiflexion restriction i.e. DRT showed a significant increase in instability (GMs,  $p < 0.05$ ) compared to an AFO free mode walk. The numerical values are mentioned in Tables 7.5 and 7.6.

**Table 7.5: Loading phases stability margins quantified in the vertical direction.**

Walking Condition	Gain Margin (decibel)	Phase Margin (degree)	% Variance Explained (PC1 + PC2)	Coefficient of Determinant (R <sup>2</sup> )
Normal (without AFO)	-72.02 3.22	92.92 3.92	86.53	99.91
AFO (free mode)	<b>-11.36</b> 6.89	<b>87.58</b> 0.84	76.61+23.37	99.98
DPRR	-68.88* 12.77	<b>90.78*</b> 2.39	87.13	99.98
DPRT	<b>-14.54</b> 4.6	<b>88.28</b> 0.39	86.33	99.96
DRR	-72.38* 6.02	<b>91.48*</b> 2.04	84.18	99.97
DRT	-68.63* 3.97	92.08* 3.42	84.27	99.97

Bold for comparison with a normal walk, \* for comparison with AFO free-mode walk.

**Table 7.6: Unloading phases stability margins in the vertical direction**

Walking Condition	Gain Margin (decibel)	Phase Margin (degree)	% Variance Explained (PC1)	Coefficient of Determinant (R <sup>2</sup> )
Normal (without AFO)	-68.13 4.55	90.01 0.31	90.14	99.99
AFO (free mode)	<b>-114.66</b> 3.38	89.88 0.21	85.23	99.99
DPRR	<b>-20.9*</b> 1.65	<b>89.63</b> 0.067	90.55	99.99
DPRT	<b>-24*</b> 1.23	<b>89.62</b> 0.15	91.63	99.99
DRR	<b>-71.9</b> 19.11	89.96 0.07	90.39	99.99
DRT	<b>-141.45*</b> 3.64	89.66 0.23	92.9	99.99

Bold for comparison with a normal walk, \* for comparison with AFO free-mode walk.

The contractile properties quantified from vertical CoM-vibrations illustrated damping ratios approaches to zero of all walking conditions. An AFO free mode showed an increase ( $p<0.05$ ) in natural frequencies compared with a normal walk. The natural frequency of oscillations decreased ( $p<0.05$ ) in all restricted conditions compared to an AFO free mode walk. However, the peak gains decreased in an AFO free mode walk compared to a normal walk. The peak gains increased in forwarding AFO restricted impairments (DPRR, DRR, and DRT) compared to AFO free mode walk. The numerical values are mentioned in Table 7.7 for loading phases of ramp ascend walk.

**Table 7.7: Contractile properties quantified using vertical CoM-vibrations.**

<b>Walking Condition</b>	<b>Damping Ratio (<math>\zeta</math>) 1.0e-15*</b>	<b>Natural Frequency (Hz)</b>	<b>Peak Gain (decibel)</b>
Normal	0.025	0.125 0.0005	380.87 6.69
AFO (free mode)	0.016	<b>6.808</b> 0.417	<b>351.41</b> 12.65
DPRR	0.069	<b>0.121*</b> 0.0005	378.62* 4.56
DPRT	0.008	<b>6.048*</b> 0.015	<b>350.95</b> 12.34
DRR	0.079	<b>0.12*</b> 0.0004	383.4* 5.59
DRT	0.021	<b>0.128*</b> 0.0005	383.81* 7.87

Bold for comparison with a normal walk, \* for comparison with AFO free-mode walk.

#### **7.4.2 Ramp Descend activity**

Like the ramp ascend activity, the CoP-velocity illustrated stable loading phases (GM: $\infty$ ; PM: $90^\circ \pm 1$ ) and unstable unloading phases (GM:  $-51\text{db} \pm 7.6$ ; PM:  $89.6^\circ \pm 0.05$ ). During loading phases, firstly, an AFO free mode walk showed decreased in stability (PMs,  $p<0.05$ ) compared to a normal walk. Secondly, the forward AFO restricted impairments showed an increase in stability (PMs,  $p<0.05$ ) compared to an AFO free mode walk. Thirdly, compared with a normal walk, an everted foot decreased in stability and an inverted foot increased in stability. During unstable unloading phases, firstly, an AFO free mode walk increased in instability (GMs and PMs,  $p<0.05$ ) compared to a normal walk. Secondly, the forward AFO restricted impairments showed a decrease in instability (GMs and PMs,  $p<0.05$ ) compared to an AFO free mode walk. Thirdly, both rotational impairments illustrated no differences compared to a normal walk. The numerical values are mentioned in Tables 7.8 and 7.9 for loading and unloading phases respectively.

**Table 7.8: Loading phases stability margins quantified using CoP-velocity.**

<b>Walking Condition</b>	<b>Gain Margin (decibel)</b>	<b>Phase Margin (degree)</b>	<b>% Variance Explained (PC1)</b>	<b>Coefficient of Determinant (R<sup>2</sup>)</b>
Normal (without AFO)	∞	90.5 0.105	81.44	99.92
<b>Forward AFO restricted Impairments</b>				
AFO (free mode)	∞	<b>90</b> 0.1	99.07	99.94
DPRR	∞	90.46* 0.15	88.14	99.91
DPRT	∞	<b>90.92*</b> 0.26	85.37	99.94
DRR	∞	90.64* 0.24	88.72	99.93
DRT	∞	<b>90.38*</b> 0.14	89.19	99.91
<b>Rotational Ankle-foot Impairments</b>				
Eversion	∞	<b>91.23</b> 0.27	89.22	99.93
Inversion	∞	<b>90.75</b> 0.15	96.33	99.93

Bold for comparison with a normal walk, \* for comparison with AFO free-mode walk.

**Table 7.9: Unloading phases stability margins quantified using CoP-velocity.**

<b>Walking Condition</b>	<b>Gain Margin (decibel)</b>	<b>Phase Margin (degree)</b>	<b>% Variance Explained (PC1)</b>	<b>Coefficient of Determinant (R<sup>2</sup>)</b>
Normal (without AFO)	-43.88 3.39	89.59 0.17	96.58	99.92
<b>Forward AFO restricted Impairments</b>				
AFO (free mode)	<b>-104.35</b> 4.16	<b>90</b> 0.1	98.68	99.94
DPRR	-43.21* 2.8	89.57* 0.15	96.55	99.91
DPRT	-43.11* 1.9	89.57* 0.08	97.87	99.94
DRR	-42.3* 2.97	89.51* 0.16	97.16	99.93
DRT	-43.55* 2.29	89.58* 0.11	97.93	99.91
<b>Rotational Ankle-foot Impairments</b>				
Eversion	-44.92 2.48	89.66 0.11	97.04	99.93
Inversion	-42.68 2.49	89.55 0.13	96.08	99.93

Bold for comparison with a normal walk, \* for comparison with AFO free-mode walk.



In the anterior-posterior direction, the stability margins quantified using CoM-vibrations illustrated unstable responses for both loading and unloading phases. During loading phases, firstly, an AFO free mode walk increased in instability (GMs,  $p < 0.05$ ). Secondly, a total restriction ‘DPRR’ showed an increase in instability (GM and PM,  $p < 0.05$ ) and all other forward AFO restrictions showed a decrease in instability (GMs,  $p < 0.05$ ) compared to an AFO free mode walk. Thirdly, compared with a normal walk, an everted foot rotational impairment showed an increase in instability (GMs and PMs,  $p < 0.05$ ) whereas an inverted foot showed a decrease in instability (GMs,  $p < 0.05$ ). During respective unloading phases, there was no difference observed in instability (GMs and PMs,  $p > 0.05$ ) compared to AFO free mode and normal walks both in forward and rotational impairments. The numerical values are mentioned in Tables 7.10 and 7.11 for loading and unloading phases respectively.

**Table 7.10: Loading phases stability margins quantified using anterior-posterior CoM-vibrations.**

<b>Walking Condition</b>	<b>Gain Margin (decibel)</b>	<b>Phase Margin (degree)</b>	<b>% Variance Explained (PC1)</b>	<b>Coefficient of Determinant (R<sup>2</sup>)</b>
Normal (without AFO)	-29.42 3.2	82.94 5.13	81.98	99.84
<b>Forward AFO restricted Impairments</b>				
AFO (free mode)	<b>-66.39</b> 7.72	86.02 2.79	85	99.45
DPRR	<b>-163.66*</b> 12.84	88.46 2.73	96.03	99.66
DPRT	-27.43* 7.3	77.03 17.24	86.38	99.15
DRR	<b>-36.27*</b> 6.77	<b>88.97</b> 1.15	95.2	99.74
DRT	-31.29* 5.26	88.18 1.28	91.85	99.57
<b>Rotational Ankle-foot Impairments</b>				
Eversion	<b>-46.42</b> 4.3	<b>89.14</b> 1.22	93.59	99.85
Inversion	<b>-11.71</b> 3.01	85.21 2.73	94.19	99.27

Bold for comparison with a normal walk, \* for comparison with AFO free-mode walk.

**Table 7.11: Unloading phases stability margins quantified using anterior-posterior CoM-vibrations.**

<b>Walking Condition</b>	<b>Gain Margin (decibel)</b>	<b>Phase Margin (degree)</b>	<b>% Variance Explained (PC1 + PC2)</b>	<b>Coefficient of Determinant (R<sup>2</sup>)</b>
Normal (without AFO)	-49.94 3.88	90.1 0.1	84.93	99.99
<b>Forward AFO restricted Impairments</b>				
AFO (free mode)	-48.96 5.55	89.92 0.09	82.7	99.96
DPRR	-51.87 5.74	89.97 0.04	80.06	99.99
DPRT	-51.26 5.93	89.92 0.04	87.69	99.99
DRR	-50.51 5.57	89.94 0.05	84.34	99.99
DRT	-51.95 10.8	89.94 0.05	76.24+12.53	99.97
<b>Rotational Ankle-foot Impairments</b>				
Eversion	-49.2 8.07	89.96 0.05	92.42	99.99
Inversion	-50.14 4.8	89.9 0.05	91.51	99.99

Bold for comparison with a normal walk, \* for comparison with AFO free-mode walk.

Considering vertical components of CoM-vibrations, firstly, an AFO free mode walk showed a decrease in instability (GM,  $p < 0.05$ ) compared to a normal walk. Secondly, All AFO restricted forward impairments increased in instability (GMs,  $p < 0.05$ ) compared to AFO free mode and normal walks. However, the instability quantified by phase margins increased only in a dorsiflexion restriction i.e. DRT compared with both AFO free mode and normal walks. During respective unloading phases, firstly, an AFO free mode walk decreased in instability (GMs,  $p < 0.05$ ) compared to a normal walk. Secondly, all AFO restricted impairments showed a decrease in instability (GMs,  $p < 0.05$ ) except ‘DRT’ walk which showed increased GMs compared to an AFO free mode walk. The numerical values are mentioned in Tables 7.12 and 7.13 for loading and unloading phases respectively.

**Table 7.12: Loading phases stability margins quantified using vertical CoM-vibrations.**

<b>Walking Condition</b>	<b>Gain Margin (decibel)</b>	<b>Phase Margin (degree)</b>	<b>% Variance Explained (PC1 + PC2)</b>	<b>Coefficient of Determinant (R<sup>2</sup>)</b>
Normal (without AFO)	-69.43 13.43	93.18 4.24	94.74	99.93
AFO (free mode)	<b>-52.1</b> 18.29	93.1 8.21	86.45	99.68
DPRR	<b>-76.52*</b> 3.25	101.78 29.59	87.53	99.56
DPRT	<b>-81.81*</b> 4.34	96.1 5.08	84.74	99.1
DRR	<b>-92.61*</b> 11.19	91.39 2.3	76.05+20.41	99.94
DRT	<b>-84.36*</b> 2.71	<b>104.94</b> 17.74	87.07	99.81

Bold for comparison with a normal walk, \* for comparison with AFO free-mode walk.

**Table 7.13: Unloading phases stability margins quantified using vertical CoM-vibrations.**

<b>Walking Condition</b>	<b>Gain Margin (decibel)</b>	<b>Phase Margin (degree)</b>	<b>% Variance Explained (PC1)</b>	<b>Coefficient of Determinant (R<sup>2</sup>)</b>
Normal (without AFO)	-135.28 3.81	89.91 0.087	90.72	99.99
AFO (free mode)	<b>-128.61</b> 1.8	89.76 0.21	88.53	99.99
DPRR	<b>-36.76*</b> 1.65	89.91 0.031	91.51	99.99
DPRT	<b>-42.87*</b> 2.3	89.98 0.03	92.52	99.99
DRR	<b>-125.82*</b> 1.72	89.85 0.07	87.93	99.98
DRT	<b>-131.9*</b> 1.01	89.89 0.031	90.1	99.99

Bold for comparison with a normal walk, \* for comparison with AFO free-mode walk.

The contractile properties during ramp descend illustrated very small damping ratios (approaches to zero) in all walking conditions. The natural frequency decreased by walking with AFO in free mode compared to a normal walk. The dorsi-plantarflexion combined AFO restricted impairments increased in natural frequency and alone dorsiflexion restriction i.e. DRT decreased ( $p < 0.05$ ) compared to an AFO free-mode walk. The peak gains increased in ‘DPRR’ and ‘DRT’ walking impairments compared to an AFO free mode walk and showed no differences compared to a normal walk. The numerical values are mentioned in Table 7.14 for the loading phase of ramp descend activity.

**Table 7.14: Contractile properties quantified using vertical CoM-vibrations.**

<b>Walking Condition</b>	<b>Damping Ratio (ζ)</b> 1.0e-14*	<b>Natural Frequency (Hz)</b>	<b>Peak Gain (decibel)</b>
Normal	0.105	0.122 0.0006	389.94 12.64
AFO (free mode)	0.02	<b>0.086</b> 0.0002	387.11 5.75
DPRR	0.031	<b>0.1*</b> 0.0001	400.25* 12.83
DPRT	0.023	<b>0.095*</b> 0.0005	385.2 7.83
DRR	0.013	<b>0.095</b> 0.0112	395.19 22.98
DRT	0.014	<b>0.084*</b> 0.0003	393.2 5.61

Bold for comparison with a normal walk, \* for comparison with AFO free-mode walk.

### 7.4.3 Variability in joints angles and moments

The lower limb joints (ankle, knee, and hip) angles and moments are illustrated in Appendix C and summarised here in Tables 7.15 and 7.16 for ramp ascend and descend activities. In ramp descending walk, initial plantarflexion, peak dorsiflexion, and peak plantarflexion ankle ROMs decreased ( $p < 0.05$ ) with forwarding impairments. Whereas initial plantarflexion angle increased and peak plantarflexion ROMs decreased for rotational impairments. Peak knee flexion ROM decreased in stance phase in all impairments, and in swing phase, this is increased for the total AFO restrictions (i.e. DRR, DPRR) and decreased in everted, inverted foot. Hip flexion angle also increased for all impairments. Considering kinetic data, peak dorsiflexion moments decreased in all impairments and peak plantarflexion moment decreased only for rotational impairments. Peak knee flexion/extension moments also decreased in rotational impairments whereas only peak knee flexion moment increased in forwarding impairments. Peak hip extension moment also decreased for the total restrictions (DRR, DPRR) forward walks.

During ramp descend, peak dorsiflexion and peak plantarflexion angles decreased in both forward and rotational impairments. Peak knee flexion angle decreased in stance for forwarding impairments and everted foot, whereas in swing phase, peak knee flexion angle decreased only for in an inverted foot walk. Overall, hip joint did not show any change in ROM during ramp ascend. Peak dorsiflexion moment increased for total ROM based AFO restrictions (DRR, DPRR) and for an inverted foot. Peak plantarflexion moment increased for dorsi-plantarflexion combined restrictions and decreased in rotational impairments. Peak knee extension moment increased and peak hip extension moment decreased in forwarding impairments.

**Table 7.15: Lower limb joints angles (ROMs) and peak moments (mean ± Std.) for Ramp Ascend activity.**

<b>Parameters</b>	<b>AFO</b>	<b>DPRR</b>	<b>DPRT</b>	<b>DRR</b>	<b>DRT</b>	<b>Normal</b>	<b>Eversion</b>	<b>Inversion</b>
Initial plantarflexion angle loading (deg)	<b>5.71</b> (1.11)	<b>1.91</b> (1.04)	<b>1.95</b> (0.92)	<b>1.93</b> (1.2)	<b>1.88</b> (0.75)	3.23 (1.68)	<b>16.57</b> (2.7)	<b>17.3</b> (2.65)
Peak dorsiflexion angle (deg)	<b>21.19</b> (2.31)	<b>9.95</b> (3.97)	<b>11.15</b> (2.82)	<b>10.51</b> (3.72)	<b>11.99</b> (2.51)	11.9 (3.73)	12.28 (4.32)	11.3 (3.64)
Peak plantarflexion angle (deg)	30.89 (3.47)	<b>13.04</b> (2.15)	<b>14.94</b> (3.13)	<b>13.63</b> (3.34)	<b>18.38</b> (3.61)	32.63 (6.13)	<b>17.63</b> (4.41)	<b>19.04</b> (4.43)
Peak knee flexion angle stance (deg)	9.11 (4.99)	<b>6.94</b> (3.26)	<b>6.69</b> (2.6)	<b>6.8</b> (2.19)	<b>6.67</b> (2.48)	9.53 (2.64)	<b>6.79</b> (1.89)	<b>6.91</b> (1.81)
Peak knee flexion angle swing (deg)	<b>38.41</b> (5.35)	<b>43.47*</b> (4.4)	40.18 (3.59)	<b>40.66*</b> (8.69)	<b>34.20</b> (2.8)	42.86 (5.23)	<b>37.38</b> (5.7)	<b>35.67</b> (5.49)
Peak hip extension angle in stance (deg)	44.33 (3.27)	42.82 (4.74)	47.84 (12.15)	44.19 (4.95)	44.73 (5.95)	46.64 (5.17)	44.21 (5.27)	<b>43.24</b> (5.05)
Peak hip flexion angle in swing (deg)	<b>5.09</b> (3.67)	<b>18.92</b> (3.03)	<b>19.41</b> (3.55)	<b>19.08</b> (2.63)	<b>20.33</b> (2.44)	15.62 (3.1)	<b>19.2</b> (2.43)	<b>19.91</b> (2.74)
Peak dorsiflexion moment (Nm/kg)	1.55 (0.11)	<b>1.29</b> (0.11)	<b>1.34</b> (0.18)	<b>1.22</b> (0.19)	<b>1.47</b> (0.24)	1.52 (0.11)	<b>1.42</b> (0.13)	<b>1.35</b> (0.18)
Peak plantarflexion moment (Nm/kg)	0.086 (0.11)	0.121 (0.03)	0.107 (0.02)	0.096 (0.03)	0.101 (0.02)	0.086 (0.063)	<b>0.037</b> (0.01)	<b>0.05</b> (0.02)
Peak knee flexion moment (Nm/kg)	<b>0.33</b> (0.07)	0.26 (0.109)	0.35 (0.103)	0.26 (0.15)	0.38 (0.13)	0.51 (0.16)	<b>0.43</b> (0.11)	<b>0.39</b> (0.12)
Peak knee extension moment (Nm/kg)	<b>0.303</b> (0.02)	<b>0.607</b> (0.14)	<b>0.51</b> (0.17)	<b>0.62</b> (0.108)	<b>0.55</b> (0.14)	0.5 (0.12)	<b>0.4</b> (0.16)	<b>0.35</b> (0.15)
Peak hip flexion moment (Nm/kg)	0.65 (0.21)	0.63 (0.4)	0.61 (0.36)	0.64 (0.32)	0.56 (0.28)	0.59 (0.3)	0.69 (0.24)	0.68 (0.29)
Peak hip extension moment (Nm/kg)	0.53 (0.17)	<b>0.47</b> (0.12)	0.5 (0.12)	<b>0.4</b> (0.13)	0.52 (0.11)	0.56 (0.09)	0.59 (0.21)	0.57 (0.23)

Bold (p<0.05) – (1) comparison made normal versus AFO (free mode), eversion, inversion; (2) AFO free-mode versus DPRR, DPRT, DRR, DRT forward impairments.

**Table 7.16: Lower limb joints angles (ROMs) and peak moments (mean ± Std.) for Ramp Descend activity.**

<b>Parameters</b>	<b>AFO</b>	<b>DPRR</b>	<b>DPRT</b>	<b>DRR</b>	<b>DRT</b>	<b>Normal</b>	<b>Everson</b>	<b>Inversion</b>
Initial plantarflexion angle loading (deg)	5.51 2.93	<b>3.89</b> 1.32	4.59 1.87	6.35 1.53	5.22 1.56	2.12 (1.3)	<b>2.47</b> 0.92	<b>1.72</b> 1.56
Peak dorsiflexion angle (deg)	<b>28.74</b> 3.55	<b>15.9</b> 2.9	<b>18.6</b> 3.27	<b>19.23</b> 3.07	<b>18.74</b> 4.03	20.16 2.86	<b>15.69</b> 6.44	<b>17.49</b> 2.86
Peak plantarflexion angle (deg)	<b>24.91</b> 5.37	<b>15.28</b> 1.88	<b>16.01</b> 1.97	<b>16.26</b> 3.17	<b>17.91</b> 3.1	23.73 5.81	<b>17.98</b> 3.1	<b>16.33</b> 3.53
Peak knee flexion angle stance (deg)	<b>18.45</b> 4.6	<b>16.13</b> 4.51	<b>14.64</b> 2.85	<b>14.4</b> 2.53	<b>15.34</b> 3.32	14.3 3.4	<b>10.58</b> 3.32	14.11 4.0
Peak knee flexion angle swing (deg)	60.23 3.27	61.02 4.63	61.88 3.85	60.73 6.76	63.07 4.47	60.76 2.94	59.69 3.52	<b>57.61</b> 4.66
Peak hip extension angle in stance (deg)	<b>27.83</b> 4.13	30.25 6.17	24.54 8.29	28.53 6.11	29.45 9.1	32.33 6.18	28.39 5.22	30.22 6.11
Peak hip flexion angle in swing (deg)	11.66 2.13	12.32 7.94	13.63 1.07	12.69 6.75	9.4 7.6	11.47 5.04	11.34 1.78	12.47 9.3
Peak dorsiflexion moment (Nm/kg)	1.35 0.26	<b>1.12</b> 0.11	1.24 0.15	<b>1.11</b> 0.15	1.27 0.16	1.3 0.14	1.26 0.14	<b>1.18</b> 0.16
Peak plantarflexion moment (Nm/kg)	0.16 0.05	<b>0.19</b> 0.03	<b>0.18</b> 0.03	0.16 0.04	0.15 0.04	0.14 0.04	<b>0.065</b> 0.04	<b>0.082</b> 0.02
Peak knee flexion moment (Nm/kg)	0.37 0.11	0.48 0.09	0.47 0.16	<b>0.52</b> 0.14	0.46 0.14	0.5 0.2	0.47 0.15	0.52 0.18
Peak knee extension moment (Nm/kg)	<b>0.15</b> 0.1	<b>0.18</b> 0.1	<b>0.24</b> 0.12	<b>0.25</b> 0.13	<b>0.2</b> 0.11	0.11 0.09	0.19 0.13	0.16 0.11
Peak hip flexion moment (Nm/kg)	0.31 0.08	0.38 0.2	0.28 0.07	0.31 0.19	0.27 0.07	0.34 0.17	0.26 0.18	0.42 0.3
Peak hip extension moment (Nm/kg)	0.61 0.09	<b>0.45</b> 0.08	<b>0.49</b> 0.11	0.5 0.12	<b>0.49</b> 0.08	0.52 0.09	0.53 0.12	0.59 0.2

## **7.5 Discussion**

This chapter quantified gait transitional stabilities by applying Nyquist and Bode methods for forward and rotational ankle-foot impairments while performing ramp ascend and descend daily living activities. The stability margins were quantified using the rate of change in CoM-acceleration (GRF) and CoP signals as resultant neuromechanical inputs and outputs (I/O's) respectively. These I/O's are modelled and analysed earlier in Chapter 4-6 for a level ground walk. The detailed methodological choice and procedures are discussed in these chapters. Here, the stability outcomes and contractile properties are discussed to verify the aforementioned hypotheses for a ramp walk. The I/O's stability margins and variations in interlimb joints are discussed in the following sections.

### **7.5.1 Stability margins quantified using Neuromotor Outputs (CoP)**

Considering neuromotor output responses, the loading phase illustrated robustness w.r.t variations in GMs for both rotational and forward impairments. That was consistent with outcomes in a level ground walk (Chapter 4). During loading phases of ramp ascend, the AFO restrictions in forwarding impairments supports the dorsiflexion muscles to provide braking torques, hence, increased in stability illustrated by PMs. The interlimb joints compensate the AFO restrictions with increased plantarflexion moments. During unloading phases of ramp ascend, the instability decreased in forwarding restrictions compared with an AFO free mode walk. That was resultant of the ankle-foot reduced push-off ability which was mainly responsible to induce instability in this phase. However, this reduced plantarflexion motion was undesirable and compensated by the knee and hip joints with increased moments and/or angles during unloading phases. In an AFO free mode walk, the stability decreased in the loading phase and instability increased in the respective unloading phase compared to a normal walk. Whereas by tuning AFO restrictions, the stability margins approached the normal walk thresholds. That implies, wearable AFO structures induced instabilities which required to be tuned from moderate to severe range restrictions to obtain normal gait stabilities.

The differences in phase margins were observed to be smaller in magnitudes, however, statistically significant. There are procedural and theoretical reasons for these. The PCA procedure adopted to linearize and remove the artefacts in the waveforms, also reduced the variances in magnitudes and reconstructed waveforms reduced in variances along both axes (x, y) after removing artefacts [130]. Theoretically, it is reported that by increasing the ankle-foot plantarflexion stiffness through AFO, there is a small but significant decrease observed in Achilles tendon length which mainly transfers the muscles forces to the ankle joint [112].

During loading phases of ramp descend activity, similar to ramp ascend, the stability increased in forwarding impairments compared to an AFO free mode walk. The interlimb compensations were illustrated in dorsi-plantarflexion combined restriction with increased peak plantarflexion moments. In comparison to ramp ascend, the knee flexion angles were greater in magnitudes during ramp descend whereas the stability margins are in close ranges for both activities. Also, during respective unloading phases, both stability margins, which quantify instability, were decreased in AFO restricted conditions to the level of a normal walk just like in ramp ascend. The knee joint compensated the reduction in ankle-foot push-off ability with an increase in peak knee extension moment in these restricted conditions. In ramp descend, a total dorsi-plantarflexion restricted 'DPRR' condition showed greater interlimb variations, despite that, the stability margins quantified from outputs (CoP) were observed in range to moderate restrictions. The wearable AFO decreased in loading phases stability and increased in unloading phase instability compared to a normal walk.

Considering rotational impairments and ramp ascend, the stability decreased in loading phases compared to a normal walk, though, the differences were small but statistically significant. The interlimb balance control adopted with increased initial plantarflexion angles. In unloading phases, there was no difference observed in rotational impairments margins, however, the peak hip flexion angle increased to compensate interlimb deficiencies. During ramp descend, the everted foot decreased in stability and inverted foot increased with respective increase and decrease in initial plantarflexion angles. The increased stability in the inverted foot was due to its increased area of foot contact towards the lateral side and wedge insole support in foot landing. During unloading phases of ramp descend, the stability margins for rotational impairments did not show any difference with a normal walk. Also, there was no significant interlimb variation observed during the descent. Overall, the interlimb compensations were more during ramp ascend compared to descend activity.

The patterns in forwarding and rotational impairments are summarised in Tables 7.17 and 7.18, and the first hypothesis concluded based on the discussion in this section.

### **7.5.2 Stability margins quantified using Neuromotor Inputs ( $a_{CoM-AP}$ )**

The stability margins quantified using the rate of change in the anterior-posterior component of CoM-acceleration (GRF/mass) are discussed for forward and rotational impairments. During loading phases of ramp ascend, the AFO free mode walk increased in instability w.r.t GMs and decreased in PMs (time delays). This is because, in a normal walk ankle-foot apply breaking moments with a gradual heel rocking mechanism, and by wearing an AFO, the carbon fibre made stiff shoe did not allow gradual foot loading. However, by restricting the ankle-foot motion e.g. in DPRR conditions the PMs approached to the range of a normal walk. The relative increase



**Table 7.17: First hypothesis concluded based on output stability margins evaluated for ramp ascend activity.**

Comparative conditions	Stability Margins	Interlimb joints variations	Hypothesis 1
<b>Loading Phases</b>			
Difference of a normal walk by wearing AFO (free mode)	stability <sup>1</sup> decreased by wearing AFO	there was no significant increase in interlimb dynamics except the initial plantarflexion angle, this was resultant of markers placements at AFO rather direct at the body, the peak knee flexion moment decreased by wearing AFO	holds true
Impact on AFO (free mode) walk by restricting ankle-foot motions	stability increased* for all AFO restrictions and approached the normal walk margins	relatively peak plantarflexion moments increased, knee flexion angles in stance decreased by applying AFO restrictions	holds true
Difference of rotational impairments with a normal walk	stability decreased for both eversion and inversion	stance phases start with maximum initial plantarflexion angles, peak knee flexion angle in stance decreased, peak knee flexion moments decreased in both conditions	holds true
<b>Unloading Phases</b>			
Difference of a normal walk by wearing AFO (free mode)	instability <sup>2</sup> increased by wearing AFO	there was no significant increase in interlimb dynamics except the peak dorsiflexion angle increased as a resultant of markers placements at AFO, knee flexion and hip flexion angles in swing decreased, peak knee extension moment decreased	holds true
Impact on AFO (free mode) walk by restricting ankle-foot motions	applying restrictions instabilities decreased* and approached towards normal walk margins	peak knee and hip flexion angles and knee extension moment increased, peak hip extension moments decreased	holds true
Difference of rotational impairments with a normal	no significant difference found	peak hip flexion angle increased, peak knee flexion angle and knee extension moment decreased	not holds true

<sup>1</sup> quantified by phase margins whereas GMs are infinite for all walking conditions, <sup>2</sup> instability quantified by GMs and PMs.

\* A recent study (LDS method) support this finding with increased AP stability in older people on inclined surfaces (up/down) compared with young [14].

**Table 7.18: The first hypothesis concluded based on output stability margins quantified for ramp descend activity.**

Comparative conditions	Stability Margins	Interlimb joints variations	Hypothesis 1
<b>Loading Phases</b>			
Difference of a normal walk by wearing AFO (free mode)	stability <sup>1</sup> decreased by wearing AFO	peak knee flexion angle increased, however, no significant decrease observed by wearing AFO	holds true
Impact on AFO (free mode) walk by restricting ankle-foot motions	stability increased* by restricting ankle-foot motions	peak plantarflexion moment increased in dorsi-plantar combined restriction and peak knee flexion moment increased in dorsiflexion restriction (DRR), peak knee flexion angle in stance phase decreased	holds true
Difference of rotational impairments with a normal walk	stability increased for inverted foot and decreased for everted foot	initial plantarflexion angle increased in everted foot and decreased for inverted foot, knee flexion angles in stance decreased in everted foot, peak plantarflexion moments decreased for both	holds true
<b>Unloading Phases</b>			
Difference of a normal walk by wearing AFO (free mode)	instability <sup>2</sup> increased by wearing AFO	peak knee extension moment increased, peak hip extension angle decreased	holds true
Impact in AFO (free mode) walk by restricting ankle-foot motions	applying restrictions to ankle-foot, the instability* decreased towards normal walk margins	peak knee extension moments increased and peak hip extension moment decreased by applying restrictions	holds true
Difference of rotational impairments with a normal walk	no difference found	no significant increase observed, inverted foot decreased in knee flexion angle in swing	not holds true

\* A recent study (Lyapunov exponent (LDS) method) support this finding with increased anterior-posterior stability in older people on inclined surfaces (up/down) compared with young and no difference reported by applying Extrapolated-CoM (MoS) method [14].

Note: A decreased in ankle joint angles and moments in loading or unloading phases is resultant of applying AFO restrictions, however in response, an increase in ankle joint and/or increase/decrease in knee and hip joints illustrate interlimb strategies to compensate ankle joint deficiencies.

in peak plantarflexion, moments in AFO restricted conditions compared to its free mode reinforce this finding through the increments were insignificant. The only exception in the loading phase was a moderate restriction 'DPRT' which was increased in gain at critical point i.e. (GMs). This is because the initial moderate plantarflexion resistance allows the interlimb joints to overcome this forcefully as illustrated by relatively more increase in knee flexion moment compared to a total restriction (DPRR).

During unloading phases of ramp ascend, the variances explained by first principal components (PC1) did not meet the criteria (>80%), hence, the PCA waveforms were reconstructed for these conditions including first two principal components (PC1 and PC2). The instability increased for dorsi-plantarflexion moderate restriction (DPRT) and decreased for alone dorsiflexion restrictions (DRR, DRT) compared to an AFO free mode walk. This increase in instability was resultant of allowable forced push-off excursion against moderated plantarflexion resistance in 'DPRT' condition. The increased dorsiflexion moment in 'DPRT' compared to 'DPRR' supported this finding. Overall interlimb compensations for restricted conditions took place with a decrease in peak dorsiflexion angles and moments, and peak hip extension moments.

During loading phase of ramp descends, an AFO free mode walk increased in instability compared to a normal walk because of increased impact during heel rocker mechanism explained earlier while walking with carbon fibre shoe of AFO. During ramp descend the braking torque is more significant for balance control [186]. Applying AFO restrictions, this instability decreased to a normal walk threshold. The interlimb compensation exhibited by decreased peak knee flexion angle in stance. The only exception was a totally restricted 'DPRR' condition which was increased in instability. A total restriction increased the heel impacts and hence the GMs at a critical point. Comparing with other AFO restrictions, this total restriction also showed a significant decrease in the initial peak plantarflexion angle and more compensatory effort by increased knee flexion angle and peak plantarflexion moment. During unloading phases of ramp descend there was no difference found in stability margins, however, the reduced dorsiflexion and plantarflexion motions were compensated by an increase in knee extension moments compared to AFO free mode.

Considering rotational impairments, in loading phases of ramp ascend, the wedged insoles illustrated a decrease in PMs (time delay). This is because of increased and instant heel impacts which took place medial-to-lateral (eversion) and lateral-to-medial (inversion) with maximum body weights towards sides of the foot. There was no controlled initial plantarflexion as illustrated by increased angles and decreased moments in these conditions. In the unloading phase, only inverted foot decreased in instability because the wedged shape from 1<sup>st</sup> metatarsal towards 5<sup>th</sup> metatarsal makes

foot inclination with the ground that supports the weight unloading without proper push-off. During the loading phase of ramp descend, everted foot increased in instability with increased initial plantarflexion angle. Oppositely, the inverted foot decreased in instability with decreased in initial plantarflexion angles. Comparing two-foot conditions, the area of heel contact in eversion decreased during loading along with decreased everter muscles strength and foot rotation along its longitudinal axis resulted in an imbalance [108]. Like in forwarding restrictions, the rotational restrictions did not impact unloading phase stabilities, also observed from least interlimb compensations except a decrease in peak dorsiflexion and plantarflexion angles.

The patterns in forwarding and rotational impairments are summarised in Tables 7.19 and 7.20, and the first hypothesis concluded based on the discussion in this section.

A comparison is made in Figure 7.8 between stability margins quantified using CoM-vibrations and CoP-velocity (I/O's) in the anterior-posterior direction. In loading phases of ramp ascend/descend, the output GMs are infinite for all conditions and respective output PMs showed increased stabilities compared in unstable PMs quantified from inputs. In unloading phases of ramp ascend, a decrease in output instabilities (GMs) was observed in forwarding impairments whereas instabilities increased in rotational impairments compared to inputs margins. However, in the unloading phase of ramp descend, the output instabilities (GMs) decreased for both forward and rotational impairments compared to inputs margins. The I/O instabilities quantified as PMs observed to be in close range for both ramps ascend and descend activities.

### **7.5.3 Stability margins quantified using Neuromotor Inputs ( $a_{\text{CoM-vertical}}$ )**

The vertical CoM-oscillations provide maximum proprioceptive feedbacks with greater magnitudes compared to the anterior-posterior component. During the loading phase of ramp ascends, an AFO free mode walk decreased in instability (GMs and PMs) compared to a normal walk at the cost of increased knee flexion angle. However, by applying AFO restrictions, the instability increased to the level of a normal walk. The only exception was a moderate restriction 'DPRT' in which a dorsi-plantarflexion moderate resistances decreased vertical impacts at a critical point ( $0\text{db}, \pm 180 \pm 2k\pi$ ). Oppositely, in the anterior-posterior direction, the impacts increased as explained in the previous section. The excursion of knee flexion moment against the restricted ankle-foot motion (DPRT) increased the anterior-posterior shear forces and decreased the vertical shocks. During unloading phases of ramp ascend, the combined dorsi-plantarflexion AFO conditions (DPRR, DPRT) decreased in instability compared to a free mode walk. This was resultant of reduced peak plantarflexion angles in these

**Table 7.19: The first hypothesis concluded based on input (AP) stability margins quantified for ramp ascend activity.**

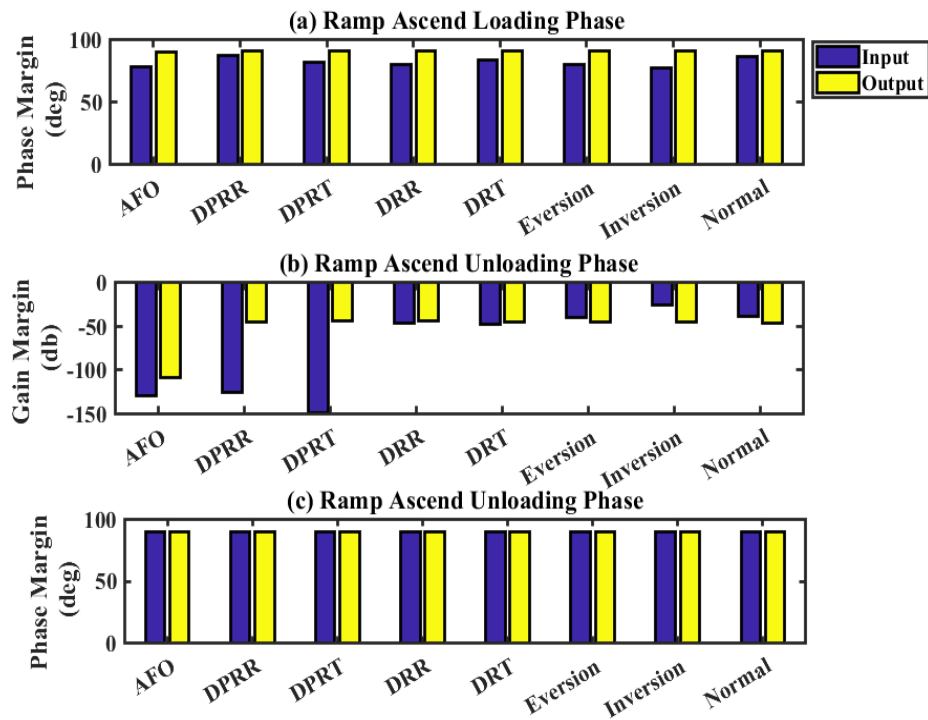
Comparative conditions	Stability Margins	Interlimb joints variations	Hypothesis 1
<b>Loading Phases</b>			
Difference of a normal walk by wearing AFO (free mode)	instability quantified by GMs and PMs, GMs increased and PMs decreased by wearing AFO, (carbon fiber rigid shoe structure did not allow gradual heel rocking and decreased PMs)	the peak knee flexion moment decreased by wearing AFO, the initial plantarflexion angle increased as a result of markers placements at AFO	holds true
Impact on AFO (free mode) walk by restricting ankle-foot motions	AFO restrictions decreased* in instability to the level of normal walk (except DPRT)	knee flexion angles decreased, relatively peak plantarflexion moments increased	holds true*
Difference of rotational impairments with a normal walk	instability quantified by GMs increased and quantified by PMs decreased, this decrease was resultant of wedged heel contacts (lateral/medial side heel contact increased impact and decreased controlled foot loading i.e. instant contact)	stance phases start with maximum initial plantarflexion angles, peak knee flexion angle in stance decreased, peak knee flexion moments decreased in both conditions	holds true
<b>Unloading Phases</b>			
Difference of a normal walk by wearing AFO (free mode)	instability (GMs) increased by wearing AFO	knee flexion and hip flexion angles in swing decreased, peak knee extension moment decreased	holds true
Impact in AFO (free mode) walk by restricting ankle-foot motions	instability (GMs) decreased* for AFO restricted conditions (except DPRT)	peak knee and hip flexion angles and knee extension moment increased, peak hip extension moments decreased	holds true
Difference of rotational impairments with a normal walk	instability (GMs) decreased for only inverted foot however PMs (time delay) slightly increased	peak hip flexion angle increased, peak knee flexion angle and knee extension moment decreased	holds true

\* A recent study (Lyapunov exponent (LDS) method) support this finding with increased anterior-posterior stability in older people on inclined surfaces (up/down) compared with young and no difference reported by applying Extrapolated-CoM (MoS) method [14].

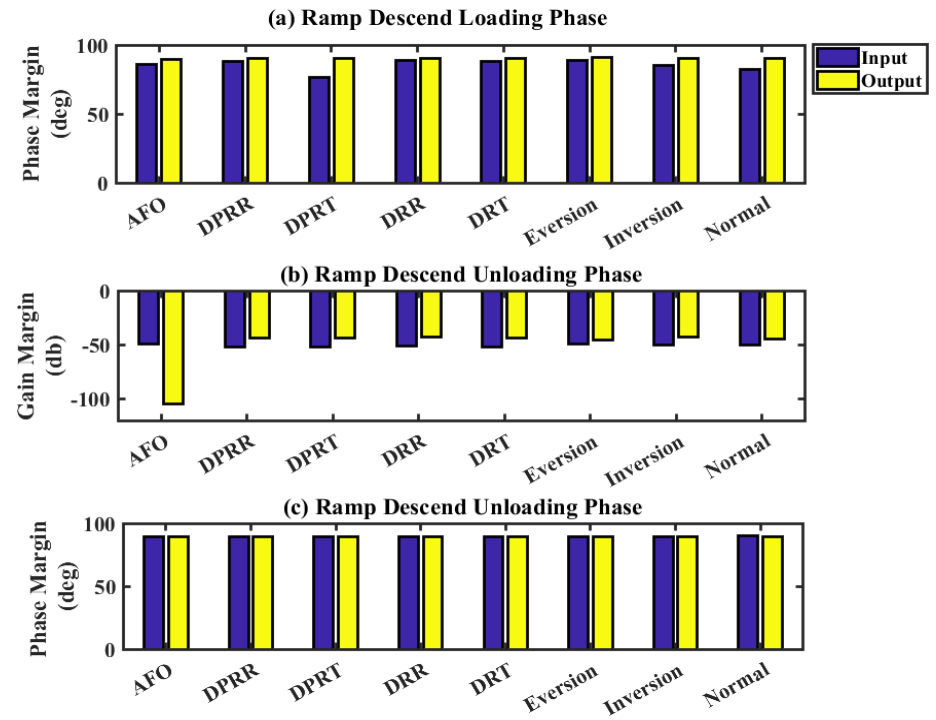
**Table 7.20: The first hypothesis concluded based on input (AP) stability margins quantified for ramp descend activity.**

<b>Comparative conditions</b>	<b>Stability Margins</b>	<b>Interlimb joints variations</b>	<b>Hypothesis 1</b>
<b>Loading Phases</b>			
Difference of a normal walk by wearing AFO (free mode)	instability (GMs) increased by wearing AFO	peak knee flexion angle increased, however, no significant decrease observed by wearing AFO	holds true
Impact on AFO (free mode) walk by restricting ankle-foot motions	instability (GMs) decreased* towards normal walk thresholds by applying restrictions except DPRR total restriction which increased in instability (GM, PM)	peak plantarflexion moment increased in dorsi-plantar combined restriction and peak knee flexion moment increased in dorsiflexion restriction (DRR), peak knee flexion angle in stance phase decreased	holds true
Difference of rotational impairments with a normal walk	everted foot increased in instability (GM, PM), inverted foot decreased in instability quantified by GMs	initial plantarflexion angle increased in everted foot and decreased for inverted foot, knee flexion angles in stance decreased in everted foot, peak plantarflexion moments decreased for both	holds true
<b>Unloading Phases</b>			
Difference of a normal walk by wearing AFO (free mode)	no difference found	peak knee extension moment increased, peak hip extension angle decreased	not holds true
Impact in AFO (free mode) walk by restricting ankle-foot motions	no difference found*	peak knee extension moments increased and peak hip extension moment decreased by applying restrictions	not holds true
Difference of rotational impairments with a normal walk	no difference found	no significant increase observed, inverted foot decreased in knee flexion angle in swing	not holds true

\* A recent study (Lyapunov exponent (LDS) method) support this finding with increased anterior-posterior stability in older people on inclined surfaces (up/down) compared with young and no difference reported by applying Extrapolated-CoM (MoS) method [14].



**(a) Ramp Ascending Walk**



**(b) Ramp Descending Walk**

**Figure 7.8: Comparison of anterior-posterior stability margins quantified from CoM-vibrations (input) and CoP-velocity (output) for a ramp ascend and descend walks.**

Note: the GMs of loading phases quantified from AP CoP-velocity (output) is infinite, hence, not illustrated in this comparison.

conditions comparative to alone dorsiflexion restricted conditions (DRR, DRT). However, the instability increased for dorsiflexion moderate restriction 'DRT'. This moderate resistance was overcome by an increase in peak dorsiflexion moment in this condition compared to other AFO restrictions.

During the loading phase of ramp descends, the instability decreased by wearing AFO like in ramp ascend. By applying restrictions, the instability (GMs) increased more than the normal walk margins despite an increase in ankle/knee joint moments. That was resultant of reduced interlimb joints ROMs and loading down the slope increased heel impact at a critical point. During respective unloading phases, the instability (GMs) decreased by wearing AFO and applying restrictions (except DRT). The interlimb joint compensate this by increased knee flexion and a decrease in hip extension moments.

The stability margins of forwarding impairments are summarised in Tables 7.21 and 7.22 and the first hypothesis is concluded based on the discussion in this section.

The contractile properties define the body's neuromuscular ability to absorb the shocks (vertical impacts) generated by heel contact. These properties investigated earlier for seated postures in various environments [92, 187], here, quantified for a ramp walk by wearing devices. The results illustrated damping ratio approached to zero i.e. undamped system for all walking conditions. During ramp ascend, the AFO (free mode) walk increased in natural frequency of CoM-oscillations and decreased to a normal walk threshold by introducing AFO restrictions (except 'DPRT'). However, the peak gains increased for respective AFO restricted conditions compared to free mode. The moderate resistance 'DPRT' condition illustrated similar patterns as explained by GMs earlier in ramp ascend with outcomes that the moderate plantarflexion resistance reduced the peak gain with increased frequency of oscillations (6 Hz). During ramp descend, the heel contact oscillations decreased by in natural frequency wearing AFO and slightly increased by applying dorsi-plantarflexion combined restriction compared to an AFO free mode. Summarising, in ramp ascend, the AFO affect the natural frequency and peak gain of CoM-oscillation with/without applying restrictions. In ramp descend only natural frequencies varied compared to a normal walk contractile properties.

The contractile properties in forwarding impairments are summarised in Tables 7.23 and the second hypothesis concluded based on the discussion in this section. This study introduces Nyquist and Bode methods for gait dynamic stability analysis as a pilot study. The results illustrated small but statistically significant variations in transitional stabilities of imitated ankle impairments. Prior gait stability analysis methods i.e. extrapolated-CoM and BoS difference (MoS) are reported as lacking for non-level walking [14, 98].



**Table 7.21: The first hypothesis concluded based on input (vertical) stability margins quantified for ramp ascend activity.**

<b>Comparative conditions</b>	<b>Stability Margins</b>	<b>Interlimb joints variations</b>	<b>Hypothesis 1</b>
<b>Loading Phases</b>			
Difference of a normal walk by wearing AFO (free mode)	instability decreased by wearing AFO	there was no significant increase in interlimb dynamics except the initial plantarflexion angle, this was resultant of markers placements at AFO rather direct at the body, the peak knee flexion moment decreased by wearing AFO	holds true
Impact on AFO (free mode) walk by restricting ankle-foot motions	instability margins attain the normal walk thresholds by applying AFO restrictions (except DPRT)	relatively peak plantarflexion moments increased, knee flexion angles in stance decreased by applying AFO restrictions	holds true
<b>Unloading Phases</b>			
Difference of a normal walk by wearing AFO (free mode)	instability increased by wearing AFO quantified by GMs	there was no significant increase in interlimb dynamics except the peak dorsiflexion angle increased as a resultant of markers placements at AFO, knee flexion and hip flexion angles in swing decreased, peak knee extension moment decreased	holds true
Impact in AFO (free mode) walk by restricting ankle-foot motions	instability decreased* by applying dorsi-plantarflexion restriction and increased for a dorsiflexion alone restriction DRT	peak knee and hip flexion angles and knee extension moment increased, peak hip extension moments decreased	holds true

\* A recent study (Lyapunov exponent (LDS) method) support this finding with increased anterior-posterior stability in older people on inclined surfaces (up/down) compared with young and no difference reported by applying Extrapolated-CoM (MoS) method [14].

**Table 7.22: The first hypothesis concluded based on input (vertical) stability margins quantified for ramp descend activity.**

<b>Comparative conditions</b>	<b>Stability Margins</b>	<b>Interlimb joints variations</b>	<b>Hypothesis 1</b>
<b>Loading Phases</b>			
Difference of a normal walk by wearing AFO (free mode)	instability (GMs) decreased by wearing AFO	peak knee flexion angle increased, however, no significant decrease observed by wearing AFO	holds true
Impact on AFO (free mode) walk by restricting ankle-foot motions	instability (GMs) increased by restricting ankle-foot motion	peak plantarflexion moments relatively increased in dorsi-plantar combined restriction, peak knee flexion moment increased in dorsiflexion restriction (DRR), peak knee flexion angle in stance phase decreased	holds true
<b>Unloading Phases</b>			
Difference of a normal walk by wearing AFO (free mode)	instability increased by wearing AFO	peak knee extension moment increased, peak hip extension angle decreased	holds true
Impact in AFO (free mode) walk by restricting ankle-foot motions	instability (GMs) decreased* in AFO restrictions except DRT where it was increased	peak knee extension moments increased and peak hip extension moment decreased by applying restrictions	holds true

\* A recent study (Lyapunov exponent (LDS) method) support this finding with increased anterior-posterior stability in older people on inclined surfaces (up/down) compared with young and no difference reported by applying Extrapolated-CoM (MoS) method [14].

Note: A decreased in ankle joint angles and moments in loading or unloading phases is resultant of applying AFO restrictions, however in response, an increase in ankle joint and/or increase/decrease in knee and hip joints illustrate interlimb strategies to compensate ankle joint deficiencies.

**Table 7.23: The second hypothesis concluded based on contractile properties evaluated for ramp ascend and descend activities.**

<b>Contractile Properties</b>	<b>Damping Ratio</b>	<b>Natural Frequency (Hz)</b>	<b>Peak Gain (decibel)</b>	<b>Hypothesis 2</b>
<b>Ramp Ascend</b>				
Difference of a normal walk by wearing AFO (free mode)	approaches to zero for all walking conditions, undamped response	oscillations increased by wearing AFO	decreased by wearing AFO	holds true*
Impact on AFO (free mode) walk by restricting ankle-foot motions	approaches to zero for all walking conditions, undamped response	oscillations decreased by applying restrictions	peak magnitudes increased by applying AFO restrictions	holds true*
<b>Ramp Descend</b>				
Difference of a normal walk by wearing AFO (free mode)	approaches to zero for all walking conditions, undamped response	oscillations decreased by wearing AFO	no significant difference	holds true <sup>^</sup>
Impact on AFO (free mode) walk by restricting ankle-foot motions	approaches to zero for all walking conditions, undamped response	oscillations increased for dorsi-plantarflexion combined restrictions	no significant difference (except DPRR)	holds true <sup>^</sup>

\* Except damping ratio, ^ only for natural frequency.

A lightweight (0.5kg) passive ankle-foot orthosis was used here to imitate ankle-foot deficiencies by tuning this device to various clinical ranges. In comparison, the active orthoses and other wearable devices (assistive exoskeleton, prosthetics) are bulkier in structures and weights and expected to produce more CoM-vibrations impacts on transitional stabilities and contractile properties. In future, the scope of current research is extended by including real patients and using active assistive devices. Also, the experiments performed in this study with a moderate range ramp ascend and descend slopes ( $\pm 5^\circ$ ). A further increase in this slope impact the gait dynamics significantly as reported earlier [186]. Lastly, the healthy subjects showed uniform imitated impairments, however, they have recovered balance control abilities for ankle-foot restrictions compared to real patients, a limitation of the current study. The vertical CoM-vibrations impacts evaluated only for forward impairments because wedged insoles used for imitating rotational impairments also damped the vertical oscillations. The stabilities are assessed only for proprioceptive feedback whereas visual and vestibular contributions are not counted.

## 7.6 Summary

Yet a little research has ever been done for balance control on an inclined surface, this study introduced Nyquist and Bode stability methods for ramp ascend and descend gait activities. The gait transitional stabilities were quantified using output and inputs neuromechanical responses in anterior-posterior and vertical directions. The orthoses restricted ankle-foot motions were used to imitate forward and rotational ankle-foot impairments illustrated by reduced ankle joint angles and moments. In response, an increase in the ankle joint and/or an increase/decrease in the knee and hip joints dynamics illustrated the compensatory strategies for simulated impairments. Overall results illustrated that by wearing an AFO in free mode the instability significantly increased compared to a normal walk (without AFO). However, by applying restrictions to ankle-foot motions through AFO (i.e. forward impairments), generally, instabilities decreased compared to an AFO free mode walk except in vertical direction where instabilities increased in loading phases. In rotational impairments, overall the stability decreased in loading phases for both ramps ascend and descend activities, however, no significant differences were observed in respective unloading phases. The variations in interlimb joints angles and moments were assessed to explain the neuromotor compensatory patterns along with stability margins. This study has important applications for evaluating stabilities over varying terrains, patients with lower limb impairments, and other wearable devices.

## **CHAPTER 8**

### **SUMMARY, CONCLUSIONS AND FUTURE WORK**

#### **8.1 Summary and Assessment of the Research Objectives**

In the first chapter, the aims and objectives of the current research were defined. The aims in this study were to introduce Nyquist and Bode (N&B) stability methods and evaluate gait transitional phases with effect to ankle-foot joint impairments and/or adjustable ankle-foot orthosis. Primarily, two hypotheses were structured to implement these methods as an initial proof of concept, first to evaluate ankle-foot impairments (forward, rotational) effect, and second to evaluate ankle-foot orthosis (AFO) effect on gait transitional stability. Since the same adjustable AFO was used in this study to imitate ankle-foot impairments in the forward direction, hence, both hypotheses were verified using the same methods and experimental data. A summary is described herein the sequence of objectives achieved in order to fill the gaps of knowledge defined in Chapter 2 (section 2.7).

- To extract appropriate biomechanical signals that can be used to evaluate transitional phases gait stabilities.

In Chapter 3, the experimental methods were presented using a motion capture system and force plates. Two types of ankle-foot orthoses were used to imitate ankle-foot impairments with uniform degrees. The first orthosis was made adjustable to tune resistive torques ( $\pm 33\text{Nm}$ ) or restrict ankle angles to imitate foot drop and Charcot-Marie-Tooth impairments. The second orthosis was designed in a pair of foot insoles wedged ( $\pm 10^\circ$ ) laterally to simulate inverted foot and medially to simulate everted foot. Further slow, normal, and fast speed trials were recorded. The variability in lower limb joints angles and moments are computed and compared with patients data from literature and later also used to explain the stability outcomes. Gait dynamic stability control signals i.e. CoP and GRF were computed. The higher order derivative of these signals illustrated impulsive responses just like what the muscles activation patterns showed during loading and unloading of gait phases. Thus, the rate of change in CoP and CoM-acceleration (GRF/mass) signals are assessed for further analyses as resultant neuromotor outputs and inputs (O/Is) respectively. The CoP signals were quantified in *forward* and *lateral* directions, whereas CoM-acceleration were quantified in *forward* and *vertical* directions.

- To establish supporting analytical techniques to these signals with clear fixed thresholds to determining stable or unstable gait.

In Chapter 2 (section 2.4), various stability assessment techniques are discussed for a dynamic gait. Among these, recently used N&B methods were reported with distinct criteria and applied in this study. The related implemented theory was discussed in Chapter 3 (section 3.6). For loading and unloading gait transitional phases, these methods were implemented using rate dependant CoP and CoM-acceleration impulsive signals. In Chapters 4-7, these signals were modelled in time and frequency domains using system identification approach with an overall best fit coefficient of determinants ( $R^2=99\pm 1\%$ ). The N&B methods were applied to these linear time-invariant frequency domain models considering lower limb as a plant with a unit impulse inputs. The gain margins (magnitude) and phase margins (time difference) were quantified from all O/I models in respective walking conditions.

- To evaluate gait transitional stabilities for varying terrains i.e. level, ramp ascends and descend ADLs.

The gait transitional stabilities (loading and unloading phases), not quantified in previous studies, are evaluated in this study for healthy and imitated ankle-foot impairments. In Chapter 4, the stability margins were evaluated using neuromotor output response (CoP-velocity) for ten walking conditions divided into three groups i.e. walking speed, forward, and rotational impairments. The outcomes were compared by applying another method (i.e. extrapolated-CoM difference from BoS). In Chapter 5, the stability margins were quantified using rate dependant *forward* CoM-acceleration as somatosensory feedback to the neuromotor in all three walking groups. The stability margins were explained by variability in peak moments and angular ROMs, variability in time series waveforms evaluated from PCA, and Spearman's correlation methods wherever required. In Chapter 7, both of these O/I signals were analysed for ramp ascend and descend activities for all three simulated walking groups. In each chapter, the outcomes from N&B methods were compared with earlier methods and summarised in tabular form (Tables 4.13, 4.14, 5.9, 6.8, 7.17-7.23) at the end of discussion sections.

- To evaluate somatosensory neuromotor feedbacks (impact forces) effect in gait stability in healthy and impaired gait, and varying terrains.

In Chapter 2, somatosensory feedback (CoM-acceleration) was reported as contributing to muscles activations during gait transitional phases. In Chapter 6, the rate of change in *vertical* CoM-acceleration showed impulsive transients which were modelled and used to evaluate gait transitional stabilities. In Chapter 5, these stabilities were quantified from *forward* CoM-acceleration. The impact of wearable ankle-foot orthosis at three self-selected walking speeds and with four different ankle-foot impairments were quantified. The rotational impairments are not evaluated in the *vertical* direction, because, the foot insoles used to imitate eversion/inversion also

attenuate *vertical* CoM-oscillations. Overall results from vertical CoM-oscillations showed that the wearable devices significantly affected gait stability in both loading and unloading phases. In Chapter 6, these methods were applied for a level walk, and in Chapter 7, these are applied for ramp ascend and descend activities.

- To evaluate lower limb contractile properties with/without the effect of ankle-foot orthosis and adjustments made to clinically prescribed ranges.

In Chapter 2, body loading impacts with wearable orthosis are highlighted to be investigated. While earlier studies used spring-mass-damper (SMD) models to characterise the attenuation of impact loading, here, the *vertical* CoM-oscillations were modelled using human subjects data and control engineering theory was applied to quantify the natural frequency, damping ratio, and peak gain. In Chapter 6, these contractile properties were evaluated for a level walk and compared with outcomes reported from SMD models. The contractile properties (natural frequency, peak gain) decreased by wearing AFO in most of level walking conditions. In Chapter 7, these properties were evaluated for ramp ascend (natural frequency increased and peak gain decreased) and ramp descend (only natural frequency decreased) activities.

- To provide a qualitative database for clinical applications with the effect of healthy and uniform ankle-foot impairments.

In Chapter 2, the stability margins were reported in fluctuating ranges because of the lack of distinct criteria and varying degree of impairment in individual subjects. In Chapter 3, a uniform degree of impairments was imitated for the ankle-foot joint, in Chapters 4-7, N&B methods were implemented with distinct cut-offs to quantify gait stability. Both the healthy and impaired gait provides a preliminary database to evaluate gait dynamic stabilities in physical patients which are deficient in either dorsiflexion, plantarflexion, eversion, inversion, or either combination of these ankle-foot motions.

## **8.2 Relevance of Research**

Considering the practical stability perspective, gait transitional stability evaluation methods are useful for the evaluation of therapeutic/rehabilitation effectiveness. For example, in the case of lower limb impairments, various physiotherapy courses are prescribed clinically or assistive orthoses are recommended to the patients. Similarly, vibration therapy is provided to such patients under foot plantar to improve balance control. An improvement in a patient's balance control before and after adopting these procedures can be evaluated using methods introduced in this research.

In a healthy walk, stability is mainly related to balancing of body's segmental masses. Within a healthy group, the body-mass-index (BMI) did not illustrate any significant

difference in stability margins during loading and unloading phases. However, by wearing a rigid AFO (0.5kg) to one side of the limb, there was a significant change observed in stability margins. Thus, any inertial change as a result of an external wearable device (prosthetics, exoskeletons) is speculated to change body's masses balance point and needed additional measures to meet the CoM movements close to healthy subjects trajectories. Regarding that, in this study, a controller design approach is adopted in this study (Chapter 4-6) with the objective to stabilizes the unstable plant models those are quantifying the body's imbalances. The simulation results illustrated that a simple proportional-integrator-derivative (PID) controller can bring back an unstable system to the stable region. In addition to that, a variation in walking speeds from very slow to very fast illustrated an increase in instability and reinforced previously reported slow walking adaptation by the elderly subjects to maintain stability. These findings suggest, using wearable robotics, the additional masses can be applied to gain the normal/healthy CoM motions which are quantifiable in terms of gain margins and phase margins. Any difference in GM and PM quantified with/without a wearable device can be retained by the addition of mass and adopting walking velocity to mimic a normal/healthy subject's stability margins. Considering these facts, the stability evaluation methods in current research can be used not only to evaluate the stability but also to control the imbalances resulted from wearable devices.

### **8.3 Conclusions**

This study has effectively implemented Nyquist and Bode methods that have the capability to quantify gait transitional phases stabilities using neuromotor O/I signals measured experimentally from human subjects. The application of these methods for ankle joint, transitional phases (loading and unloading), and varying terrains is a pilot work assessed in this study. The findings of current research are concluded here as:

1. The biomechanical signals such as rate of change in CoP and CoM-acceleration showed transient impulses with decaying and rising magnitudes and illustrated potentially suitable for transitional phases stability evaluations which have been unquantified in previous studies.
2. The N&B methods implemented here to evaluate these transient impulses have fixed distinct cut-off thresholds, that resolves the standardization issue (i.e. a clear reference to define stability/instability margins) as reported in previous methods with fluctuating stability outcomes and confusion in stability criteria. The hypotheses verified by applying N&B methods (stability margins) are summarised in Table 8.1 and 8.2 for level and inclined walks respectively.



**Table 8.1: Overall Stability Margins and Hypothesis evaluation for a Level ground Walk.**

<b>Hypothesis (effect on stability)</b>	<b>Compared with</b>	<b>CoP- velocity (forward)</b>	<b>CoM- oscillations (forward)</b>	<b>CoM- oscillations (vertical)</b>
<b>Loading Phases</b>				
Wearable ankle orthosis	Normal walk	holds true	holds true	holds true
Forward ankle impairments	AFO (free mode)	not holds true	holds true	holds true
Rotational impairments	Normal walk	holds true	holds true	not evaluated
Preferred walking speed	Normal walk	holds true	holds true	not holds true
<b>Unloading Phases</b>				
Wearable ankle orthosis	Normal walk	holds true	holds true	holds true
Forward ankle impairments <sup>1</sup>	AFO (free mode)	holds true	holds true	holds true
Rotational impairments <sup>2</sup>	Normal walk	holds true	holds true	not evaluated
Preferred walking speed <sup>3</sup>	Normal walk	holds true	holds true	holds true

Above hypotheses are evaluated in following walking groups: <sup>1</sup>**Group 1 – Forward Impairments:** dorsiflexion resistance torque (DRT), dorsi-plantarflexion resistive torques (DPRT), dorsiflexion range-of-motion restriction (DRR), dorsi-plantarflexion range of motion restrictions (DPRR); <sup>2</sup>**Group 2 – Rotational Impairments:** Everted foot (medially wedged insoles), Inverted foot (laterally wedged insoles); <sup>3</sup>**Group 3 – Preferred Walking speeds:** Slow, Normal, Fast.

3. The stability margins quantified from CoP signals give a measure of a resultant neuromotor output response, and CoM-acceleration signals measure resultant impact forces acting as somatosensory feedback in neuromotor balance control. These parameters (O/Is) and methods provide a comprehensive way-out to evaluate neuropathy patients e.g. diabetic, multiple sclerosis, CMT, stroke patients who lost their sensory feedback and exhibited poor balance control.

**Table 8.2: Overall Stability Margins and Hypothesis evaluation for Ramp Ascend (A) and Descend (D) Walks.**

<b>Hypothesis (effect on stability)</b>	<b>Compared with</b>	<b>CoP- velocity (forward)</b>	<b>CoM- oscillations (forward)</b>	<b>CoM- oscillations (vertical)</b>
<b>Loading Phases</b>				
Wearable ankle orthosis	Normal walk	holds true (A/D)	holds true (A/D)	holds true (A/D)
Forward ankle impairments	AFO (free mode)	holds true (A/D)	holds true (A/D)	holds true (A/D)
Rotational impairments	Normal walk	holds true (A/D)	holds true (A/D)	not evaluated (A/D)
<b>Unloading Phases</b>				
Wearable ankle orthosis	Normal walk	holds true (A/D)	holds true (A) not hold true (D)	holds true (A/D)
Forward ankle impairments	AFO (free mode)	holds true (A/D)	holds true (A) not hold true (D)	holds true (A/D)
Rotational impairments	Normal walk	not holds true (A/D)	holds true (A) not hold true (D)	not evaluated (A/D)

4. The results in this study illustrated that adjustable ankle-foot orthosis significantly affects loading and unloading phases stabilities. Overall patterns presented that stability margins have either maximum or minimum thresholds by wearing AFO (free mode) and on applying restrictions the stability margins gained the normal walk thresholds as shown in Figures 8.1-8.3.
5. Results from rotational impairments illustrated the significant difference in inverted foot stability margins and hence stands more sensitive along with the reduced area of foot contact with the ground. Similarly, in self-selected walking speeds, the results showed a greater decrease in stability at slow speed during the loading phase and at fast speed during unloading phase compared to a normal walk (associated figures in Appendix E).

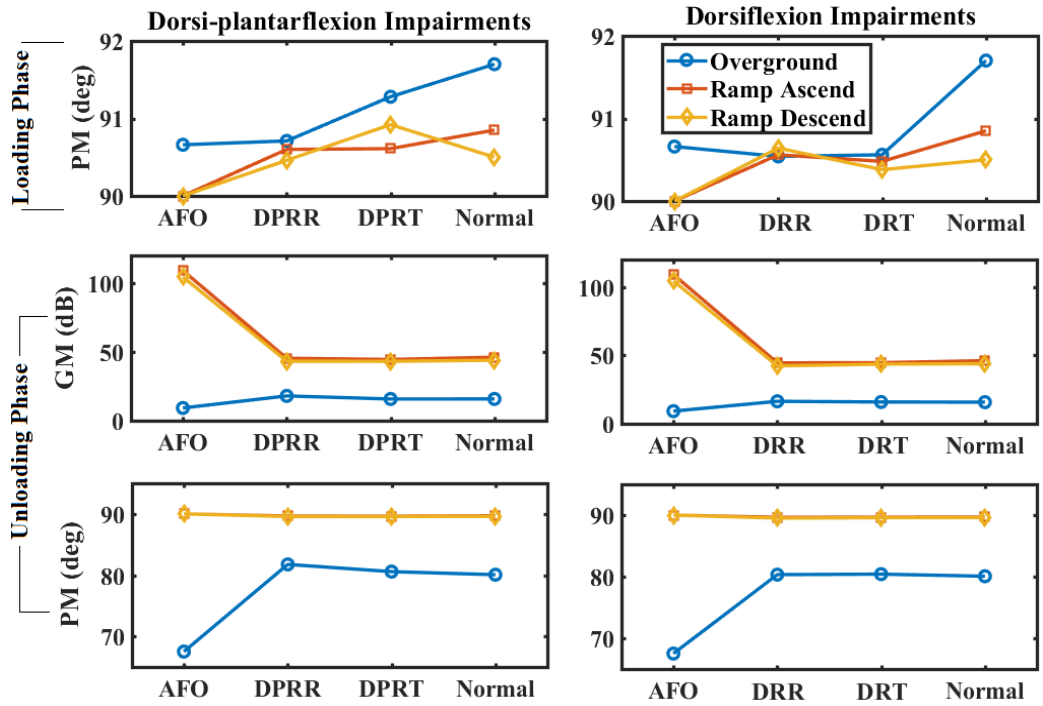


Figure 8.1: Mean Stability margins quantified from neuromotor outputs (CoP).

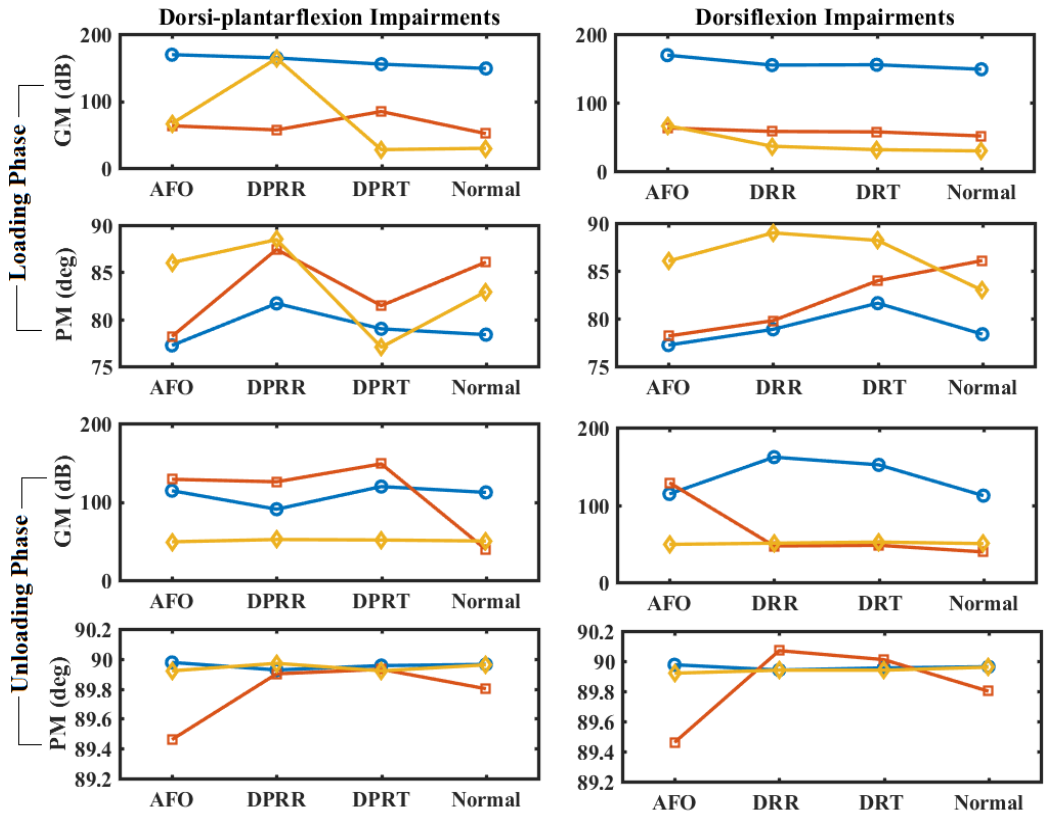
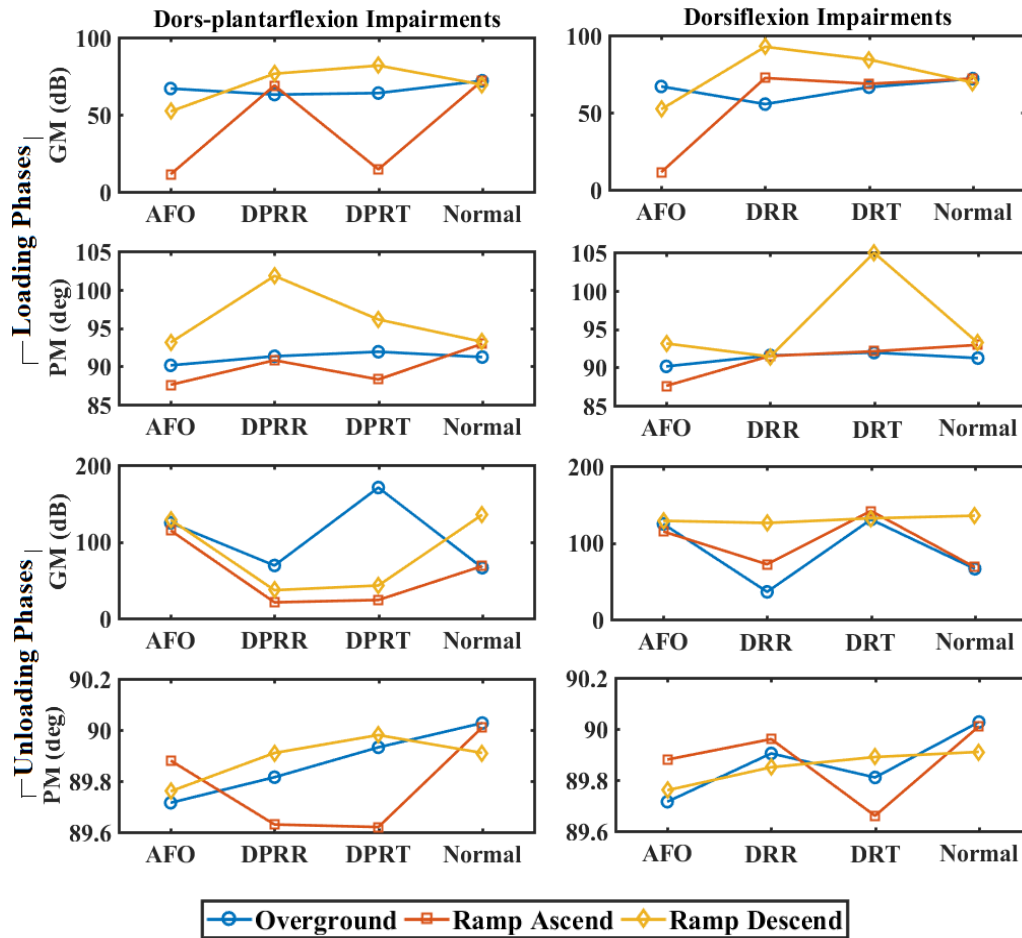


Figure 8.2: Mean Instability margins quantified from *forwarding* CoM-acceleration (somatosensory Input).



**Figure 8.3: Mean Instability margins quantified from *vertical* CoM-acceleration (somatosensory Input).**

6. The use of resultant O/I signals also optimise the computational cost and analytical descriptions compared with multiple signals being used in Lyapunov exponent methods, in parametric variability, and extrapolated-CoM and BoS difference (two variables) methods described in Chapter 2.
7. In this study, the efficiency of stability evaluation algorithms can be predicted from an average of variability explained by principal components (%) and best-fit coefficient of determinants ( $R^2$ ) values as mentioned in Table 8.3 for a level walk. This was not predictable in earlier assessments except intraclass correlation (ICC) methods. (Appendix F includes ramp walk data)

**Table 8.3: Efficiency of stability evaluation for level walking conditions.**

Signals	CoP-velocity (forward)		CoM-acceleration (forward)		CoM-acceleration (vertical)	
	L	U	L	U	L	U
walk cond.						
AFO (free)	98.73	98.51	98.69	91.20	94.21	97.18
DPRR	98.05	98.63	94.16	92.6	92.54	94.53
DPRT	96.80	98.26	95.27	92.07	91.23	96.97
DRR	98.42	98.05	94.38	91.35	88.82	95.23
DRT	98	98.30	95.77	89.98	92.55	95.83
Eversion	98.54	98.78	96.88	96.66	-	-
Inversion	98.36	98.73	95.95	92.55	-	-
Slow	98.4	99.04	96.16	94.05	92.79	95.23
Normal	98.04	98.22	96.82	94.54	95.03	96.03
Fast	98.37	98.32	94.47	95.61	93.13	95.38

8. The results from ramp ascend/descend walks (Table 8.2) showed consistency in hypothesis outcomes. The only exception is found during ramp descend unloading phases for forwarding CoM-acceleration. Only, a couple of studies [13, 14, 98] have evaluated ramp walk stabilities with healthy and elderly subjects. The N&B methods are a new addition in this series that has successfully evaluated stabilities on inclined surfaces.
9. This study improvises uniform restrictions to imitate forward and rotational ankle-foot impairments and outcomes provide qualitative reference data for both methodological and patients related stability evaluations. Considering previous studies, only gait dynamic stabilities are assessed with the effect of age-related differences and there is no study found that has evaluated stability with lower limb deficiencies mainly due to a varying degree of impairments.

## 8.4 Limitations

The limitations of the current study are described in the respective chapters and are summarised here:

1. The N&B models require plant transfer functions (TF) and are modelled in this study using a system identification approach. These TFs are sensitive to the best fit coefficient of the determinant ( $R^2$ ) such that a slight compromise

to reduce the order of a model has a significant effect in output stability margins. This is particularly important while modelling CoM-oscillations (Chapter 5-7).

2. The rate-dependent resultant biomechanical signals (CoP, CoM-acceleration) were demonstrated to be suitable for evaluating transitional stabilities in which signals showed transient impulses and remained steady state for the rest of the gait phases. This implies that the implementation of N&B with mentioned signals is not appropriate for stability evaluation in single limb support time (i.e. mid-stance, terminal stance, and swing phases).
3. The results from N&B methods were compared with extrapolated-CoM method (for a level walk) and explained by interlimb joints (angles, moments) compensations wherever necessary (Chapter 4-7). The exact comparison with prior assessments is instead impossible because earlier methods involved either whole gait cycle waveforms or evaluate stabilities at discrete gait events such as heel contact and toe-off. To the author's knowledge, there is no study found that has evaluated gait stabilities during loading and unloading transitional phases.
4. There were small but statistically significant differences found in gain (dB) and phase (degree) margins wherever exists, that was consistent with extrapolated-CoM methods in which MoS(s) differences were reported in a fraction of a meter [29, 38, 39]. It can be presumed further that treadmill based trials can illustrate relatively more differences among comparative conditions along with a uniform degree of impairments.
5. Lastly, though the previous researches also used imitation approaches and it helps in establishing new methods with a uniform degree of impairments, however, the patients are required to be evaluated further by applying these methods.

## 8.5 Future Works

The current study introduced N&B methods for walking stability assessments as a preliminary study. However, there is great potential to improve or extend the scope of this research. Future work included the following aspects to be considered:

1. The N&B methods are required to be directly applied to patients and evaluate the differences between practical and ideal stability margins as quantified in this study from uniformly restricted imitated ankle-foot impairments.
2. In the current research, rotational impairments are simulated in a moderate range i.e. using  $\pm 10^\circ$  wedged insoles, further ranges are required to be evaluated by applying these methods to examine stability trends. Further,

forward impairments are imitated at fixed stiffness (Nm) and ROM (degree) restrictions, a further range can show stability patterns w.r.t degree of impairments.

3. Considering great research in developing wearable exoskeletons (assistive and enhance) and lower limb prosthetics, there is a little work done so far considering the stability aspects of these devices. To the author's knowledge, this is the first study that has evaluated orthosis impact on walking stabilities and contractile dynamics of lower limbs using a passive device. Whereas, the active devices are bulkier and produce greater initial changes in the body's CoM. Considering these facts, there is a requirement to evaluate the impact of these devices on dynamic stabilities as shown in Figure 8.4.
4. On an inclined surface, stabilities are evaluated for  $\pm 5^\circ$  slopes, the other slope angles can illustrate the stability trends further.
5. The effectiveness of these methods for other dynamic walking activities (e.g. stairs up/down, turning, start and stop transitions, obstacles) are required to be evaluated with/without impairments.
6. These methods are applied in this study in an indoor lab environment. However, further advancement requires it to be applied in real life outdoor environments using portable GRF measurement systems e.g. Tekscan pressure insoles (F-Scan) [188] as shown in Figure 8.4.
7. In this study, resultant CoP and GRF are used to quantify transitional phases (loading and unloading), however, other signals such as joint angles or angular velocity, or moments can differentiate mid-stance, terminal stance, and swing phases stabilities as an earlier study used knee angle [34].
8. The use of resultant signals also has a benefit of applying these methods for evaluating the stability of any lower limb joints (ankle, knee, hip). A reduction in stability due to either joint can be measured using resultant signals. Therefore, the potential application of these biomechanical signals (CoP and GRF) for hip or knee joints' stability assessment require an investigation in future.
9. Lastly, these methods are required to be assessed in patients of different age groups. For example, most of the ankle-foot impairments start to show off an early age (1-15 years), similarly, many associated impairments start to appear elderly age (above the '50s). The early evaluation of gradually developing impairments (lower limb neuropathies) and clinical measurements can prevent or slow down the further growth of such diseases.

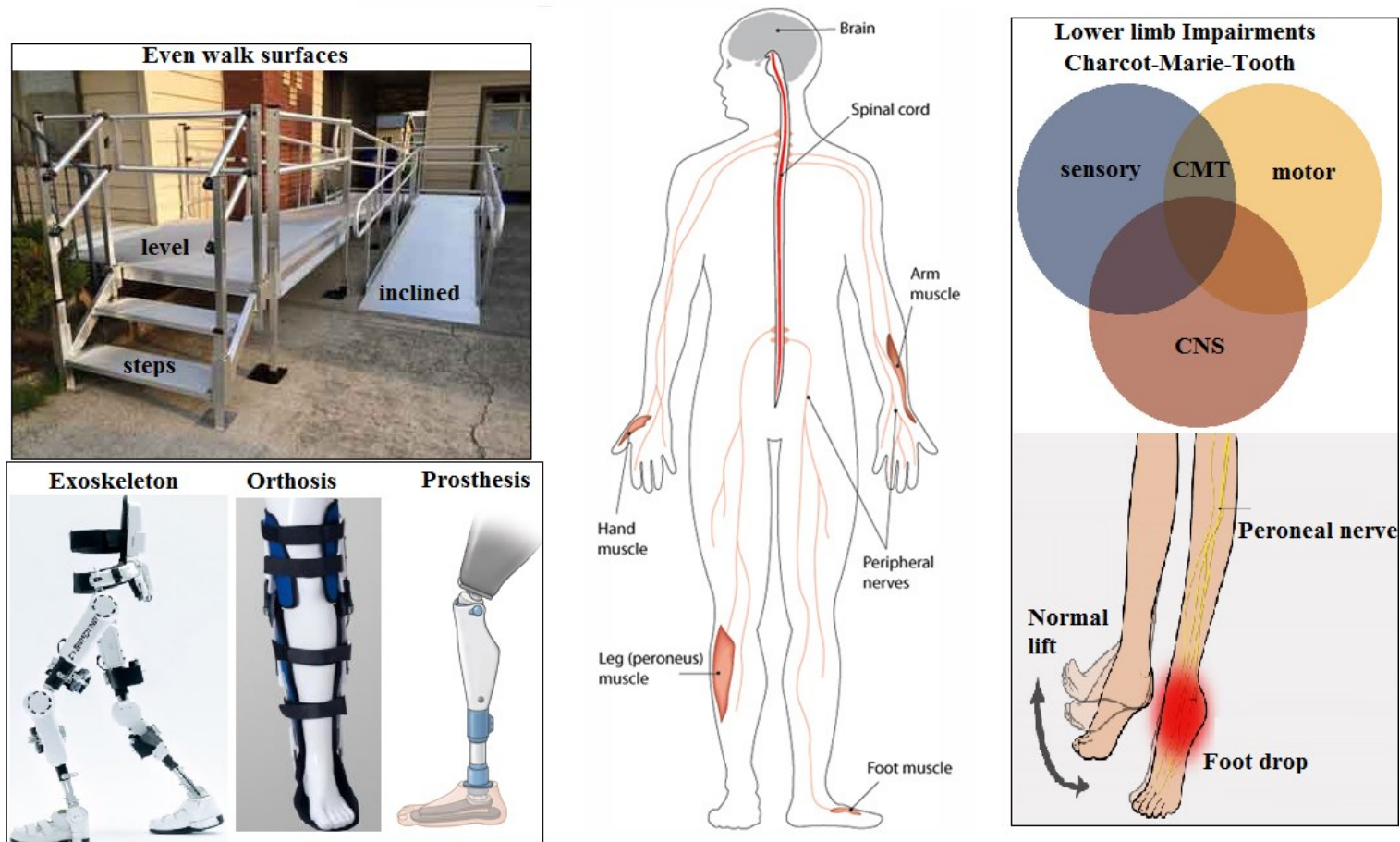


Figure 8.4: Applications of the current study for Neuromotor balance control evaluation during gait transitional phases. images adapted from [189-194]



## REFERENCES

- [1] U. R. a. Innovation. (2018). Available: <https://gtr.ukri.org/projects?ref=EP%2FM026388%2F1>
- [2] M. Rabuffetti, G. Bovi, P. L. Quadri, D. Cattaneo, F. Benvenuti, and M. Ferrarin, "An experimental paradigm to assess postural stabilization: no more movement and not yet posture," *IEEE Transactions on Neural Systems and Rehabilitation Engineering*, vol. 19, pp. 420-426, 2011.
- [3] CDC. (2018). Available: <https://www.cdc.gov/homeandrecreationalafety/falls/adultfalls.html>
- [4] F. P. Society. (2019).
- [5] M. M. Wu, G. Brown, and K. E. Gordon, "Control of locomotor stability in stabilizing and destabilizing environments," *Gait & Posture*, vol. 55, pp. 191-198, 2017/06/01/ 2017.
- [6] S. Mehdizadeh, "The largest Lyapunov exponent of gait in young and elderly individuals: A systematic review," *Gait & Posture*, vol. 60, pp. 241-250, 2018/02/01/ 2018.
- [7] A. Doğğan, M. Mengüllüoğğlu, and N. Özgirgin, "Evaluation of the effect of ankle-foot orthosis use on balance and mobility in hemiparetic stroke patients," *Disability and Rehabilitation*, vol. 33, pp. 1433-1439, 2011/01/01 2011.
- [8] S. F. Tyson and R. M. Kent, "Effects of an Ankle-Foot Orthosis on Balance and Walking After Stroke: A Systematic Review and Pooled Meta-Analysis," *Archives of Physical Medicine and Rehabilitation*, vol. 94, pp. 1377-1385, 2013/07/01/ 2013.
- [9] D. Cattaneo, M. Rabuffetti, G. Bovi, E. Mevio, J. Jonsdottir, and M. Ferrarin, "Assessment of postural stabilization in three task oriented movements in people with multiple sclerosis," *Disability and Rehabilitation*, vol. 36, pp. 2237-2243, 2014/12/01 2014.
- [10] S. Bruijn, O. Meijer, P. Beek, and J. Van Dieën, "Assessing the stability of human locomotion: a review of current measures," *Journal of the Royal Society Interface*, vol. 10, p. 20120999, 2013.
- [11] A. L. Simon, B. Ilharreborde, P. Souchet, and K. R. Kaufman, "Dynamic balance assessment during gait in spinal pathologies - a literature review," *Orthop Traumatol Surg Res*, vol. 101, pp. 235-46, Apr 2015.
- [12] A. L. Hof, "The 'extrapolated center of mass' concept suggests a simple control of balance in walking," *Human Movement Science*, vol. 27, pp. 112-125, 2008/02/01/ 2008.
- [13] M. F. Vieira, F. B. Rodrigues, G. S. de Sá e Souza, R. M. Magnani, G. C. Lehnen, N. G. Campos, *et al.*, "Gait stability, variability and complexity on inclined surfaces," *Journal of Biomechanics*, vol. 54, pp. 73-79, 2017/03/21/ 2017.
- [14] M. F. Vieira, F. B. Rodrigues, G. S. de Sá e Souza, R. M. Magnani, G. C. Lehnen, and A. O. Andrade, "Linear and Nonlinear Gait Features in Older Adults Walking on Inclined Surfaces at Different Speeds," *Annals of Biomedical Engineering*, vol. 45, pp. 1560-1571, June 01 2017.
- [15] L. Houx, M. Lempereur, O. Rémy-Néris, and S. Brochard, "Threshold of equinus which alters biomechanical gait parameters in children," *Gait & Posture*, vol. 38, pp. 582-589, 2013/09/01/ 2013.

- [16] Brace. (2018). Available: <http://www.richiebrace.com/index.php/treatment-guide.html>.
- [17] Prosthetics. (2018). Available: <https://www.llop.com/alternative-kafo-orthosis/>.
- [18] State. (2018). Available: <http://www.treasurestateoandp.com/orthotics/>.
- [19] Ultraflex. (2018). <https://orthoactive.com/product/6841-ultraflex-uss-adult-afo-joint/>.
- [20] C. Grech, C. Formosa, and A. Gatt, "Shock attenuation properties at heel strike: Implications for the clinical management of the cavus foot," *Journal of Orthopaedics*, vol. 13, pp. 148-151, 2016/09/01/ 2016.
- [21] K.-J. Chi and D. Schmitt, "Mechanical energy and effective foot mass during impact loading of walking and running," *Journal of Biomechanics*, vol. 38, pp. 1387-1395, 2005/07/01/ 2005.
- [22] J. M. Wakeling, A.-M. Liphardt, and B. M. Nigg, "Muscle activity reduces soft-tissue resonance at heel-strike during walking," *Journal of biomechanics*, vol. 36, pp. 1761-1769, 2003.
- [23] M. W. Creaby, K. May, and K. L. Bennell, "Insole effects on impact loading during walking," *Ergonomics*, vol. 54, pp. 665-671, 2011.
- [24] A. Jamali, E. Sadeghi-Demneh, N. Fereshtenajad, and S. Hillier, "Somatosensory impairment and its association with balance limitation in people with multiple sclerosis," *Gait & Posture*, vol. 57, pp. 224-229, 2017/09/01/ 2017.
- [25] A. A. Butler, S. R. Lord, M. W. Rogers, and R. C. Fitzpatrick, "Muscle weakness impairs the proprioceptive control of human standing," *Brain Research*, vol. 1242, pp. 244-251, 2008/11/25/ 2008.
- [26] F. Yang, G. A. King, L. Dillon, and X. Su, "Controlled whole-body vibration training reduces risk of falls among community-dwelling older adults," *Journal of biomechanics*, vol. 48, pp. 3206-3212, 2015.
- [27] D. A. Winter, "Human balance and posture control during standing and walking," *Gait & posture*, vol. 3, pp. 193-214, 1995.
- [28] V. Lugade, V. Lin, and L.-S. Chou, "Center of mass and base of support interaction during gait," *Gait & posture*, vol. 33, pp. 406-411, 2011.
- [29] S. M. Bruijn, A. Van Impe, J. Duysens, and S. P. Swinnen, "White matter microstructural organization and gait stability in older adults," *Frontiers in Aging Neuroscience*, vol. 6, 2014-June-10 2014.
- [30] C. Beyaert, R. Vasa, and G. E. Frykberg, "Gait post-stroke: Pathophysiology and rehabilitation strategies," *Neurophysiologie Clinique/Clinical Neurophysiology*, vol. 45, pp. 335-355, 2015/11/01/ 2015.
- [31] L. Bizovska, Z. Svoboda, P. Kutilek, M. Janura, A. Gaba, and Z. Kovacicova, "Variability of centre of pressure movement during gait in young and middle-aged women," *Gait & Posture*, vol. 40, pp. 399-402, 2014/07/01/ 2014.
- [32] C. Kirtley, "Chapter 9 - Gravity and centre of mass," in *Clinical Gait Analysis*, C. Kirtley, Ed., ed Edinburgh: Churchill Livingstone, 2006, pp. 157-173.
- [33] V. La Scaleia, Y. P. Ivanenko, K. E. Zelik, and F. Lacquaniti, "Spinal motor outputs during step-to-step transitions of diverse human gaits," *Frontiers in Human Neuroscience*, vol. 8, p. 305, 05/15 10/29/received 04/25/accepted 2014.
- [34] K. D. Morgan, Y. Zheng, H. Bush, and B. Noehren, "Nyquist and Bode stability criteria to assess changes in dynamic knee stability in healthy and

- anterior cruciate ligament reconstructed individuals during walking," *Journal of Biomechanics*, vol. 49, pp. 1686-1691, 2016/06/14/ 2016.
- [35] K. D. Morgan, C. J. Donnelly, and J. A. Reinbolt, "Empirical Based Modeling for the Assessment of Dynamic Knee Stability: Implications for Anterior Cruciate Ligament Injury Risk," in *2018 40th Annual International Conference of the IEEE Engineering in Medicine and Biology Society (EMBC)*, 2018, pp. 1676-1679.
- [36] M. M. Ardestani, C. ZhenXian, H. Noori, M. Moazen, and Z. Jin, "Computational Analysis of Knee Joint Stability Following Total Knee Arthroplasty," *Journal of Biomechanics*, 2019/01/25/ 2019.
- [37] P. Hur, B. A. Duiser, S. M. Salapaka, and E. T. Hsiao-Wecksler, "Measuring Robustness of the Postural Control System to a Mild Impulsive Perturbation," *IEEE Transactions on Neural Systems and Rehabilitation Engineering*, vol. 18, pp. 461-467, 2010.
- [38] D. Mandeville, L. R. Osternig, and L.-S. Chou, "The effect of total knee replacement surgery on gait stability," *Gait & Posture*, vol. 27, pp. 103-109, 2008/01/01/ 2008.
- [39] K. Koh, Y. S. Park, and J. K. Shim, "Analysis of the Dynamic Balance Recovery Ability by External Perturbation in the Elderly," *Korean Journal of Sport Biomechanics*, vol. 27, pp. 205-210, 2017.
- [40] S. Sivakumaran, A. Schinkel-Ivy, K. Masani, and A. Mansfield, "Relationship between margin of stability and deviations in spatiotemporal gait features in healthy young adults," *Human Movement Science*, vol. 57, pp. 366-373, 2018/02/01/ 2018.
- [41] D. F. Graham, C. P. Carty, D. G. Lloyd, and R. S. Barrett, "Muscle contributions to the acceleration of the whole body centre of mass during recovery from forward loss of balance by stepping in young and older adults," *PLOS ONE*, vol. 12, p. e0185564, 2017.
- [42] J. L. Allen and L. H. Ting, "Why Is Neuromechanical Modeling of Balance and Locomotion So Hard?," in *Neuromechanical Modeling of Posture and Locomotion*, B. I. Prilutsky and D. H. Edwards, Eds., ed New York, NY: Springer New York, 2016, pp. 197-223.
- [43] V. Lugade and K. Kaufman, "Center of pressure trajectory during gait: A comparison of four foot positions," *Gait & Posture*, vol. 40, pp. 719-722, 2014/09/01/ 2014.
- [44] S. Fuchioka, A. Iwata, Y. Higuchi, M. Miyake, S. Kanda, and T. Nishiyama, "The Forward Velocity of the Center of Pressure in the Midfoot is a Major Predictor of Gait Speed in Older Adults," *International Journal of Gerontology*, vol. 9, pp. 119-122, 2015/06/01/ 2015.
- [45] C. Kirtley, "Chapter 10 - Power," in *Clinical Gait Analysis*, C. Kirtley, Ed., ed Edinburgh: Churchill Livingstone, 2006, pp. 175-198.
- [46] S. Junfen, "Finite element analysis of total knee replacement considering gait cycle load and malalignment," Doctoral, University of Wolverhampton, University of Wolverhampton, 2007.
- [47] T. Stöckel, R. Jacksteit, M. Behrens, R. Skripitz, R. Bader, and A. Mau-Moeller, "The mental representation of the human gait in young and older adults," *Frontiers in Psychology*, vol. 6, 2015-July-14 2015.
- [48] C. Kirtley, "Introduction," in *Clinical Gait Analysis*, C. Kirtley, Ed., ed Edinburgh: Churchill Livingstone, 2006, pp. 5-14.

- [49] M. G. Benedetti, F. Catani, A. Leardini, E. Pignotti, and S. Giannini, "Data management in gait analysis for clinical applications," *Clinical Biomechanics*, vol. 13, pp. 204-215, 1998/04/01/ 1998.
- [50] R. Don, M. Serrao, P. Vinci, A. Ranavolo, A. Cacchio, F. Ioppolo, *et al.*, "Foot drop and plantar flexion failure determine different gait strategies in Charcot-Marie-Tooth patients," *Clinical Biomechanics*, vol. 22, pp. 905-916, 2007/10/01/ 2007.
- [51] D. A. Winter, *Biomechanics and motor control of human movement*: John Wiley & Sons, 2009.
- [52] J. Chern, C. Kao, P. Lai, C. Lung, and W. Chen, "Severity of spine malalignment on center of pressure progression during level walking in subjects with adolescent idiopathic scoliosis," in *2014 36th Annual International Conference of the IEEE Engineering in Medicine and Biology Society*, 2014, pp. 5888-5891.
- [53] E. M. J. Bekkers, K. Dockx, E. Heremans, S. Vercruyssen, S. M. P. Verschueren, A. Mirelman, *et al.*, "The contribution of proprioceptive information to postural control in elderly and patients with Parkinson's disease with a history of falls," *Frontiers in human neuroscience*, vol. 8, pp. 939-939, 2014.
- [54] "https://courses.cs.washington.edu/courses/cse490i/07wi/lectures/lect02.pdf," ed, 2017.
- [55] T. Kiemel, A. J. Elahi, and J. J. Jeka, "Identification of the Plant for Upright Stance in Humans: Multiple Movement Patterns From a Single Neural Strategy," *Journal of Neurophysiology*, vol. 100, pp. 3394-3406, 2008.
- [56] K. P. Blum, B. Lamotte D'Incamps, D. Zytnecki, and L. H. Ting, "Force encoding in muscle spindles during stretch of passive muscle," *PLOS Computational Biology*, vol. 13, p. e1005767, 2017.
- [57] S. K. Au, P. Dilworth, and H. Herr, "An ankle-foot emulation system for the study of human walking biomechanics," in *Proceedings 2006 IEEE International Conference on Robotics and Automation, 2006. ICRA 2006.*, 2006, pp. 2939-2945.
- [58] A. BONNEFOY, ARMAND, Stéphane., *Normal Gait. In: Orthopedic Management of Children With Cerebral Palsy: A Comprehensive Approach.*: Nova Science Publishers, Inc., 2015.
- [59] Y. Park, B. Chen, D. Young, L. Stirling, R. J. Wood, E. Goldfield, *et al.*, "Bio-inspired active soft orthotic device for ankle foot pathologies," in *2011 IEEE/RSJ International Conference on Intelligent Robots and Systems*, 2011, pp. 4488-4495.
- [60] NHS. (2018). Available: <https://www.nhs.uk/conditions>
- [61] Charcot-Marie-Tooth. (2019). Available: <http://cmt.org.uk/about-cmt/what-is-cmt/>
- [62] artilimb. (2018). Available: <http://www.artlimb.com/more-details/lower-limb-articles/prosthetic-alignment-part1-basics/>
- [63] Braceability. (2018). Available: <https://www.braceability.com/collections/ankle-braces>
- [64] Heliosbracing, 2018.
- [65] S. Ortho. (2018). Available: <https://www.sourceortho.net/rebound-air-walker-tall/>
- [66] Orthobmi. (2018). Available: <http://orthobmi.com/index.php/product/ankle-foot-orthosis/>

- [67] Ottobock. (2018). Available: <https://www.ottobock.co.uk/orthopaedic-rehabilitation/solution-overview/goon/>
- [68] Rehabmart. (2018). Available: <https://www.rehabmart.com/product/praf-fo-fo-kodel-44729.html>
- [69] Becker. (2018). Available: <https://www.beckerorthopedic.com/>
- [70] S. Hwang, J. Kim, J. Yi, K. Tae, K. Ryu, and Y. Kim, "Development of an active ankle foot orthosis for the prevention of foot drop and toe drag," in *2006 International Conference on Biomedical and Pharmaceutical Engineering*, 2006, pp. 418-423.
- [71] S. Tanida, T. Kikuchi, T. Takehashi, K. Otsuki, T. Ozawa, T. Fujikawa, *et al.*, "Intelligently controllable Ankle Foot Orthosis (I-AFO) and its application for a patient of Guillain-Barre syndrome," in *2009 IEEE International Conference on Rehabilitation Robotics*, 2009, pp. 857-862.
- [72] K. A. Shorter, Y. Li, E. A. Morris, G. F. Kogler, and E. T. Hsiao-Wecksler, "Experimental evaluation of a portable powered ankle-foot orthosis," in *2011 Annual International Conference of the IEEE Engineering in Medicine and Biology Society*, 2011, pp. 624-627.
- [73] K. E. Gordon, G. S. Sawicki, and D. P. Ferris, "Mechanical performance of artificial pneumatic muscles to power an ankle-foot orthosis," *Journal of Biomechanics*, vol. 39, pp. 1832-1841, 2006/01/01/ 2006.
- [74] L. Deberg, M. Taheri Andani, M. Hosseinipour, and M. Elahinia, "An SMA Passive Ankle Foot Orthosis: Design, Modeling, and Experimental Evaluation," *Smart Materials Research*, vol. 2014, p. 11, 2014.
- [75] H. Nancy, W. Wendi, and L. Kathryn, *Kinesiology : scientific basis of human motion*: The McGraw-Hill Companies, Inc. .
- [76] M. H. van der Linden, S. C. van der Linden, H. T. Hendricks, B. G. M. van Engelen, and A. C. H. Geurts, "Postural instability in Charcot-Marie-Tooth type 1A patients is strongly associated with reduced somatosensation," *Gait & Posture*, vol. 31, pp. 483-488, 2010/04/01/ 2010.
- [77] H.-M. Chai. Stance and Stability [Online]. Available: [http://www.cq.com.pl/publikacje/cqstabosc\\_art4.pdf](http://www.cq.com.pl/publikacje/cqstabosc_art4.pdf)
- [78] P. contributors. (2018). *Berg Balance Scale*. Available: [https://www.physio-pedia.com/index.php?title=Berg\\_Balance\\_Scale&oldid=185349](https://www.physio-pedia.com/index.php?title=Berg_Balance_Scale&oldid=185349)
- [79] A. Sabet, G. Taghizadeh, and T. Mohammadi-Nezhad, "Clinical assessment of Persian translation of Fullerton Advanced Balance Scale in community-dwelling older adults AU - Azad, Akram," *Disability and Rehabilitation*, pp. 1-7, 2019.
- [80] I. M. Schut, D. Engelhart, J. H. Pasma, R. G. K. M. Aarts, and A. C. Schouten, "Compliant support surfaces affect sensory reweighting during balance control," *Gait & Posture*, vol. 53, pp. 241-247, 2017/03/01/ 2017.
- [81] A. Maslivec, T. M. Bampouras, S. Dewhurst, G. Vannozzi, A. Macaluso, and L. Laudani, "Mechanisms of head stability during gait initiation in young and older women: A neuro-mechanical analysis," *Journal of Electromyography and Kinesiology*, vol. 38, pp. 103-110, 2018/02/01/ 2018.
- [82] T. Krasovsky, A. Lamontagne, A. G. Feldman, and M. F. Levin, "Effects of walking speed on gait stability and interlimb coordination in younger and older adults," *Gait & Posture*, vol. 39, pp. 378-385, 2014/01/01/ 2014.
- [83] T. Lencioni, M. Rabuffetti, G. Piscoquito, D. Pareyson, A. Aiello, E. Di Sipio, *et al.*, "Postural stabilization and balance assessment in Charcot-Marie-Tooth 1A subjects," *Gait & Posture*, vol. 40, pp. 481-486, 2014/09/01/ 2014.

- [84] T. K. Koo and M. Y. Li, "A Guideline of Selecting and Reporting Intraclass Correlation Coefficients for Reliability Research," *Journal of Chiropractic Medicine*, vol. 15, pp. 155-163, 2016/06/01/ 2016.
- [85] H. G. Kang and J. B. Dingwell, "Dynamics and stability of muscle activations during walking in healthy young and older adults," *Journal of Biomechanics*, vol. 42, pp. 2231-2237, 2009/10/16/ 2009.
- [86] J. B. Dingwell and L. C. Marin, "Kinematic variability and local dynamic stability of upper body motions when walking at different speeds," *Journal of Biomechanics*, vol. 39, pp. 444-452, 2006/01/01/ 2006.
- [87] J. B. Dingwell, J. P. Cusumano, P. R. Cavanagh, and D. Sternad, "Local Dynamic Stability Versus Kinematic Variability of Continuous Overground and Treadmill Walking," *Journal of Biomechanical Engineering*, vol. 123, pp. 27-32, 2000.
- [88] R. Neptune and A. Vistamehr, "Dynamic Balance during Human Movement: Measurement and Control Mechanisms," *Journal of Biomechanical Engineering*, 2018.
- [89] Y.-C. Pai and J. Patton, "Center of mass velocity-position predictions for balance control," *Journal of Biomechanics*, vol. 30, pp. 347-354, 1997/04/01/ 1997.
- [90] A. L. Hof, M. G. J. Gazendam, and W. E. Sinke, "The condition for dynamic stability," *Journal of Biomechanics*, vol. 38, pp. 1-8, 2005/01/01/ 2005.
- [91] C. McCrum, K. Eysel-Gosepath, G. Epro, K. Meijer, H. H. C. M. Savelberg, G.-P. Brüggemann, *et al.*, "Deficient recovery response and adaptive feedback potential in dynamic gait stability in unilateral peripheral vestibular disorder patients," *Physiological reports*, vol. 2, p. e12222, 2014.
- [92] J. M. Hidler, R. L. Harvey, and W. Z. Rymer, "Frequency Response Characteristics of Ankle Plantar Flexors in Humans Following Spinal Cord Injury: Relation to Degree of Spasticity," *Annals of Biomedical Engineering*, vol. 30, pp. 969-981, July 01 2002.
- [93] J. E. Smeathers, "Transient Vibrations Caused by Heel Strike," *Proceedings of the Institution of Mechanical Engineers, Part H: Journal of Engineering in Medicine*, vol. 203, pp. 181-186, 1989.
- [94] K. D. Morgan, C. J. Donnelly, and J. A. Reinbolt, "Empirical based modeling approach for the quantification of dynamic knee stability," presented at the Proceedings of 41st Annual Meeting of the American Society of Biomechanics, Boulder, CO, USA, 2017.
- [95] I. Mahmood, U. Martinez-Hernandez, and A. A. Dehghani-Sani, "Rate-Dependant Gait Dynamic Stability Analysis for Motor Control Estimation," in *Advances in Cooperative Robotics*, ed: WORLD SCIENTIFIC, 2016, pp. 454-463.
- [96] I. Mahmood, U. Martinez-Hernandez, and A. A. Dehghani-Sani, "Gait dynamic stability analysis and motor control prediction for varying terrain conditions," in *Mechatronics (MECATRONICS)/17th International Conference on Research and Education in Mechatronics (REM), 2016 11th France-Japan & 9th Europe-Asia Congress on*, 2016, pp. 290-295.
- [97] I. Mahmood, U. Martinez-Hernandez, and A. A. Dehghani-Sani, "Towards Behavioral Based Sensorimotor Controller Design for Wearable Soft Exoskeletal Applications," in *Converging Clinical and Engineering Research on Neurorehabilitation II: Proceedings of the 3rd International Conference on NeuroRehabilitation (ICNR2016), October 18-21, 2016, Segovia, Spain*, J. Ibáñez, J. González-Vargas, J. M. Azorín, M. Akay, and J.

- L. Pons, Eds., ed Cham: Springer International Publishing, 2017, pp. 1281-1286.
- [98] N. T. Pickle, J. M. Wilken, N. P. Fey, and A. K. Silverman, "A comparison of stability metrics based on inverted pendulum models for assessment of ramp walking," *PLOS ONE*, vol. 13, p. e0206875, 2018.
- [99] B. M. Nigg, "The role of impact forces and foot pronation: a new paradigm," *Clin J Sport Med*, vol. 11, pp. 2-9, Jan 2001.
- [100] F. G. Benjamin C. Kuo, *Automatic Control Systems*, 9 ed.: Prentice Hall PTR, 2003.
- [101] N. S. Nise, *Control Systems Engineering*: John Wiley & Sons, Inc., 2000.
- [102] H. Hong, S. Kim, C. Kim, S. Lee, and S. Park, "Spring-like gait mechanics observed during walking in both young and older adults," *Journal of biomechanics*, vol. 46, pp. 77-82, 2013.
- [103] S. Kim and S. Park, "Leg stiffness increases with speed to modulate gait frequency and propulsion energy," *Journal of Biomechanics*, vol. 44, pp. 1253-1258, 2011/04/29/ 2011.
- [104] H. Enders, V. von Tscherner, and B. M. Nigg, "Analysis of damped tissue vibrations in time-frequency space: A wavelet-based approach," *Journal of Biomechanics*, vol. 45, pp. 2855-2859, 2012/11/15/ 2012.
- [105] A. Khassestarash, R. Hassannejad, H. Enders, and M. M. Etefagh, "Damping and energy dissipation in soft tissue vibrations during running," *Journal of Biomechanics*, vol. 48, pp. 204-209, 2015/01/21/ 2015.
- [106] A. A. Zadpoor and A. A. Nikooyan, "Modeling muscle activity to study the effects of footwear on the impact forces and vibrations of the human body during running," *Journal of Biomechanics*, vol. 43, pp. 186-193, 2010/01/19/ 2010.
- [107] S. Öunpuu, E. Garibay, M. Solomito, K. Bell, K. Pierz, J. Thomson, *et al.*, "A comprehensive evaluation of the variation in ankle function during gait in children and youth with Charcot–Marie–Tooth disease," *Gait & Posture*, vol. 38, pp. 900-906, 2013/09/01/ 2013.
- [108] P. Vinci and S. L. Perelli, "Footdrop, foot rotation, and plantarflexor failure in Charcot-Marie-Tooth disease," *Archives of Physical Medicine and Rehabilitation*, vol. 83, pp. 513-516, 2002/04/01/ 2002.
- [109] V. Lugade and K. Kaufman, "Dynamic stability margin using a marker based system and Tekscan: A comparison of four gait conditions," *Gait & Posture*, vol. 40, pp. 252-254, 2014/05/01/ 2014.
- [110] M. Rabiei, M. Eslami, and A. F. Movaghar, "The assessment of three-dimensional foot pronation using a principal component analysis method in the stance phase of running," *The Foot*, vol. 29, pp. 11-17, 2016/12/01/ 2016.
- [111] P. H. Tzu-wei, K. A. Shorter, P. G. Adamczyk, and A. D. Kuo, "Mechanical and energetic consequences of reduced ankle plantarflexion in human walking," *Journal of Experimental Biology*, p. jeb. 113910, 2015.
- [112] H. Choi, K. M. Peters, M. B. MacConnell, K. K. Ly, E. S. Eckert, and K. M. Steele, "Impact of ankle foot orthosis stiffness on Achilles tendon and gastrocnemius function during unimpaired gait," *Journal of biomechanics*, vol. 64, pp. 145-152, 2017.
- [113] D. P. Soares, M. P. de Castro, E. Mendes, and L. Machado, "Influence of wedges on lower limbs' kinematics and net joint moments during healthy elderly gait using principal component analysis," *Human Movement Science*, vol. 38, pp. 319-330, 2014/12/01/ 2014.

- [114] B. J. Addison and D. E. Lieberman, "Tradeoffs between impact loading rate, vertical impulse and effective mass for walkers and heel strike runners wearing footwear of varying stiffness," *Journal of Biomechanics*, vol. 48, pp. 1318-1324, 2015/05/01/ 2015.
- [115] J. Romkes and K. Schweizer, "Immediate effects of unilateral restricted ankle motion on gait kinematics in healthy subjects," *Gait & Posture*, vol. 41, pp. 835-840, 2015/03/01/ 2015.
- [116] S. Perry and M. Lafortune, "Influences of inversion/eversion of the foot upon impact loading during locomotion," *Clinical Biomechanics*, vol. 10, pp. 253-257, 1995.
- [117] H. Kondo, "Changes in the Ground Reaction Force, Lower-Limb Muscle Activity, and Joint Angles in Athletes with Unilateral Ankle Dorsiflexion Restriction During A Rebound-Jump Task," *Journal of Functional Morphology and Kinesiology*, vol. 3, p. 52, 2018.
- [118] J. Pauser, A. Jendrissek, M. Brem, K. Gelse, B. Swoboda, and H.-D. Carl, "Foot loading with an ankle-foot orthosis: the accuracy of an integrated physical strain trainer," *International Orthopaedics*, vol. 36, pp. 1411-1415, July 01 2012.
- [119] M. Deharde and Y. Vinshtok, "Ambulating ankle and knee joints with bidirectional dampening and assistance using elastomeric restraint," 2012.
- [120] H. H. C. M. Savelberg, N. C. Schaper, P. J. B. Willems, T. L. H. de Lange, and K. Meijer, "Redistribution of joint moments is associated with changed plantar pressure in diabetic polyneuropathy," *BMC musculoskeletal disorders*, vol. 10, pp. 16-16, 2009.
- [121] S. Stucke, D. McFarland, L. Goss, S. Fonov, G. R. McMillan, A. Tucker, *et al.*, "Spatial relationships between shearing stresses and pressure on the plantar skin surface during gait," *Journal of Biomechanics*, vol. 45, pp. 619-622, 2012/02/02/ 2012.
- [122] <https://www.oastaug.com/ankle-sprains-high-vs-low/>. (2018).
- [123] C-motion. (2018). [http://c-motion.com/v3dwiki/index.php?title=Tutorial:\\_Force\\_Platforms](http://c-motion.com/v3dwiki/index.php?title=Tutorial:_Force_Platforms).
- [124] C-Motion, "[http://www.c-motion.com/v3dwiki/index.php?title=YouTube\\_Tutorial:\\_Model\\_Building](http://www.c-motion.com/v3dwiki/index.php?title=YouTube_Tutorial:_Model_Building)," 2018.
- [125] C. A. Rábago, J. Aldridge Whitehead, and J. M. Wilken, "Evaluation of a Powered Ankle-Foot Prosthesis during Slope Ascent Gait," *PLOS ONE*, vol. 11, p. e0166815, 2016.
- [126] K. L. Loverro, A. Khuu, P.-C. Kao, and C. L. Lewis, "Kinematic variability and local dynamic stability of gait in individuals with hip pain and a history of developmental dysplasia," *Gait & Posture*, 2019/01/07/ 2019.
- [127] E. Wojciechowski, A. Sman, K. Cornett, J. Raymond, K. Refshauge, M. P. Menezes, *et al.*, "Gait patterns of children and adolescents with Charcot-Marie-Tooth disease," *Gait & Posture*, vol. 56, pp. 89-94, 2017/07/01/ 2017.
- [128] C. J. Newman, M. Walsh, R. O'Sullivan, A. Jenkinson, D. Bennett, B. Lynch, *et al.*, "The characteristics of gait in Charcot-Marie-Tooth disease types I and II," *Gait & Posture*, vol. 26, pp. 120-127, 2007/06/01/ 2007.
- [129] Z. Svoboda, L. Bizovska, M. Janura, E. Kubonova, K. Janurova, and N. Vuillerme, "Variability of spatial temporal gait parameters and center of pressure displacements during gait in elderly fallers and nonfallers: A 6-month prospective study," *PLOS ONE*, vol. 12, p. e0171997, 2017.



- [130] S. R. Anderson, J. Porrill, S. Sklavos, N. J. Gandhi, D. L. Sparks, and P. Dean, "Dynamics of Primate Oculomotor Plant Revealed by Effects of Abducens Microstimulation," *Journal of Neurophysiology*, vol. 101, pp. 2907-2923, 03/18 09/17/received 03/12/accepted 2009.
- [131] S. Sklavos, J. Porrill, C. R. S. Kaneko, and P. Dean, "Evidence for wide range of time scales in oculomotor plant dynamics: Implications for models of eye-movement control," *Vision Research*, vol. 45, pp. 1525-1542, 2005/06/01/ 2005.
- [132] M. H. Tan and J. K. Hammond, "A non-parametric approach for linear system identification using principal component analysis," *Mechanical Systems and Signal Processing*, vol. 21, pp. 1576-1600, 2007/05/01/ 2007.
- [133] D. P. Soares, M. P. de Castro, E. A. Mendes, and L. Machado, "Principal component analysis in ground reaction forces and center of pressure gait waveforms of people with transfemoral amputation," *Prosthetics and Orthotics International*, vol. 40, pp. 729-738, 2016.
- [134] H. Yli-Ollila, M. P. Tarvainen, T. P. Laitinen, and T. M. Laitinen, "Principal Component Analysis of the Longitudinal Carotid Wall Motion in Association with Vascular Stiffness: A Pilot Study," *Ultrasound in Medicine & Biology*, vol. 42, pp. 2873-2886, 2016/12/01/ 2016.
- [135] T. P. Downes, D. Welch, K. S. Scott, J. Austermann, G. W. Wilson, and M. S. Yun, "Calculating the transfer function of noise removal by principal component analysis and application to AzTEC deep-field observations," *Monthly Notices of the Royal Astronomical Society*, vol. 423, pp. 529-542, 2012.
- [136] S. Xu, P. Wang, and Y. Dong, "Measuring Electrolyte Impedance and Noise Simultaneously by Triangular Waveform Voltage and Principal Component Analysis," *Sensors*, vol. 16, p. 576, 2016.
- [137] R. Patel, S. Sengottuvel, M. P. Janawadkar, K. Gireesan, T. S. Radhakrishnan, and N. Mariyappa, "Ocular artifact suppression from EEG using ensemble empirical mode decomposition with principal component analysis," *Computers & Electrical Engineering*, vol. 54, pp. 78-86, 2016/08/01/ 2016.
- [138] K. Lankinen, E. Smeds, P. Tikka, E. Pihko, R. Hari, and M. Koskinen, "Haptic contents of a movie dynamically engage the spectator's sensorimotor cortex," *Human brain mapping*, vol. 37, pp. 4061-4068, 2016.
- [139] S. M. Robbins, J. L. Astephen Wilson, D. J. Rutherford, and C. L. Hubley-Kozey, "Reliability of principal components and discrete parameters of knee angle and moment gait waveforms in individuals with moderate knee osteoarthritis," *Gait & Posture*, vol. 38, pp. 421-427, 2013/07/01/ 2013.
- [140] K. P. Clark, L. J. Ryan, and P. G. Weyand, "A general relationship links gait mechanics and running ground reaction forces," *The Journal of Experimental Biology*, vol. 220, pp. 247-258, 2017.
- [141] A. Elhasairi and A. Pechev, "Humanoid robot balance control using the spherical inverted pendulum mode," *Frontiers in Robotics and AI*, vol. 2, p. 21, 2015.
- [142] A. Simpkins, "System Identification: Theory for the User, 2nd Edition (Ljung, L.; 1999) [On the Shelf]," *IEEE Robotics & Automation Magazine*, vol. 19, pp. 95-96, 2012.
- [143] I. liung. (2018). <https://www.youtube.com/watch?v=cst4DkDdacc&t=1892s>.
- [144] D. E. Seborg, D. A. Mellichamp, T. F. Edgar, and F. J. Doyle III, *Process dynamics and control*: John Wiley & Sons, 2010.

- [145] Y. B. Toosi, "A Note on the Gain and Phase Margin Concepts," *Journal of Control and Systems Engineering*, vol. 3, pp. 51-59, 2015.
- [146] Y. Bavafa-Toosi, "6 - Nyquist plot," in *Introduction to Linear Control Systems*, Y. Bavafa-Toosi, Ed., ed: Academic Press, 2017, pp. 471-575.
- [147] E. M. Ficanha, M. Rastgaar, and K. R. Kaufman, "A two-axis cable-driven ankle-foot mechanism," *Robotics and Biomimetics*, vol. 1, p. 17, November 02 2014.
- [148] N. Karavas, A. Ajoudani, N. Tsagarakis, J. Saglia, A. Bicchi, and D. Caldwell, "Tele-impedance based assistive control for a compliant knee exoskeleton," *Robotics and Autonomous Systems*, vol. 73, pp. 78-90, 2015/11/01/ 2015.
- [149] S. M. M. Rahman and R. Ikeura, "A Novel Variable Impedance Compact Compliant Ankle Robot for Overground Gait Rehabilitation and Assistance," *Procedia Engineering*, vol. 41, pp. 522-531, 2012/01/01/ 2012.
- [150] Y. Itoh, K. Akataki, K. Mita, M. Watakabe, and H. Nonaka, "Frequency response model of skeletal muscle and its association with contractile properties of skeletal muscle," *Journal of Electromyography and Kinesiology*, vol. 23, pp. 572-579, 2013/06/01/ 2013.
- [151] C. Orizio, R. V. Baratta, B. He Zhou, M. Solomonow, and A. Veicsteinas, "Force and surface mechanomyogram frequency responses in cat gastrocnemius," *Journal of Biomechanics*, vol. 33, pp. 427-433, 2000/04/01/ 2000.
- [152] C. Orizio, M. Solomonow, B. Diemont, and M. Gobbo, "Muscle-joint unit transfer function derived from torque and surface mechanomyogram in humans using different stimulation protocols," *Journal of Neuroscience Methods*, vol. 173, pp. 59-66, 2008/08/15/ 2008.
- [153] M. AlShabi, W. Araydah, H. ElShatarat, M. Othman, M. B. Younis, and S. A. Gadsden, "Effect of Mechanical Vibrations on Human Body," *World Journal of Mechanics*, vol. Vol.06No.09, p. 32, 2016.
- [154] [http://dev.mri.cnrs.fr/projects/imagej-macros/wiki/Velocity\\_Measurement\\_Tool](http://dev.mri.cnrs.fr/projects/imagej-macros/wiki/Velocity_Measurement_Tool), 2018.
- [155] A. K. Buldt, S. Forghany, K. B. Landorf, G. S. Murley, P. Levinger, and H. B. Menz, "Centre of pressure characteristics in normal, planus and cavus feet," *Journal of Foot and Ankle Research*, vol. 11, p. 3, February 05 2018.
- [156] Z. Mei, G. Zhao, K. Ivanov, Y. Guo, Q. Zhu, Y. Zhou, *et al.*, "Sample entropy characteristics of movement for four foot types based on plantar centre of pressure during stance phase," *BioMedical Engineering OnLine*, vol. 12, p. 101, 2013.
- [157] A. J. Strang, A. DiDomenico, W. P. Berg, and R. W. McGorry, "Assessment of differenced center of pressure time series improves detection of age-related changes in postural coordination," *Gait & Posture*, vol. 38, pp. 345-348, 2013/06/01/ 2013.
- [158] R. Cuisinier, I. Olivier, M. Vaugoyeau, V. Nougier, and C. Assaiante, "Reweightings of Sensory Inputs to Control Quiet Standing in Children from 7 to 11 and in Adults," *PLOS ONE*, vol. 6, p. e19697, 2011.
- [159] E. Carbonneau, R. Fontaine, and C. Smeesters, "A practical approach to determine appropriate cutoff frequencies for motion analysis data," in *37th Annual Meeting of the American Society of Biomechanics*, 2013.
- [160] J. J. B. Allen, "<http://apsychoserver.psych.arizona.edu/JJBAREprints/PSYC501A/pdfs2004/PCAEXPL.pdf>," 2002.

- [161] J. J. B. Allen, "<https://jallen.faculty.arizona.edu/content/psy696b-lectures-handouts-and-podcasts>," ed, 2018.
- [162] E. A. F. Ihlen, "Age-related changes in inter-joint coordination during walking," *Journal of Applied Physiology*, vol. 117, pp. 189-198, 2014.
- [163] A. Hernández, A. Silder, B. C. Heiderscheit, and D. G. Thelen, "Effect of age on center of mass motion during human walking," *Gait & Posture*, vol. 30, pp. 217-222, 2009/08/01/ 2009.
- [164] E. A. F. Ihlen, T. Goihl, P. B. Wik, O. Sletvold, J. Helbostad, and B. Vereijken, "Phase-dependent changes in local dynamic stability of human gait," *Journal of Biomechanics*, vol. 45, pp. 2208-2214, 2012/08/31/ 2012.
- [165] T. E. D. Robroy L. Martin, Stephen Paulseth , Dane K. Wukich, Joseph J. Godges, "Ankle Stability and Movement Coordination Impairments: Ankle Ligament Sprains," *Journal of Orthopaedic & Sports Physical Therapy*, vol. 43, pp. A1-A40, 2013.
- [166] R. Gigi, A. Haim, E. Luger, G. Segal, E. Melamed, Y. Beer, *et al.*, "Deviations in gait metrics in patients with chronic ankle instability: a case control study," *Journal of Foot and Ankle Research*, vol. 8, p. 1, 01/21 06/15/received 12/15/accepted 2015.
- [167] S. M. Bruijn, J. H. van Dieën, O. G. Meijer, and P. J. Beek, "Is slow walking more stable?," *Journal of Biomechanics*, vol. 42, pp. 1506-1512, 2009/07/22/ 2009.
- [168] Y. Fan, Z. Li, S. Han, C. Lv, and B. Zhang, "The influence of gait speed on the stability of walking among the elderly," *Gait & Posture*, vol. 47, pp. 31-36, 2016/06/01/ 2016.
- [169] J. J. Kavanagh, "Lower trunk motion and speed-dependence during walking," *Journal of NeuroEngineering and Rehabilitation*, vol. 6, p. 9, April 09 2009.
- [170] H.-L. Lu, M.-Y. Kuo, C.-F. Chang, T.-W. Lu, and S.-W. Hong, "Effects of gait speed on the body's center of mass motion relative to the center of pressure during over-ground walking," *Human Movement Science*, vol. 54, pp. 354-362, 2017/08/01/ 2017.
- [171] H.-L. Lu, T.-W. Lu, H.-C. Lin, H.-J. Hsieh, and W. P. Chan, "Effects of belt speed on the body's center of mass motion relative to the center of pressure during treadmill walking," *Gait & Posture*, vol. 51, pp. 109-115, 2017/01/01/ 2017.
- [172] R. R. Neptune, K. Sasaki, and S. A. Kautz, "The effect of walking speed on muscle function and mechanical energetics," *Gait & posture*, vol. 28, pp. 135-143, 12/26 2008.
- [173] J. Stenum, S. M. Bruijn, and B. R. Jensen, "The effect of walking speed on local dynamic stability is sensitive to calculation methods," *Journal of Biomechanics*, vol. 47, pp. 3776-3779, 2014/11/28/ 2014.
- [174] A. L. Hof and J. Duysens, "Responses of human ankle muscles to mediolateral balance perturbations during walking," *Human Movement Science*, vol. 57, pp. 69-82, 2018/02/01/ 2018.
- [175] J. L. Cook, S.-J. Blakemore, and C. Press, "Atypical basic movement kinematics in autism spectrum conditions," *Brain : a journal of neurology*, vol. 136, pp. 2816-2824, 2013.
- [176] Á. M. d. S. Soares, L. C. S. Góes, and L. C. G. d. Souza, "Modeling and control of multibody system with flexible appendages," *Journal of the Brazilian Society of Mechanical Sciences*, vol. 21, pp. 463-476, 1999.

- [177] G. L. C. M. d. e. a. ABREU, "System identification and active vibration control of a flexible structure.," *Journal of the Brazilian Society of Mechanical Sciences and Engineering*, vol. 34, pp. 386-392, 2012.
- [178] Q. H. Ly, A. Alaoui, S. Erlicher, and L. Baly, "Towards a footwear design tool: Influence of shoe midsole properties and ground stiffness on the impact force during running," *Journal of Biomechanics*, vol. 43, pp. 310-317, 2010/01/19/ 2010.
- [179] K. Gruber, H. Ruder, J. Denoth, and K. Schneider, "A comparative study of impact dynamics: wobbling mass model versus rigid body models," *Journal of Biomechanics*, vol. 31, pp. 439-444, 1998/05/01/ 1998.
- [180] J. M. Wakeling and B. M. Nigg, "Modification of soft tissue vibrations in the leg by muscular activity," *Journal of Applied Physiology*, vol. 90, pp. 412-420, 2001.
- [181] M. Lee, S. Kim, and S. Park, "Resonance-based oscillations could describe human gait mechanics under various loading conditions," *Journal of Biomechanics*, vol. 47, pp. 319-322, 2014/01/03/ 2014.
- [182] B. M. Nigg and W. Liu, "The effect of muscle stiffness and damping on simulated impact force peaks during running," *Journal of Biomechanics*, vol. 32, pp. 849-856, 1999/08/01/ 1999.
- [183] M. Ferrarin, G. Bovi, M. Rabuffetti, P. Mazzoleni, A. Montesano, E. Pagliano, *et al.*, "Gait pattern classification in children with Charcot–Marie–Tooth disease type 1A," *Gait & Posture*, vol. 35, pp. 131-137, 2012/01/01/ 2012.
- [184] H. Bao, "Multiple solutions to impulsive differential equations," *Advances in Difference Equations*, vol. 2017, p. 20, January 18 2017.
- [185] J.-P. Kulmala, M. T. Korhonen, S. Kuitunen, H. Suominen, A. Heinonen, A. Mikkola, *et al.*, "Which muscles compromise human locomotor performance with age?," *Journal of The Royal Society Interface*, vol. 11, p. 20140858, 2014.
- [186] M. S. Redfern and J. DiPasquale, "Biomechanics of descending ramps," *Gait & Posture*, vol. 6, pp. 119-125, 1997/10/01/ 1997.
- [187] S. Rakheja, R. G. Dong, S. Patra, P. É. Boileau, P. Marcotte, and C. Warren, "Biodynamics of the human body under whole-body vibration: Synthesis of the reported data," *International Journal of Industrial Ergonomics*, vol. 40, pp. 710-732, 2010/11/01/ 2010.
- [188] Tekscan. (2019). Available: <https://www.tekscan.com/products-solutions/systems/f-scan-system>
- [189] T. T. M. Appliance. (2018). Available: <https://www.made-in-china.com/productdirectory.do?word=Knee+Ankle+Foot+Orthosis+Kafo+Brace+Orthoses&subaction=hunt&style=b&mode=and&code=0&comProvince=nolimit&order=0&isOpenCorrection=1>
- [190] M. D. association. (2018). Available: <https://www.mda.org/disease/charcot-marie-tooth>
- [191] Bodyorganic. (2018). Available: <https://www.bodyorganics.com.au/pilates-strategies-foot-drop/>
- [192] K. Orthopedics. (2018). Available: <https://www.kenneyorthopedics.com/about/news/view/416/moving-from-a-temporary-to-a-definitive-prosthesis>
- [193] A. Prakash. (2018). Available: <https://www.roboticsbusinessreview.com/robo-dev/china-and-japan-lead-asian-exoskeleton-development/>

- [194] A. T. Quadros Santos Monteiro Fonseca and E. Zanoteli, "Charcot-Marie-Tooth disease," *Revista Médica Clínica Las Condes*, vol. 29, pp. 521-529, 2018/09/01/ 2018.
- [195] A. DiDomenico, R. W. McGorry, and J. J. Banks, "Methodological considerations of existing techniques for determining stabilization times following a multi-planar transition," *Gait & Posture*, vol. 38, pp. 541-543, 2013/07/01/ 2013.
- [196] C.-J. Chen and L.-S. Chou, "Center of mass position relative to the ankle during walking: A clinically feasible detection method for gait imbalance," *Gait & Posture*, vol. 31, pp. 391-393, 2010/03/01/ 2010.
- [197] D. Martelli, V. Vashista, S. Micera, and S. K. Agrawal, "Direction-Dependent Adaptation of Dynamic Gait Stability Following Waist-Pull Perturbations," *IEEE Transactions on Neural Systems and Rehabilitation Engineering*, vol. 24, pp. 1304-1313, 2016.
- [198] L. Hak, H. Houdijk, P. van der Wurff, M. R. Prins, A. Mert, P. J. Beek, *et al.*, "Stepping strategies used by post-stroke individuals to maintain margins of stability during walking," *Clinical Biomechanics*, vol. 28, pp. 1041-1048, 2013/11/01/ 2013.
- [199] I. Mahmood, U. Martinez Hernandez, and A. A. Dehghani-Sanij, "Gait Dynamic Stability Analysis for simulated Ankle-foot impairments and Bipedal robotics applications," presented at the 6th Mechatronics Forum International Conference, 2018.
- [200] P. C. Fino, "A preliminary study of longitudinal differences in local dynamic stability between recently concussed and healthy athletes during single and dual-task gait," *Journal of Biomechanics*, vol. 49, pp. 1983-1988, 2016/06/14/ 2016.
- [201] T. A. Worden, S. M. Beaudette, S. H. M. Brown, and L. A. Vallis, "Estimating Gait Stability: Asymmetrical Loading Effects Measured Using Margin of Stability and Local Dynamic Stability," *Journal of Motor Behavior*, vol. 48, pp. 455-467, 2016/09/02 2016.
- [202] H. G. Kang and J. B. Dingwell, "Dynamic stability of superior vs. inferior segments during walking in young and older adults," *Gait & Posture*, vol. 30, pp. 260-263, 2009/08/01/ 2009.
- [203] S. V. Yalla, R. T. Crews, A. E. Fleischer, G. Grewal, J. Ortiz, and B. Najafi, "An immediate effect of custom-made ankle foot orthoses on postural stability in older adults," *Clinical Biomechanics*, vol. 29, pp. 1081-1088, 2014/12/01/ 2014.
- [204] M. Guerra Padilla, F. Molina Rueda, and I. M. Alguacil Diego, "Effect of ankle-foot orthosis on postural control after stroke: A systematic review," *Neurología (English Edition)*, vol. 29, pp. 423-432, 2014/09/01/ 2014.

## Appendix A: Literature Review Summary

**Table A.1: A Review of Gait Dynamic Stability Assessment Techniques**

Study	Purpose (subjects – H: healthy, I: impaired, Y: young, E: elderly)	Equipment/Method Used	Measurement Signals	Outcomes
<b>Gait Parameters Variability (section 2.4.1)</b>				
Bizivska et. al. [31]	age-related variations in stability compared to healthy subjects, (H=25)	Force plates (200Hz)	GRF, CoP	significant variations observed in CoP displacements in loading and pre-swing phases
Svoboda et. al. [129]	stability evaluation in faller/non-faller elderly at self-selected walking speeds, (E=125)	Force plates (200Hz), photocells for time measures at a fixed distance	step length, step width, step time, speed, CoP	in general no difference found in faller and non-faller w.r.t variability in mentioned parameters
Lugade et. al. [43]	balance control with four imitated foot conditions i.e. plantigrade, equinus, inverted, and everted foot, (H=13)	Force plates (720Hz) and motion cameras (120Hz)	CoP, CoP velocity, ankle angles ROM	CoP was 83% and 27% of foot length and width respectively in plantigrade, reduced ROM of CoP and velocity in AP for equinus walk

Fuchioka et. al. [44]	gait speed decline in elderly people as a predictor of poor stability, (E=68)	F-scan pressure sensitive foot insole (50Hz)	absolute CoP-velocity, step length, speed etc.	midfoot CoP velocity is a strong predictor of gait speed in elderly people
Strang et. al. [157]	postural coordination with growing age, (H=45)	Force plates (100Hz)	CoP, CoP-velocity (AP, ML)	significant age related mean frequency spectrum relation found with resultant CoP-velocity (abs)
Linden et. al. [76]	stability issues in Charcot-Marie tooth patients, (H=11, CMT=09)	Force plate, Rydel-Seiffer tuning fork,	RMS CoP-velocity, vibrations	a decrease in postural stability correlated with decreased in vibration sensing in CMT patients
Maslivec et. al. [81]	mechanism of head stability in young and elderly women, (Y=11, E=12)	Motion cameras (100Hz), force plate (1000Hz), EMG	CoM, BoS, angular displacement, rms accelerations	elderly showed higher variability in head angular displacement and decreased attenuations in the trunk to head,
Hof et. al [174]	ankle muscles role in medial-lateral imbalances	perturbator, EMGs (800Hz), treadmill, force transducer	CoP, EMG data three muscles	muscles activated with breaking reaction towards ML instability
<b>Correlation Coefficient Methods (section 2.4.2)</b>				
Rabuffetti et. al. [2]	stability evaluation for three tasks: a step forward, sit-to-stand, bending the trunk forward, (H=40)	Force platform (960Hz), the negative exponential model fitted	GRF, RMS value of AP CoM-acceleration	the intra-class correlation coefficient (ICC) determined for model parameters with variable outcomes

Cattaneo et. al. [9]	balance control assessment in multiple sclerosis patients during sit-to-stand, step forward and bending, (H=20, I=20)	Force plate, the negative exponential model fitted, Spearman correlation	GRF, RMS value of AP CoM-acceleration	longer stability time in bending and step forward, transitional sway higher in bending and sit-to-stand, static sway higher in all tasks
Lencioni et. al. [83]	stability assessment in Charcot-Marie tooth (1A) patients for sit-to-stand activity, (CMT=47)	Force platform (960Hz), the negative exponential model fitted, Spearman correlation	GRF, RMS value of AP CoM-acceleration	CMT1A patients found less stable and hard to maintain erect posture than healthy
DiDomenico et. al. [195]	postural stability evaluation after multiplanar perturbations using sliding window & model fits, (H=45)	MOCAP, Force plate, (100Hz) negative exponential model fitted	absolute and mean CoP-velocity	a negative exponential model was found more promising to determine stabilization times
<b>Extrapolated-CoM and BoS Difference (section 2.4.6)</b>				
Lugade et. al. [109]	extrapolated CoM difference with BoS by measuring BoS using markers and pressure sensors, (H=13)	F-scan pressure sensor, Motion cameras (120Hz)	CoM, CoM-velocity, CoP	stability margins underestimated with markers based BoS and over-estimated based on pressure sensors
Sivakumaran et. al. [40]	dynamic stability evaluated by a margin of stability (MoS) compared with variabilities in spatiotemporal, (H=11)	Force plate, motion cameras, (100Hz) treadmill, three walking speeds	CoM, BoS, step length, width, swing time, GRF	MOS was lower before long and wide steps, quick steps, and slower, spatiotemporal variability reflect transient period mechanical stability



Lugade et. al. [28]	margin of stability computed in relation to the interaction between CoM and BoS at different events, (H=20, E=10)	Force plate, motion cameras (60Hz)	CoM, CoP, foot markers	results showed reduced MoS in elderly
Mary Wu et. al. [5]	evaluate control on lateral stability with/without spine injuries in haptic walking environments, (H=10, I=08)	Force plate, motion cameras, motor actuated destabilizing platform	CoM, BoS (foot markers), step width, step time	step width decreased in stabilizing field and variability increased in impaired subjects, in the destabilizing field these subjects showed faster steps and increased lateral MoS
Mandeville et. al. [38]	stability evaluation in knee replacement patients (pre and post-surgery) compared with control subjects, (H=22, I=21)	Force plate (960Hz), motion cameras (60Hz), safety harness	CoM, CoP	MoS quantified by difference in CoM and CoP decreased in knee replacement than control subjects
Chen et. al. [196]	stability evaluation in elderly using angles between CoM and COP/ankle markers, (H=12, I=12)	Force plate (960Hz), motion cameras (60Hz)	CoM, CoP	CoM-ankle inclination angles are a good predictor of elderly stability in single stance compared with control
Martelli et. al. [197]	stability evaluation with wait-pull perturbations in AP and ML directions, (H=18)	motion cameras, FSR pressure pads, unexpected perturbations applied pelvic region	CoM, BoS (foot markers)	MoS shows balance recovery for AP perturbations, aftereffects modify stability control w.r.t type and extent of perturbation

Hak. L. et al. [198]	post-stroke patients stability evaluation in the backward and medial-lateral direction, (H=10)	motion cameras, treadmill, safety harness, virtual environment	CoM, BoS (foot markers)	at higher speed both backward and medial-lateral MoS increased slightly – reduce fall risks
Park. W. D. et al. [39]	age-related balance control under perturbations in standing, (Y=6, E=6)	motion cameras (100Hz)	CoM, BoS (foot markers)	Elderly subjects showed decreased regularity in MoS than younger
Mahmood et al. [199]	Impact of forwarding and rotational ankle-foot impairments on walking stability, (H=7)	Force plate (1000Hz), Motion cameras (400Hz)	CoP, GRF	rotational impairments decrease in MoS both at HC and TO, forward remains intact
<b>Lyapunov Exponent and Floquet Multiplier Methods (sections 2.4.3 &amp; 2.4.4)</b>				
Ihlen A.F. et al. [164]	local dynamic stability evaluation based on gait phases, (H=10)	motion cameras (100Hz), Lyapunov exponent method	position, velocity of toe, heel markers	subjects illustrated intra-stride changes in transitional gait phases
Fino. C. P. [200]	neuromotor stability control estimation in recently concussed athletes in single and dual task gait, (H=09)	IMU sensors placed at trunk and head (128Hz), Lyapunov exponent method	stride time, trunk tri-axial accelerations	decreased local dynamic stability during dual-tasks and no difference found in single task compared to healthy subjects
Worden et al. [201]	dynamic stability evaluated in response to unilateral masses added in lower limb extremity, (H=14)	light emitting diodes (60Hz) at head, trunk, pelvis, foot, margin of stability and local dynamic stability methods	CoM estimated from a weighted average of three	both methods showed more unstable upper body movements and only local dynamic stability method also

			segments head, trunk, pelvis	illustrated changes in upper body stability using temporal parameters
Kang et. al. [85]	stability evaluation in young and elderly using muscles activations, (Y=17, E=18)	surface EMGs (1080Hz), Lyapunov exponent and Floquet multiplier	EMG waveforms	elderly illustrated greater instability by both methods, kinematic & EMG correlated with Lyapunov exponent
Stenum et. al. [173]	walking speed effect of local dynamic stability, (H=10)	an accelerometer at the sternum (64Hz), treadmill	3D acceleration	local dynamic stability evaluated using fixed time interval and strides, walking speed effect significantly different from these methods
Kang et. al. [202]	age-related stability evaluation with the effect of superior/inferior sensory measurements (H=17, E=18)	motion cameras, treadmill, Lyapunov exponent and Floquet multiplier	markers data from trunk, pelvis, thigh, shank, feet	LE was larger for elderly and in inferior segments, FM was larger in elderly but in superior segments
Bruijn et. al. [167]	walking speed effect on human stability during walking, (H=15)	LED cluster at the trunk, Optotrack system (50Hz), treadmill	thorax marker 3D position data	inconsistent pattern in Lyapunov exponents (short & long divergence) slow speed not necessarily stable
Loverro et. al. [126]	gait stability evaluation in patients having hip pain and dysplasia at different walking speeds, (H=12)	Motion cameras (120Hz), force plate (1000Hz), treadmill, Lyapunov	joints angles, spatiotemporal, trunk markers	patients showed greater kinematic variability and no difference in Lyapunov exponent (stability) compared to control subjects

		exponent, variability (Std.) methods		
Bruijn et. al. [29]	age-related changes in gait stability in relation to the brain structure, (Y=15, E=12)	motion cameras, MRI scanner, extrapolated-COM and Lyapunov exponent	CoM, pelvis markers, CoP, step width, stride time	among different stability measures, the stride time and Lyapunov exponent decreased for elderly subjects
<b>Linear System Identification and Bode Stability Methods (section 2.4.7)</b>				
Morgan et. al. [34]	stability difference in healthy and knee ligament reconstructed patients, (H=16, I=16)	MOCAP (200Hz), Force plate (1200Hz), Nyquist and Bode algorithms	knee joint angle	Nyquist and Bode methods introduced for gait stability assessment with improved criteria
Morgan et. al. [35]	stability evaluation in football players during the weight acceptance phase	MOCAP (250Hz), Force plate (2000Hz), N&B algo.	knee abduction moment, GRF-V	N&B methods successfully illustrated stable and unstable knee dynamics
Ardestani et al. [36]	knee joint stability evaluation in patients with total knee arthroplasty, (I=6)	MOCAP (200Hz), Force plate (1000Hz), Bode algo.	knee power o/p, angular velocity and moment i/ps	the impaired knee can potentially impair knee power in the presence of perturbations
Hur et al., [37]	evaluation of robustness in posture in the presence of perturbations, (H=30)	Force plate (1000Hz), Bode plot, system identification,	ankle angle, the impulsive force	the robustness found smaller in older than younger and middle age subjects
Hidler et al., [92]	Contractile properties evaluated for a spastic gait stimulated at tibial nerve and	Biodex Medical system, a tibial nerve stimulator,	Ankle joint moment, EMG signals	Patients with higher spasticity preserved contractile dynamics and

	Bode plots constructed from ankle moments signals, (H=10, I=10)	EMGs (1000Hz), system identification		with less spasticity showed fast response in contractile properties
Schut et. al. [80]	walking surfaces compliances effect sensory reweighting towards balance control, (H=11)	bilateral ankle perturbator (BAP), spectral analysis system identification	ankle angle amplitude from BAP dynamics	compliant mats reweight the sensory feedback with an inverse relationship
Mahmood et. al. [95, 96]	gait dynamic stability evaluation for a level walk and inclined surfaces (H=4)	Force plate (1000Hz), Motion cameras (400Hz)	CoP, GRF, GM, PM	inputs showed unstable and outputs showed a stable response, ramp ascend is less stable than descending walk
Mahmood et. al. [97]	neuromotor control estimation using biomechanical signals (H=4, I=4)	Force plate (1000Hz), Motion cameras (400Hz)	CoP, GRF, GM, PM	Toe walk is least stable comparing with inverted and normal feet.
<b>Gait Stability Evaluation Review Studies (section 2.4)</b>				
Bruijn et. al. [10]	gait stability evaluation methods – a review study	Lyapunov, Floquet, Extrapolated-CoM, ICC, variability, forced perturbations methods		future direction – new stability measures to validating these methods
Simon et. al. [11]	dynamic stability evaluation in spine patients – a review study	Lyapunov exponent, Floquet multiplier, variability, extrapolated-CoM methods		Reproducibility and clinical evaluation of these methods need
<b>Studies included AFO for Stability Evaluations (section 2.4)</b>				
Yalla et. al. [203]	custom made AFO impact of postural stability in elderly	Romberg balance, timed up and go test, IMUs	observations and time of tasks	AFO decreased postural sway and improve stability in elderly

Tyson et. al. [8] (review study)	effectiveness of AFO on balance, mobility and walking in stroke patients	Motion cameras, Force plates, Timed up and go test, Berge balance test	walking speed, step length, body sway, stride length	AFOs improve balance and walking in stroke patients
Dogan et. al. [7]	effect of AFO on balance and mobility in hemiparetic patients	Timed up and go test, Berge balance test	observations and scaling	AFO improved balance and ambulation activities
Padilla et. al. (review study) [204]	AFOs impact on postural control in stroke patients	Timed up and go test, Berge balance test, Fall risks and functional reach tests, symmetry	Spatiotemporal, CoP, GRF, angles, moments, observations, scaling	Gait parameters such as cadence and speed improved, however, no evidence regarding improvement in gait symmetry and balance

## Appendix B: Ethical Approval

Performance, Governance and Operations  
 Research & Innovation Service  
 Charles Thackrah Building  
 101 Clarendon Road  
 Leeds LS2 9LJ Tel: 0113 343 4873  
 Email: [ResearchEthics@leeds.ac.uk](mailto:ResearchEthics@leeds.ac.uk)



**UNIVERSITY OF LEEDS**

Imran Mahmood  
 Mechanical Engineering  
 University of Leeds  
 Leeds, LS2 9JT

**MaPS and Engineering joint Faculty Research Ethics Committee (MEEC FREC)  
 University of Leeds**

12 February 2017

Dear Imran

**Title of study**            **Wearable Soft Robotics for Independent Living.**  
**Ethics reference**        **MEEC 15-050**

I am pleased to inform you that the application listed above has been reviewed by the MaPS and Engineering joint Faculty Research Ethics Committee (MEEC FREC) and following receipt of your response to the Committee's initial comments, I can confirm a favourable ethical opinion as of the date of this letter. The following documentation was considered:

Document	Version	Date
MEEC 15-050 Ethical_Review_Form_V3.pdf	3	13/07/16
MEEC 15-050 Supporting Documents for ethical approval.pdf	3	13/07/16
MEEC 15-050 Faculty Risk Assessment Form 208 Imran_final.pdf	3	13/07/16
MEEC 15-050 Letter of Authority_Imran.doc	1	13/07/16

Committee members made the following comments:

- The wording of the recruitment poster will need some checking/ amending before use.

Please notify the committee if you intend to make any amendments to the original application as submitted at date of this approval as all changes must receive ethical approval prior to implementation. The amendment form is available at <http://ris.leeds.ac.uk/EthicsAmendment>.

Please note: You are expected to keep a record of all your approved documentation. You will be given a two week notice period if your project is to be audited. There is a checklist listing examples of documents to be kept which is available at <http://ris.leeds.ac.uk/EthicsAudits>.

We welcome feedback on your experience of the ethical review process and suggestions for improvement. Please email any comments to [ResearchEthics@leeds.ac.uk](mailto:ResearchEthics@leeds.ac.uk).

Yours sincerely

Jennifer Blaikie  
 Senior Research Ethics Administrator, Research & Innovation Service  
 On behalf of Professor Gary Williamson, Chair, [MEEC FREC](#)  
 CC: Student's supervisor(s)

### Appendix C: Angles and Moments Ramp walk

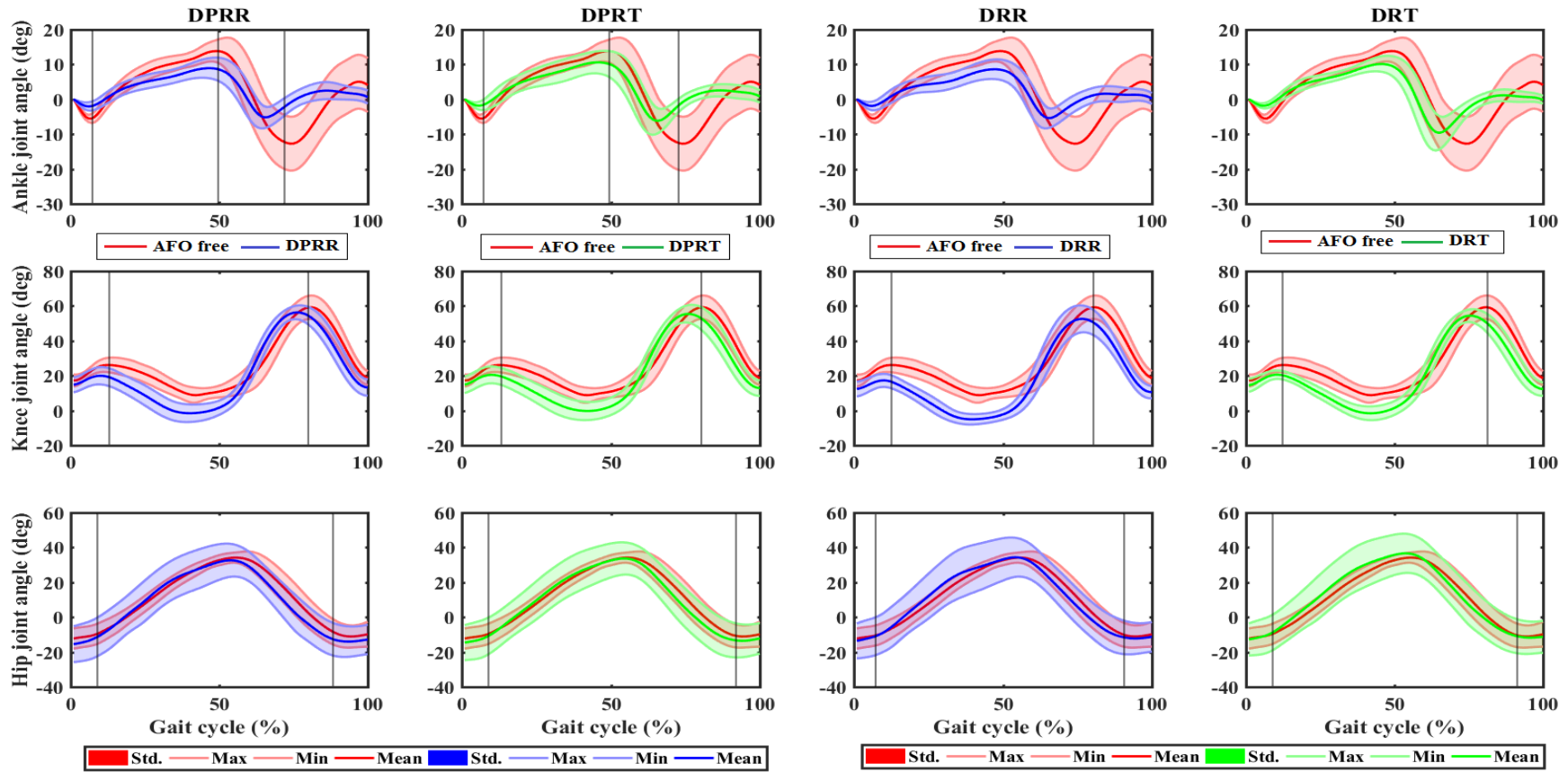


Figure C.1: Lower limb joints angles comparison between normal and forward ankle-foot impairments for Ramp Ascend.



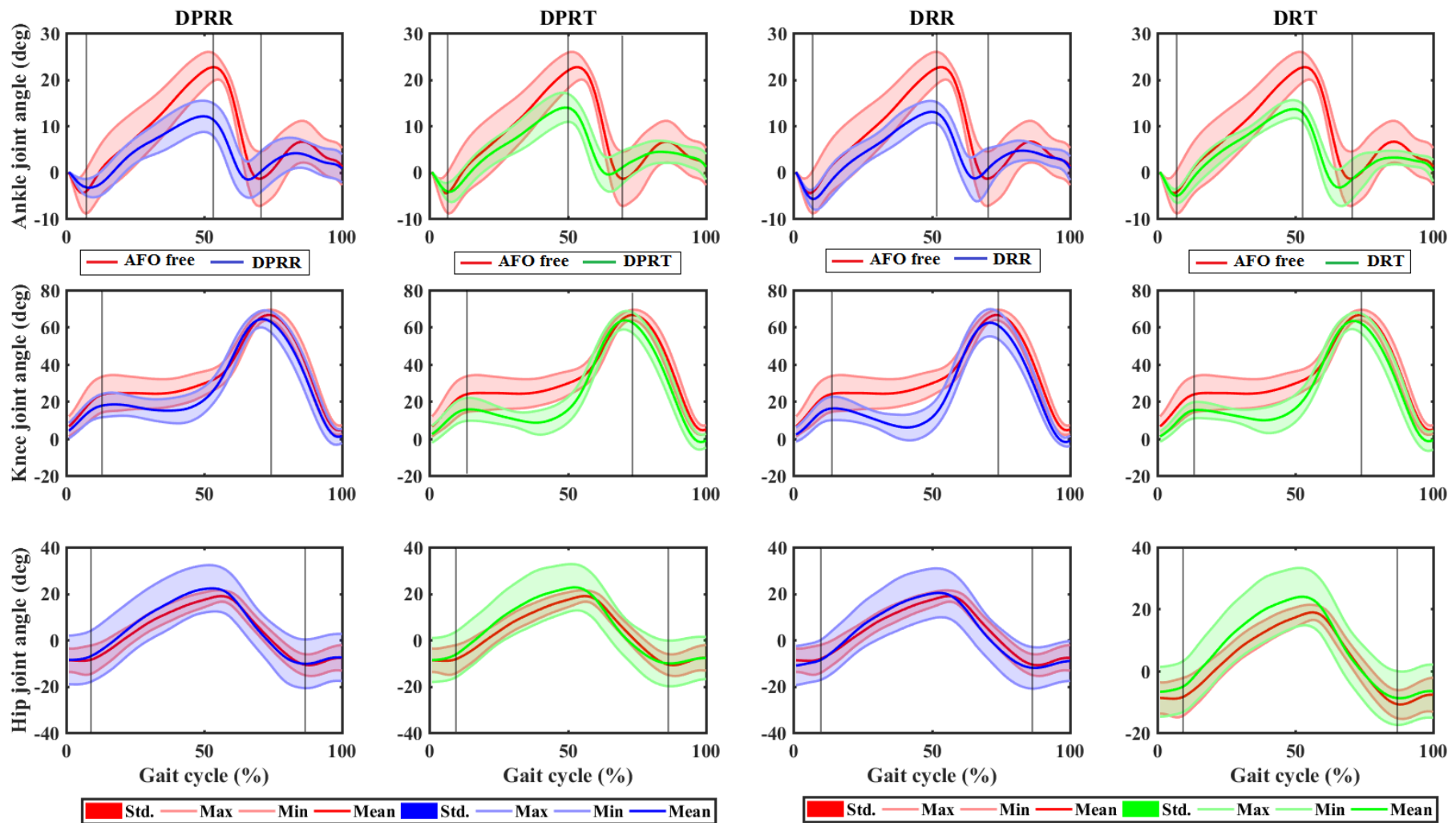


Figure C.2: Lower limb joints angles comparison between normal and forward ankle-foot impairments for Ramp Descend.

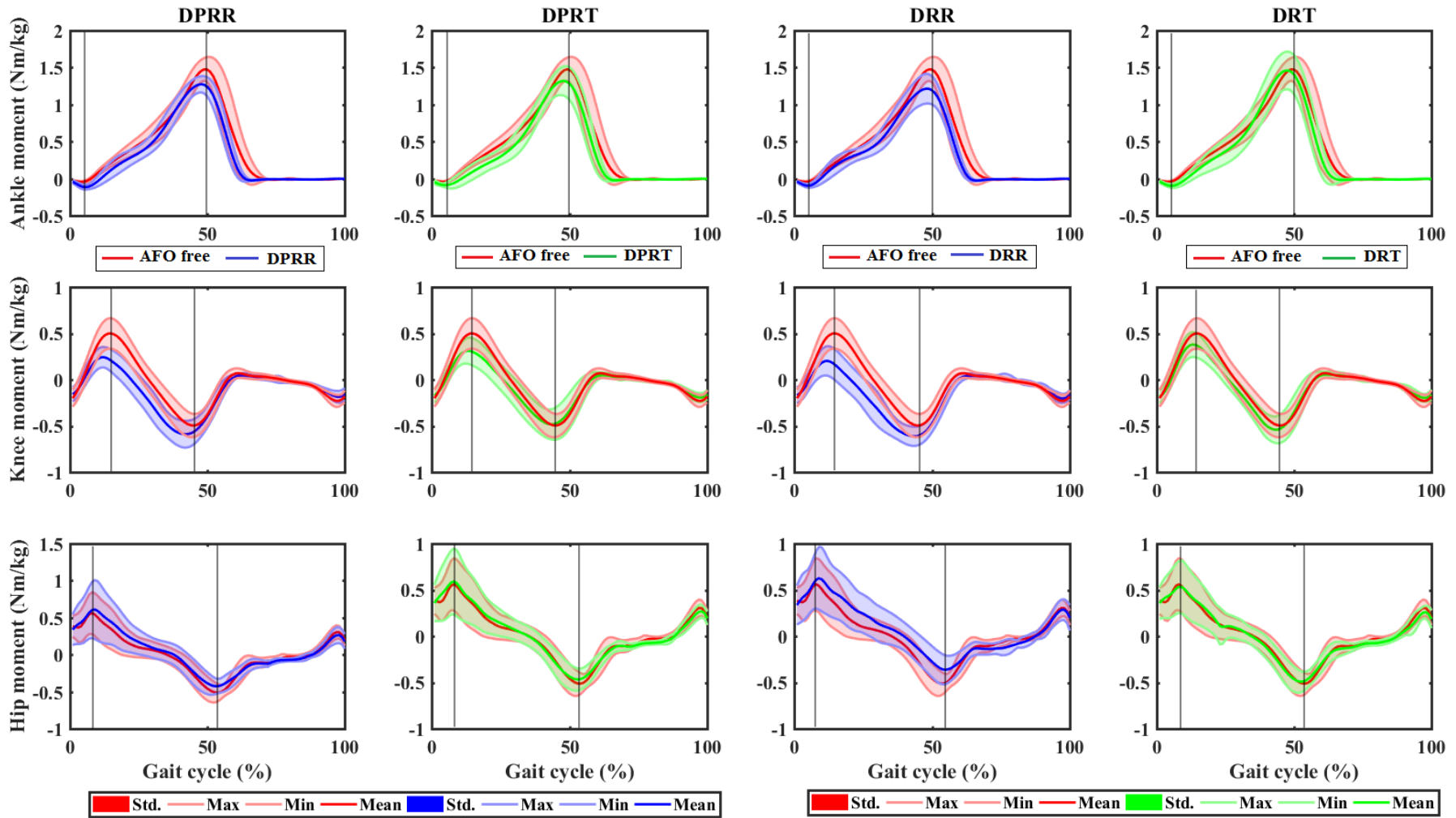


Figure C.3: Lower limb joints moments comparison between normal and forward ankle-foot impairments for Ramp Ascend.

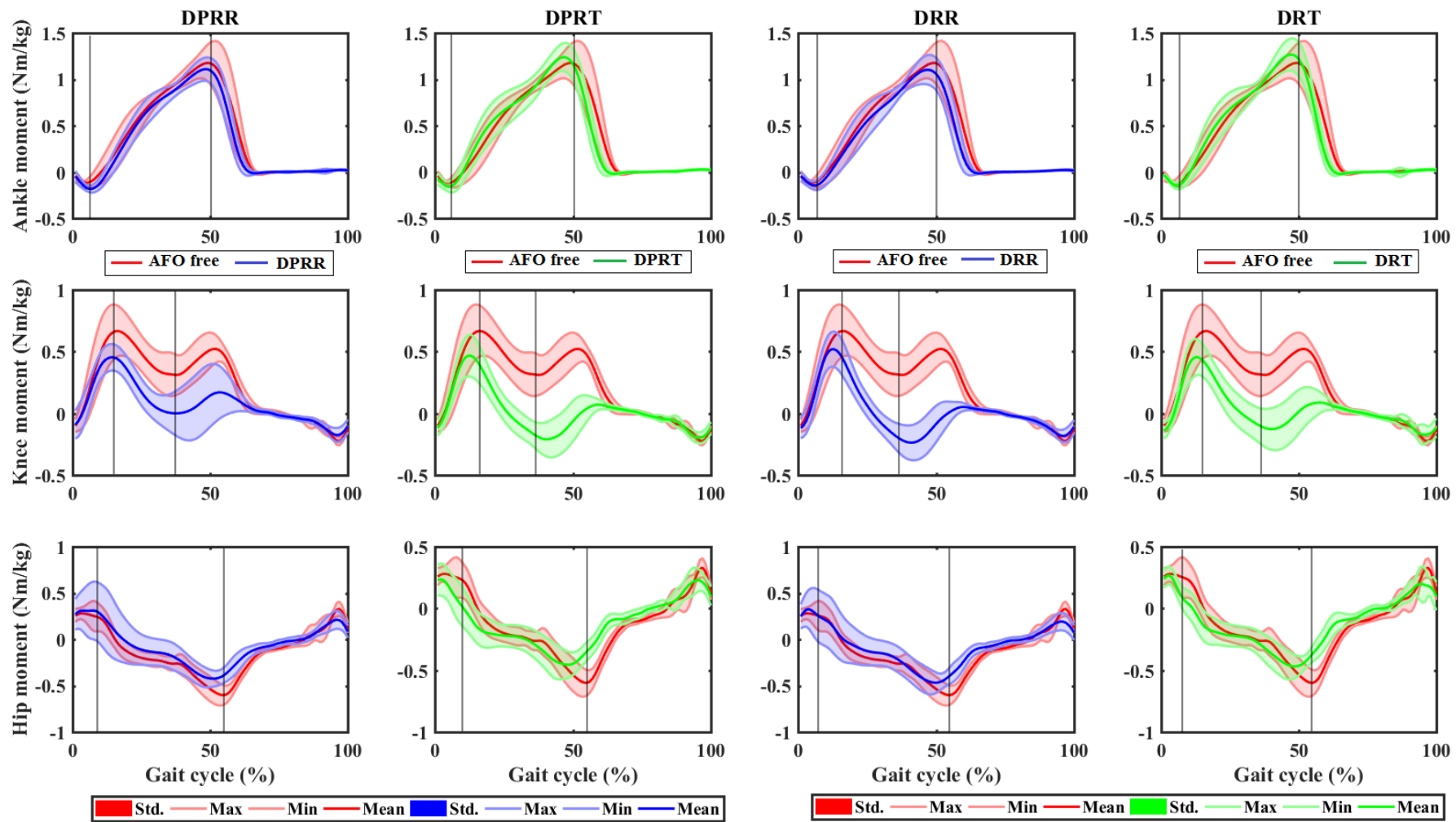


Figure C.4: Lower limb joints moments comparison between normal and forward ankle-foot impairments for Ramp Descend.

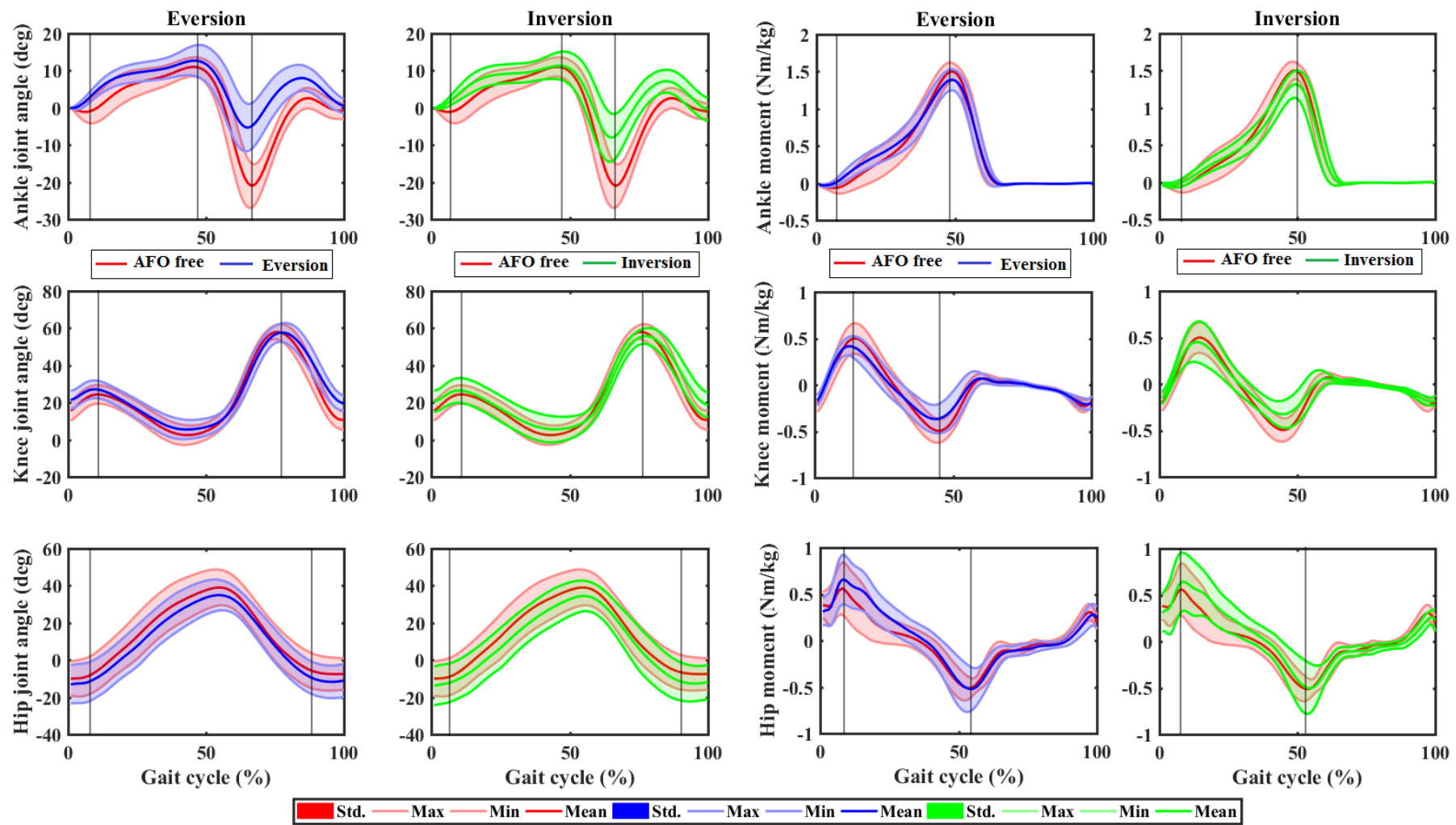


Figure C.5: Lower limb joints angles & moments comparison between normal and rotational foot impairments for Ramp Ascend.

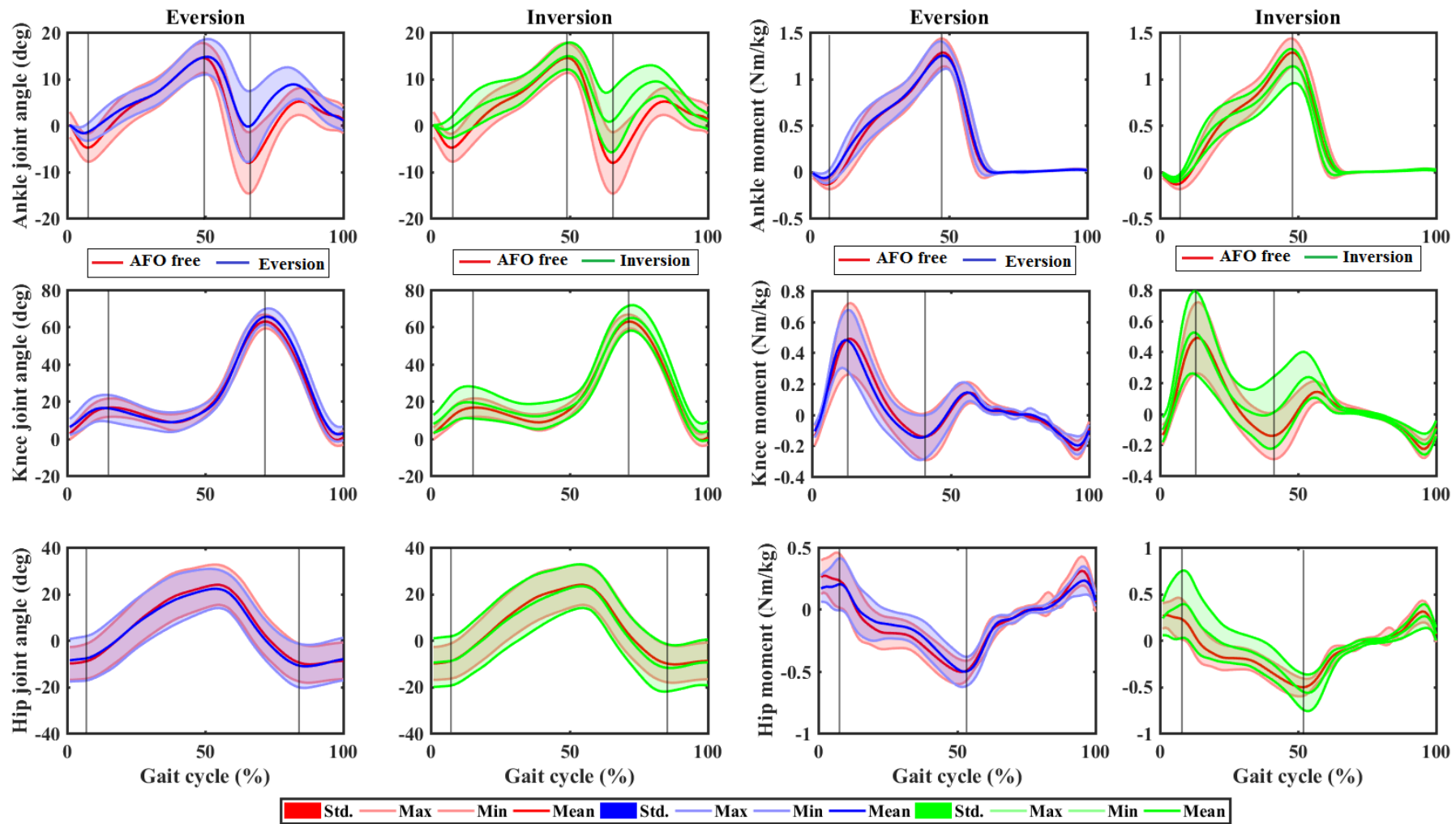


Figure C.6: Lower limb joints angles & moments comparison between normal and rotational foot impairments for Ramp Descend.

## Appendix D: Demographic data

Table B.1: Subjects demographic data.

Subjects	Age	Height (cm)	Weight (kg)	Foot length (cm)	BMI* kg/m <sup>2</sup>
1	30	173.9	83.5	26	27.6
2	34	179.2	72.2	28	22.5
3	27	166	70.2	25	25.5
4	31	166.6	70.6	25	25.4
5	29	174.1	76.3	26	25.2
6	28	167.4	78.8	25	28.1
7	33	162	63.6	23	24.2
8	29	171	67	27	22.9
9	32	180.8	89.7	28	27.4
10	28	165.4	54.1	25	19.7
11	35	171	81.2	25.5	27.8
12	28	191.7	94.8	29	25.8

\*Body mass index calculated ([https://www.diabetes.ca/en-CA/managing-my-diabetes/tools---resources/body-mass-index-\(BMI\)-calculator](https://www.diabetes.ca/en-CA/managing-my-diabetes/tools---resources/body-mass-index-(BMI)-calculator))

## Appendix E: Stability Margins

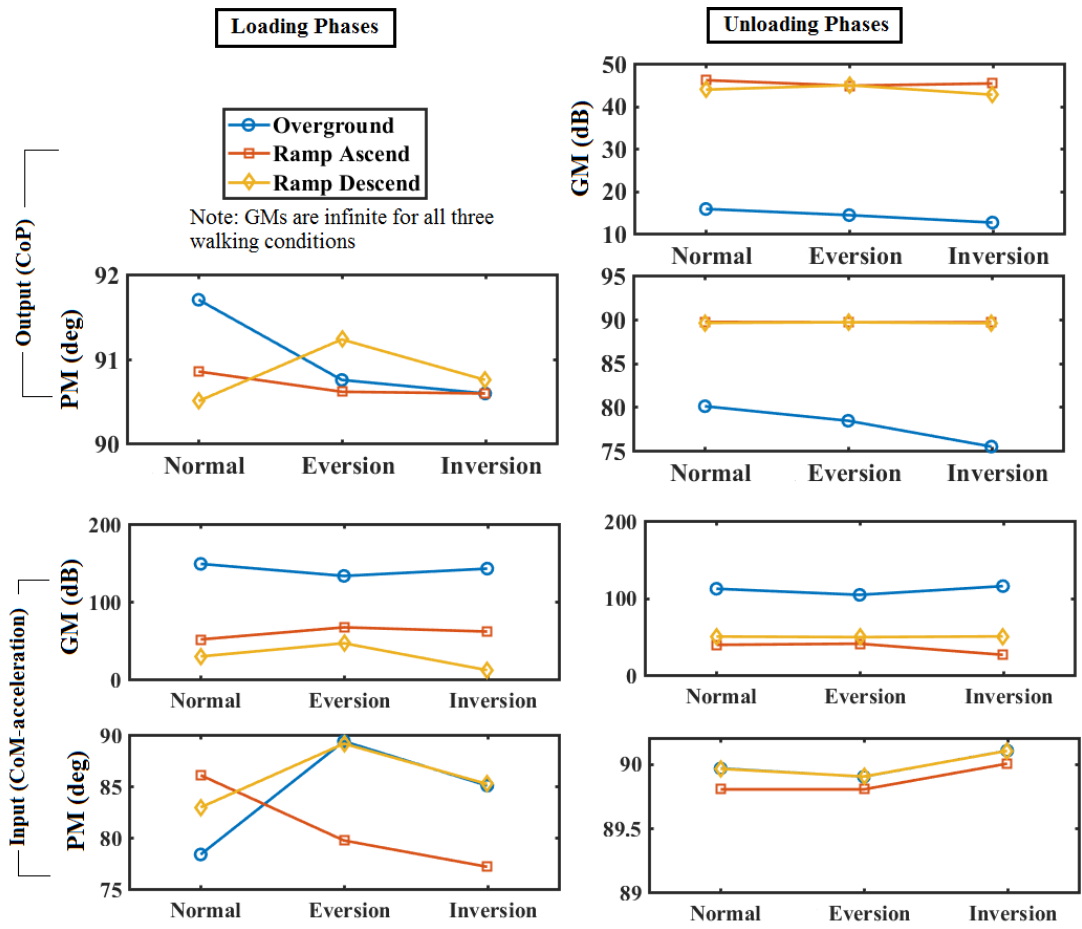
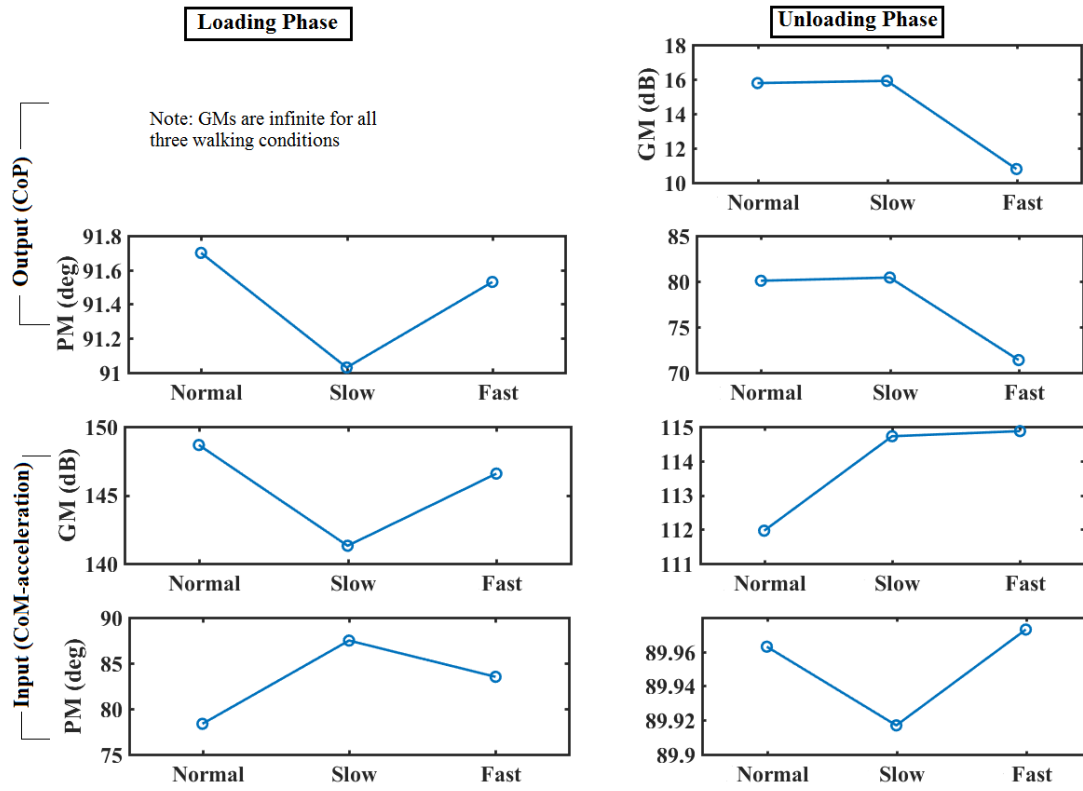


Figure E.1: Mean stability margins comparison for rotational impairments in the forward direction.



**Figure E.2: Mean stability margins comparison in walking speed group in the forward direction.**



**Appendix F: Efficiency of predictively**

**Table F.1: Efficiency of stability evaluation for ramp ascend and descend.**

Signals	CoP-velocity (forward)		CoM-acceleration (forward)		CoM-acceleration (vertical)	
	L	U	L	U	L	U
<b>Ramp Ascend</b>						
AFO (free)	97.17	99.54	95.22	93.54	99.98	92.61
DPRR	97.14	98.17	98.31	90.16	93.55	95.27
DPRT	97.74	98.19	96.15	96.8	93.14	95.81
DRR	98.5	97.98	99.39	94.3	92.07	95.19
DRT	97.00	98.76	99.25	91.41	92.12	96.44
Eversion	98.52	98.81	98.39	93.06	-	-
Inversion	98.61	98.68	97.84	91.17	-	-
Normal	97.34	97.85	94.35	93.46	93.22	95.06
<b>Ramp Descend</b>						
AFO (free)	99.50	99.31	92.22	91.33	93.06	94.26
DPRR	94.02	98.23	97.84	90.02	93.54	95.75
DPRT	92.65	98.90	92.76	93.84	91.92	96.25
DRR	94.32	98.54	97.47	92.16	98.2	93.95
DRT	94.55	98.92	95.71	94.37	93.44	95.04
Eversion	94.57	98.48	96.72	96.20	-	-
Inversion	98.13	98.00	96.73	95.75	-	-
Normal	90.68	98.25	90.91	92.46	97.33	95.35

L: loading, U: unloading.

## Appendix G: List of all Publications

### G.1 Publications from Thesis (I. Mahmood, main author)

1. I. Mahmood, U. Martinez-Hernandez, and A. A. Dehghani-Sanij, "Rate-Dependant Gait Dynamic Stability Analysis for Motor Control Estimation," in *Advances in Cooperative Robotics*, ed: WORLD SCIENTIFIC, 2016, pp. 454-463. DOI: <https://doi.org/10.1142/10261>
2. I. Mahmood, U. Martinez-Hernandez, and A. A. Dehghani-Sanij, "Gait dynamic stability analysis and motor control prediction for varying terrain conditions," in *IEEE Mechatronics (MECHATRONICS)/17th International Conference on Research and Education in Mechatronics (REM), 2016 11th France-Japan & 9th Europe-Asia Congress on*, 2016, pp. 290-295. DOI: [10.1109/MECATRONICS.2016.7547157](https://doi.org/10.1109/MECATRONICS.2016.7547157)
3. Mahmood I., Martinez-Hernandez U., Dehghani-Sanij A.A. (2017) Towards Behavioral Based Sensorimotor Controller Design for Wearable Soft Exoskeletal Applications. In: Ibáñez J., González-Vargas J., Azorín J., Akay M., Pons J. (eds) *Converging Clinical and Engineering Research on Neurorehabilitation II. Biosystems & Biorobotics*, vol 15. Springer, Cham. DOI: [https://doi.org/10.1007/978-3-319-46669-9\\_209](https://doi.org/10.1007/978-3-319-46669-9_209)
4. I. Mahmood, U. Martinez Hernandez, and A. A. Dehghani-Sanij, "Gait Dynamic Stability Analysis for simulated Ankle-foot impairments and Bipedal robotics applications," presented at the 6th Mechatronics Forum International Conference, 2018.

Following Journal papers are submitted (1 and 2) or planned to be submitted (3) including level ground walk stability evaluations in Chapter 3-6 of current thesis:

5. Mahmood, U. Martinez Hernandez, and A. A. Dehghani-Sanij, "Evaluation of Neuromotor Balance Control during Gait Transitional Phases," *ASME Journal of Biomechanical Engineering*. (Under review, 2019)
6. Mahmood, U. Martinez Hernandez, and A. A. Dehghani-Sanij, "Evaluation of Neuromotor Balance Control during Gait Transitional Phases with Rotational ankle-foot Impairments," *Human Movement Science*. Elsevier. (Under review, 2019)
7. Mahmood, U. Martinez Hernandez, and A. A. Dehghani-Sanij, "Wearable orthosis impacts on vertical dynamics of lower limbs during weight loading and unloading gait transitions," *Journal of Biomechanics*. Elsevier. (Submitted, 2019)

The outcomes from Chapter 7 (Ramp Ascend Descend walk) are planned to be published accordingly.

## **G.2 Other Publications (I. Mahmood, co-author)**

1. Mahmood I, Raza A. Therapeutic Equipment for Brain-Hyperthermia Using Convective Spray Cooling. ASME. J. Med. Devices. 2017;11(3):031010-031010-11. doi:10.1115/1.4036652.
2. U. Martinez-Hernandez, I. Mahmood and A. A. Dehghani-Sanij, "Simultaneous Bayesian Recognition of Locomotion and Gait Phases With Wearable Sensors," in IEEE Sensors Journal, vol. 18, no. 3, pp. 1282-1290, 1 Feb.1, 2018. doi: 10.1109/JSEN.2017.2782181
3. U. Martinez-Hernandez, M. I. Awad, I. Mahmood and A. A. Dehghani-Sanij, "Prediction of gait events in walking activities with a Bayesian perception system," 2017 International Conference on Rehabilitation Robotics (ICORR), London, 2017, pp. 13-18. doi: 10.1109/ICORR.2017.8009214
4. Martinez-Hernandez U., Mahmood I., Dehghani-Sanij A.A. (2017) Probabilistic Locomotion Mode Recognition with Wearable Sensors. In: Ibáñez J., González-Vargas J., Azorín J., Akay M., Pons J. (eds) Converging Clinical and Engineering Research on Neurorehabilitation II. Biosystems & Biorobotics, vol 15. Springer, Cham.